EGE UNIVERSITY INSTITUTE OF SCIENCE

(PhD OF SCIENCE THESIS)

PREPARATION OF METAL NANOPARTICLES AND/OR METAL FILM MODIFIED ELECTRODES THEIR CHARACTERIZATION AND ELECTROCHEMICAL APPLICATIONS

Aydan ELÇİ

Supervised by : Prof. Dr. Zekerya DURSUN

Co-Supervisor : Prof. Dr. F. Nil ERTAŞ

Department of Chemistry

Department Code : 405.03.01

Date of Presentation : 20.09.2013

Bornova-İZMİR

2013

Sayın **Aydan ELÇİ** tarafından **Doktora Tezi** olarak sunulan **"Preparation Of Metal Nanoparticles And/Or Metal Film Modified Electrodes Their Characterizations And Electrochemical Applications"** başlıklı bu çalışma E.Ü. Lisansüstü Eğitim ve Öğretim Yönetmeliği ile E.Ü. Fen Bilimleri Enstitüsü Eğitim ve Öğretim Yönergesi'nin ilgili hükümleri uyarınca tarafımızdan değerlendirilerek savunmaya değer bulunmuş ve 20.09.2013 tarihinde yapılan tez savunma sınavında aday oybirliği/oyçokluğu ile başarılı bulunmuştur.

<u>Jüri Üyeleri:</u>   **<u>İmza</u>**

Jüri Başkanı   : **Prof. Dr. Zekerya DURSUN**   ....

Raportör Üye   : **Prof. Dr. F. Nil ERTAŞ**   ....

Üye   : **Prof. Dr. Ahmet EROĞLU**   ....

Üye   : **Prof. Dr. Ümran YÜKSEL**   ....

Üye   : **Prof. Dr. Berin Yenigül**   ....

Üye   : **Doç. Dr. Nuri NAKİPOĞLU**   ....

ÖZET

METAL NANO PARTİKÜL VE/VEYA METAL FİLM MODİFİYE ELEKTROTLARIN HAZIRLANMASI, KARAKTERİZASYONU VE ELEKTROKİMYASAL UYGULAMALAR

ELÇİ, Aydan

Doktora Tezi, Kimya Bölümü
Tez Yöneticisi: Prof. Dr. Zekerya DURSUN
İkinci Tez Danışmanı: Prof. Dr. F. Nil ERTAŞ
Eylül 2013, 226Sayfa

Analitik kimyadaki önemli çalışma alanlarından birisi organik ve inorganik maddelerin elektrokimyasal tayinidir. Bu alandaki araştırma konularının çoğu, organik ve inorganik analitlerin tayini için, yüksek duyarlık, doğruluk ve düşük belirtme sınırı elde etmek için yöntem geliştirmeyi esas alır. Son yıllarda nanoteknoloji ve nanobilimdeki gelişmeler, fiziksel ve kimya ve biyolojik konusunda bilgi sağlayan çalışmalar hız kazanmıştır. Özellikle nano boyuttaki malzemelerin geliştirilmesi sonucu, elektrokimyasal çalışmalarda kullanılan geleneksel elektrotların kimi uygulamalardaki yetersizliğini gidermek amacıyla, analitlere karşı katalitik etkinliği ve seçimliliği yüksek, farklı yüzeylere gereksinim duyulmuştur. Bu amaca yönelik yüksek iletkenlik, geniş ve etkin yüzey alanlarına sahip karbon naotüp veya iletken polimer filmlerin metal nanoparçacıklar ile birleştirilmesi önemli yeni elektrot malzemeleri olarak kullanılmaktadır.

İki bölümden oluşan bu tez çalışmasının ilk kısmında, metal nanoparçacıklar (Au, Pd, Ni) hem elektrokimyasal hemde kimyasal indirgeme yöntemiyle elektrot yüzeyinde hazırlanarak etanol ve metanol gibi yakıt olarak kullanılabilecek küçük alkol moleküllerinin elektrokatalitik yükseltgenmesine olan etkileri incelenmiştir.

Etanol ve metanolün yükseltgenmesine karşı en yüksek katalitik etkinlik Pd-Au-Ni metal nanoparçacık modifiye MWCNT/GCE' da gözlenmiştir. Üçlü metal nano parçacık modifiye elektrotlarla elde edilen sonuçlar diğer elektrotlarla elde edilen voltammetrik sonuçlarla karşılaştırıldığında, gerek etanol gerekse metanol alkali ortamdaki hem pik akımları artmış hem de yükseltgenme pik potansiyelleri daha negatif değerlere kaymıştır. Pd, Au ve Ni nano parçacığın tekli, ikili ve üçlü olarak MWCNT/GCE yüzeyindeki morfolojik ve kimyasal karakterizasyonları SEM-EDX, XRD ve XPS tekniklerle yapılmıştır.

İkinci bölümde ise modifiye karbon pasta elektrotlar ile çevre için zararlı olan ağır metallerden kurşun ve kadmiyumun nicel tayinleri gerçekleştirilmiştir. Yalın karbon pasta elektrot; $Ca_3(PO_4)_2$, $Ca_3(PO_4)_2+ZrO(H_2PO_4)_2$, $Ca_3(PO_4)_2+Cu_2Fe(CN)_6$, $CNT+K_4Fe(CN)_6$, Sn-Bi film gibi parçacıklarla modifiye edilmiştir. Modifiye edilmiş karbon pasta elektrotlarla yalın karbon pasta elektroda göre daha duyar ve düşük belirtme sınırı elde edilmiştir.

Pb(II) iyonunun belirtme alt sınırı 0.1584×10^{-7} mol $L^{-1} \pm 0.035$ ($X_{ort} \pm 3S$) ve tayin sınırı 0.528×10^{-7} mol $L^{-1} \pm 0.172$ ($X_{ort} \pm 10S$) olarak for Sn-Bi Film modifiye karbon pasta elektrot kullanılarak bulunmuştur. Cd(II) iyonunun belirtme alt sınırı 1.2654×10^{-7} mol $L^{-1} \pm 0.042$ ($X_{ort} \pm 3S$) ve tayin sınır4.218×10^{-7} mol $L^{-1} \pm 0.196$ ($X_{ort} \pm 10S$) olarak for Sn-Bi Film modifiye karbon pasta elektrot kullanılarak bulunmuştur.

Tüm elektrot yüzeyleri taramalı elektron mikroskobu, X-ışınları fotoelektron spektroskopisi ve elektrokimyasal impedans spektroskopisi ile karakterize edilmiştir.

Anahtar Kelimeler: Diferansiyel puls voltammetri, döngüsel voltammetri, etanol, kadmiyum, karbon nanotüpler**,** karbon pasta elektrot, kurşun, metal nano partikül, metanol, modifiye elektrot, taramalı elektron mikroskobu.

ABSTRACT

PREPARATION OF METAL NANOPARTICLES AND/OR METAL FILM MODIFIED ELECTRODES THEIR CHARACTERIZATION AND ELECTROCHEMICAL APPLICATIONS

ELÇİ, Aydan

(PhD) Thesis in Chemistry Department
Supervisors: Prof. Dr. Zekerya DURSUN
Co-Supervisor: Prof. Dr. F. Nil ERTAŞ
September 2013, 226 Pages

The main research area of analytical chemistry is organic and inorganic compounds determined by electrochemical techniques. In this research area, to determine organic and inorganic analytes needs high sensitivity, accuracy and low detection limits for methods. Sensor applications that provide information on our physical, chemical and biological environment were increased with the progress on nanoscience and nanotechnology. The insufficient behaviour of bare electrodes lead to necessity of different catalytically active surfaces. Carbon nanotubes or polymer films were canditates for overcome this problem with their active sited high surface area.

In the first part of this thesis which consisted of two different sections, metal nanoparticles (Au, Pd, Ni) prepared with electrochemical and chemical reduction methods on modified multiwall carbon nanotube electrodes and their effect on electrocatalytic oxidation of ethanol and methanol as a fuel for cells were investigated. The best catalytic activity for ethanol and methanol oxidations were supplied with Pd-Au-Ni metal nanoparticles modified MWCNT/GCE. Trimetallic nanoparticles covered carbon nanotube electrode compare with other electrodes the peak current was increased also oxidaiton peak potential was shifted to negative values for ethanol and methanol in alkaline media. Pd, Au ve Ni nanoparticles, bi and tri metalic covered MWCNT/GCE surfaces morphology and chemical characterization were characterizied by SEM-EDX, XRD ve XPS techniques.

In second part of this thesis, the quantitative determinations of lead and cadmium which was harmfull for environment were investigated by modified carbon paste electrode. Bare carbon paste electrode modified with $Ca_3(PO_4)_2$, $Ca_3(PO_4)_2+ZrO(H_2PO_4)_2$, $Ca_3(PO_4)_2+Cu_2Fe(CN)_6$, $CNT+K_4Fe(CN)_6$, Sn-Bi Film. Modified carbon paste electrode compare with bare carbon paste electrode, modified carbon paste electrode show more sensitive and low limit of dedection. Differential puls voltammetry and square wave voltammetry were used quantitative determination of lead and cadmium.

Limit of dedection of Pb(II) ions was 0.1584×10^{-7} mol $L^{-1} \pm 0.035$ ($X_{ort} \pm 3S$) and limit of quantitaion of Pb(II) ions was 0.528×10^{-7} mol $L^{-1} \pm 0.172$ ($X_{ort} \pm 103S$) for Sn-Bi Film modified carbon paste electrode. Limit of dedection of Cd(II) ions was 1.2654×10^{-7} mol $L^{-1} \pm 0.042$ ($X_{ort} \pm 3S$) and limit of quantitaion of Cd(II) ions was 4.218×10^{-7} mol $L^{-1} \pm 0.196$ ($X_{ort} \pm 103S$) for Sn-Bi Film modified carbon paste electrode.

All electrode surfaces were characterizied by scanning electrone microscopy, X-Ray photoelectrone spectroscopy and electrochemical impedance spectroscopy.

Keywords: Cadmium, carbon nanotubes, carbon paste, cyclic voltammetry, differential pulse voltammetry, ethanol, lead, metal nanoparticles, methanol, modified electrode, scanning electrone microscopy.

ACKNOWLEDGEMENT

x

CONTENTS

CONTENTS(continued)

CONTENTS(continued)

CONTENTS(continued)

CONTENTS(continued)

CONTENTS(continued)

LIST OF FIGURES

LIST OF FIGURES(continued)

LIST OF FIGURES(continued)

LIST OF FIGURES(continued)

LIST OF FIGURES(continued)

LIST OF FIGURES(continued)

LIST OF FIGURES(continued)

LIST OF FIGURES(continued)

LIST OF FIGURES(continued)

LIST OF FIGURES(continued)

LIST OF FIGURES(continued)

LIST OF FIGURES(continued)

LIST OF TABLES

LIST OF TABLES(continued)

ABBREVIATIONS

Symbol	Explanation
CNTs	Carbon nanotubes
MWCNT	Multi carbon nanotubes
SWCNT	Single walled carbon nanotubes
CPEs	Carbon pasta electrodes
MNPs	Metal nanoparticles
CV	Cyclic voltammetry
SEM	Scanning electron microscopy
EDX	Energy dispersive x-ray spectroscopy
XPS	X-ray photonelectron spectroscopy
EIS	Electrochemical impedance spectroscopy
ESD	Electrostatic spray deposition
ICP-MS	Inductively coupled plasma-mass spectrometry
Red	Reduction
FETs	Field-effect transistors
PE	Plasma-enhanced
CVD	Chemical vapor deposition
PVD	Physical vapor deposition
A	Amper
US	Ultrasound
PLA	Laser ablation
AAS	Atomic absorption spectrometry
AFS	Atomic fluorescence spectrometry
NAA	Neutron activation analysis
SCF	Supercritical fluids
DMFC	Direct methanol fuel cell
SPM	Scanning probe microscopes
DMF	Dimethyl foramide
DEFC	Direct ethanol fuel cell
XRD	X-ray diffraction
TEM	Transmission electron microscopy
CNTPE	Carbon nanotube paste electrode
Adsv	Adsorptive stripping voltammetry
ICP-MS	Inductively coupled plasma mass spectrometry
ICP-OES	Inductively coupled plasma optical emission spectrometry
STM	Scanning tunnelling microscopy
SE	Secondary electrons
BSE	By backscattered electrons
ASV	Anodic stripping voltammetry
Ox	Oxidation

1. INTRODUCTION

1. 1 General Information

The application of nano-materials in various fields of science and technology has been widely studied due to their unique optical, electrical, catalytic and magnetic properties of these materials. These types of materials, possesses some interesting properties such as high specific area, subtle electronic characteristics, strong adsorptive ability and promote the electron-transfer reactions of electroactive molecules. The property of these materials is usually different from that of their bulk counterparts due to their extremely small size, special structure and large surface-to-bulk ratio. The increasing surface area to volume ratio provides to an increase in the dominance of the surface atoms of the nanoparticle over those in its inside structure (Abid et al., 2013).

In recent years, metal/metal oxide nanoparticles, carbon based nanomaterials, nano composites and hybride structures have been used for preparation of novel metarials. Initially, studies on nanoparticles have been focused on single nanoparticles because such particles have several better properties than the bulk materials. Later, the studies showed that heterogeneous, composite or hybride nano material particles have better efficiency than their corresponding single particles. Thus, nanomaterials have potential applications in electronics and photonics, catalysis, information storage, chemical sensing and imaging, environmental remediation, drug delivery and biological labelling (Guo et al., 2005).

The most of composite nanomaterials are based on the use of carbon materials. Among these nanoparticles, the carbon nanotubes (CNTs) have been the target of numerous investigations due to their unique properties (Iijima et al., 1991; Baughman et al., 2002). The conductivity of carbon nanotubes, as a consequence of their special electronic properties, is very important for the use of these nanomaterials in electrochemistry. CNTs have the ability to promote electron-transfer reactions on the electrode reactions. The first application of nanotubes in electrochemistry was a study where a paste of muliwall carbon nanotubes in bromoform. The obtaining paste was packed into a glass tube and used to study the oxidation of dopamine (Gooding, 2005).

Recent researches on carbon nanotubes have demonstrated that CNTs could serve as potential supports for heterogeneous catalysts and possess good electrocatalytic activities (Xu et al., 2008). Therefore, the CNT film-coated electrodes are presently attractive for many researchers (Sherigara et al., 2003). Because, carbon nanotubes are regarded entirely as metallic conductors, which in some respects makes them more suitable for electrochemical applications. The electrochemical properties of both multi walled (MWCNT) and single walled (SWCNT) carbon nanotubes have been examined and still gone on to be examine. These materials should serve as excellent candidates for nanoelectrodes and platforms for nanoelectrochemical cells and amperometric biosensor devices (Lyons and Keeley, 2008).

The other nanoparticles type used in nanoscience and nanotechnology is metal nanoparticles. Metal nanoparticles among the nanomaterials have played an important role in applications such as optics, electronics, magnetics, catalysis, and biology because of various unusual chemical and physical properties compared with those of metal atoms or bulk metal. It is well known that the optical, electronic, and catalytic properties of metal nanoparticles are mostly affected from their size, shape, composition, and crystal structure (Ghosh and Pal, 2007). Furthermore, the metal nanoparticles provide very fast kinetics and enhanced sorption capacity due to their high surface to volume ratio (Sarkar et al., 2012). On the other hand, both metal and metal oxide nanoparticles such as silver, gold, copper, palladium and platinum, iron and its oxides have found applications in catalytic reactions (Nair et al., 2007).

Nanoparticles can be classified as single or multiple materials into simple and composite or hybride nanoparticles, respectively. In general, simple nanoparticles are made of a single material, whereas, composite and hybride nanoparticles are composed of two or more materials. These mixture nanoparticles can consist of a wide range of different combinations in close interaction, including inorganic/inorganic, inorganic/organic, organic/inorganic, and organic/organic materials. In electrochemical studies, the typical composite and hybride nanoparticals are based on mixture of carbon and metal nanoparticles.

For this purpose, carbon pasta electrodes (CPEs) due to their ease of construction, renewability, and compatibility with various types of modifiers, have been widely used as a suitable matrix for preparation of modified electrodes (Arepalli et al., 2004).

In recent years, application of the CNT-modified CPEs showed considerable improvements in electrochemical behavior of materials (Ko et al., 2004; Iijima, 1991). The CNT modified cabon paste electrode has been applied for the voltammetric detection of several compounds. Furthermore, these developed electrodes have been modified with metal nanoparticles such as; gold, palladium, platium, copper and nickel, etc. On the other hand, metal nanoparticles (MNPs) provide three important functions for electroanalysis: the roughening of the conductive sensing interface, catalytic properties, and conductivity properties. MNPs have some special advantages such as higher mass transport, lower influence of the solution resistance, low detection limit, and better signal-to noise ratio over the conventional macroelectrodes (Parvin et al., 2012). Those properties are closely related to their size and shape.

However, because of the extremely high surface area to volume ratios and surface energies, the stabilization of metal nanoparticles is one of the primary challenges for their use as a catalyst electrode. To obtain better catalytic properties, the metal nanoparticles are stabilized by various substrate materials. Until now, many stabilization materials such as; polymers, ceramics, and grafite, garphene, carbon nanotubes etc. have been used for metal nanoparticle (Jiang, 2007). Among them, CNTs have excellent electronic properties, good chemical stability, and large surface area (Lee et al., 2007).

These unique properties make CNTs promising substrates for supporting metal nanoparticles. CNT-stabilized metal nanoparticles are important due to their potential electrochemical applications as using electrode material (Guo and Li, 2005) and catalysts (Xue et al., 2001). By combining, the two classes of nano-materials (CNTs and MNPs) novel hybrid materials can be synthesized and so the properties of the two counter components are successfully incorporated. In preparation of metal nanoparticles modified CNTs, the reduction of metal salts is commonly used to generate MNPs. The reduction process is carried out by physical, chemical and electrochemical reduction prosedures. The NPs are bounded to the CNTs through van der Waals or other weak interactions. Commonly used metals are Pt, Au, Pd, Ru, Ni, Sn, Bi, Sb, Cu, Ag and etc. These metals often are active as heterogeneous catalysts and their performance can be enhanced by use of CNTs as support materials. However, several researches on the catalyst electrodes have been employed by use of CNTs coated on glassy carbon and carbon pasta as the supporting material (Ardakani et al., 2010).

1.2 Carbon Nanotubes and Structures

Although carbon nanotube structures were characterized with transmission electrone microscopy (TEM) in 1991 by Ijima, the first report on the carbon based material called later CNTs came from Radushkevich and Lukyauovich in 1952. CNTs are one dimensional well-ordered, hollow graphitic nanostructure made of sp^2-hybridized carbon atoms. These long hollow cylindrical carbon molecules have revealed being remarkable nanostructures for several aspects from they discovered. Carbon nanotubes are composed of carbon, and they can be easily produced by several techniques. A carbon nanotube can bend easily but still is very robust. These nanotubes are concentric graphitic cylinders closed at either end due to the presence of five-membered rings (Iijima, 2002).

CNTs have two different structure as multi-walled carbon nanotubes (MWCNTs) and single-walled carbon nanotubes (SWCNTs) (Figure 1.1). MWCNT is composed of several concentric tubes of graphite sharing a common longitudinal axis whereas SWCNTs are composed of a single layer of graphene rolled into a tube. Generally, CNTs length can range from several hundred nanometers to several micrometers while diameters are 0.4-2 nm and 2-100 nm for SWCNTs and MWCNTs, respectively (Gooding, 2005). The CNTs has higher conductivity compare to graphite, therefore they can behave either like a metal or semiconducter.

The unique properties of CNTs such as superb strength, stiffness, chemical and thermal stability, electrical conductivity, high surface area of 1600 m^2 g^{-1} (SWCNTs), and the presence of a hollow core suitable for storing guest molecules, have revolutionized various fields such as electronics and medicine (Kim, 2007).

CNTs have been applied various energy storage devices (supercapacitors, fuel cells, and accumulators), transistors, photovoltaic devices, sensors and biosensors (Nenkova et al., 2010; Larsen et al., 2012; Li et al., 2013). Their final usage, however, may be limited by their potential toxicity and controlling their property changes in response to chemical treatment.
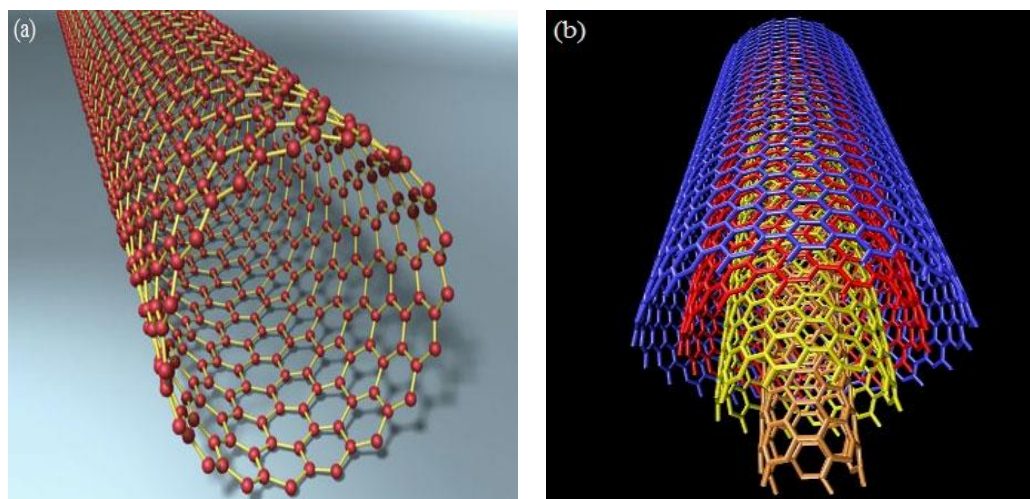
Figure 1.1 Structures of a) Single-walled carbon nanotube b) Multi-walled carbon nanotube

SWCNTs were discovered by Iijima and Ichihashi in 1993 and most of these nanostructures have a diameter close to 1 nm, with a tube length that may be many thousands of times larger and up to orders of centimeters (Zhu, 2002). The electrical conductivity of SWCNTs depends on their chirality and diameter while for MWCNTs such dependence is not observed. SWCNTs possess a cylindrical nanostructure. The carbon atoms are arranged in a single sheet called a graphene layer in a hexagonal repeating pattern (Figures 1.2). The sheet is rolled into a seamless, tube hence the name SWCNT. Therefore, SWCNTs are considered as molecular wire with every carbon atom on the surface.
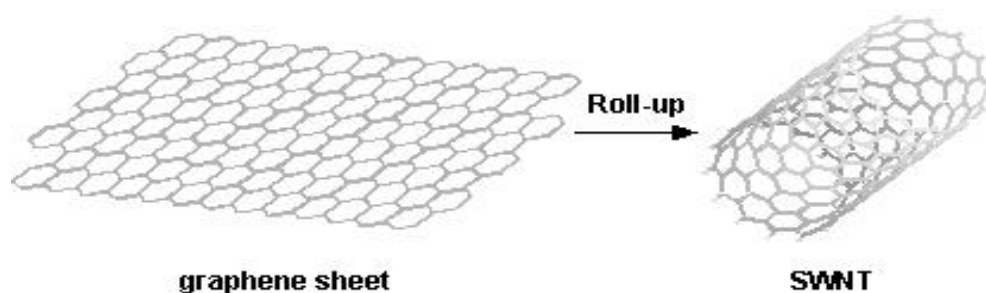
Figure 1.2 Roll-up of a graphene sheet to form SWCNT

A graphene sheet can be rolled more than one way, producing different types of CNTs and the three main types are armchair, zig-zag, and chiral (Figure 1.3).
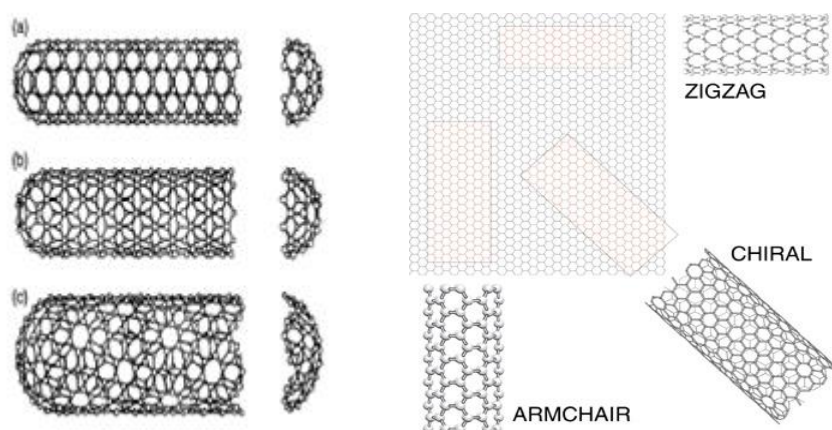
Figure 1.3 Main types of SWCNT a) Zigzag b) Armchair c) Chiral

Because of its structure, SWCNTs display excellent chemical stability, good mechanical strength and a range of electrical conductivity. They are at least ten times stronger than steel, around six times lighter and, depending on their chirality and diameter, can behave as metals, semiconductors or insulators. In a typical sample, around one third can be thought of as metallic. Due to their high surface energies, SWCNTs are usually found in bundles composed of tens to hundreds of tubes in parallel and in contact with each other. Thus, SWCNTs exhibit important electric properties that are not shown by MWCNTs. The most basic building block of these systems is the electric wire and these are excellent conductors.

SWCNTs were used in the development of the first intramolecular field-effect transistors (FETs) and intramolecular logic gate using SWCNT FETs (Derycke, 2001). To create a logic gate, a p-FET and an n-FET are required. Because SWCNTs are p-FETs when exposed to air and n-FETs when unexposed to oxygen, they were able to protect half of a SWCNT from oxygen exposure, while exposing the rest to oxygen. This results in a single SWCNT that acts as a NOT logic gate with both p- and n-type FETs within the same molecule. CNT can be metallic or semiconducting and offers amazing possibilities to create future nanoelectronics devices, circuits, and computers.

MWCNTs consist of multiple layers of graphite rolled on themselves to form a tube shape with an interlayer spacing of 3.4 Å. The outer diameter of MWCNTs may range from 1 to 50 nm while the inner diameter is usually of several nanometers. There are two models to describe the structures of MWCNTs;

1. The Russian Doll model where the sheets of graphite are arranged in concentric cylinders, e.g., a (0,8) SWCNT within a larger (0,10) SWCNT which the separation between tubes is about equal to that between the layers in natural graphite (Figure 1.1a)

2. The Parchment model where a single sheet of graphite is rolled in around itself, resembling a scroll of parchment or a rolled up newspaper.

CNTs are regarded entirely as metallic conductors, which in some respects makes them more suitable for electrochemical applications. However, SWCNTs are more well-defined systems, making their electrochemical properties easier to understand. Because of their electrical properties, the electrochemical properties of both multi walled (MWCNT) and single walled (SWCNT) carbon nanotubes have been examined and still gone on to be examine. These materials should serve as excellent candidates for nanoelectrodes and platforms for nanoelectrochemical cells and amperometric biosensor devices (Lyons and Keeley, 2008).

At present, there are several approaches to producing carbon nanotubes. Each procedure has its strengths and weaknesses. Techniques like electric carbon arc-discharge, laser ablation, and thermal or plasma-enhanced (PE) chemical vapor deposition (CVD) are employed to synthesize CNTs of sizeable quantities.

Laser ablation and arc discharge are modified physical vapor deposition (PVD) techniques and involve the condensation of hot gaseous carbon atoms generated from the evaporation of solid carbon (Louchev and Growth, 2002; Hester and Louchevet, 2002; Eres et al., 2004). Of these, the carbon arc discharge is a most convenient way to produce a variety of carbon materials because of high temperature of the arc-plasma (3700 $^{\circ}$C). In arc discharge, a vapor is created by an arc discharge between two carbon electrodes with or without a catalyst. Nanotubes self-assemble from the resulting carbon vapor. The types of carbon products are depend on the type and pressure of the gas surrounding gas the arc. The arc-evaporation method, which produces the best quality nanotubes, involves applying a current of about 50 amper (A) between two graphite electrodes in a helium atmosphere. This results in graphite evaporation, part of which condenses on the walls of the reactor vessel and part on the cathode. Deposit on the cathode usually contains the CNTs.The yield of MWCNT is 30-50 % in the electric arc discharge method using pure carbon. The remains of product are SWCNTs.

The yield requires careful control of the arc working parametres (Ebbesen, 1997). However, many researchers currently prefer to work with SWCNTs. To obtain SWCNTs, Co, Fe and Ni or some other metal having catalytic properties is added to the anode (Bethune et al., 1993). However, some researchers have also used the mixture of catalysts (Ni-Co, Co-Y, or Ni-Y) in the synthesis of SWCNTs.

In laser-ablation technique, intense laser pulses are used to ablate a carbon target. The pulsed laser-ablation of graphite rod in the presence of an inert gas and catalyst yields CNTs in the form of ropes or bundles of 5 to 20 nm diameter and tens to hundreds of micrometers long. Graphite rod is heated to 1000 ^{o}C or higher temperatures. Laser-ablation methods produce SWCNTs in high yields (more than 70 %). Laser ablation produces a small amount of clean nanotubes, whereas arc discharge methods generally produce large quantities of impure material. Both the laser ablation and arc discharge techniques produce powder-type nanotubes with impurities in the form of amorphous carbon and catalyst particles because of the high temperature of the heat source.

The CVD technique involves the reaction of a carbon-containing gas (such as methane, acetylene, ethylene, ethanol, etc.) with a metal catalyst particle (usually, cobalt, nickel, iron, or a combination of these such as cobalt/iron or cobalt/molybdenum) at temperatures in the range of 500-1000 ^{o}C. Carbon has a low solubility in these metals in this temperature range and thus, carbon precipitates to produce carbon nanotubes.

The CVD method is a better technique for high yield and low impurity production of CNT arrays at moderate temperatures (Yun et al., 2006; Kang et al., 2007; Denysenko et al., 2008; Vijayaraghavan et al., 2007). PECVD can grow individual, free-standing nanofibers with spatial controllability. On the other hand, high-density, aligned nanotubes can be mass produced using thermal CVD. The CVD method also provides good control over the size, shape, and alignment of the nanotubes. Recently, Kang (2007) have synthesized dense, perfectly aligned arrays of SWNTs and Vijayaraghavan (2007) have been able to horizontally align individual nanotubes on a large scale using dielectrophoretic force.

Nanotube materials for analytical applications should be clean, with low impurities from metal catalysts and amorphous carbon (Arepalli et al., 2004). Most CNT samples contain carbonaceous impurities such as amorphous carbon, fullerenes, nanoparticles, and especially transition metals introduced as catalysts during the synthesis of SWCNTs. These impurities change the properties of CNTs. Thus, the CNT products are purified to achive their good physico-chemical properties. The methods adopted include hydrothermal, gaseous, or catalytic oxidation, nitric acid reflux, peroxide reflux, cross-flow filtration and chromatography, and chemical functionalization. Although purification based on an initial selective oxidation to remove amorphous carbon followed by a reflux in concentrated nitric acid is effective in removing metal from the reaction products, the refluxing in nitric acid induces wall damage in the nanotubes. SWCNTs of more than 90% purity were produced using ultrasonically assisted microfiltration from amorphous and crystalline carbon impurities and metal particle. A suitable purification is possible using microwave heating in the presence of air followed by treatment with hydrochloric acid. Microwave assisted purification is also used for purification of MWCNTs (Luo et al., 2001). Synthesis of nanotubes with a uniform size and spatial density is critical before postprocessing or functionalization. The CNTs owing to following advantages: small size with large surface area, high sensitivity to target analyte, higher conductivity supply fast response time in analyte detection, and diminishing surface fouling effects have found wide application in the electrochemical sensing (Yanez-Sedeno et al., 2010).

Recently, many investigators have demonstrated that CNTs possess good electrocatalytic activities toward biomolecules such as dopamine and epinephrine (Luo et al., 2001) dihydronicotinamide adenine dinucleotide (NADH) (Musameh et al., 2002), uric acid (Pedano and Rivas, 2004; Wang et al., 2002), Cytochrome C (Wang et al., 2002), and ascorbic acid (Wang et al., 2002), quercetin and rutin (Lin et al., 2006), tryptophan (Shahrokhian and Fotouhi, 2007) and glucose. The CNT film-coated electrodes are presently attractive for many researchers (Sherigara et al., 2003).

Recent experiments have shown that carbon nanotube surfaces provide enhanced electron transfer rates when used as electrodes in electrochemical reactions. The role of MWCNT in the electrocatalysis of oxygen reduction has been demonstrated, and charge transfer on CNTs is seen to occur faster compared to graphite (Qu et al., 2004).

Dai and Shiu in 2004 have demonstrated that MWCNT-modified electrode could be employed as an amperometric oxygen sensitive electrode to construct a glucose biosensor offering good performance for glucose determination. However, many claims of enhanced electrocatalytic performance have been questioned by other researchers (Banks et al., 2005) on the basis that the electrocatalysis stems from the transition metal impurities introduced during the CNT synthesis step.

On the other hand, CPEs, due to their ease of construction, renewability, and compatibility with various types of modifiers, have been widely used as a suitable matrix for preparation of modified electrodes (Rubianes and Rivas, 2003). Further, they show rather low background current compared to the solid graphite or noble metal electrodes. In recent years, application of the CNT-modified CPEs showed considerable improvements in electrochemical behavior of materials (Valentini et al., 2003; Antiochia et al., 2004). The CNT-paste electrode is applied for the voltammetric detection of homocysteine and a 120 mV decrease in the anodic overpotential, along with greatly enhanced signal-to-noise characteristics is reported (Lawrence et al., 2004).Large number of electrochemical applications for CNTs can be found as modifier material and catalysts in analytical voltammetry. The preparation and the characterization of new type of CNT-based electrodes were accomplished by using four different orientations via chemical vapor deposition.

Multiple oriented MWCNTs were obtained via CVD onto silicon substrates. The chemical treatments improve the nanotube electrochemical reactivity by creating edge-like defects on their exposed sidewalls and nanostructured electrodes were treated with sulfuric acid. For sensing applications, sensitivity and detection limit, were investigated by CV. By using potassium ferricyanide and hydrogen peroxide solutions, CNTs with tilted tips show the best electrochemical behavior. CNTs with tilted tips become hydrophilic after the treatment showing a contact angle of $22°±2°$. The electrode has shown also the best electrochemical performance. Sensitivity and detection limit values are $110.0±0.5$ $\mu A/(mM\ cm^2)$ and 8 μM for potassium ferricyanide solutions and $16.4±0.1$ $\mu A/(mM\ cm^2)$ and 24 μM using hydrogen peroxide as target compound. Electrochemical responses at the electrode surface depend on the type of target. The introduction of wall defects influences more nanotube-potassium ferricyanide interaction rather than the interaction between MWCNTs and hydrogen peroxide (Taurino et al., 2011).

The preparation of a CNT film electrode by a novel fabrication method involving electrostatic spray deposition (ESD) was described (Kim et al., 2006). The CNT film electrode showed well-entangled and interconnected porous structures on the nanometer scale with good adherence to the substrate. The cyclic voltammograms of the CNT film electrode were mostly featureless in 1.0 M H_2SO_4 solution in the potential window of -0.2 to 0.8 V SCE, indicating typical electric double layer capacitive behavior. A specific capacitance of 108 F/g at a potential scan rate at 10.0 mV/s was achieved for the electrodes in 1.0 M H_2SO_4 and it decreased slightly to 103 F/g at a potential scan rate of 100 mV/s.

1.2.1 Metal nanoparticles and metal nanoparticles modified carbon nanotubes

Because of the problems on ethanol and methanol oxidation, most of the researchs in electroanalytical chemistry have been focused on the electrooxidation mechanism of alcohols and development of suitable catalysts. The use of metal nanoparticle catalysts in fuel cells is an area of research which is continually expanding. The unique properties of metal nanoparticle materials (e.g. enhanced mass transport, high surface area, improved performance) provide often be advantageous in electroanalytical techniques. Until now, metal nanoparticle based catalysts have been evaluated to be the most promising electrode materials.

Metal nanoparticles, defined as nanoparticles produced from metals, among the nanomaterials have played an important role in applications such as optics, electronics, magnetics, catalysis, and biology because of various unusual chemical and physical properties compared with those of metal atoms or bulk metal. In biomedical and catalyst applications the particles mostly include the noble metals, especially platinum, gold and silver. It is well known that the optical, electronic, and catalytic properties of metal nanoparticles are mostly affected from their size, shape, composition, and crystal structure (Ghosh and Pal, 2007).

Metal nanoparticles generally exhibit small sizes in a narrow size distribution, and well defined, regular shapes. Thus, metal nanoparticles of different forms may catalyze the reactions with different efficiencies due to nanocrystals of different shape and sizes. Furthermore, the nanoparticles provide very fast kinetics and enhanced sorption capacity due to their high surface to volume ratio (Sarkar et al., 2012).

Therefore, both metal and metal oxide nanoparticles such as silver, gold, copper, palladium and platinum, iron and its oxides have found applications in catalyzing reactions (Naır et al., 2007). Iron and its oxide nanoparticles are also used for environmental remediation (Zhang, 2003).

Metal oxide nanoparticles are used as sorbents for contaminants and preconcentration of trace metals (Türker et al., 2012). The use of metal nanoparticles in sensing researches may provide a revolution in healthcare, military and day-to-day life (Naır et al., 2007; Doria et al., 2012). For this aim noble metal nanoparticles like gold and silver are among the most extensively studied nanometals and have been used for the development of innumerous methods for molecular diagnostics, imaging, drug delivery and therapeutics (Doria et al., 2012; Chaudhuri and Paria, 2012). Also, metal oxide nanoparticles are finding increasing application in nanotechnologies that include environmental sensing (Abid et al., 2013).

The production of many semiconductors can be made of nanoparticles of heavy metal (Cd, Zn, etc), lantanides and their compounds (Doria et al., 2012). On the other hand, inorganic lanthanide based nanoparticles are applied in a range of biotechnologies (Abid et al., 2013).

The electrocatalytic activity of catalyst materials is depended on many factors. Particularly the supporting materials and their surface condition are most important for any catalyst to produce high catalytic activity (Qu et al., 2010). Carbon support materials like glassy carbon, active carbon, graphite carbon nanotubes and graphite carbon nanofibres are commonly used as a catalyst support. CNTs are most popular owing to a large specific surface area, chemical inertness, excellent electrical conductivity, thermal property and mechanical strength. Especially, glassy carbon and CNTs modified glassy carbon have been used to be the suitable materials as electrodes or electrocatalyst supports (Parra et al., 2008; Danaee et al., 2008).

Recently, many researches in the areas of catalysis had focused on the evaluation and preparation of metal nanoparticles as nanostructured materials on glassy carbon and CNTs modified glassy carbon for the catalytic electrooxidation of methanol and ethanol. The metallic nanoparticles (MNPs) modified electrodes like MNP modified MWCNT/GCE and bare electrodes have been used as the catalytic surface for electrocatalytic reduction of oxygen in alkaline media (Bakır, 2010).

Moreover, in general, MNPs have began to be more attractive and more interest over the past decade, compared to organic nanoparticles, owing to their relatively higher chemical activity and specificity of interaction (White et al., 2009).

The use of nanocomposite metal alloys has provided high catalytic efficiency for the nanostructured catalysts. But it is a great important task to prepare the catalysts into a specific structure that can efficiently perform catalysis. To date different preparation strategies to MNPs, such as physical (e.g. sonication, microwaves and UV), chemical (e.g. electrochemical, impregnation) and physicochemical routes (i.e. sonoelectrochemical) have been developed. Among these, chemical strategy including electrochemical and chemical reducing procedures is preferred because of their simplicities to quickly prepare nanoparticles modified electrodes. However, the electrochemical deposition procedure for synthesis of metal nanoparticles provides one of the approaches of producing uniformly and directly dispersed catalytic nanoparticles on electrode surface and supporting materials. Moreover, the advantage of electrodeposition procedure offer a high purity of the particles, more easily control the nanoparticles dimensions, lower particle size distribution compare to chemical and physical methods (Ulubay, 2008). The choice of reducing reagent in chemical reduction procedure is important to obtain metallic or alloy nanoparticles without contamination. The excess of reducing reagent and undesired side products must be removed easily. The most important drawback of chemical reducing procedure is to be time consuming and labour-intensive preparation.

1.2.1.1 Preparation methods of supported metal nanoparticles as catalyst

The metal nanoparticles have been prepared to modify the various electrode systems by different preparation methods. Such approaches can be classified at three main categories, depending on the methodology: chemical, physical and physicochemical methods (Ulubay, 2008). In this section, these, especially chemical methods, are explained in more detail.

Chemical methods: The classical chemical synthesis methods are impregnation, co-precipitation and deposition-precipitation. However, there are more new chemical methods including emulsions, photochemical reduction, chemical vapor impregnation, electrochemical reduction and chemical reduction. Here, these are briefly introduced:

Impregnation method commonly referred to as wetness impregnation is carried out in succesive four steps like mixing (wetting) the supporting material with metal salt (e.g. metal nitrate, chloride) as a solution for a suitable duration, removing the solvent from the mixture of support and metal salt, drying (calcining) the solid mixture and finanly reducing the metal ions impregnated on the solid support by a reducing agents. The supported metal nanoparticle catalysts prepared by impregnation methods have been highly active for oxidation of CO and alcohol (Luque et al., 2008).

Coprecipitation involves the simultaneous precipitation of the metal precursor and the supporting material which is mostly inorganic oxide. The method can not control the pore size and shape of metal nanoparticles. Furthermore, this approach has limited applicability to many supports.

Deposition–precipitation includes the complete precipitation of the metal hydroxide of the metal precursor from the solution adjusted to a suitable pH, for its deposition on the support material. The resulting solid supported metal hydroxide is then calcined to reduce nanoparticles to elemental metal.

Microemulsions are defined as clear, thermodynamically stable and isotropic homogeneous-like mixtures of water with oil and/or surfactants. In general, a solid support is impregnated with a microemulsion containing a dissolved metal salt as a precursor in a similar approach to the conventional chemical impregnation. The metal nanopatricles perpared by microemulsion approcah have been found to have a more uniform and controllable size and pore distribution compared to the previous chemical methods given above. The catalysts have been used for hydrogenation and oxidation reactions. With this method, Pd, Rh and Pd–Rh MNPs with sizes ranging from 2 to 10 nm have been homogeneously deposited on the surface of MWCNT.

Photochemical reduction approach is based on the photochemical reduction of metal precursors to prepare the supported metal nanoparticle catalysts. This procedure minimises the use of chemicals and solvents, so it is more eco friendly than most of the reported approcahes. The formation of well-dispersed Ag, Au and Pd nanoparticles on the graphene support has been provided under UV radiation.

Chemical vapor deposition (CVD) is carried out in gas-phase. The method generates well-dispersed metal nanoparticle catalyts in controllable and reproducible size distribution. The MNPs prepared with this method have a relatively narrow particle size distribution (2-8 nm). It includes the vaporisation (sublimation in real) of metal precursors and growth of the metal nanoparticles under high vacuum in the presence of an excess of stabilizing organic solvents (e.g. aromatic hydrocarbons, alkenes, THF) and/or reducing agent (e.g. H_2 and CO).

Electrochemical reduction has been widely used for the electrochemical deposition of metal nanoparticles on mainly for carbonaceous supports. The literature survey shows that the method is limited noble metals such as Pd, Pt, Au and Ag. Size and distiribution of metals are controlled by variying the electrodeposition potential, support material and deposition time. Especially, it is well-known that the catalysyts prepared on the carbon nanotube with this approach is effective for alcohol oxdation.

Chemical reduction of metal precursors using the suitable reducing reagents (e.g. hydrazine and $NaBH_4$) in presence of support material is another alternative electrochemical reduction method. The generated nanoparticles mix with the support material particles. The excess of reducing reagent is used to ensure the complete reduction of metal precursors but it needs to be removed the resideu reagent, prior to the use of the catalysts.

Physical Methods: Physical methods use sonication, microwaves, UV, laser, plasma and supercritical fluids, in the preparation of supported metal nanoparticles.

Sonoelectrochemistry used in various fields is succesively employed to prepare the nanoparticle catalysts.The method can be explained as a combination of ultrasonic waveleght with electrode processes forming at surface of electrodes immersed in electrochemical cell. Ultrasound (US) remarkably enhances mass transport, reducing the diffusion layer thickness and also affect the surface morphology of the treated materials; typically enhancing the surface contact area.

Microwave irradiation is known to be a very effective technology used to initiate chemical reaction and for synthesis of organic compounds. Therefore, in the case of preparation of metal nanoparticle catalyts the microwave has several advantages such as shorter reaction time, smaller size (i.e. 1-5 nm) of the metal nanoparticle with narrow size distribution than those of the others.

These approaches typically employ metal salts in solutions as the precursor metal source.

Laser ablation (PLA) is used to vaporise a metal or mixture of metals, and typically employs a pulsed laser (e.g. Nd-YAG) controlled deposition of the metals on a given support. The laser assisted approach offers a number of other advantages for the preparation of supported metal nanometal particles such as use of no solvent, easy to automate, operation under the controlled conditions to obtain the uniform particle size and distribution, etc.

Supercritical fluids (SCF) as another efficient and potentially eco friend approach to the preparation of a wide range of supported metal nanoparticles has been employed. The most common procedure involves the dissolution of a metallic precursor in a supercritical fluid (e.g. supercritical carbon dioxide, $scCO_2$) and subsequent incorporation on a substrate/support under various conditions. The impregnated metallic precursor can be reduced to its elemental form by different reducing techniques. This approach was applied to the preparation of ruthenium and rhodium MNPs supported on MWCNTs.

Physicochemical methods: The most commonly employed physicochemical methods have been sonoelectrochemistry and flame spray pyrolysis.

Sonoelectrochemistry technique uses a combination of US waves and electrochemistry. So it can be explained as a combination of ultrasonic waves with electrode processes forming at surface of electrode immersed into the elecctrochemical cell. The process is carried out the electrode-electrolyte interface under the ultrasonic radiation.

Flame spray pyrolysis is applied as another alternative method of preparation for the catayltic electrode. The metal precursor solution was fed in the center of a methane-oxygen flame by a syringe pump and dispersed by oxygen, forming a fine spray. The spray flame was surrounded and ignited by a small flame ring issuing from an annular gap (0.15 mm spacing, at a radius of 6 mm).

The formed metal nanoparticles were then collected on a glass fibre fitler (Whatmann GF/D, 25.7 cm in diameter) by means of a vacuum pump. The technique provides highly stable supported metal nanoparticles with small particle size (<5 nm for palladium) for various applications.

1.2.2 Electrochemical properties of ethanol and methanol

The investigation of ethanol and methanol electrochemical behaviours in presence of new catalysts systems is important to obtain high efficiency in fuel cell. Among the fuels used in fuel cells, alcohols have an important place. Because, they are liquids to easy storage and their mass energy density is rather high, almost close to that of gasoline (Vigier et al., 2006).

Methanol and ethanol are mostly used as a fuel. In the case of methanol, the methanol is converted to carbon dioxide and hydrogen at the anode. Then, the hydrogen ions act with oxygen to form the water. Each fuel has particular advantages and disadvantages (Wongyao et al., 2011). Methanol is more efficiently oxidized than other alcohols. The disadvantage of methanol as a fuel is methanol crossover through Nafion™ membrane to the oxygen electrode, and anode poisoning by strongly adsorbed intermediates (mainly CO). The fuel cell efficiency is decreased by the methanol crossover. Moreover, methanol is relatively toxic for human beings, and especially for optical nevre, easily volatile and inflammable. Therefore, ethanol is used as an alternative fuel since it can be produced from agricultural raw materials, which helps diminish global concentrations of greenhouse gases. Furthermore, ethanol has a lower crossover rate and affects cathode performance less severely than methanol. It has non-toxicity and higher power density.

The methanol or ethanol as fuel were oxidized on the anode in the anodic compartment of direct methanol fuel cell (DMFC) and direct ethanol fuel cell (DEFC), respectively. At the anode, alcohol molecules combine with water to give up electrons, forming hydrogen ions. In the case of methanol, the methanol is converted to carbon dioxide and hydrogen at the anode. The hydrogen ions then go on to react with oxygen. These reactions for methanol at the electrodes are shown as follows:

Anode Reaction: $CH_3OH + H_2O \rightarrow CO_2 + 6\ H^+ + 6e^-$

Cathode Reaction: $3/2\ O_2 + 6H^+ + 6e^- \rightarrow 3\ H_2O$

Cell Reaction: $CH_3OH + 3/2\ O_2 \rightarrow CO_2 + 2\ H_2O$
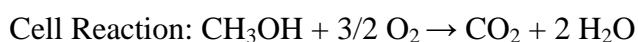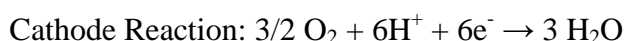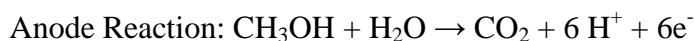
For example, ethanol or methanol is oxidized at the anode with the potential to release twelve electrons or six electrons, respectively. For all twelve electrons to be released in case of ethanol, the carbon-carbon (C-C) bond must be broken so that ethanol is oxidized completely. However the breaking of the C-C bond is not easy and usually the reaction proceeds slowly. The breaking is also not complete. Thus the anodic process is carried out mostly using a catalyst. An effective catalyst for ethanol oxidation is one that can break the C-C bond, freeing all twelve electrons and leading to the formation of CO_2. Ideally, the catalyst should be effective even at room conditions.

On the other hand, the catalyst is not required for methanol as a fuel because methanol has good kinetics of oxidation compared to other alcohols at low temperatures. It oxidizes completely to CO_2, meaning the maximum transfer of electrons is occurring (Rao et al., 2007). However it has very low oxidation rate. The problem of the slow methanol oxidation rate has been solved to some extent by alloying Pt with other elements such as Ru, Sn, Mo etc. (Lee, 2010). However, the CO poisoning of the anode catalysts is one of the most important drawbacks for the application of direct methanol fuel cell (DMFC) and direct ethanol fuel cell (DEFC) (Hall et al., 2004).Besides, both methanol and ethanol as a fuel have drawbacks because of their poor electrochemical activity on the cathode reaction. The complete electrooxidation of alcohol to CO_2 involving carbon-carbon bond rupture is not carried out by insufficient catalyst performance of present electrode systems. This limitation reduces the cell voltage of them, almost 0.4 V.

Thus, in the electrochemical oxidation of liquid fuels like methanol and ethanol, the electrode material is a crucial factor to obtain power densities from the fuel cells. It is required to prepare catalyst materials with high activity and develop new catalyst preparation method for the electrooxidation of methanol and ethanol. More studies are needed, however, to further enhance the electrocatalytic activity, stability and CO tolerance of these catalysts.

Due to these requirements explained above, until now, most of the research in both methanol and ethanol oxidations have been focused on the electrooxidation mechanism of alcohols and development of suitable catalysts.

Application and integration of CNTs and metal-NPs to voltammetric electrode systems are referred to investigation of electrochemical behaviour of ethanol and methanol using different modified electrode systems. Bimetallic Pt-Fe supported MWCNTs were synthesized for methanol electrooxidation. The catalyst was prepared by a spray-cooling process. The higher electrocatalytic activity was observed with Pt-Fe/MWNTs electrode for methanol oxidation. The results imply that the Pt-Fe/MWNTs composite has good potential applications in fuel cells (Xu et al., 2006).

The methanol electrooxidation reaction was studied on carbon dispersed Pd-nickel oxide nanocatalysts in KOH/CH_3OH solutions. X-Ray diffraction (XRD) and X-Ray photoelectron spectroscopy (XPS) were used to characterize PdNiO/C catalysts. The electrochemical behaviors for the methanol electrooxidation reaction were measured in a powder microelectrode by cyclic voltammetry and Tafel plots. The result showed that the adding NiO enhances the anti-poison ability of PdNiO/C catalyst, but the reaction mechanism didnt change. The anti-poison ability of PdNiO/C catalyst can be enhanced by three ways: (1) the NiOOH on the surface of catalyst improves the activity of composite catalyst for methanol oxidation; (2) the catalytic role of NiO for methanol dehydration; (3) the promotion of large amount active species-PdO (low oxidation state) for methanol oxidation (Wang et al., 2009).

Babaei et al, were used Pd-impregnated Ni-GDC anode electrode for the oxidation reaction of methane, methanol and ethanol fuels was investigated at open circuit potential and under dc bias.

The results showed that the presence of Pd nanoparticle catalyst significantly promotes the electrocatalytic activity of Ni/GDC for the electrooxidation reaction in methane and in particularly in methanol and ethanol fuels. Alcohol fuels like methanol and ethanol, the results indicate that carbon deposition on the surface of the anode is relatively lower as compared to that on pure Ni/GDC. A comparison between molecular structures of methane, methanol and ethanol and the probable dissociation routes for these three hydrocarbons suggest that existence of hydroxide groups in the molecular structure of alcohols may facilitate partial carbon removal from the electrode surface (Babaei et al., 2012).

Long and co-workers were presented the poly (vinylpyrrolidone) (PVP) protected shape-controlled synthesis of Pt-Pd core-shell nanoparticles modified with AgNO$_3$. The Pt-Pd alloy and core-shell nanoparticles were characterized by TEM, high-resolution TEM, and electrochemical measurements. The catalytic comparisons of electrocatalytic properties of alloy, cluster, and core-shell bimetallic nanoparticles were done to confirm the best nanostructures for high catalytic activity. The best catalytic performance was observed with Pt-Pd core-shell nanoparticles in developing novel and efficient electrocatalysts in DMFCs (Long et al., 2011).

Kumar et al. have been used microwave induced reactions for immobilizing platinum and palladium (Pd) nanoparticles on MWCNTs to investigate oxidation of methanol, ethanol and formic acid in acidic media. The electrodes are formed by simply mixing the hybrids with graphite paste, thus using a relatively small quantity of the precious metal. The Tafel slopes confirmed that Pd composite in alkaline medium and platinum composite in acid medium were suitable electro-catalysts for methanol oxidation. The activation energy values were low for ethanol oxidation with Pd nanohybrids which was an advantage due to the low cost of former compared to Pt and ethanol is easily available from bio mass (Kumar et al., 2012).

Hu and Chen have reported the useage of Pd based catalyst with end-opened carbon nanotube arrays (CNTA) to improve the electrode performance for alcohol oxidation in alkaline media. As a result that the Pd based end-opened CNTA electrode performed significantly better than the unprocessed Pd based CNTA electrode.

The femtosecond laser cutting technique can be very useful in fabricating 3D CNTA structures/devices with controllable dimensions and may yield unique advantages in terms of maximizing the potentials of CNTAs for application in energy conversion and energy storage (Hu and Chen, 2011).

Azizia et al. have prepared mesoporous SBA-15 nanoparticles with the use of Stem Sweep Ash (SSA) as silica source in the presence of co-templates as structure-directing agents using sol-gel and hydrothermal methods. To investigate electrooxidation of methanol, the new material siliceous (SBA-15)-modified carbon paste electrode based on mesoporous nickel modified SBA-15 were used. The synthesized mesoporous SBA-15 nanoparticles were characterized by the XRD, SEM, TEM, TGA and BET. Mesoporous silica (SBA-15) can be modified with Ni(II) ions (Ni/SBA) by dispersion in a 0.1 M nickel chloride solution. The results showed that Ni/SBACPE could enhance the oxidation of methanol by a catalytic process through a decrease in overpotential of methanol oxidation with compare to Ni/CPE and overcome the low kinetic of reaction in alkaline solution and the rate constant for the catalytic reaction (k) of methanol is obtained (Azizia et al., 2013).

Yan et al. have used highly mesoporous hollow carbon hemispheres (HCHs). The electrodes were prepared using glucose as carbon source and solid core mesoporous shell silica (SCMSS) as template. The HCHs has presented an ultrahigh surface area of 1095.59 m^2 g^{-1} and an average mesopore size of 9.38 nm.The results show that the structure improve the mass transfer and also more concentrated ethanol solution can be used to increase the energy density. The current densities of ethanol oxidation on Pd nanoparticles supported on HCH (Pd/HCH) electrocatalyst are 3 times as many as on Pd/C at the same Pd loadings (Yan et al., 2010).

Raoof has prepared novel poly (m-toluidine) Triton X-100 film (Raoof et al., 2011). The film was prepared by electropolymerization of MT at the surface of carbon nanotube paste electrode (CNTPE), in the presence of TX-100. The performance of the electrode was investigated as a novel matrix for dispersion of platinum particles. Electrochemical response of the poly (m-toluidine) film prepared in the presence of TX-100 (PMT/TX-100) is, at least, 20 times higher than that obtained in the absence of the surfactant. The as-prepared substrate is used as porous matrix for dispersion of platinum particles by potentiodynamic method.

The electrochemical methanol oxidation reaction (MOR) was studied at the surface of this modified electrode and this electrode was improved the electrochemical signal. The results showed that the PMT/TX-100 at the surface of CNTPE improves the catalytic efficiency of the deposited platinum particles toward MOR.

Zhang et al. were synthesized Ni-Pd core/shell nanoparticles supported on MWCNTs (Ni-Pd/MWCNTs) by impregnation-reduction and replacement method and also used as electrocatalyst for alcohol oxidation in alkaline media for fuel cells. The Ni-Pd/MWCNTs has uniform dispersion of Ni-Pd nanoparticles with the average particle size of 3.4 nm indicating less thickness of Pd shell. For ethanol oxidation, the Ni-Pd/MWCNTs showed 2.3 times peak current density as high as that on Pd/MWCNTs electrocatalyst at the same Pd loadings. The electrochemical results demonstrated that the electrocatalytic activity and stability of the Ni-Pd/MWCNTs composites for alcohol oxidation are significantly enhanced (Zhang et al., 2012).

Tayal et al. have preapared bi-metallic and tri-metallic Pt, Ir, Sn electro-catalysts by impregnation reduction method on carbon Vulcan XC-72 to improve upon electrooxidation of ethanol in direct ethanol fuel cell. Their electrocatalytic activities were characterized by CV, linear sweep voltammetry (LSV) and chronoamperometry (CA) techniques. The single direct ethanol fuel cell (DEFC) test at 90 ^{o}C, 1 bar with catalyst loading of 1.0 mg cm^{-2} and 2.0 M ethanol as anode feed showed an enhancement of catalytic activity with Pt-Ir-Sn/C (20 % Pt, 5 % Ir and 15 % Sn by wt) system (Tayal et al., 2011).

Chen et al. have used SWNTs, MWNTs and Vulcan XC-72 carbon (XC-72) as supporting carbon materials to prepare Pt/XC-72, Pt/SWNTs and Pt/MWNTs catalysts in tetrahydrofuran/water/ethanol mixture solution. Among them, the Pt/SWNTs catalyst exhibited the highest current density, the lowest onset oxidation potential and the best stability for methanol electro-oxidation. It was indicated that SWNTs are an ideal anode catalyst supporting material for the practical application of direct methanol fuel cells (Chen et al., 2010).

The synthesis and characterization of a new Pd-electrocatalyst supported on MWCNTs were described along with its use to manufacture anodes for the oxidation of methanol, ethanol or glycerol in either passive or active DAFCs equipped with an anion-exchange membrane. Electrodes coated with Pd/MWCNT were investigated in detail for the oxidation of methanol, ethanol or glycerol in 2.0 M KOH solution in half cells. The catalyst is very active for the oxidation of all alcohols with glycerol providing the best performance in terms of specific current density and ethanol showing the lowest onset potential. Pd/MWCNT exhibits unrivalled activity as anode electrocatalyst for alcohol oxidation. The analysis of the anode exhausts that ethanol is selectively oxidized to acetic acid, detected as acetate ion in the alkaline media of the reaction, while methanol yields carbonate and formate. A comparison with a DMFC containing a Pt-Ru/MWCNT anode catalyst has completely confirmed the superior performance of Pd/MWCNT in alkaline media (Bambagioni et al., 2009).

The Au-modified Pd catalysts with the alloy, coreshell and physically-mixed structures with carbon nanotubes as the support were prepared. Their catalytic activities for oxygen reduction and ethanol oxidation have been examined by electrochemical measurements. The researchers have indicated that the Au-modified Pd catalyst by comparison with the mono-Pd catalyst exhibits increased catalytic activity for oxygen reduction, but decreased catalytic activity for ethanol oxidation in alkaline media (Xu et al., 2010).

Jiang et al have investigated effect of preparation procedure on the performance of PtSn/C anode electrocatalyst for direct ethanol fuel cells. For this purpose, carbon-supported platinum-tin (PtSn/C) electrocatalysts has been prepared by reducing platinum and tin salts with various reducing agents (such as ethylene glycol (EG, HCHO, and $NaBH_4$) in H_2O or EG. Of the three catalysts PtSn/C (EG) has the smallest mean particle size (about 1.8 nm) in a narrow size distribution. Tin is found in multi-valence states in this catalyst. Cyclic voltammetry and single cell performance tests have shown that PtSn/C(EG) has the highest activity for ethanol electro-oxidation, which is attributed to the small metal particles and the oxygen-containing species supplied by the tin oxide at a lower potential (Jiang et al., 2006).

Lin and co-workers have studied the influence of the effect of Sn content in Pt-SnO$_2$/CNTs for methanol electrooxidation. For this, they prepared Pt-SnO$_2$/CNTs with atom ratio at) Pt/Sn = 1.5, 2, 3 and 4. The addition of tin oxide has decreased the conductivity of the electrode, but the electrochemical activity has been improved by the addition of Sn. After electrochemical analysis in sulfuric acid, it was proved that the electrochemical performance for methanol oxidation and endurance against adsorptive intermediates were impressive while Pt/Sn=2.0 in atom ratio. The study indicated that electrochemical activity of Pt–SnO$_2$/CNTs show positive correlation with Sn content (Lin et al., 2012).

Ha and co-workers have investigated to increase the durability enhancement of low-temperature fuel cells by platinum-catalyzed carbon nanotubes. For this purpose, Pt-catalyzed carbon nanotubes (CNT(Pt)) were synthesized using Pt nanoparticles supported on Vulcan XC-72 (Pt/C) and methane by chemical vapor deposition (CVD) for oxygen reduction reaction (ORR) catalysts in LTFCs. The results suggest that the durability of Pt nanoparticle catalysts can be improved by locating Pt nanoparticles inside of one-dimensional CNTs and by making the Pt nanoparticles subsequently released from the CNT tips as smaller particles during usage of the catalysts (Ha and Han, 2013).

Yang has suggested a simple and cost effective method to prepare an excellent catalyst for fuel cell. So, PtRu/POB-MWCNTs, in which the MWCNTs were first wrapped by POB molecules, and then PtRu nanoparticles were uniformly deposited on the surface POB-MWCNTs. Cyclic voltammetry and electrochemical endurance experiments indicate that PtRu/POB-MWCNT catalyst has a higher EAS from CO stripping voltammograms and better electrocatalytic activity and stability for ethanol electro-oxidation in acid solution than those PtRu nanoparticles on acid-treated MWCNTs and carbon black. These results have shown that PtRu/POB-MWCNTs would be an excellent candidate for catalysts in fuel cells (Yang et al., 2012).

Zhu et al. have investigated to use BCNTs as the support material of high loaded Pt nanoparticles for improving the efficiency of ethanol/methanol fuel cell. For this, synthesis of BCNTs through CVD using an acetonitrile nitrogenous gas was carried out and then deposited Pt nanoparticles onto the BCNTs surface by aqueous phase reduction.

Cyclic voltammogram indicated that the Pt-BCNTs catalyst displayed excellent electrocatalytic activity and long-term stability toward ethanol oxidation. The excellent performance may be attributed to the high dispersion of nanoscale Pt catalysts and the unique nature of BCNTs. The results imply that doping N atom introduces some defective sites and active sites onto the surface of CNTs. The paper explored that BCNTs are promising support material for Pt-nanoparticles catalyst and can be used to enhance the efficiency of fuel cell. Also, it was shown that the technique is suitable for production beyond the laboratory-scale (Zhu et al., 2010).

1.3 Modified Carbon-Paste and Carbon-Paste Film Electrodes for Determination of Some Metals in Electrochemistry

Lead and cadmium at trace level are widely present in the environmental samples such as waters, soils, sediment, plant samples, etc. as a result of anthropogenic processes (Martinez and Blasco, 2012). Lead is widely used in industry, mainly in the manufacturing of pigments, coatings, containers, ointments, electric batteries and even liquor. Cadmium is an important metal which is largerly used in production of various materials such as various alloys, nickel-cadmium batteries, dyes and pigments, plastic stabilizers and metal plating (Jha et al., 2012). Also, the the content of cadmium in soils, sediments and waters is increased by agricultural activities such as the excessive use of fertilisers and pesticides, irrigation with waste water.

On the other hand, lead and cadmium are considered to be some of the most toxic elements in the world. Therefore, lead and cadmium have been long known as the most important environmental contaminants. These elements are toxic metallic elements for both humans and animals when absorbed in the body. Accumulation of lead and cadmium in the body of both humans and animals can cause poisoning, cancer and brain damage, amongst others. Cadmium can accumulate in kidney, liver and lung. So, it could affect kidney function and bone metabolism, even at exposure levels found in the general population. Accumulation of cadmium at high level can cause a wide variety of acute and chronic effects on human health (Zhou et al., 2013). Lead is highly toxic to nervous, immune and gastrointestinal systems of both humans and animals (Jang et al., 2005). If lead poisoning is left untreated, it may damage kidneys, the nervous system, and the brain. Lead is also an important risk factor for hypertension in women (Houston and Johnson, 1999).

The maximum acceptable levels of cadmium and lead in drinking water were allowed by United States Environmental protection Agency (EPA) are 5 and 15 µg L^{-1}, respectively (US EPA, 2009). Because of the above reasons, monitoring the heavy metal ions of lead and cadmium at trace levels in various samples such as natural water, drinking water, soil and plant, etc. are essential and indeed a requisite for human health and safety.

Several analytical techniques have been employed for the determination of lead and cadmium, inlcuding spectrophotometry, inductively coupled plasma mass spectrometry (ICP-MS), inductively coupled plasma optical emission spectrometry (ICP-OES), atomic absorption spectrometry (AAS), atomic fluorescence spectrometry (AFS) and neutron activation analysis (NAA) (Jha et al., 2012). However, most of these techniques require some time consuming manipulation steps, sophisticated instruments and special trainings. For these reasons, electroanalytical techniques, combining high precision, selectivity, sensitivity and accuracy by low-cost instrumentation, are mostly employed for the determination of heavy metals like cadmium and lead.

The most fequently used electroanalytical techniques are anodic stripping voltammetry (ASV) in differential pulse, linear sweep modes and potentiometric stripping analysis (Senthilkumar and Saraswathi, 2009; Li et al., 2009). Conventional working electrodes for voltammetric determination were widely based on a hanging drop mercury electrode. Unfortunately, the toxicity of mercury limits its use. Thus it is very important task to develop a better sensitive, more selective and non-toxic electrode for the simultanously determination of heavy metals by stripping techniques. Thus, the various modified composite and hybride electrodes have been developed.

The modified electrodes are generally prepared by combining CNTs and MNPs including different intrinsic properties. On the other hand, the carbon paste and glassy carbon are the most popular supporting electrode materials for the laboratory preparation of various modified catalyst electrodes in electrochemistry studies (Ardakani et al., 2010). As a result, in the literature, several studies based on use of various single and multible noble and non-noble metals as modifier for GCEs and CPEs could be found for voltammeric heavy metal determinations. Recent literatures relevant studies are shortly explained below.

Wonsawat et al. have aimed to develop an environment friendly electrode for determining Cd^{2+} and Pb^{2+} levels by using an automated flow system. CV and square wave anodic stripping voltammetry (SWASV) coupled with sequential injection analysis (SIA) were applied to examine the electrochemical performance of the electrode.

The bismuth-modified graphene-carbon paste electrode (Bi-GCPE) has exhibited excellent electrooxidation of Cd(II) and Pb(II) with a significantly higher peak current for both metal ions compared with the unmodified CPE. The limits of detection have been found to be 0.07 and 0.04 mg L^{-1} for Cd(II) and Pb(II), respectively.The Bi-GCPE has been also applied to determine Cd(II) and Pb(II) in low-(tap water) and high-(sea bass fish and undulated surf clam tissues) matrix complexity samples by automate flow system. It has been found that the recoveries were acceptable and ranged from 70.4 % to 120 % for Cd(II) and 65.8 % to 113.5 % for Pb(II) (Wonsawat et al., 2012).

Mhammedi et al. have aimed to evaluate the analytical performance of hydroxyapatite $Ca_{10}(PO_4)_6(OH)_2$(Hap) screen-printed sensors designed for the detection of metals. In this work, it has been shown that the HAp-modified carbon-paste electrode (HAp-CPE) for the electrochemical determination of lead is suitable by using cyclic and square-wave voltammetry in the potential range between -0.3 and -0.8 V. Perchlorate acid solution (1.0 mol L^{-1}) has been used as the supporting electrolyte. The voltammetric measurements have been carried out using as working electrode HAp-CPE, and a platinum electrode and an SCE electrode as auxiliary and reference electrodes, respectively. Under the optimized working conditions, calibration graph is linear for 5 min of preconcentration time with the detection limit 7.68×10^{-10} mol L^{-1}. The results have been indicated that this electrode is sensitive and effective for the determination of Pb(II) (Mhammedi et al., 2009).

Sánchez et al. have prepared chemically modified CPE for Pb(II) determination in aqueous media by AdSV. For this purpose, they have examined the effect of the mesostructural order of four types of hybrid mesoporous silicas, referred to as MPS1-MPS4, functionalized with 5-mercapto-1-methyltetrazole (MTTZ). The effect of the mesostructure of the MPS on the analytical performance of the sensors has been evaluated with respect to linear ranges, sensitivities, selectivities, precision and limits of detection.

They have found that the CPE modified with MPS1 exhibited the best inter-electrode reproducibility and sensitivity, a linear range between 1and 30 ppb and a limit of detection of 0.8 ppb. But the CPE modified with MPS4 exhibited the poorest interelectrode reproducibility and sensitivity, a linear range between 5.0 and 100.0 ppb, and a limit of detection of 2.6 ppb. As consequence of its highest inter-electrode reproducibility and sensitivity, good linear range and low LOD, MPS1 have been found as the better MPS material to prepare MCPE for Pb(II) determination in aqueous media by AdSV (Sánchez et al., 2013).

Gomez has investigated CPEs modified at various kaolinite or TPP-kaolinite to graphite ratios for the detection of lead, by differential pulse voltammetry. Kaolinite clay has been modified with tripolyphosphate (TPP) by impregnation method. The results have indicated that TPP in kaolinite clay has an important role in the accumulation process of Pb(II) on the modified electrode surface and the determination of lead using a CPE modified with TPP-kaolinite was improved when compared to unmodified CPE and modified kaolinite/CPE. The range for quantitative detection was 3×10^{-7} mol L^{-1} to 2×10^{-5} mol L^{-1} with a preconcentration time of 7 min. Pb^{2+} analysis has been carried out succesfully in the presence of Cu(II), Cd(II) and Ag(I) ions (Gomez et al., 2011).

Shams have developed a new CPE modified with zirconium-phosphate chemically grafted onto the silica gel surface (SiZrPH) for determination of nanomolar concentrations of cadmium by differential pulse anodic-stripping voltammetry. Due to the low solubility of the SiZrPH in aqueous solutions, a single electrode surface has been used for multiple analytical determinations over several weeks. The electrode has demonstrated linear response over a wide range of Cd(II) concentration (3-1400 ng mL^{-1}) with an accumulation time of 120 s. It has been found that the electrode system was free from most interference. The prepared electrode has been applied for determination of Cd(II) in some artificial synthetic samples (Shams and Torabi, 2006).

Cao and co-workers have investigated the operational parameters affecting the analytical performances of the bismuth-modified zeolite doped CPE (BiF-ZDCPE) for trace Cd(II) and Pb(II) analysis by differential pulse stripping voltammetry. It has been foun that the in situ plated (zeolite/graphite powder/silicone, 10/190/80 w/w/w) BiF-ZDCPEs exhibited the most sensitive response to Cd(II) and Pb(II) in 0.10 mol L^{-1} acetate buffer (pH 4.5). The detection limits of the modified electrode have been calculated to be 0.08 µg L^{-1} for Cd(II) and 0.10 µg L^{-1} for Pb(II) based on three times the standard deviation of the baseline with a preconcentration time of 120 s under optimal conditions, respectively.The electrode as-prepared has been applied to determine Cd(II) and Pb(II) ions at trace level in tap-water and sewage water samples, and the results were compared with those of atomic absorption spectroscopy (AAS) (Cao et al., 2008).

The carbon paste electrodes modified with 1-furoylthioureas for the analysis of cadmium by dp ASV. Two series of 1-furoylthioureas (FTHD) have been tried as modifiers of carbon paste electrodes. The experimental data have provided that some of the FTHD-modified CPEs have high sensitivity, adequate selectivity and reproducibility, and a wide operative linear range of concentrations, for the determination of Cd(II) in water samples. The system has been used for spiked superficial water (collected from San Pedro River, Puerto Real, C´adiz, Spain) and spiked drinking water samples. The results have been compared with the results obtained the real samples was tested by ICP-AES (inductively coupled plasma-atomic emission spectrometry) (Estevez-Hernandez et al., 2007).

A 1,4-bis(prop-2-enyloxy)-9,10-anthraquinone (AQ) modified carbon paste electrode has been developed to determine Pb(II) by DPASV. The method is based on non-electrolytic preconcentration via complex formation with modifier, followed by an accumulation period with a negative potential (-1.5 V). The analytical performance was considered with respect to the quantity of modifier in the paste, concentration of electrolyte solution, preconcentration time, Pb(II) concentration, and other variables. The linear calibration graph was obtained in the concentration range 2.00×10^{-9}-1.06×10^{-5} mol L^{-1} Pb(II) (n=21, r=0.9999) with 30 s preconcentration time. The detection limit was found to be 1×10^{-9} mol L^{-1}. After eight preconcentration/determination cycles, the DPV response was reproduced with 5.0 and 3.7% RSD at 2.0×10^{-8} and 2.0×10^{-6} mol L^{-1} Pb(II), respectively. The purposed method was applied to lead determination in waste waters (Mousavi et al., 2001).

Saadeh et al., have prepared chemically modified carbon paste electrode based on a new thiosalicylamide-functionalized polysiloxane as ionophore. The new electrode was used for lead determination in real samples and showed a Nernstian response for lead ion over a wide concentration range of 4.3×10^{-6}-1.0×10^{-2} mol L^{-1} with a detection limit of 8.7×10^{-7} mol L^{-1} within pH range 4.5-7.2 in a short response nearly 5 s. The electrode exhibits high sensitivity, reasonable selectivity, fast static response, long term stability and a wide concentration range with minimal sample pretreatment. The electrode was satisfactorily used as an indicator electrode in complexometric titration with EDTA and determination of Pb(II) in miscellaneus samples such as water samples and commercial lipsticks (Saadeh et al., 2012).

Carbon paste electrode modified with carbamoylphosphonic acid (acetamide phosphonic acid) self-assembled monolayer (SAM) on mesoporous silica (Ac-Phos SAMMS) were used to determine cadmium (Cd(II)), copper (Cu(II)), and lead (Pb(II)) by adsorptive stripping voltammetry (AdSV) technique which was involves preconcentration of the metal ions onto Ac-Phos SAMMS under an open circuit, then electrolysis of the preconcentrated species, followed by a square wave potential sweep towards positive values. The voltammetric responses increased linearly with the preconcentration time from 1 to 30 min or with metal ion concentrations ranging from 10 to 200.0 μg L^{-1}. The pH of the preconcentration solution strongly affected the voltammetric responses of metal ions; the best operating pH range was between 4.5 and 6. The electrolysis step was performed at -1.0V in an acidic solution for 60 s and the stripping step was also performed in highly acidic solution. The Ac-Phos SAMMS modified electrode will be incorporated into a flow system to test the simulated and real waste samples. The metal detection limits were 10 ppb after 2 min preconcentration and improved to 0.5 μg L^{-1} after 20 min preconcentration (Yantasee et al., 2004).

Ghiaci et al, have evolved an inexpensive, simple, selective and especially highly selective modified mixed-oxide (SiO_2-Al_2O_3 mixed-oxide) CPE for voltammetric determination of Pb(II). The electroanalytical procedure for determination of the Pb(II) comprises two steps: the chemical accumulation of the analyte under open-circuit conditions followed by the electrochemical detection of the preconcentrated species using dp ASV. The voltammetric response was linear in the concentration range of 2.0×10^{-9} to 5.2×10^{-5} mol L^{-1} for 5.0 min preconcentration time at fixed accumulation potential.

The detection limit (three times signal-to-noise) was found to be 1.07×10^{-9} mol L^{-1} Pb(II). This CMCPE can also be used as a relatively simple, selective, sensitive and quick method to determine Pb(II) in the real samples (Ghiaci et al., 2007).

Tesarova et al, have investigated the preparation and electroanalytical characteristics of the antimony film electrode (SbF-CPE) prepared in situ on the surface of the carbon paste electrode serving as a substrate transducer. Its aptitude for measuring Cd(II) and Pb(II) ions has been demonstrated in combination with square-wave anodic stripping voltammetry in nondeaerated model solutions of 0.01 M hydrochloric acid with pH 2.0. The newly developed sensor revealed highly linear behavior in the examined concentration range from 5 to 50 μg L^{-1}, with limits of detection (3σ) of 0.8 μg L^{-1} for Cd(II), and 0.2 μg L^{-1} for Pb(II) in connection with 120 s deposition step, offering good reproducibility of ±3.8 % for Cd(II), and ±1.2 % for Pb(II) (30 μg L^{-1}, n=10). Preliminary experiments disclosed that SbF-CPE and MF-CPE exhibit comparable performance for measuring trace concentration levels of Zn(II) in acidic medium with pH 2.0, whereas its detection with BiF-CPE was practically impossible. Finally, the practical applicability of SbF-CPE was demonstrated via measuring Cd(II) and Pb(II) in a real water sample (Tesarova et al., 2009).

Cd(II) ions were determined by using SWASV equipped with bismuth-antimony film (Bi-SbFE) electrode. The Bi-Sb film electrode has been reported for the first time as a possible alternative for electrochemical stripping analysis of trace heavy metals. The Bi-SbFE was prepared in situ on a GCE and employed in combination with square wave anodic stripping voltammetry in hydrochloric acid solution (pH 2.0). Compared with the bismuthfilm electrode (BiFE) and antimony-film electrode (SbFE), it has been found that the Bi-SbFE had better electroanalytical performance than the bismuth film or antimony film electrodes. The linear regression equation of Cd(II) is ip=0.95C+7.16 (ip: μA, C: μg L^{-1}) with a correlation coefficient of 0.998, and the detection limit is 0.15 μg L^{-1}. The Bi-SbFE has been applied to the analysis of Cd(II) in tap water sample (Yi et al., 2012).

Li et al have introduced bismuth-film modified graphite nanofibers-Nafion glassy carbon electrode (BiF/GNFs–NA/GCE) for simultaneous determination of Cd(II) and Pb(II) by differential pulse anodic stripping voltammetry.

Operational parameters have been optimized for the determination of trace metal ions in 0.10 M acetate buffer solution (pH 4.5). Under optimized conditions, the limits of detection were 0.09 µg L^{-1} for Cd(II) and 0.02 µg L^{-1} for Pb(II) with a 10 min preconcentration. The prepared electrode has been applied to the determination of trace metals in river water and blood samples, and the results were compared with those of inductively coupled plasma mass spectrometry (Li et al., 2010).

Kokkinos and co-workers have fabricated photolithographically a disposable bismuth-film electrodes (BiFEs) using a thin-film deposition approach. The electrode has been applied for the simultaneous trace determination of Cd(II) and Pb(II) by SWASV. The analytical sensitivities have beed found as Pb: 0.75 µA $µg^{-1}$ (R^2=0.996) and Cd: 0.32 µA $µg^{-1}$ (R^2=0.994). The electrode has been used for at least 15-20 preconcentration/stripping cycles without loss of sensitivity allowing operation in the semi-disposable mode. The limits of detection, calculated at a signal-to-noise ratio of 3 at a preconcentration time of 4 min, were 0.5 µg L^{-1} for Pb(II) and 1 µg L^{-1} for Cd(II). The proposed BiFEs have been successfully applied to the determination of Cd(II) and Pb(II) in a phosphate fertilizer and a river water sample (Kokkinos et al., 2008).

Wu et al, were developed a novel sensor for simultaneous detection of Pb(II), Cd(II) and Zn(II) ions, based on the dp ASV response at a bismuth/poly(p-aminobenzene sulfonic acid) (Bi/poly(p-ABSA)) film electrode which was created in situ by depositing simultaneously bismuth and the metals by reduction at -1.40 V on the poly(p-ABSA) modified electrode. Under the optimum conditions, a linear response was observed for Cd(II) and Zn(II) in the range from 1.00 to 110.00 µg L^{-1} and for Pb in the range from 1.00 to 130.00 µg/L. The detection limits of Pb(II), Cd(II) and Zn(II) were 0.80, 0.63 and 0.62 µg L^{-1}, respectively. The electrode were used as a sensor to determine Pb(II), Cd(II) and Zn(II) in river water samples the results were quite corresponding to the value obtained by AAS (Wu et al., 2008).

A bismuth-modified carbon nanotube electrode (Bi-CNT electrode) which was prepared by in situ plating of bismuth onto the screen-printed CNT electrode was employed for the determination of trace lead, cadmium and zinc. Preconcentration potential, bismuth concentration, preconcentration time and rotation speed during preconcentration were optimized for the purpose of determining trace metals in 0.1 M acetate buffer solution (pH 4.5) by using square wave anodic stripping voltammetry.

The Bi-CNT electrode presented well-defined, reproducible and sharp stripping signals compared to commonly use glassy carbon, activated carbon and graphite. The peak current response increased linearly with the metal concentration in a range of 2-100 μg L^{-1}. The limit of detection was 1.3 μg L^{-1} for Pb(II), 0.7 μg L^{-1} for Cd(II) and 12 μg L^{-1} for Zn(II) (S/N=3). The Bi-CNT electrode was successfully applicable to analysis of trace metals in real environments (Hwanga et al., 2008).

1.4 Surface Characterization Techniques

The developments in material sciences have increased demand for surface characterization techniques to improve the function and quality of target surface. Characterization of surface properties is important in many research fields of material science, including heterogeneous catalysis, activity of metal surfaces, semiconductor thin-film technology, corrosion resistance and studies of the behavior and functions of biological membranes. Desired surface properties such as optical, electrical, chemical or mechanical are affected from the surface structure and composition. In this connection, also, surface characterization techniques such as scanning electron microscopy (SEM), transmission electron microscopy (TEM), scanning tunnelling microscopy (STM) and atomic force microscopy (AFM) and X-Ray Photoelectron Spectroscopy (XPS) are very usefull instruments for the understanding of catalytic activities of modified electrode surface having a important place in electrochemical studies.

1.4.1 Scanning electron microscopy

The SEM is the most important electron-optical instrument for the investigation of bulk specimens. An electron probe is produced by two- or three-stage demagnification of the smallest cross section of the electron beam after acceleration.

This electron probe, 2-10 nm in diameter, is scanned in a raster over a region of the specimen. The smallest diameter of the electron probe is limited by the minimum acceptable probe current, which lies in the range 10^{-12}-10^{-11} A. This value is determined by the need to generate an adequated signal-to-noise ratio and by the spherical and chromatic aberration of the finel probe-forming lens. The image is displayed on a cathode-ray tube (CRT) scanned in synchrony.

The CRT beam intensity can be modulated by any of the different signals that result from the electron-specimen interactions.
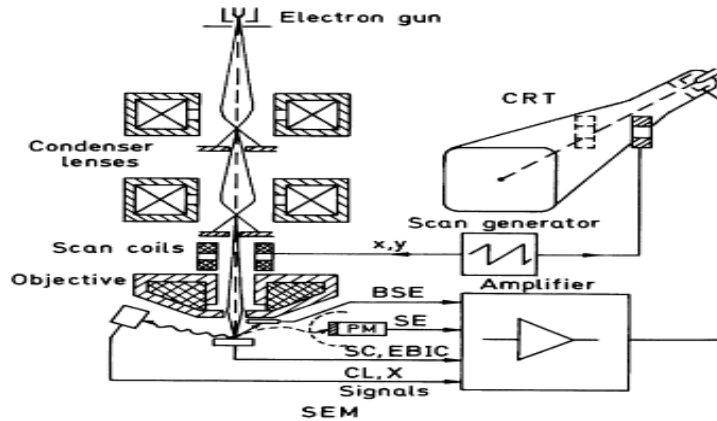
Figure 1.4 Schematic Ray Path for a Scanning Electron Microscope

The most important signals are those produced by secondary electrons (SE) with most probable exit energies of 2-5 eV and by backscattered electrons (BSE) with energies taht range from the energy of the primary electrons to about 50 eV. The secondary-electron yield and the backscattering coefficient depend on the angle of electron incidence (topographic contrast), the mean atomic number (material contrast), the crystal orientation (channeling contrast), and electrostatic and magnetic fields near the surface (potential and magnetic contrast). A signal can also be produced by the specimen current and by electron-beam-induced currents in semiconductors. Analytical information is available from the X-Ray spectrum and Auger electrons or from light quanta emitted by cathado-luminescence. The crystallographic structure and orientation can be obtained from electron channelling patterns, electron-backscattering patterns, and X-Ray Kossel diagrams. An environmental SEM can work with a high partial pressure between the specimen and the objectivelens diaphragm.

The resolution of the different modes operation and types of contrast depend on the information volume that contributes to the signal. Secondary electrons provide the best resolution because the exit depth is very small of the order of a few nanometers. The information depth of backscattered electrons is much greater, of the order of half electron range, which is as much as 0.1-1.0 μm, depending on the density of the specimen and the electron energy.

The secondary electron signal also contains a large contribution from the backscattered electrons when these penetrate the surface layer. At higher energies, the electron range and the diameter for the electron-diffusion region are greater. Conversely, higher energies are of interest for X-Ray microanalysis if K shells of heavy elements are to be excited. The progress in Schottky and field-emission gun design has increased the gun brightness at low electron energies, so that low-voltage scanning electron microscopy (LVSEM) in the range 0.5-5.0 eV is attractig interest because information can be extracted from a volume nearer to the surface. Unlike in TEM, special specimen-preparation methods are rarely needed in SEM. Nevertheless, charging effects have to be avoided by coating a non-conductive specimen with a thin conductive film, for example, and organic speciments have to be protected from surface distortions by chemical fixation or cryo-fixation (Reimer and Kohl, 2008).

1.4.2 X-Ray photoelectron spectroscopy

X-Ray Photoelectron Spectroscopy (XPS) provides a great deal of information about elemental distributions, layer or coating structure and thicknesses, surface functionality, and even particles sizes on the 1-20 nm scale for sample types that may not be readily analyzed by other methods. This information is important for both synthetic nanostructured or nanosized materials and a variety of natural materials with nanostructure.

The surface analysis technique called XPS is also known as ESCA, electron spectroscopy for chemical analysis. It is the most widely used surface analysis technique because of its relative simplicity in use and data interpretation. XPS is chosen when the samples are insulating or when chemical state information is desired.

The sample is irradiated with mono-energetic X-Rays causing photoelectrons to be emitted from the sample surface. An electron energy analyzer determines the binding energy of the photoelectrons. The energy of photoelectrons is characteristic of the target material, and measurement of the energy spectrum (number of count vs kinetic/binding energy) provides valuable information about the top 2-20 atomic layers, depending on the material studied. From the binding energy and intensity of a photoelectron peak, the elemental identity, chemical state, and quantity of an element are determined.

XPS analysis is usually conducted in two parts. During the first portion, a complete surface elemental analysis is obtained. XPS detects atomic number range 3-92, within 50 Å of the surface. There is good light element sensitivity, with a detectability limit of approximately 0.1 atomic percent. The second portion of a typical XPS experiment is used to determine the chemical binding energy of the surface elements. This portion is the true strength of XPS in that the binding energy furnishes some information about compounds present on the surface. Argon profiling is also available to determine concentration as a function of depth.

The kinetic energy, E_k, of these photoelectrons is determined by the energy of the X-Ray radiation, $h\nu$, and the electron binding energy, E_b, as given by:

$E_k = h\nu - E_b$

The experimentally measured energies of the photoelectrons are given by:

$E_k = h\nu - E_b - E_w$

E_w is the work function of the spectrometer.

The electron binding energies are dependent on the chemical environment of the atom, making XPS useful to identify the oxidation state and ligands of an atom.
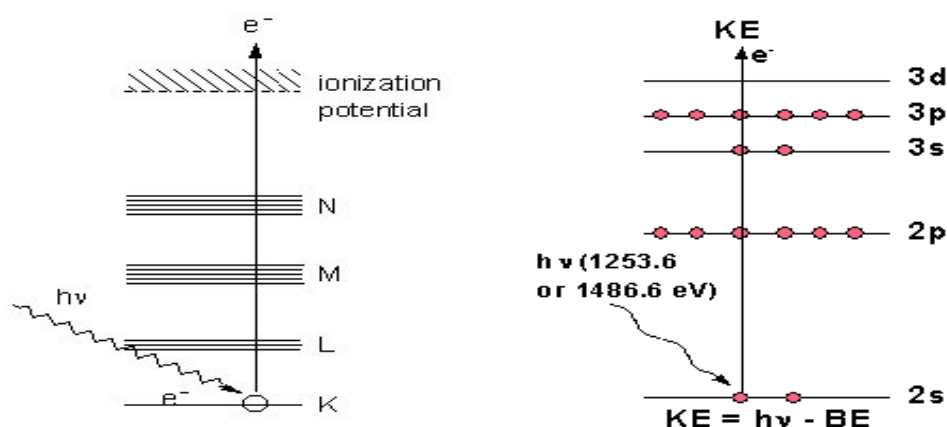
Figure 1.5 XPS photoelectron emission process

XPS instruments consist of an X-Ray source, an energy analyzer for the photoelectrons and an electron detector. The analysis and detection of photoelectrons requires that the sample be placed in a high-vacuum chamber. Since the photoelectron energy depends on X-Ray energy, the excitation source must be monochromatic.

The energy of the photoelectrons is analyzed by an electrostatic analyzer, and the photoelectrons are detected by an electron multiplier tube or a multichannel detector such as a microchannel plate.

The working tecnique of XPS is;

1. Energy spectrum: XPS research spectra (typically 0-1000 eV) are measured to estimate the composition.High-resolution spectra (within 10-20 eV) provide information about the chemical bonds.

2. Mapping: Choosing the energy of a single peak and scanning the focal point of the lenses across the sample one gets information about the lateral distribution of the corresponding species (elemental or chemical state) on the surface.

3. Imaging: Parallel imaging of the whole field of view e.g. by using a second hemispherical analyser allows real-time capability for chemical state and elemental imaging with high spatial resolution (<10-15 microns) and high sensitivity.

The information XPS provides about surface layers or thin film structures is of value in many industrial applications including: polymer surface modification, catalysis, corrosion, adhesion, semiconductor and dielectric materials, electronics packaging, magnetic media, and thin film coatings used in a number of industries.

1.4.3 X-Ray diffraction

X-Rays are electromagnetic radiation of wavelength about 1 Å (10-10 m), which is almost the same size as an atom. They are found in that part of the electromagnetic spectrum between gamma-rays and the ultraviolet. X-Ray diffraction (XRD) is used in two main areas, for the fingerprint characterization of crystalline materials and the determination the chemical composition and crystallographic structure of natural and manufactured materials.

Each crystalline solid material has a unique characteristic X-Ray pattern which is used as a "fingerprint" for the identification. Once the material has been identified, X-Ray crystallography may be used to determine its structure, i.e. how the atoms pack together in the crystalline state and what the interatomic distance and angle are etc.

XRD is one of the most important characterization tools used in solid state chemistry and materials science. XRD is one of the most powerful non-destructive analytical technique qualitative and quantitative analysis of crystalline compounds.

Diffraction is a scattering phenomenon. When a parallel beam of monochromatic X-Rays is irradiated on a crystalline sample, they are scattered in all directions but specific angles by the atomic lattice of the sample. The scattered X-radiation is produced by all the atoms. The scattered X-Rays can add together in few directions and reinforce each other to form the diffracted X-Ray beams. This is known as constructive interference. Constructive interference occurs when the waves are moving in same phase with each other. Thus, XRD occurs as a result of constructive interference of monochromatic scattered X-Rays coming from a crystalline sample. On the other hand, it is known that the diffraction occurs when any electromagnetic radiation interacts with a periodic structure like the planes or lattices of the atoms in a crystalline sample. XRD pattern is obtained by X-Ray diffraction (Figure 1.6) (Binnig et al., 1986).
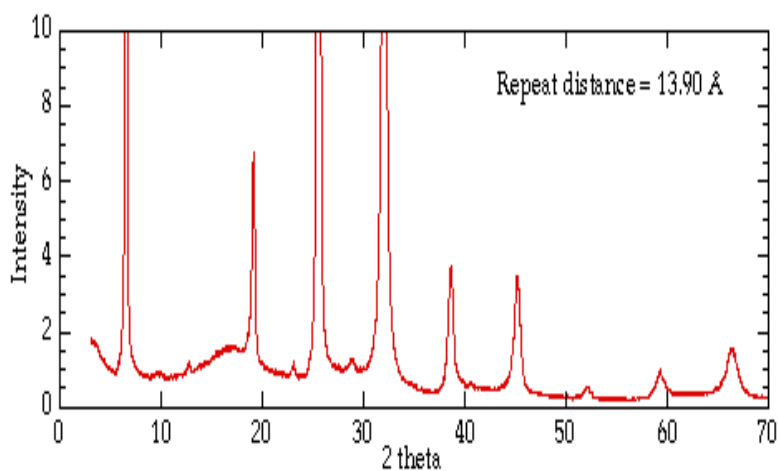
Figure 1.6 X-Ray diffraction patterns from layered structure vermiculite clay

The distances between the planes of the atoms in the sample are measured by applying Bragg's Law. Bragg's Law is n l = 2 d sin q, where the integer n is the order of the diffracted beam, l is the wavelength of the incident X-Ray beam, d is the distance between adjacent planes of atoms (the d-spacings), and q is the angle of incidence of the X-Ray beam. Since we know l and we can measure q, we can calculate the d-spacings.

Because the positions of the peaks in a powder pattern are determined by the size, shape, and symmetry of the unit cell and the peak intensities are determined by the arrangement of atoms within the cell, the powder pattern is a characteristic "fingerprint" of a phase.

As the concentration of a phase in a mixture varies, the intensities of all of the peaks from this phase vary in concert (ideally). Thus, the concentrations of phases in a mixture can be determined by measuring the intensities of peaks in the powder pattern.

1.4.4 Atomic force microscope

The atomic force microscope (AFM) was first described in 1986 (Binnig et al., 1986). Then it was evolved to be a powerful tool for a variety of disciplines such as material sciences, polymer research, etc (Venkataramanı, 2010). An AFM basically consists of a sharp tip mounted at the end of a cantilever.

Normally, the probe is a sharp tip, which is a 3-6 μm tall pyramid with 15-40 nm end radius (Figure 1.7). It commonly consists of a silicon nitride pyramid.
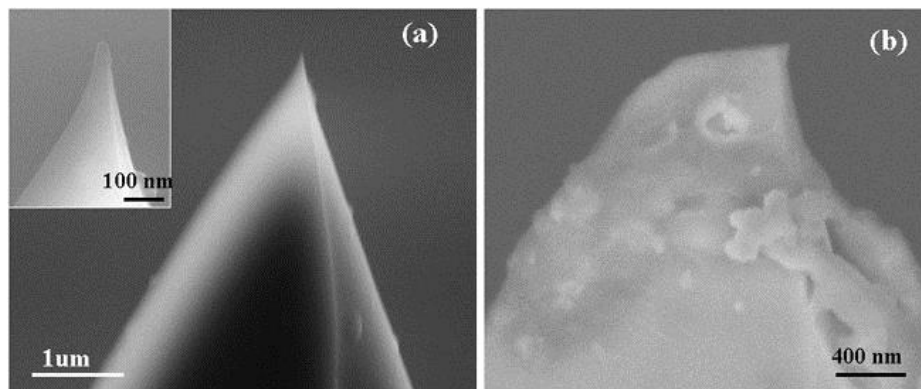
Figure 1.7 a) A new AFM tip; inset: The end of the new tip. b) A used AFM tip.

When the tip is in close proximity to the surface, the forces between the tip (probe) and the surface causes the cantilever beam to deflect (Figure 1.8). AFMs operate by measuring force between a probe and the sample. The cantilever operation obeys Hookes Law. The bending of cantilever during the tip is scanned over the sample and detected by a sensitive detector based on use of an optical beam deflection method.

The measured cantilever deflections are used to generate a map of the surface topography. Magnifications of the AFM may be between 100X and 100,000,000X in the horizontal (x-y) and vertical axis.

AFM is one kind of scanning probe microscopes (SPM). The primary difference in instrumentation design is how the forces between the probe and sample surface are monitored. The modes of operation of AFM are classified as contact and non-contact modes respectively.

In the contact mode, the tip is in contact with the surface and the AFM is operated in the repulsive force. In the non-contact mode, the tip never touches the surface in contrast to the contact mode. In this mode the cantilever with the tip is vibrated at its resonance frequency or close to the resonance frequency with constant amplitude when the tip is in close proximity to the sample surface.

In this mode, the AFM is operated in the attractive force (mostly van der Waals). This prevents the tip from destructive interactions with sample surface that can ruin the tip sharpness and also prevent the sample from being permanently deformed. There is a third mode which is a hybrid between the two known as the tapping mode.
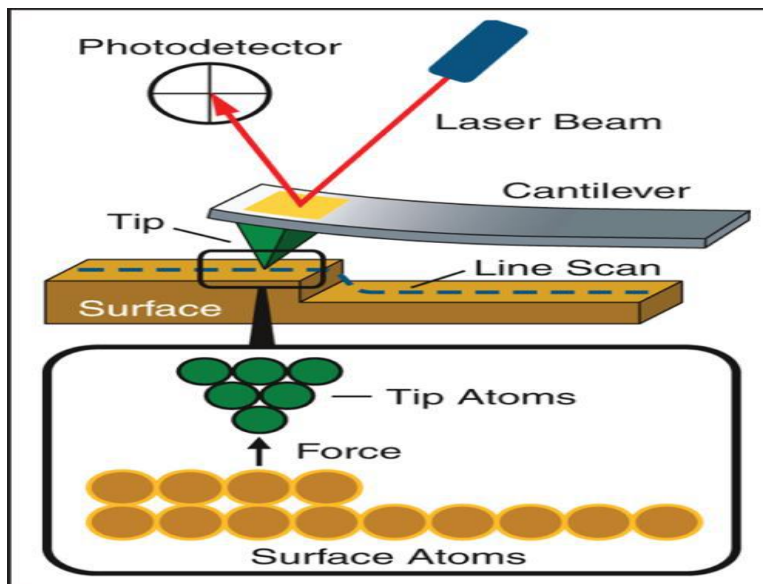
Figure 1.8 A schematic representation of the principle and working of AFM

AFM is a powerful technique, capable of imaging surfaces at nanometre or sub-nanometre resolution. Therefore, this instrument has found many applications in material and biological sciences. Atomic force microscopy is efficiently and widely used in the studies of different electrochemical processes, as well.

Metal electrodeposition as a method of synthesis of metal nanoparticles on different supporting materials as well as adsorptive and catalytic properties of nanomaterials objects is widely studied. It is well known that atomic-force microscopy is one of suitable and important methods for control of the structure of obtained electrodeposit objects in general and the morphology of electrodeposit catalysts.

1.4.5 Electrochemical impedance spectroscopy

Since many years, electrochemical impedance spectroscopy (EIS) is known to the electrochemists. However, the application of EIS has increased dramatically in the past few years due to its ability to explain physical and electronic properties of electrochemical systems such as diffusion coefficients, electron transfer rate constants, adsorption mechanisms, charge transfer resistances, capacitances and pore sizes. EIS offers all tools for the investigation of impedance in surface engineering, electrochemical power generation, corrosion research, catalysis or even in basic electrochemical research.

So far, many studies were carried out on composite electrodes and thin-film electrodes (Wang et al., 2012). EIS is now well established as a powerful tool for investigating the mechanisms of electrochemical reactions, for measuring the dielectric and transport properties of materials, for exploring the properties of porous electrodes, and for investigating passive surfaces. As a result, electrochemical impedance spectroscopy propvides a useful non-intrusive measurement method that can be used to characterize the electrical performance of fuel cells and other electrochemical devices.

The use of EIS records the response of the system to a small applied perturbation (i.e. AC signal), over a pre-determined frequency range. The applied AC voltage and the resultant AC current are measured and the impedance calculated ($Z^*=V/I$).

In general, a sinusoidal potential excitation is applied and an AC current signal is measured as a response to this potential. This current signal can be analyzed as a sum of sinusoidal functions (a Fourier series). During EIS experiments, because of applying a small amplitude AC signal to the system being studied, it is a non-destructive method for the evaluation of coated or modified surfaces.

For the study of electrochemical systems, EIS can give accurate kinetic and mechanistic information with a variety of techniques and output formats. For this reason, EIS is becoming a powerful tool in the study of corrosion, semiconductors, batteries, electroplating, electro-organic synthesis and electrocatalysis. EIS is also one of the best techniques for analyzing the performance of metallik nanoparticle coated electrodes.

General advantages of EIS:

1. Measurements can be made under real-world fuel cell operating conditions, e.g., open circuit voltage or under load (DC voltage or current).

2. Multiple parameters are determined from a single experiment.

3. Relatively simple electrical measurement is automated.

4. Bulk and interfacial properties of the system, e.g., membrane resistance and electrocatalysts are idendified.

5. Reaction models are verified.

6. A high precision measurement-the data signal can be averaged over time to improve the signal-to-noise ratio.

1.5 Electroanalytical Teqniques

Electrochemistry is a study of electron transfer reactions between electrodes (typically, but not always, metallic) and reactants, the latter usually in a located solution phase. If a general aqueous, heterogeneous electron transfer reactions is considered:

$Ox_{(aq)} + ne^- \leftrightarrows Red_{(aq)}$
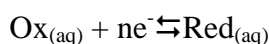
Ox symbolizes the oxidised species, Red represents the reduced species, n is the number of electrons transferred, and kc and ka are the reduction and oxidation rate constants, respectively. If k_c and k_a are so fast that the electrolysis is effectively equilibrium, the concentration of Ox and Red at the electrode surface can be given by the Nernst equation:

$$E = E^o + nF/RT \ln (Ox_{surface})/(Red_{surface})$$

E^o is the formal electrode potential when all species have unit concentration; this relates to the standard electrode potential via inclusion of activity coefficient effects. R is the molar gas constant (8.314 J mol^{-1} K^{-1}), T is the absolute temperature (K), n is the number of electrons participating in the reaction per mole of analyte, F is Faraday's constant (96485 C mol^{-1}) (Fernandez, 2009).

The interfacial region is the region between the electrode and solution, where electrode reactions actually occur and where the greatest potential differences across the electrical circuit appear. In dynamic electrochemical experiments, a potential difference is applied between an electrode and a solution containing an electrolyte. The applied potential leads to breakdown in electrochemistry of the solution close to the electrode surface.

Stern proposed a model for this region consisting of a Helmholtz double layer in series with a Guay-Clapman diffuse layer (Figure 1.9). In the double layer, solvated ions arrange themselves along the electrode surface forming a sheet of ionic charge called the Outer Helmholtz Plane (OHP) which is ~1nm from the electrode surface. The ions can also discard their solvation shell and adsorb onto the electrode surface forming an Inner Outer Helmholtz Plane (IHP).

The disordering effect of thermal motion is taken into account in the diffuse layer where an ionic atmosphere, similar to that described in the Debye-Huckel theory, is present. The potential drop is shoved across the whole region. Electron transfer occurs via tunnelling over distances no greater than the OHP. Therefore, it is the potential drop across the double layer which influences the redox process.
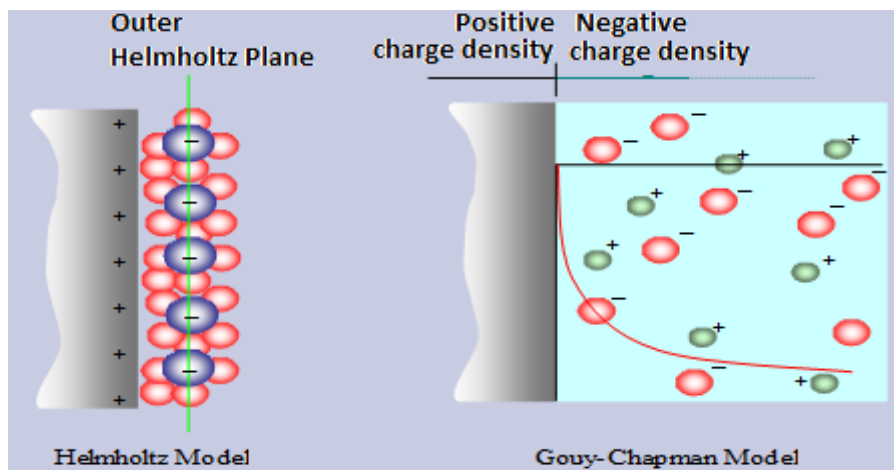
Figure 1.9 The electrical double layer

1.5.1 Electrochemical cells

All electrochemical cells require at least two electrodes (conductors) and a contacting sample (electrolyte) solution, which constitute the electrochemical cell. One of the two electrodes responds to the target analyte(s) and is thus termed the *working* (or indicator) *electrode*.

The second one, termed the *reference electrode*, is of constant potential (i.e. dependent of the properties of the solution). The two electrode system is the simplest approach to the study of current/voltage characteristics. In the experiments where the iR may be high (e.g, in large-scale electrolytic, galvanic cells or in experiments involving non-aqueous solutions with low conductivities), a three electrode cell is often preferable and one of the most common configurations used to study electrochemical reactions.

In a three electrode cell, the current is passed between the working electrode (where the reaction takes place) and *counter electrode* (or auxiliary). The auxiliary electrode can be one of convenience since its electrochemical properties do not affect the behaviour of the electrode of interest, the working electrode. It is only used to polarise the working electrode and usually chosen to be an electrode that does not produce substances by electrolysis that will reach the working electrode surface and cause interference with the reaction of interest (Schwarz and Irving, 1964).

In order that the potential (voltage) on the working electrode is precisely known, as third electrode known as the reference electrode is held close to the surface of the working electrode and the potential difference measured. This is because the reference electrode has no current passing through it, but merely maintains an invariant constant potential, no matter what is happening around it. In voltammetric experiments the three elecrode system is used (Figure 1.10).

This cell consists of working, reference and counter electrodes. The potential is applied between the working and reference electrodes, and the current flow is measured between the working and counter electrodes. The working electrode provides the surface for electron transfer to occur for the system under investigation.
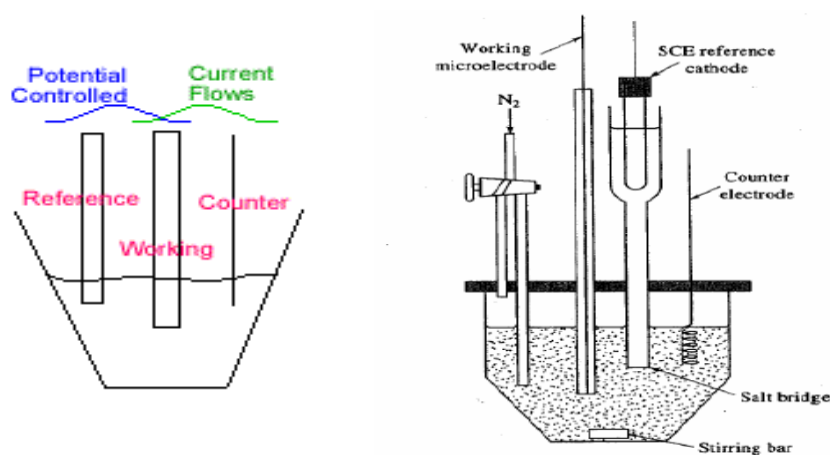
Figure 1.10 Electrode electrochemical cell used in voltammetry

The electrode place where redox occurs surface area few mm^2 to limit current flow is known as working electrode (microelectrode). In voltammetric instrumentation, microelectrodes are used as working electrode. Many types of electrodes can be used as the working electrode: dropping mercury, glassy carbon, gold, copper, platimun, a metal coated with mercury etc. and the timing of the applied potential can be varied to extract a variety of information. Potential ranges for three types of electrode materials in various supporting electrolytes are shown in Figure 1.11.
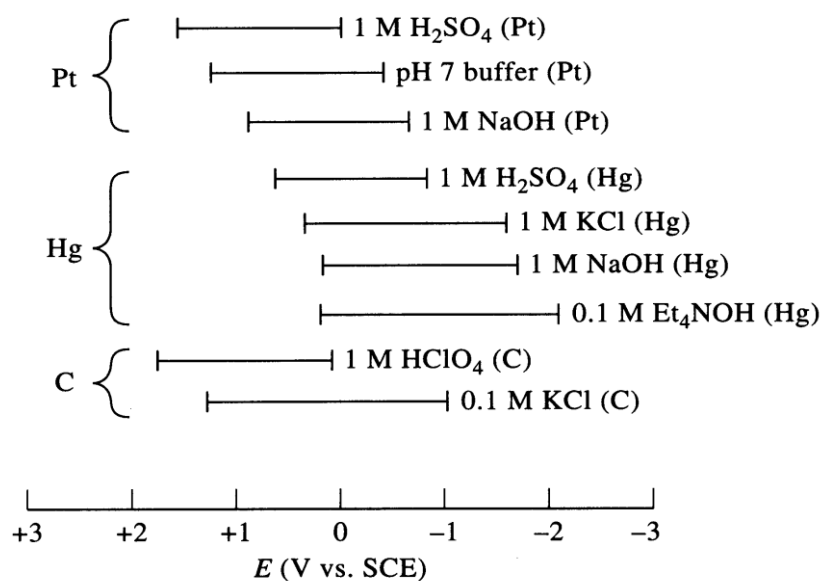
Figure 1.11 Potential ranges of some electrode materials

Reference electrode is an electrode having constant potential reference (Saturated Calomel Reference Electrode, SCE or silver-silver chloride electrode). Counter electrode made of inert material (Hg, Pt) plays no part in redox but completes circuit. It carries the bulk of the current (instead of reference electrode). In the cell, supporting electrolyte alkali metal salt does not react with electrodes but has conductivity.

1.5.2 Voltammetry and voltammetric techniques

Historically, the branch of electrochemistry we now call voltammetry developed from the discovery of polarography in 1922 by the Czech chemist Jaroslav Heyrovsky, received the 1959 Nobel Prize in chemistry. The early voltammetric methods experienced a number of difficulties, making them less than ideal for routine analytical use.

Voltammetry is one of the most important electroanalytical methods used in analytical chemistry and various industrial processes. Voltammetry is the name of a group of electrochemical techniques. In voltammetry, information about an analyte is obtained by measuring the current as the potential is varied.

The common characteristic of all voltammetric techniques is that they involve the application of a potential (E) to an electrode and the monitoring of the resulting current (i) flowing through the electrochemical cell. In many cases the applied potential is varied or the current is monitored over a period of time (t). Thus, voltammograms are obtained as some function of E, i and t. Voltammetric techniques are considered active techniques because the applied potential does a change in the concentration of an electroactive species at the electrode surface by electrochemically reducing or oxidizing it.

The various voltammetric techniques have many analytical advantages including excellent sensitivity with a very large useful linear concentration range for both inorganic and organic species (10^{-12} to 10^{-1} mol L^{-1}), a large number of useful solvents and electrolytes, a wide range of temperatures, rapid analysis times (seconds) and simultaneous determination of several analytes. Analytical chemists routinely use voltammetric techniques for the quantitative determination of a variety of dissolved inorganic and organic substances. Inorganic, physical and biological chemists widely use voltammetric techniques for a variety of purposes, including fundamental studies of oxidation and reduction processes in various media, adsorption processes on surfaces, electron transfer and reaction mechanisms, kinetics of electron transfer processes, and transport, speciation and thermodynamic properties of solvated species.

Voltammetry is an electrochemical technique in which the current-potential behaviour at an electrode surface is measured. The potential is varied in some systematic manner to cause electroactive chemical species to be reduced or oxidized at the electrode. The resultant current is proportional to the concentration of the electrochemical species. The voltammetric techniques are based on Farady's Law and Fick's Laws. In voltammetry the current corresponding to the quantity of material transported by diffusion and reacting at the electrode surface is usually measured. This current is proportional to the concentration of the electroactive component (analyte) present in the test solution. The current measured is usually the current due to a specific oxidation or reduction process involving the analyte species at the surface of one of the electrodes.

In voltammetry, the applied potential, as calculated by the Nernst equations, controls the concentrations of the redox species at the electrode surface (c_O^0 and c_R^0).

The current resulting from the redox process, (known as the faradaic current) is related to the material flux at the electrode-solution interface and is described by Fick's diffusion law.

For a reversible electrochemical reaction, which can be described by Oxidation (Ox)+ne$\leftrightarrows$Reduction (Red), the application of a potential E forces the respective concentrations of Ox and Red at the surface of the electrode (that is, c^0_{Ox} and c^0_{Red}) to a ratio in compliance with the Nernst equation:

$E=E^0+2.3\ RT/nF\log c^0_{Ox}/\ c^0_{Red}$

R is the molar gas constant ($8.3144\ J\ mol^{-1}K^{-1}$), T is the absolute temperature (K), n is the number of electrons transferred, F=Faraday constant (96,485 C/equiv), and E^0 is the standard reduction potential for the redox couple. If the potential applied to the electrode is changed, the ratio $c^0_{Red}/c^0_{Ox}{}^0$ at the surface will also change so as to satisfy. If the potential is made more negative the ratio becomes larger (that is, Ox is reduced) and conversely, if the potential is made more positive the ratio becomes smaller (that is, Red is oxidized).

The current resulting from redox reactions at the working and auxiliary electrodes is called a faradaic current. Thus, electroactive species diffuses from the bulk solution to the electrode surface and the reduction products diffuse from the electrode surface towards the bulk solution. This creates what is called the faradaic current. The magnitude of the faradaic current is determined by the rate of the resulting oxidation or reduction reaction at the electrode surface. Two factors contribute to the rate of the electrochemical reaction:

1. The rate at which the reactants and products are transported to and from the surface of the electrode (mass transport)

2. The rate at which electrons pass between the electrode and the reactants and products in solution (kinetics of electron transfer at the electrode surface)

There are three modes of mass transport to and from the electrode surface: diffusion, migration, and convection.

The flux of material to and from the electrode surface is a complex function of all three modes of mass transport. In the limit in which diffusion is the only significant means for the mass transport of the reactants and products, the current in a voltammetric cell is given by İlkovic:

$i=nFAD (c_A- c_A^o)/\delta$

where n is the number of electrons transferred in the redox reaction, F is Faraday's constant($C \cdot mol^{-1}$), A is the area of the electrode (cm^2), D is the diffusion coefficient for the reactant or product ($cm^2 \cdot s^{-1}$), c_A and c_A^o are the concentration of the analyte in bulk solution and at the electrode surface, and δ is the thickness of the diffusion layer.

$nFAD/\delta$ is contant due to each constant of them, rate can be rewritten as

$i = k_A (c_A- c_A^o)$

At maximum current, c_A^o, in this case, the current (i) known as the limiting current or diffussion current is proportional to analyte concentration by the Ilkovic equation

$i_l = k_A \times c_A$
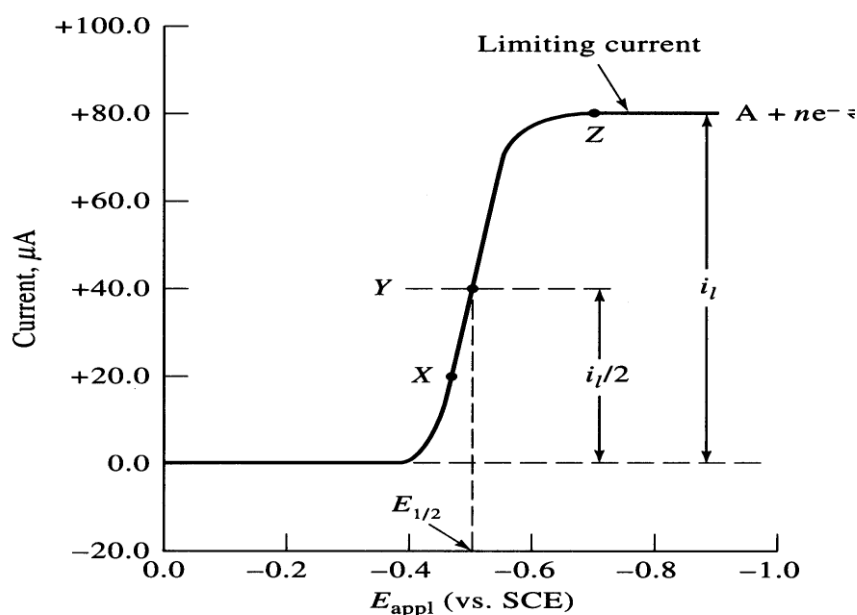
Figure 1.12 A typical linear-sweep voltammogram at slow scan rate

Voltammetric methods of analysis involve the application of a potential (volts) in an electrochemical cell, and measuring the current (amps) that flows. Voltammograms (voltammetric waves) are graphs of current (i) vs.applied voltage (Figure 1.12).

Many different voltammetric techniques have been developed based on this current-voltage relationship, and have proven to be be extremely valuable tools for analyzing trace metals in solutions, determining complexation in organic and inorganic systems, studying kinetics and diffusion, etc.The most widely used voltammetric methods can be classified as:

a) Direct current methods: i) D.C. Polarography, ii) Linear sweep voltammetry, iii) Sampled D.C. Polarography, iv) Hydrodynamic voltammetry

b) Pulse methods: v) Normal Pulse voltammetry, vi) Differential Pulse voltammetry, vii) Square wave voltammetry, viii) Cyclic voltammetry

c) Stripping voltammetry: ix) Anodic stripping voltammetry, x) Cathodic stripping voltammetry, xi) Adsorptive stripping voltammetry

d) Alternating current methods

The voltammetric techniques used in this thesis will be discussed in following section.

1.5.2.1 Cyclic voltammetry

Cyclic voltammetry (CV) is a simple, rapid, and powerful method for characterizing the electrochemical behavior of analytes that can be electrochemically oxidized or reduced. It is mostly used for the study of redox processes, for understanding reaction intermediates, and for obtaining stability of reaction products (Kounaves, 1997).

This technique is based on varying the applied potential at a working electrode in both forward and reverse directions (at some scan rate) while monitoring the current. For example, the initial scan could be in the negative direction to the switching potential. At that point the scan would be reversed and run in the positive direction. Usually the scan is reversed at a specific switching potential, hence the name cyclic voltammetry.

The potential is scanned back and forth linearly with time between two extreme values-the switching potentials using triangular potential waveform (Figure 1.13a).

Since the scan rate is constant and the initial andswitching potentials are known, one can easily convert time to potential, and the usual protocol is to record current vs. applied potential. A typical voltammogram is given in Figure 1.13b (Wang, 2000).
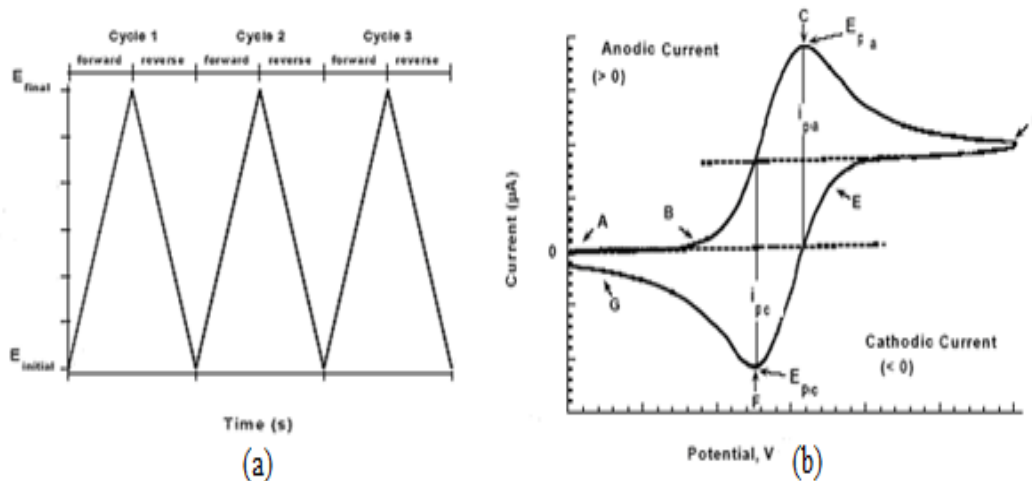
Figure 1.13 a) A cyclic voltammetry potential waveform with switching potentials

b) The expected response of a reversible redox couple during a single potential cycle

In cyclic voltammetry, the system is described as "reversible" when the electrode kinetics is much faster than the rate of diffusion. The Nernst equation is the final boundary condition for a reversible system. The system is described as "irreversible" when the electrode kinetics is slower than the rate of diffusion.

For an irreversible reaction of the type one-electron, one-step reaction $Ox+e^-$ $\leftrightarrows$Red, linear scan and cyclic voltammetry give the same voltammetric profile, since no inverse peak emerges on changing the scan direction.

1.5.2.2 Stripping voltammetry and preconcentration

The preconcentration techniques have the lowest limits of detection of any of the commonly used electroanalytical techniques. Sample preparation is minimal and sensitivity and selectivity are excellent.

The three most commonly used variations are anodic stripping voltammetry (ASV), cathodic stripping voltammetry (CSV), and adsorptive stripping voltammetry (AdSV).

Even though ASV, CSV, and AdSV have their own unique properties, these methods have two steps in common. First step, the analyte species in the sample solution is concentrated onto or into a working electrode. It is a preconcentration step that results in the high sensitivity that can be achieved. During the second step, the preconcentrated analyte is measured or stripped from the electrode by the application of a potential scan. Any number of potential waveforms can be used for the stripping step. The most common are differential pulse and square wave due to the discrimination against charging current. However, square wave has the added advantages of aster scan rate and increased sensitivity relative to differential pulse.

1.5.2.3 Anodic stripping voltammetry

Anodic stripping voltammetry (ASV) is a voltammetric method for quantitative determination of specific ionic species. The analyte of interest is electroplated or electrodeposited on the working electrode during a deposition step, and oxidized from the electrode during the stripping step. The current is measured during the stripping step.

The oxidation of species is registered as a peak in the current signal at the potential at which the species begins to be oxidized. The stripping step can be eitherlinear, staircase, squarewave or pulse. Advantages are as follows;

1. Very sensitive and reproducible (RSD<5%) method for trace metal ion analysis in aqueous media.

2. Concentration limits of detection for many metals are in the low ppb to high ppt range (S/N=3) and this compares favorably with AAS or ICP analysis.

3. Field deployable instrumentation that is inexpensive.

4. Approximately 12-15 metal ions can be analyzed for by this method.

5. The stripping peak currents and peak widths are a function of the size, coverage and distribution of the metal phase on the electrode surface (Hg or alternate).

1.5.2.4 Cathodic stripping voltammetry

Cathodic stripping voltammetry (CSV) can be used to determine substances that form insoluble salts with the mercurous ion. Application of a relatively positive potential to a mercury electrode in a solution containing such substances results in the formation of an insoluble film on the surface of the mercury electrode. A potential scan in the negative direction will then reduce (strip) the deposited film into solution. This method has been used to determine inorganic anions such as halides, selenide, and sulfide, and oxyanions. In addition, many organic compounds, such as nucleic acid bases, also form insoluble mercury salts and may be determined by CSV.

1.5.2.5 Adsorptive stripping voltammetry

Adsorptive stripping voltammetry is quite similar to anodic and cathodic stripping methods. In this technique, analyte is adsorbed on the electrode surface and there is no electrolysis step. The adsorbed species is quantified by using a voltammetric technique such as DPV or SWV in either the anaodic or cathodic direction, depending on whether the analyte is to be oxidized or reduced, to give a peak-shaped voltammetric response with amplitude proportional to concentration.

Many organic species (such as heme, chlorpromazine, codeine, and cocaine) and inorganic species have been determined at micromolar and nanomolar concentration levels using AdSV.

1.5.2.6 Square wave stripping voltammetry

Pulse voltammetric techniques were introduced by Barker and Jenkin in 1952 to improve the sensitivity of voltammetric measurements (Barker and Jenkin, 1952). The improvement in sensitivity is achieved by a significant increase of the ratio between the Faradaic and capacitive currents. By using these techniques, the detection limits for analyte can be as low as 10^{-8} M. One of the newest pulse techniques is square-wave voltammetry (SWV) (Osteryoung and Osteryoung, 1985). It was little used in the beginning owing to difficulties with the controlling electronics. With advances in instrumentation SWV became more popular as an important voltammetric technique (Shah, 2010).

This technique consists of the application of a square-wave of constant amplitude superimposed on a staircase wave form (Figure 1.14). The current is sampled twice in each pulse period; at the reverse half cycle and the forward half cycle. During each square-wave cycle, once at the end of the forward pulse that gives rise to the oxidative current component, and once at the end of the backward pulse that gives rise to the reduction current component. The difference between the two currents is then displayed as a function of the resultant potential. This minimizes the effect of charging current and so high sensitivity is achieved. The resulting peak-shaped voltammogram is symmetrical about the half-wave potential and the peak current is proportional to the concentration. The detection limit for SWV is 10^{-7} to 10^{-8}. It seems that this technique will gain considerable use for the analysis of inorganic and organic species. The SWV is rapid, sensitive and consumed less analyte than the other pulsed techniques.
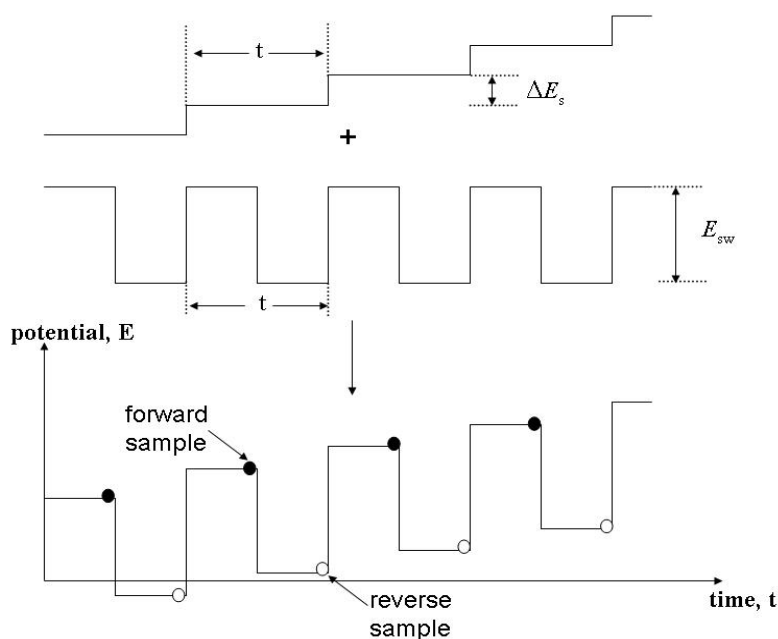
Figure 1.14 Schematic waveform of pulses superimposed on a staircase for square wave voltammogram

1.6 The aim of the thesis

In this thesis, the attention was paid to mainly two goals; the first aim was to design and develop metal nanoparticles modified, based nickel, gold and palladium nanoparticles modified multiwall carbon nanotubes (MWCNT)/glassy carbon electrode (GCE) toward oxidation of ethanol and methanol molecules. For this purpose, The MWCNT/GC electrodes were modified with each single metal, bimetallic and triple metal nanoparticle of nickel, gold and palladium by electrochemical deposition. The obtaining results about electrocatalytic oxidation of methanol and ethanol with electrochemically modification of those electrodes were compared with same metal nanoparticles modified electrodes prepared by chemical reduction methods. The performances of the catalytical system for methanol and ethanol electrooxidation were evaluated by cyclic voltammetry (CV) in both acidic and alkaline media. The modified electrode surfaces as a catalytist were characterized with cyclic voltammetry, scanning electron microscopy (SEM), X-Ray diffraction (XRD), energy dispersive X-Ray spectroscopy (EDX) and X-Ray photonelectron spectroscopy (XPS).

The second goal of this thesis was to prepare the carbon pasta electrodes modified with various modifiers for selective determination of trace lead and cadmium with high sensitivity and accuracy using square wave and differantial puls anodic stripping voltammetry. For qualitatively new, more sensitive and selective composite ($K_4Fe(CN)_6$+CNT and $Ca_3(PO_4)_2$+$Cu_2Fe(CN)_6$) CPEs and bismuth, tin and antimony alloy film electrodes for voltammetric stripping analysis of lead and cadmium ions were fabricated and those prepared electrodes were used to detection of lead (Pb(II)) and cadmium (Cd(II)) in real samples.

The results obtained by square wave anodic stripping voltammetry and inductively coupled plasma-mass spectrometry (ICP-MS) were compared each other for validation of real sample analysis.The modified electrode surfaces were characterized by cyclic voltammetry (CV), scanning electron microscopy (SEM), electrochemical impedance spectroscopy (EIS) and X-Ray photoelectron spectroscopy (XPS).

In addition, the carbon paste electrodes coated with bismuth (Bi), antimony (Sn) and their mixture in the film by use of electrochemical method was evaluated for determination of lead and cadmium by square wave anodic stripping voltammetry in acidic media. The electrode surfaces of the bare carbon pasta and carbon pasta electrodes coated with the metal films were characterized by SEM and XPS.

2. EXPERIMENTAL

2.1 Apparatus

Voltammetric and electrochemical impedance measurements (EIS) were carried out using BAS 100B and Autolab/302 N Electrochemical Analysers with a three electrodes system consisted of a working electrode (bare GCE, MWCNT/GCE, Au-MWCNT/GCE, Pd-MWCNT/GCE, Ni-MWCNT/GCE, Pd-Au-MWCNT/GCE, Pd-Ni-MWCNT/GCE, Au-Ni-MWCNT/GCE, Pd-Au-Ni-MWCNT/GCE, Sb/Bi-MWCNT/GCE and different modified carbon paste electrodes ($Ca_3(PO_4)_2$, $Ca_3(PO_4)_2+ZrO(H_2PO_4)_2$, $Ca_3(PO_4)_2+Cu_2Fe(CN)_6$, $CNT+K_4Fe(CN)_6$, Bi/MWCNTs-CP-FE, Sn/MWCNTs-CP-FE, Sn-Bi/MWCNTs-CP-FE), a platinum wire counter electrode and an Ag/AgCl (sat.KCl) reference electrode, respectively. Cyclic voltammetry (CV), differential puls anodic stripping voltammetry (DPASV) and square wave anodic stripping voltammetry (SWASV) were used throughout the electroanalytical studies. The pH measurements were made with WTW handheld 330i ion analyzer meter pH. Magnetic stirrer model was MSH-20A which was produced by Wisd Laboratory Instruments. Philips XL30 SFEG Scanning Electron Microscopy was used for the charecterization of bare and modified elecrode surfaces. The crysttallic structure of metal nanoparticles on the electrode surfaces were characterized by Riguka Ultima IV X-Ray Diffractometer, using Cu Kα as the radiation source at the operating voltage of 40 kV and scan rate of 4 ^{o}min^{-1}. Surface chemistry of each metal nanoparticle modified electrodes was studied by X-Ray-photoelectron Spectroscopy (XPS) using Thermo K-Alpha-monochromated high-performance XPS spectrometer.

2.2 Reagents and Materials

All reagents were analytical reagent greade. MCNTs with purity 95% (110–170 nm diameter) and 5-9 μm length were purchased from Aldrich. Acetic acid (CH_3COOH), sodium acetate (CH_3COONa), sodium dihydrogen phosphate (NaH_2PO_4), disodium monohydrogen phosphate (Na_2HPO_4), boric acid (H_3BO_3), sodium meta borate ($NaBO_2$), sodium hydroxide (NaOH), hydrochloric acid (HCl), lead(II) acetate trihydrate ($Pb(CH_3COO)_2.3H_2O$), cadmium acetate dihydrate ($Cd(CH_3COO)_2.2H_2O$), ethanol (C_2H_5OH), methanol (CH_3OH), cloroplatinic acid (H_2PtCl_6), gold wire, silver wire were supplied from Merck, Sigma and Aldrich.

Addition to them, chloroauric acid ($HAuCl_4$), nickel sulphate ($NiSO_4$), calcium nitrate tetrahydrate [$Ca(NO_3)_2.4H_2O$], diammonium hydrogen phosphate [$(NH_4)_2HPO_4$], potassium carbonate (K_2CO_3), tartaric acid ($C_4H_6O_6$), potassium ferrocyanide ($K_4Fe(CN)_6$), bismuth oxychloride (BiOCl), antimony chloride ($SbCl_3$), tin (II) chloride ($SnCl_2$), potassium hydrogen tartrate (KHT), graphite, mineral oil, silica gel, alimuna (Al_2O_3), N,N-dimethylformamide (DMF) were supplied from Merck, Sigma and Aldrich. Stock standart solution of ethanol and methanol were freshly prepared from the required amount of reagent in ultrapure water.

Buffer solutions were prepared from acetic acid/sodium acetate, sodium dihydrogen phosphate/disodium monohydrogen phosphate (PBS), boric acid/sodium metaborate and Britton-Robinson buffer in the pH range from 2.0 to 10.0. To prepare chloroauric acid ($HAuCl_4$) solution, a 0.05 g Au wire was dissolved concentrated HNO_3:HCl (1:3) and the solution was boiled until evaporation of the acid. Then the residual was dissolved in 100.0 mL 0.1 mol L^{-1} HCl solutions. Palladium solution was prepared by dissolving 0.01 g ($1.0x10^{-3}$ mol L^{-1}) $PdSO_4$ in 100.0 mL 0.1 mol L^{-1} H_2SO_4 solution. Nickel solution was prepared by dissolving 0.07 g $NiSO_4$ ($1.0x10^{-3}$ mol L^{-1}) in 250.0 mL 0.1 mol L^{-1} H_2SO_4 solution. All solutions were prepared and diluted with ultrapure water. Stock standart solution ($5.0x10^{-3}$ mol L^{-1}) of Pb (II) and Cd (II) were freshly prepared by dissolving the required amount of reagents in ultrapure water (Millipore Milli Q system, 18.2 MΩ).

2.3 Methods

2.3.1 Pre-conditioning of glassy carbon electrode

GCE was activated by polishing with different grade of Al_2O_3 slurry (0.05-3 micron) on a synthetic cloth then rinsing with pure water and then ultrasonicated for 3 minutes in ethanol/ultra pure water (1:1 v/v) mixture. GCE was also electrochemically cleaned by keeping 10 minutes at constant potential at 1.0 V.

2.3.2 Pre-treatment of multiwall carbon nanotubes

Multiwalled carbon nanotube was pretreated with concentrated HNO_3 for purification and activation of nanotubes as follow; a 0.1 g MWCNT was boiled in approximately 4.0 mL concentrated HNO_3 for 8 hours and then washed many times with ultrapure water.

The acid-treated MWCNT was dispersed in dimethyl formamide (DMF) to get a black suspension after 30 minutes ultrasonication. A 10 μL of MWCNT suspension was injected on the pre-conditioned bare GCE surface. The solvent (DMF) of the suspension on the GCE surface was evaporated at 55˚C for more then one hour.

2.3.3 Preparation of gold, palladium and nickel metal nanoparticles modified multiwall carbon nanotubes/ glassy carbon electrode

The metal nanoparticles modified composite electrodes were obtained by a straight forward electrochemical method. The electrochemical deposition of metal particles of palladium (Pd), gold (Au) and nickel (Ni) were deposited using electrochemical reduction of, 1.0×10^{-3} mol L^{-1} $PdSO_4$+0.1 mol L^{-1} H_2SO_4, 1.0×10^{-3} mol L^{-1} $HAuCl_4$+0.1 mol L^{-1} HCl and 1.0×10^{-3} mol L^{-1} $NiSO_4$+0.1 mol L^{-1} H_2SO_4 solutions, respectively on the MWCNT/GCE.

For MWCNT/GCE modification, Au nanoparticles deposited by cyclic voltammetry in the potential range from 0.5 V to -0.8 V in $HAuCl_4$ with a scan rate of 50 mV/s for 10 cycles, and Pd nanoparticles were deposited by CV in the potential range from 0.6 V to -0.9 V, and Ni nanoparticles were deposited by CV in the potential range from 0.65 V to -0.8 V at a sweep rate of 50mV/s. Bimetallic and trimetalic nanoparticles modified MWCNT/GC electrodes were obtained by applying the same prosedure consecutively that mentioned above. The obtained metal nanoparticles modified MWCNT/GCE electrodes were ready for use after the final wash with ultra pure water and denoted as Au-MWCNT/GCE and Pd-MWCNT/GCE, Ni-MWCNT/GCE, Pd-Au-MWCNT/GCE, Pd-Ni-MWCNT/GCE, Au-Ni-MWCNT/GCE and Pd-Au-Ni-MWCNT/GCE etc.

2.3.4 Preparation of chemically modified multiwall carbon nanotube electrodes

A 10.0 mg of treated MWCNTs were kept in 10.0 mL single metal precursor solution (1.0×10^{-3} mol L^{-1} $PdSO_4$, $NiSO_4$ or $HAuCl_4$). Ultrasonically dispersed carbon nanotube metal precursor solutions were heated to 80 $^{\circ}$C in vacuum oven and kept constantly over night.

After then, the metal ions (Pd) impregnated carbon nanotubes were reduced by 0.05 mol L^{-1} sodium borohydride and washed with ultrapure water and dried in vacuum oven at 80 ^{o}C for 12 hours. The modified MWCNT was separately dispersed in DMF to get a black suspension. A 10.0 μL of each MWCNT suspension was injected on the pre-conditioned bare GCE surface and then the solvent of the suspension on the GCE surface was evaporated at 55˚C for one hour to fabricate modified MWCNT/GCE. For the reduction of metal with citric acid, the process given above was carry out using 15.0 mL of 0.1 mol L^{-1} citric acid solution, instead of sodium borohydride.

2.3.5 Potassium ferrocyanide immobilized silica modified carbon paste electrode preparation

Silica gel was activated by HCl for a day then washed with pure water until free chloride removed and was dried at 150 ^{o}C in oven. 4.0 mmol $K_4Fe(CN)_6$ was mixed with activated silica gel for 1 hour then washed with ultrapure water for many times to remove phsically adsorbed $K_4Fe(CN)_6$ on the silica surface, the final product was blue in colour. The mixture was dried at 50 ^{o}C in oven for a day. $K_4Fe(CN)_6$ immobilized silica modified carbon paste electrode was prepared by throughly mixing the 10.0 % modified silica, 25.0 % mineral oil, 1.0 % CNT and spectroscopic grade graphite powder until obtaining uniformly wetting paste. The paste was then packed into home-made glass cylindrical tube (i.d. 3 mm). A silver wire was inserted into the opposite end to establish electrical contact.

The external electrode surface was smoothed with tracing paper until obtain to shiny surface. After electrochemical study, a new electrode surface was produced by scraping out the old surface and replacing the modified carbon paste.

2.3.6 Procedure of voltammetric measurements for potassium ferrocyanide immobilized silica modified carbon paste electrode

DPASVs were recorded directly after immersion of the modified electrode into 10.0 mL solution of 0.2 mol L^{-1} CH_3COOH supporting electrolyte or Pb(II) ions containing supporting electrolyte.

ASV responses were obtained by immersing the modified electrode for a selected period of time in accumulation voltammetric cell (in situ accumulation) containing Pb (II) solution in acidic medium, under constant stirring rate. After 10 s for quiescent conditions, the stripping was achived by potantial scanning from -0.8 to +0.1 V in differential pulse mode (deposition time, 5 min; pulse amplitude, 10 mV; range of scan potential, -0.80 to -0.20 V and scan rate, 20.0 mV s^{-1}).

2.3.7 Calcium phosphate modified carbon paste electrode preparation

Calcium nitrate tetrahydrate [Ca(NO$_3$)$_2$.4H$_2$O] and diammonium hydrogen phosphate [(NH$_4$)$_2$HPO$_4$] were used as the precursors for the synthesis of the Ca$_3$(PO$_4$)$_2$ nanocrystals. An aliqouat of 50.0 mL of Ca(NO$_3$)$_2$ and (NH$_4$)$_2$HPO$_4$ solutions were mixed in a beaker and allowed over night. The product in the beaker was seperated from the solution with decantation and then dried at the room temperature. The dried product was mixed with 2.0 g graphite powder and the mixture was put into a porcelain crucible at 900 ^{o}C oven for 5 hours. Thus, the graphite powder modified with Ca$_3$(PO$_4$)$_2$ was obtained.

The modified carbon pasta electrode was prepared by mixing the 73.0 % modified graphite powder and 27.0 % mineral oil. The paste was then packed into home-made glass cylindrical tube (i.d. 3 mm). A silver wire was inserted into the opposite end to establish electrical contact. The external electrode surface was smoothed with clean weighing paper until obtain to shiny surface. After each use electrochemical study, the new fresh electrode surface of the paste electrode surface was simply renewed by scrapping off about 2-3 mm of the old surface and polished the new surface on a piece of tracing paper.

2.3.8 Voltammetric measurements with calcium phosphate modified electrode

DPASVs were recorded directly after immersion of the modified electrode into 10.0 mL solution of 0.2 mol L^{-1} CH$_3$COOH supporting electrolyte or Pb(II) ions containing supporting electrolyte. The preconcentration of lead was carried out at -0.70 V for 300.0 seconds. The equilibration time was 10 s, after the voltammogram in differential pulse mode was recorded with an anodic scan (step potential 20 mV, pulse amplitude 10 mV; pulse width 50 ms, scan range: -0.7 to -0.3 V).

2.3.9 Calcium phosphate and zirconium phosphate modified carbon paste electrode preparation

The calcium phosphate ($Ca_3(PO_4)_2$) nanocrystals has been synthesized using calcium nitrate tetrahydrate and diammonium hydrogen phosphate mixture as the precursor. On the other hand, 8.34 g zirconium oxichloride ($ZrOCl_2$) was mixed with 143.0 mL of 2.0 mol L^{-1} HCl acid and 133.0 mL of 1.25 mol L^{-1} H_3PO_4 solution. A white gelly product was obtained and it was dried at room temperatute.The final product was zirconium phosphate ($ZrO(H_2PO_4)_2$). $ZrO(H_2PO_4)_2$ and $Ca_3(PO_4)_2$ curds were mixed nearly 5 hours using magnetic stirrer. The mixed curd was dried in an oven set at 40 ^{o}C overnight. $ZrO(H_2PO_4)_2+Ca_3(PO_4)_2$ modified carbon paste electrode was prepared by througly mixing the 10.0 % $ZrO(H_2PO_4)_2+Ca_3(PO_4)_2$ modifier, 27.0 % mineral oil and 63.0 % spectroscopic grade graphite powder until obtaining uniformly wetting paste. The modified paste was then packed into home-made glass cylindrical tube (i.d. 3 mm). A silver wire was inserted into the opposite end to establish electrical contact. The exterior electrode surface was smoothed with weighing paper until obtain to shiny surface. After each use electrochemical study, the new fresh electrode surface of the paste electrode surface was simply renewed by scrapping off about 2-3 mm of the old surface and polished the new surface on a piece of tracing paper.

2.3.10 Voltammetric measurements with calcium phosphate and zirconium phosphate modified carbon paste electrode

Differential pulse anodic stripping voltammetry studies were carried out by immersing the modified electrode for a selected accumulation (in situ) time into voltammetric cell containing Pb(II) solution and without Pb(II) inos, in acidic medium, under constant stirring. After 10 seconds for quiescent conditions, the stripping was achived by scanning from -0.70 to -0.30 V in dp mode.

2.3.11 Calcium phosphate and copper(II) ferrocyanide modified carbon paste electrode preparation

The $Ca_3(PO_4)_2$ nanocrystals has been synthesized using calcium nitrate tetrahydrate and diammonium hydrogen phosphate mixture as the precursor. On the other hand, silica gel was activated by HCl for a day then washed with pure water until free chloride and was dried at 150 ^{o}C in oven. 4.0 mmol copper(II) ferrocyanide ($Cu_2Fe(CN)_6$) was mixed with activated silica gel for 1 hour, then washed with ultrapure water for many times to remove excess $Cu_2Fe(CN)_6$ on the silica surface.

The final product was red in colour. The mixture was dried at 50 ^{o}C in an oven for 24 hours. $Cu_2Fe(CN)_6$+$Ca_3(PO_4)_2$ modified carbon paste electrode was prepared by throughly mixing the 10.0 % $Ca_3(PO_4)_2$, 5.0 % $Cu_2Fe(CN)_6$, 5.0 % carbon nanotubes, 20.0 % mineral oil and 60.0 % spectroscopic grade graphite powder until obtaining uniformly wetting paste. The paste was then packed into home-made glass cylindrical tube (i.d. 3 mm). A silver wire was inserted into the opposite end to establish electrical contact. The exterior electrode surface was smoothed with weighing paper until obtain to shiny surface. After each use electrochemical study, the new fresh electrode surface of the paste electrode surface was simply renewed by scrapping off about 2-3 mm of the old surface and polished the new surface on a piece of tracing paper.

2.3.12 Voltammetric measurements with calcium phosphate and copper(II) ferrocyanide modified carbon paste electrode

Differential pulse anodic stripping voltammograms were recorded directly after immersion of the modified electrode into 10.0 mL solution of 0.20 mol L^{-1} CH_3COOH supporting electrolyte or Pb(II) ions at increasing concentration, containing supporting electrolyte with a selected period of time in accumulation. After 10 seconds for quiescent conditions, the stripping was achived by scanning from -0.60 to -0.30 V in dp mode.

2.3.13 Preparation of antimony-bismuth film modified multiwall carbon nanotubes coated glassy carbon electrode

The bare GCE was polished to a mirror using 0.30 micron Al_2O_3 powder, respectively, and rinsed thoroughly with ultrapure water between each polishing step. 10.0 μL of MWCNT suspension was injected on the bare GCE surface and then DMF of the suspension on the GCE surface was evaporated at 55˚C for one hour to fabricate modified MWCNT/GCE. A 10.0 mL supporting electrolyte solution was put into electrochemical cell to prepare Sb-Bi film electrode. From the 100.0 mg L^{-1} Sb(III) and 100.0 mg L^{-1} Bi(III) stock solution, 0.05 mL of Sb(III) ions and 0.03 mL of Bi(III) ions solutions were added into the electrolyte. Then, nitrogen gases get through 3 minutes to repel oxygen gases from the supporting electrolyte. During the preparetion of film electrode, a computer-controlled magnetic stirrer was employed to supporting electrolyte at 500 rpm. The preconcentration was carried out at -0.90 V for 180.0 s under stirring. After 180.0 seconds the film electrode was ready for measurement.

2.3.14 Voltammetric measurement for antimony-bismuth film modified multiwall carbon nanotubes coated glassy carbon electrode

10.0 mL potassium hydrogen tartrate was added into an electrochemical cell. Nitrogen was bubbled through the solution for 180.0 s to remove dissolved oxygen. The preconcentration was carried out at -0.90 V for 180.0 s under stirring to prepaire Sb-Bi-FE. The stirrer was shut off for 20 s to allow for quiescence After a 20 s equilibration period, the voltammogram was recorded by applying a positive-going SWASV potential scan from -0.90 to 0.40 V with a frequency of 15.0 Hz, a potential step of 4.0 mV, and an amplitude of 25.0 mV.

2.3.15 Preparation of tin-bismuth film modified mixture of multiwall carbon nanotubes and carbon paste electrode

The bismuth-tin-unmodified MWCNTs doped CPE was prepared. For this, 63.0 % graphite powder (0.315 g), 7.0 % MWCNTs (0.035 g) and 30.0 % mineral oil (0.15 g) were mixed in an agate mortar and the mixture was homogenized by hand-mixing. The mixed active carbon paste was subsequently packed into electrode shell (3.0 mm in diameter, 5.0-6.0 mm in depth).

The carbon paste electrode and the MWCNTs-CPE were manufactured by the same method. Tthe electrode surface was smoothed by polishing on a piece of paper. After then the electrodes were polished, the modification of MWCNTs-CPE with Bi-Sn film was carried out by in situ plating in the detection process. So, Bi-film modified mixture of MWCNT and CPE (Bi/MWCNTs-CP-FE), Sn- film modified mixture of MWCNT and CPE (Sn/MWCNTs-CP-FE) and Bi-Sn film modified mixture of MWCNT and CPE (Bi-Sn/MCNTs-CP-FE) were obtained.

2.3.16 Voltammetric measurement of tin-bismuth film modified mixture of multiwall carbon nanotubes and carbon paste electrode

Square wave anodic stripping voltammograms were recorded directly after immersion of the modified electrode into 10.0 mL solution of pH=4.5 CH_3COOH/CH_3COONa as a supporting electrolyte or the supporting electrolyte containing Cd(II). The preconcentration of Cd(II) ions was carried out at -1.0 V for 210.0 seconds with stirring. Then the stirring was stopped and after a 10.0 seconds equilibration period, the voltammogram was recorded by applying a positive-going SWASV potential scan from -1.0 to 0.4 V with a frequency of 25 Hz, pulse amplitude of 25 mV, and step increment of 10 mV. Prior to the next measurement, the electrode surface must be refreshed by a weighing paper.

3. RESULTS AND DISCUSSIONS

The thesis consists of mainly two parts. First section was dedicated to design and develop metal nanoparticles modified, based nickel, gold and palladium nanoparticles modified multiwall carbon nanotube glassy carbon electrode toward oxidation of ethanol and methanol molecules. The second section consists of the preparation of carbon pasta electrodes modified with various modifiers for selective determination of trace lead and cadmium.

3.1 Preparation and Characterization of Palladium, Gold and Nickel Nanoparticles Modified Multiwall Carbon Nanotubes/Glassy Carbon Electrodes

Voltammetric behaviour of MWCNT-GCE in the presence of $PdSO_4$+0.1 mol L^{-1} H_2SO_4 was studied (Figure 3.1). The deposition of Pd nanoparticles on the MWCNT/GCE surface corresponds to a reduction peak at -0.32 V and a partially reoxidation of Pd at 0.11 V in Figure 3.1. Stable peak currents were observed for both reduction and oxidation on the electrode reaction after the 10 CV cycles. A well-established feature of hydrogen adsorption and desorption was obatined at -0.85 V during the Pd nanoparticles decorated on the MWCNT/GCE. The hydrogen adsorption and desorption on the electrode surface indicating that the activity of Pd nanoparticles modified MWCNT/GCE is quite high (Casella and Contursi, 2006).
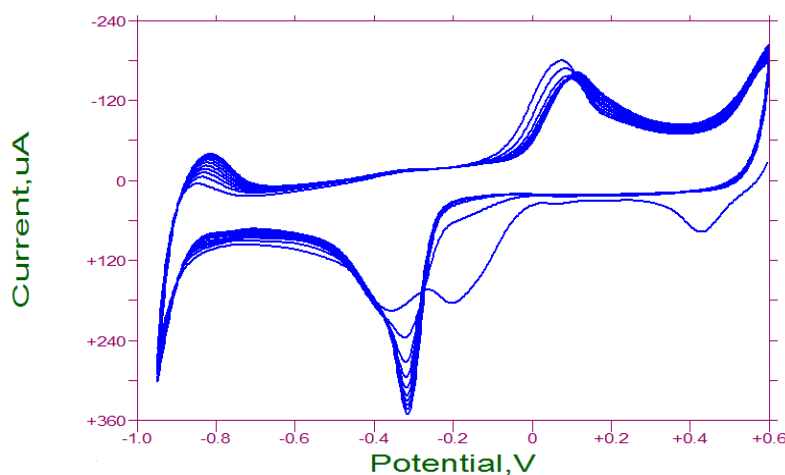
Figure 3.1 Consecutive cyclic voltammograms of palladium nanoparticles on MWCNT-GCE in a solution containing 1.0x10^{-3} mol L^{-1} PdSO$_4$ + 0.1 mol L^{-1} H$_2$SO$_4$ at 50 mV s^{-1} scan rate

Deposition of gold nanoparticles on the MWCNT/GCE electrodes in $HAuCl_4$+0.1 mol L^{-1} HCl solution was obtained in potential range between 0.6 V to -0.8 V (Figure 3.2). Figure 3.2 of CV showed that, Au nanoparticles obtained by Au(III) ions reduction at -0.371 V and partially reoxidation at 0.235 V. These datas are well aggrement with previous study (Bakır et al., 2011).
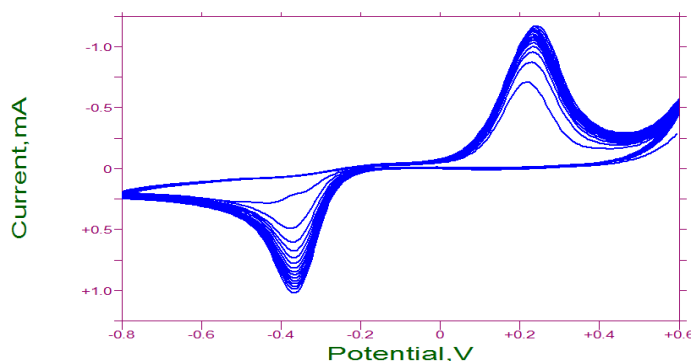
Figure 3.2 Consecutive cyclic voltammograms of gold nanoparticles on MWCNT-GCE in a solution containing 1.0x10^{-3} HAuCl$_4$ + 0.1 mol L^{-1} HCl at 50 mV s^{-1} scan rate

To formation of Ni nanoparticles on the MWCNT/GCE surface, cyclic voltammograms were recorded in the potential range between 0.65 V to -0.8 V in 1.0 mM $NiSO_4$+0.1 mol L^{-1} H_2SO_4 solution (Figure 3.3). A cathodic peak was observed at -0.195 V by reduction of Ni^{2+} to Ni metal. A partially reoxidation of metallic formed Ni was seen at -0.1 V during the anodic potential scan.
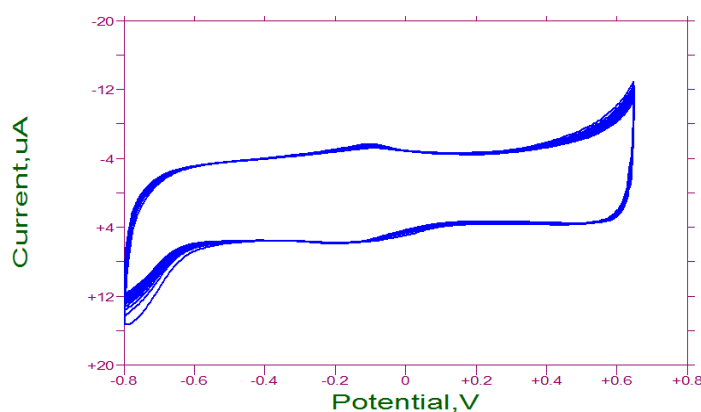
Figure 3.3 Consecutive cyclic voltammograms of nickel nanoparticles on MWCNT-GCE in a solution containing 1.0x10^{-3} NiSO$_4$ + 0.1 mol L^{-1} H$_2$SO$_4$ at 50 mV s^{-1} scan rate

3.2 Surface Characterization of The Electrodes

SEM images can effectively prove the morphological surface characterization of the modified electrodes. In the current study, the surface chemistry and morphologies of electrodes prepared using electrochemical deposition and chemical reduction prosedures were characterized by scanning electron microscopy, energy dispersive X-ray spectroscopy (EDX) and X-ray photoelectron spectoscopy.

3.2.1 Scanning electron microscopy images of the electrodes prepared by electrochemical deposition

Figures 3.4 a-g show the typical SEM images of the bare GCE, MWCNT/GCE and Pd, Au and Ni nanoparticles decorated MWCNT/GCE prepared by electrochemical deposition. As it is expected, the SEM image of smooth and homogeneous surface referes to the bare glassy carbon electrode (Figure 3.4 a). Compared with bare glassy carbon electrode surface, the morphology of the MWCNT on GC electrode showed a network-like structure (Figure 3.4 b).

On the other hand, the SEM image of Ni- MWCNT/GCE shows many observable light dots on network-like structure in SEM image of MWCNT/GCE given in Figure 3.4c. The average particle size of Ni-MWCNT/GCE was 96.0 nm. This SEM image confirms that nickel nanoparticles were bounded to MWCNT with almost uniform distribution. In contrast to the Ni-MWCNT/GCE, the distribution of gold nanoparticles on the end of MWCNT shows a few bright round-shaped aggregates (Figure 3.4d). The average particle size of Au-MWCNT/GCE was 102.0 nm.

Compared with the gold nanoparticles image, the SEM image shows that palladium nanoparticles are decorated on MWCNT ropes inside of network-like structure of carbon nanotubes. Also, palladium nanoparticles having smaller brigth dots were decorated with high particle density on the ropes (Figure 3.4e). The average particle size of Pd-MWCNT/GCE was 135.0 nm.
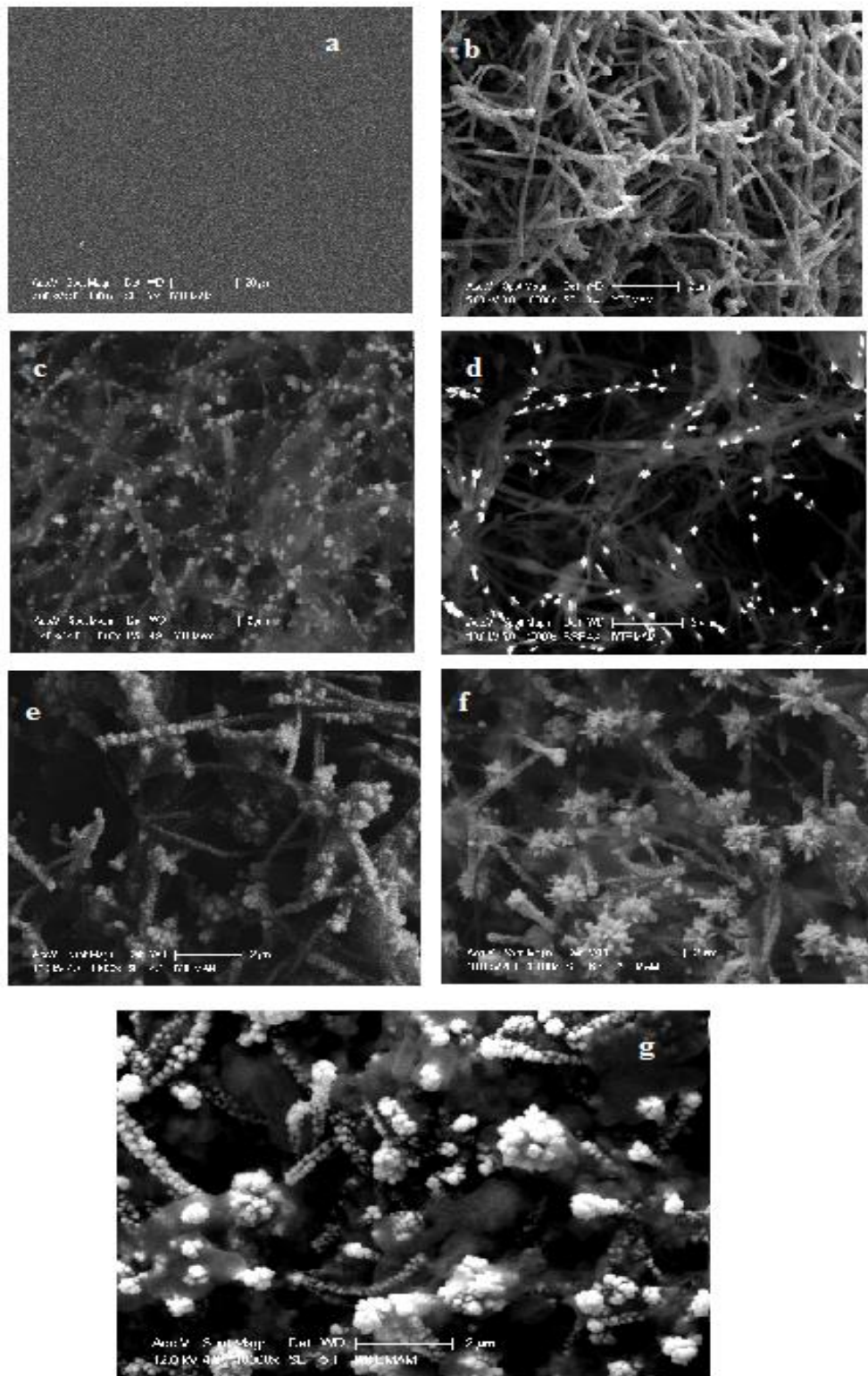
Figure 3.4 SEM image of a) Bare GCE b) MWCNT/GCE c) Ni-MWCNT/GCE d) Au-MWCNT/GCE e) Pd-MWCNT/GCE f) Pd-Au-MWCNT/GCE g) Pd-Au-Ni-MWCNT/GCE

In particular, the comparision of single metal nanoparticle decoreted carbon nanotubes with bimetallic nanoparticles was important. Because, the catalytic effect of bi-metallic nanoparticles modified electrodes is better than that of single metal nanoparticle. In this connection, the dispersed nanoparticles decorating as needle-like structure on through the ropes surface and as aggregates on the end of MWCNT ropes can be seen easly from the SEM images of Pd-Au-MWCNT/GCE (Figure 3.4f). This image corresponds to the large surface area. Probably, the large surface area which is seen in Figure 3.4f is responsible for better catalytic effect bi-metallic nanoparticles. The average particle size of Pd-Au-MWCNT/GCE was 165.0 nm.

The SEM image of Pd-Au-Ni-MWCNT/GC electrode surface shows more dense and big aggregate having larger surface area (Figure 3.4f). The aggregates were mostly decorated the end of MWCNT ropes. On the other hand, Pd, Au and Ni nanoparticles were decotated through the MWCNT ropes. This decoration is understandable from the bright round-shaped dots in the image. Among single, bi-metallic and tri metallic nanoparticles, tri metallic nanoparticles have largest surface area, which was provided the best catalytic effect. The average particle size of Pd-Au-Ni-MWCNT/GCE was 215.0 nm.
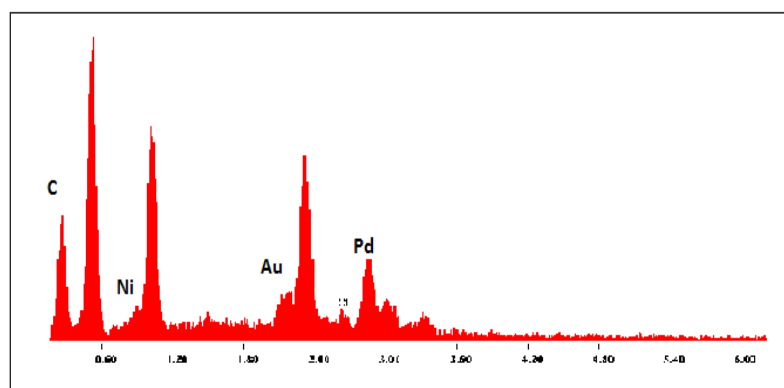
Figure 3.5 EDX spectrum of Pd-Au-Ni-MWCNT/GCE

EDX study confirmed the presence of nano Pd, Au and Ni particles decorating MWCNT/GCE, with the electrochemical deposition (Figure 3.5). The weight gain of the MWCNTs due to the Pd, Au and Ni loading were about 21.71 %, 8.64 % and 5.66 %, respectively. Finally, it can be claimed that a uniformly covered layer of Pd, Au and Ni nanoparticles modified MWCNT on the GCE can easily be prepared with the presence technique applied here according to SEM images.

71

3.2.2 Scanning electron microscopy images of the electrodes prepared by chemically reduction procedure

In this section, in stead of electrodeposition procedure to prepare metal nanoparticle modified electrodes, chemical reduction procedure was used. The surface properties of prepared electrode system such as palladium, gold and nickel nanoparticles decorated on MWCNTs were characterized. Figure 3.6a shows that nano nickel particles like light dots were formed as which homogeneously dispersed particles decorating on the electrode surface of MWCNT/GCE.

On the other hand, it was found that gold nanoparticles decorated on the MWCNTs have more homogeneous distribution than those of palladium and nickel nanoparticles. It can be seen from Figure 3.6 b, gold nanoparticles decorated on the multiwall carbon nanotubes wall surfaces were also more fine than the others. Compared with gold and nickel nanoparticles, the SEM image of palladium nanoparticles showed bright round-shaped which homogeneously dispersed particles decorating on the electrode surface, but not high particle density (Figure 3.6 c).
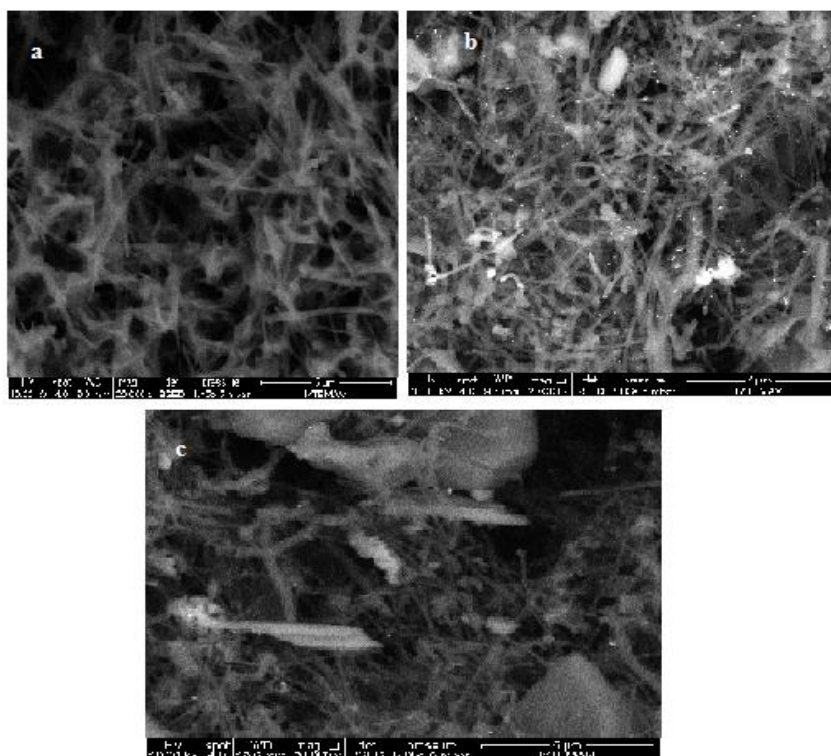
Figure 3.6 SEM images of a) Ni-MWCNT/GCE b) Au-MWCNT/GCE c) Pd-MWCNT/GCE

With comparision of both the decorating procedures used for the each modified electrodes, their SEM images show that electrodeposition procedure provides more homogeneous distrubition and higher particle density. As a result, we were prefered to use the electrodeposition procedure for the decorating of metal nanoparticles on the MWCNTs for alcohol oxidation.

3.2.3 Chemical characterization of modified electrodes by X-Ray photoelectron spectroscopy

The surface chemistry of the Pd-MWCNT, Au-MWCNT and Ni-MWCNT electrode systems were characterized by XPS. The state of palladium deposited on CNTs can be further identified from Figure 3.7 a. The XPS spectrum of Pd illustrates 3d regions of Pd-MWCNT composites which reveals the presence of Pd 3d5/2 and 3d3/2 peaks at binding energy of 335.2 and 340.5 eV, respectively. Such binding energy values are in accordance with those reported for metallic Pd (Bera et al., 2004).

XPS spectrum of the Au-MWCNT hybrid (Figure 3.7 b) shows the 4f7/2 and 4f5/2 doublet with the binding energies (BE) of 86.7 and 90.4 eV, respectively, which are typically characteristic of Au0 (Zhang et al., 2006).

The high-resolution XPS spectra of the Ni 2p3/2 core energy level for the Ni-MWCNT sample is shown in Figure 3.7c. The Ni 2p3/2 energy level was centered around 856.0 eV with asymmetry in the higher binding energy side. The Ni 2p3/2 spectrum was deconvoluted for four differently bound Ni species with the BE values 859.6, 865.6, 877.7 and 883.7 eV.
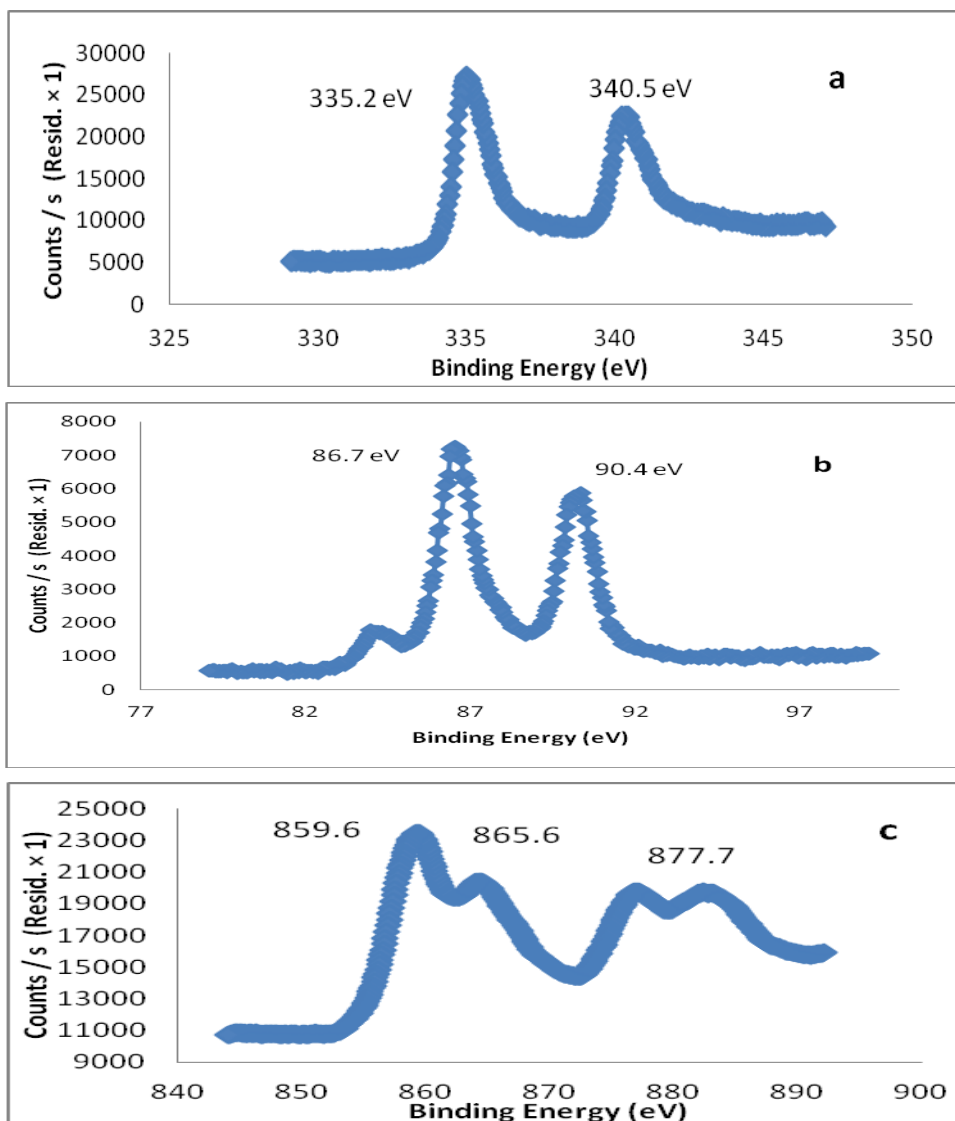
Figure 3.7 XPS of a) Pd-MWCNT hybrid b) Au-MWCNT hybrid c) Ni-MWCNT hybrid

3.2.4 X-Ray diffraction studies for metal nanoparticles modified electrodes decorated by electrochemical deposition

Figure 3.8 shows the X-Ray diffraction (XRD) patterns of the Pd-Au-Ni-MWCNT/GCE. It can be seen that the first double peak located at a 2θ value of about 23.5° belongs to multiwall carbon nanotubes.

The other three peaks corresponds to Au (1 1 1), Pd (1 1 1) and Ni (1 1 1) at 2θ values of about 38.1°, 40.0° and 43.3°, respectively, in gold, palladium and nickel structures.
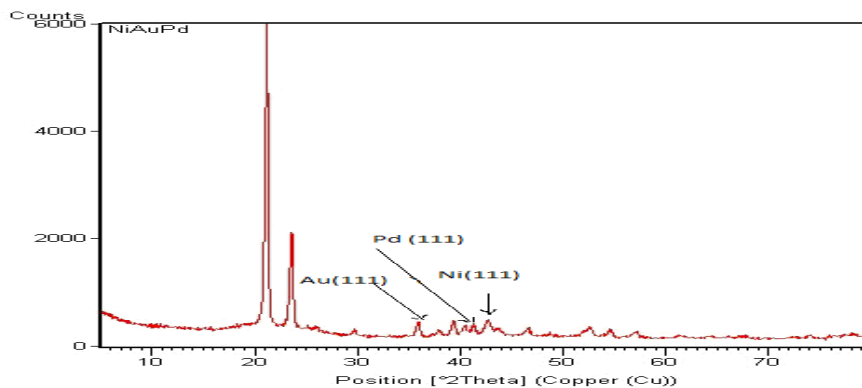
Figure 3.8 XRD patterns of Pd-Au-Ni-MWCNT/GCE

3.2.5 Tafel slopes for metal nanoparticles modified electrodes decorated by electrochemical deposition
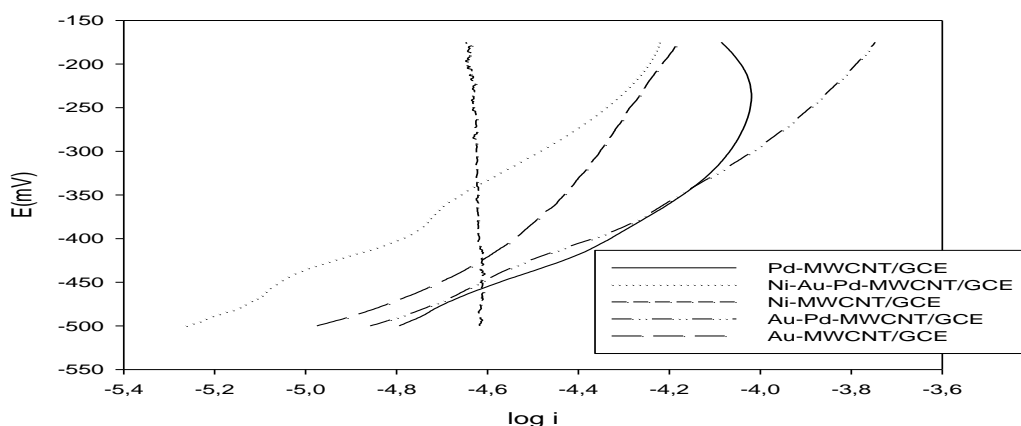
Figure 3.9 Tafel slopes of ethanol oxidation on different electrodes for 3mV s^{-1} scan rate

Tafel behavior was studied in the mixed kinetic diffusion control region with 3.0 mVs^{-1} scan rate at different types of electrodes. Figure 3.9 shows the Tafel plot of the Pd-MWCNT/GCE, Pd-Au-Ni-MWCNT/GCE, Ni-MWCNT/GCE, Pd-Au-MWCNT/GCE, Au-MWCNT/GC electrodes.

In the low potential range of -0.5 V to -0.4 V, we can assume that the adsorption process of ethoxi is independent of the potential and follows the Temkin-type isotherm. Therefore, the kinetics of the ethanol in the potential region of -0.5 V to -0.4 V is dominated by the adsorption of hydroxyl on the Ni-Au-Pd-MWCNT/GC electrode.

As the potential increases, Tafel slope indicates that the kinetics of the ethanol is not controlled only by the adsorption of hydroxyl, but it is also affected by other surface reactions. At the higher potentials, the oxide layer might form on the surface of the Pd-Au-Ni-MWCNT/GC electrode, causing the kinetics. These indicated that the Tafel slope of the ethanol increases with the potential.

3.3 Voltammetric Behaviour of Ethanol

In this thesis, ethanol and methanol electrocatalytic oxidation behaviours were investigated using cyclic voltammetry. For this, the effect of pH, alcohol concentration, scan rate on their oxidation behaviours were evaluated by use of various electrode types such as; bare GCE, MWCNT/GCE, Au-MWCNT/GCE, Pd-MWCNT/GCE, Ni-MWCNT/GCE, Au-Pd-MWCNT/GCE, Au-Ni-MWCNT/GCE, Pd-Ni-MWCNT/GCE and Ni-Au-Pd-MWCNT/GCE. The modified electrodes used in these experiments were prepared by electrochemical and chemical reduction procedures. The results obtained for alcohol oxidation behavior were discussed following sections.

3.3.1 Voltammetric behaviour of ethanol at different electrolyte systems

The voltammetric behaviour of ethanol at various electrode systems was investigated at different pHs of electrolyte solution. pH is one of important parameters on electrocatalytic oxidation of methanol and ethanol (Pereira et al., 2013).

Therefore, the effect of pH on oxidation of ethanol was examined using different buffer solutios such as; acetate buffer (3.76-5.76), phosphate buffer (6.0-8.0), borate buffers (8.2-8.6) and Britton-Robinson buffers (3.0-10.0) and also alkaline solutions at bare and modified electrodes.

To test Britton-Robinson (BR) buffers as the supporting electrolyte, firstly the effect of pH on the ethanol oxidation peak current and peak potential was investigated in pH range of 3.0 to 10.0 at bare GCE, MWCNT/GCE, Au-MWCNT/GCE and Pd-MWCNT/GC electrodes.
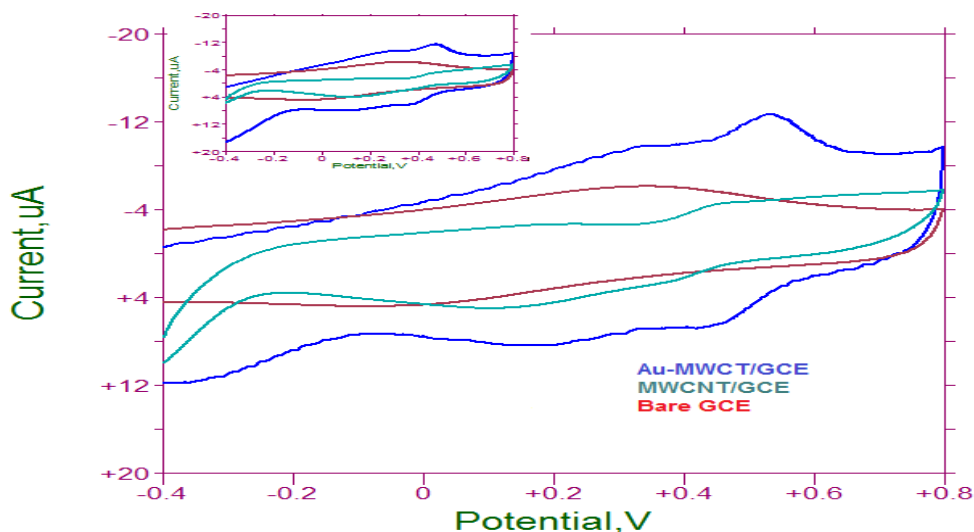
Figure 3.10 Cyclic voltammograms of 0.5 mol L^{-1} ethanol at Britton-Robinson buffers (pH=4) on bare GCE, MWCNT/GCE and Au-MWCNT/GCE at 50 mV s^{-1} scan rate (the inset shows blanks at the same conditions)

Figure 3.10-3.12 indicate that the voltammograms of supporting electrolyte (pH=4.0-9.0 BR Buffer) and ethanol oxidation were in similar to each other with GCE, MWCNT/GCE and Au-MWCNT/GC electrodes. Therefore, it may be concluded that these electrodes was not show any catalytic effect for ethanol oxidation, by comparing both the voltammograms.
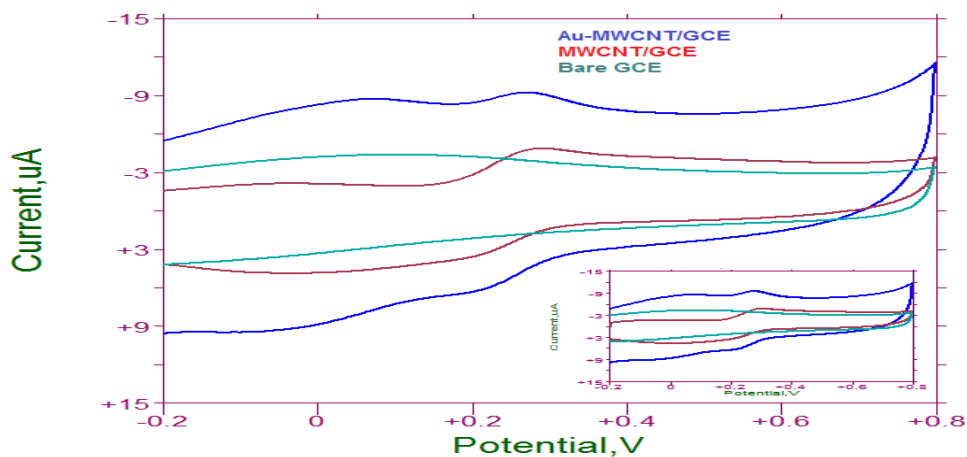
Figure 3.11 Cyclic voltammograms of 0.5 mol L^{-1} ethanol at Britton-Robinson buffers (pH=7) on bare GCE, MWCNT/GCE and Au-MWCNT/GCE at 50 mV s^{-1} scan rate (the inset shows blanks at the same conditions)
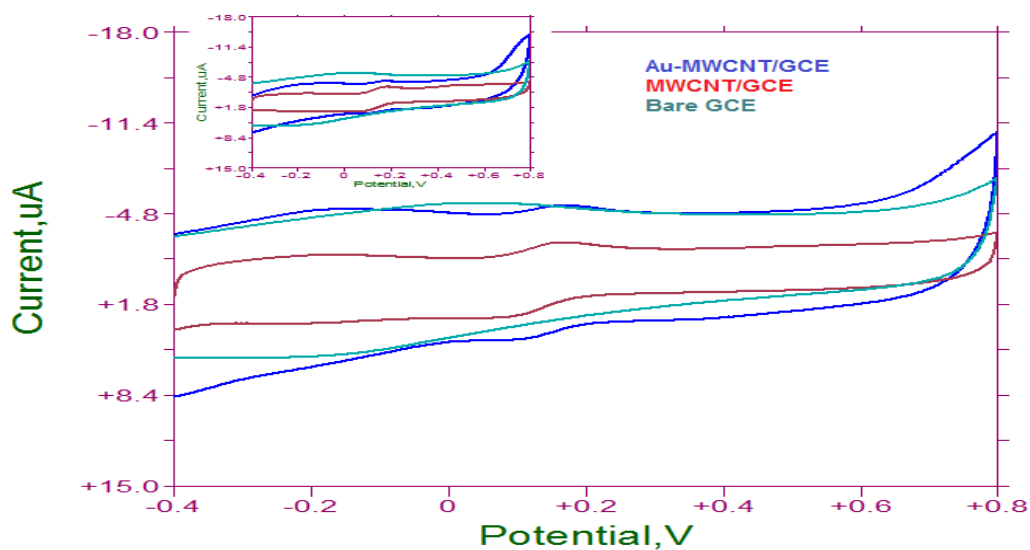
Figure 3.12 Cyclic voltammograms of 0.5 mol L^{-1} ethanol at Britton-Robinson buffers (pH=9) on bare GCE, MWCNT/GCE and Au-MWCNT/GCE at 50 mV s^{-1} scan rate (the inset shows blanks at the same conditions)
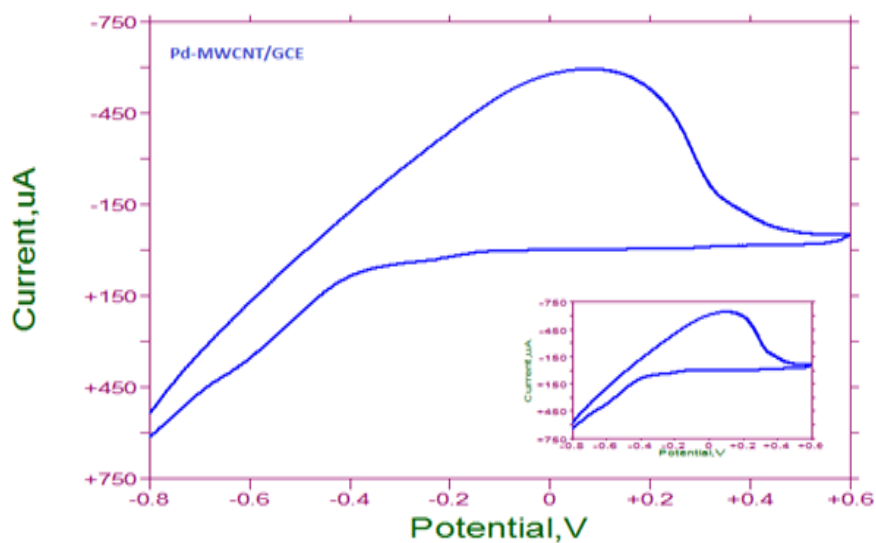
Figure 3.13 Cyclic voltammograms of 0.5 mol L^{-1} ethanol at Britton-Robinson buffers (pH=4) on Pd-MWCNT/GCE at 50 mV s^{-1} scan rate (the inset shows blanks at the same conditions)

As can be seen from Figure 3.13, at anodic potential scan, a broad oxidation peak was observed at Pd-MWCNT/GCE in the presence and in the absence of ethanol. The broad peak was related with adsorption of hydrogen on the Pd nanoparticles. Therefore, it may be concluded that the Pd-MWCNT/GCE does not show any catalytic effect for ethanol oxidation in the presence conditions.
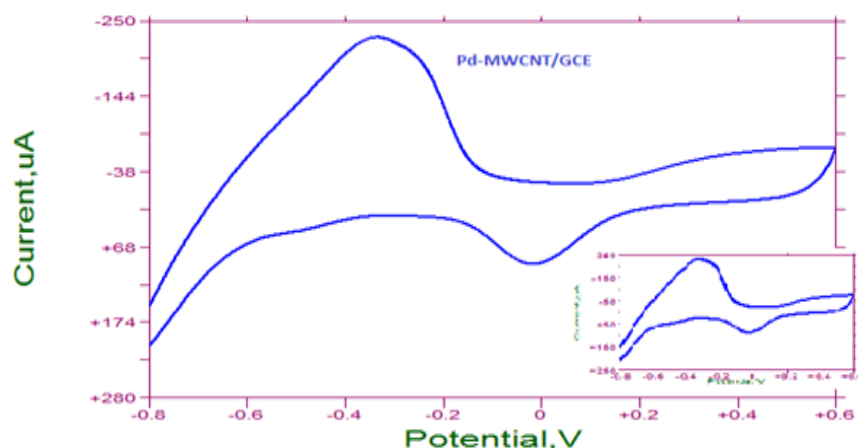
Figure 3.14 Cyclic voltammograms of 0.5 mol L^{-1} ethanol at Britton-Robinson buffers (pH=7) on Pd-MWCNT/GCE at 50 mV s^{-1} scan rate (the inset shows blanks at the same conditions)

Figure 3.14 displayed voltammetric behaviour of Pd-MWCNT/GCE in pH 7.0 BR buffer solution in the absence (the inset voltammograms) and in the presence of ethanol. The CV responses of the Pd-MWCNT/GCE were in general similar for both in the absence and presence of ethanol in pH 7.0 BR buffer solution. Two oxidation peaks at -0.50 V and 0.35 V were observed for both voltammograms during the anodic potential scan and a reduction peak at 0.01 V in the presence and the absence of ethanol for cathodic scan.
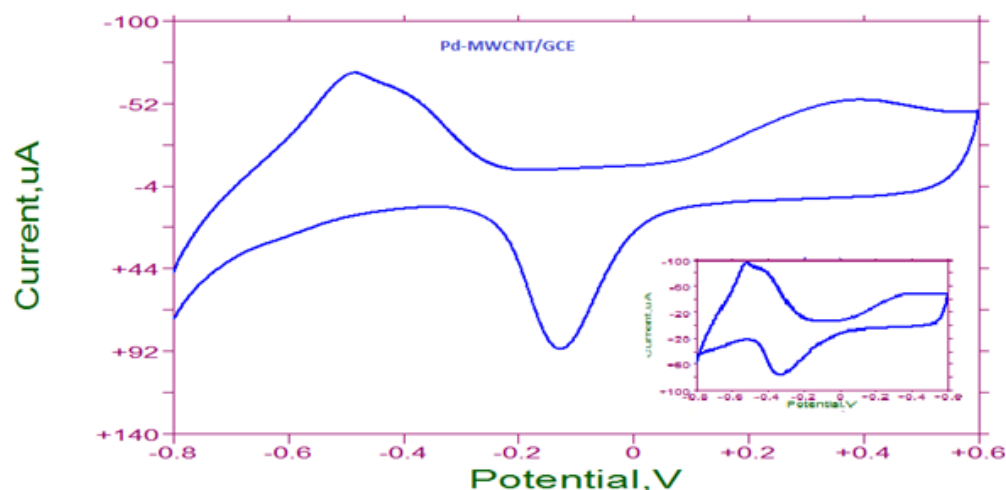
Figure 3.15 Cyclic voltammograms of 0.5 mol L^{-1} ethanol at Britton-Robinson buffers (pH=9) on Pd-MWCNT/GCE at 50 mV s^{-1} scan rate (the inset shows blanks at the same conditions)

Figure 3.15 displayed voltammetric behaviour of Pd-MWCNT/GCE in pH 9.0 BR buffer solution in the absence (the inset voltammograms) and in the presence of ethanol. The CV responses of the Pd-MWCNT/GCE were in general similar for both in the absence and presence of ethanol in pH 9.0 BR buffer solution. Two oxidation peaks at -0.50 V and 0.35 V were observed for both voltammograms during the anodic potential scan and a reduction peak at -0.13 V in the presence of ethanol and at -0.33 V in the absence of ethanol for cathodic scan. The current peak at -0.50 V related to adsorption hydrogen evaluation and oxidation peak at 0.35 V to Pd oxide formation and reduction of this Pd oxide at -0.13 or -0.33 V on Pd-MWCNT/GCE surface. From the cyclic voltammograms, Pd-MWCNT/GCE was not also show any electrocatalytic oxidation of ethanol in pH 9.0 BR buffer solution.

3.3.2 Electrochemical behaviour of ethanol in the presence of alkaline solutions at bare glassy carbon and modified multiwall carbon nanotubes/glassy carbon electrodes

The studies above showed that there was no any cataytic actvity on ethanol oxidation at all electrodes. Therefore, to find an electrocatalytic activty with both bare glassy carbon and modified MWCNT/GC eletrodes the experimentals were performed in alkaline solutions.

In initial stuides, the cyclic voltammetric behaviour of ethanol was studied at bare GCE in different concentration of NaOH solutions (in the range of 0.1-4.0 M). The obtained voltammograms in the absence and presence of ethanol were given in Figure 3.16-3.18.However, there was no any oxidation or reduction for all NaOH solution in the absence of ethanol at bare GCE but an irreversible oxidation peak for ethanol was appeared at -0.07 V at bare GCE. The peak current was also increased by increasing ethanol concentration (Figure 3.17). A reverse oxidation peak was appeared during the cathodic potential scan due to the adsorption of ethanol oxidation product on the electrode surface as obtained published data (Mahapatra and Datta, 2011).

The studies above showed that the evaluation of catalytic effects of bare GCE, MWCNT/GCE, Pd-MWCNT and Pd-Au-MWCNT/GCE and Pd-Au-Ni-MWCNT/GCE systems for ethanol oxidation was required alkaline media as a supporting electrolyte.

Thus, electrochemical behaviour of ethanol using these catalytic systems was investigated in NaOH solution at different concentrations in detail. A significant oxidation current of ethanol in the range of 0.1-3.0 mol L^{-1} was not obtained in presence of different concentrations of NaOH as a supporting electrolyte (Figure 3.16).
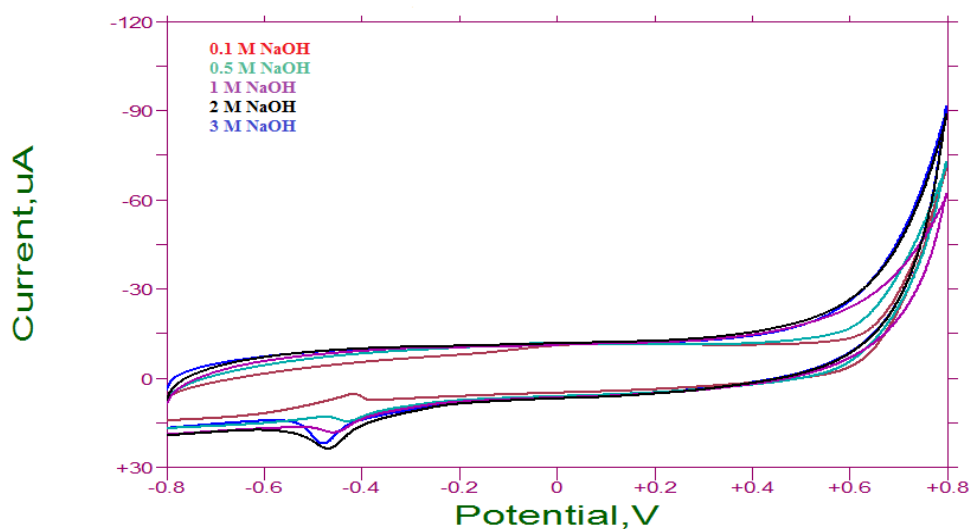
Figure 3.16 Cyclic voltammetric behaviour of bare GCE in alkaline solutions as a supporting electrolyte. The scan rate was 50 mV s^{-1}
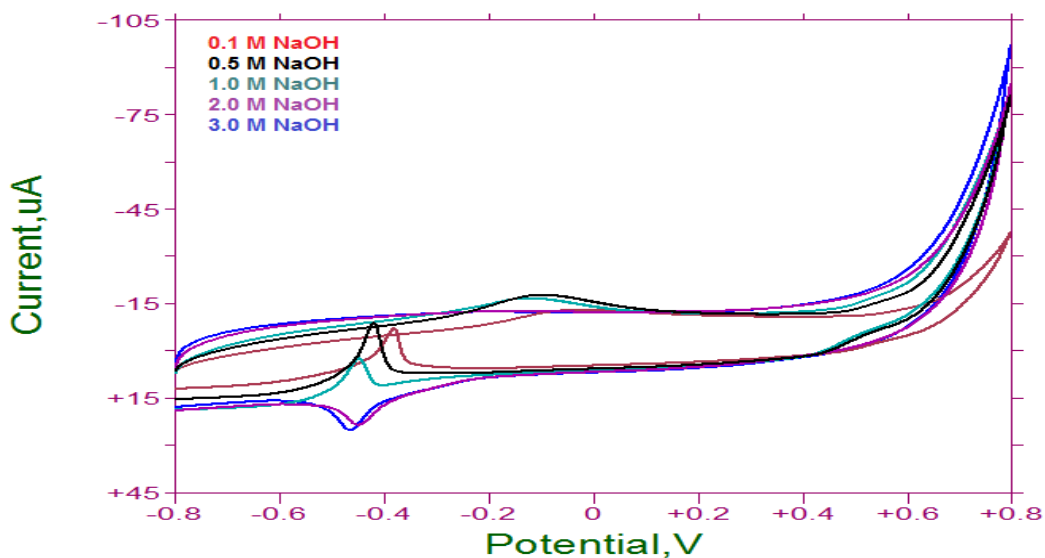
Figure 3.17 Cyclic voltammetric behaviour of bare GCE in the presence of 2.0 mol L^{-1} ethanol for different concentration of NaOH solutions. The scan rate was 50 mV s^{-1}
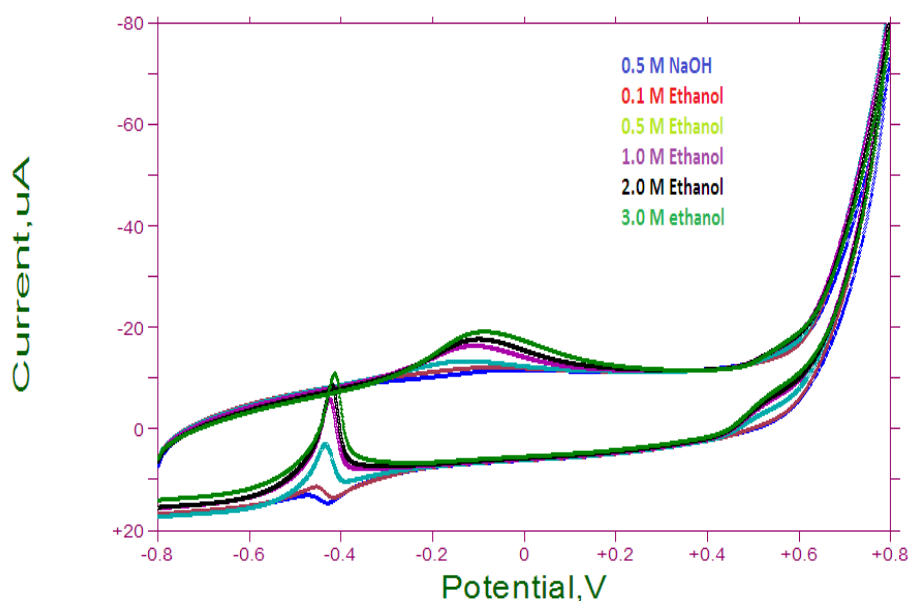
Figure 3.18 Cyclic voltammograms of ethanol oxidation at increasing concentration in presence of 0.5 mol L^{-1} NaOH with bare GCE at 50 mV s^{-1} scan rate

Although, the bare GC electrode was shown a weak electrocatalytic activity toward on the oxidation of ethanol in alkaline media, but the obtained cyclic voltammograms were not significant for ethanol based fuel cell catalytic anode electrode surfaces. Therefore, to improve the catalytic activity for ethanol, the GCE surface was modified with MWCNT and different mono, bi and three metal nanoparticles modified MWCNT/GCE and compare to bare polycrystalline gold, palladium electrodes.

Figure 3.19-3.20 shows cyclic voltammograms of MWCNT/GCE in alkaline solutions in the absence and in the presence of ethanol. There was no any oxidation or reduction signal in the presence of different NaOH concentration on MWCNT/GC electtrode.
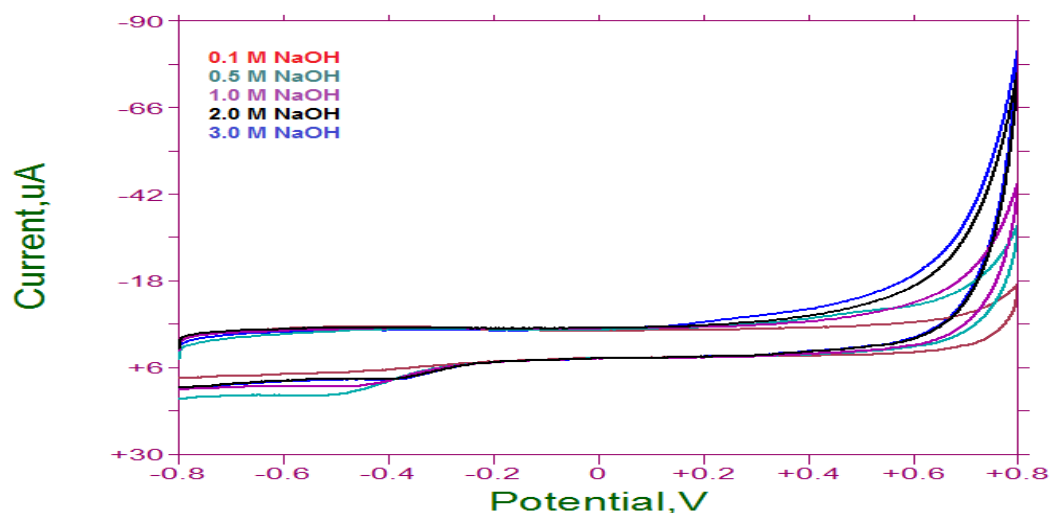
Figure 3.19 Cyclic voltammetric behaviour of MWCNT/GCE in alkaline solutions as a supporting electrolyte. The scan rate was 50 mV s^{-1}

A small oxidation peak for 2.0 mol L^{-1} ethanol was observed about 0.329 V with 5.223 μA in the presence of 3.0 mol L^{-1} NaOH at MWCNT/GCE.
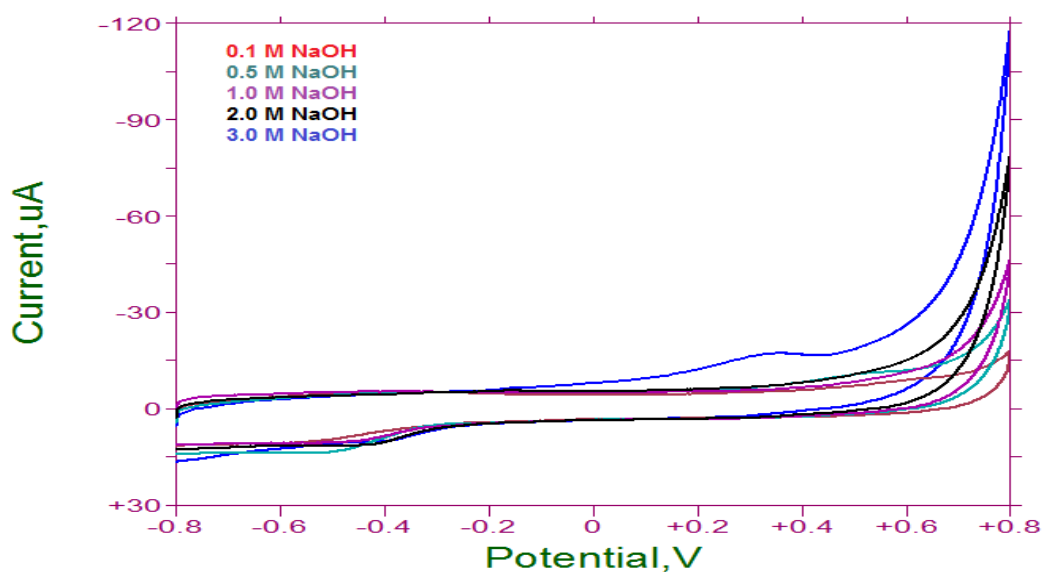
Figure 3.20 Cyclic voltammetric behaviour of MWCNT/GCE in the presence of 2.0 mol L^{-1} ethanol for different concentration of NaOH solutions. The scan rate was 50 mV s^{-1}

The results show that bare glassy carbon electrode and MWCNT/GCEs have not higher catalytic actvity towards ethanol oxidation in the presence conditions.

On the other hand, the electrochemical reactivity of ethanol is slightly lower at bare and without metal nanoparticles modified electrodes. It is necessary to achieve its complete oxidation to CO_2 with 12 electrons per molecule for maximum energy recovery from ethanol in fuel cell technology. Nevertheless, breaking the C-C bond is difficult to promote by electrochemical means. Partial oxidation of ethanol can lead to the formation of acetaldehyde, acetic acid, or carbon monoxide, which can be easily adsorbed on the electrode surface and decrease its catalytic activity towards ethanol oxidation (Calvillo et al., 2013).

To improve electrocatalytic activity of MWCNT/GCE on ethanol oxidation, the electrode surfaces were modified with Au, Pd and Ni metal nanoparticels as single, binary and triple metallic forms. In our preliminary experiments with metal based electrodes the polycrystalline noble metal electrodes were used for electroctalytic oxidation of ethanol to obtaine optimum experimental conditions and the compared the results with metal nanoparticles modified electrodes.

3.3.2.1 Voltammetric behaviour of ethanol at palladium and gold disk electrode in alkaline solutions

Figure 3.21 shows the cyclic voltammograms for the Pd disk electrode in concentration range of 0.1-3.0 mol L^{-1} NaOH solution. An oxidation signal was observed at more positive potential for Pd disk electrode during anodic potential scan. There was a reduction peak for palladium oxide species in the reverse potential scan in all NaOH concnetrations. However, the peak current was increased, but the reduction peak potential was shifted towards negative potential by increasing of NaOH concentration. The ethanol oxidation voltammograms on the Pd disk electrode in concentration of 0.1-3.0 mol L^{-1} NaOH solutions were presented in Figure 3.22 and they were all characterized by two well defined oxidation peaks in the anodic sweep voltammograms and revers oxidation peaks in the cathodic sweep voltammograms. The oxidation peak potential was shifted to negative potential by increasing NaOH concentration. The reverse oxidation peak was occured due to the partial oxidation of ethanol and the formation of acetaldehyde, acetic acid, or carbon monoxide, which can be easily adsorbed on the electrode surface and decrease its catalytic activity towards ethanol oxidation.

By comparing with above all results cyclic voltammograms in the absence and presence of ethanol, the Pd disk electrode has higher catalytic activity towards ethanol oxidation.
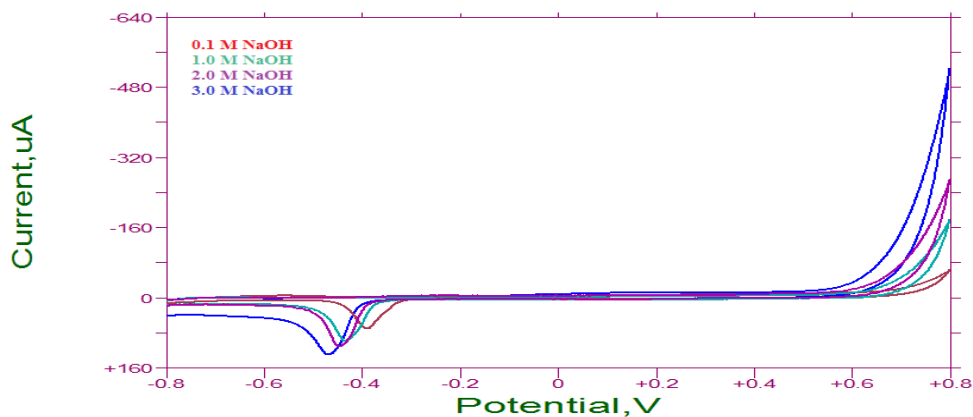
Figure 3.21 Cyclic voltammetric behaviour of polycrystalline Pd disk electrode in alkaline solutions. The scan rate was 50 mV s^{-1}
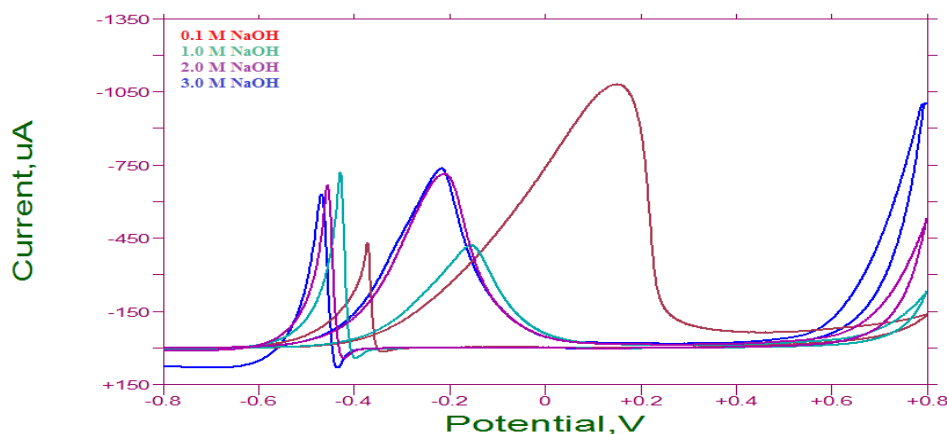
Figure 3.22 Cyclic voltammetric behaviour of polycrystalline Pd disk electrode in the presence of 2.0 mol L^{-1} ethanol for different concentration of NaOH solution. The scan rate was 50 mV s^{-1}

The cyclic voltammetric behaviour of Au disk electrode in alkaline solution was also examined in the absence and presence of ethanol in manner of Pd disk electrode studies. Figure 3.23 shows the cyclic voltammograms for the Au disk electrode in concentration range of 1.0-3.0 mol L^{-1} NaOH solution. An oxidation peak and two reduction peaks were appeared for Au species during the both anodic and cathodic potential scan in the presence conditions. An ethanol oxidation was observed at about 0.1 V on Au disk electrode and a small reverse oxidation peak was also apperaed at 0.0 V during the cathodic potentail scan. The main oxidation peak current was increased by increasing of NaOH concentration (Figur 3.24).
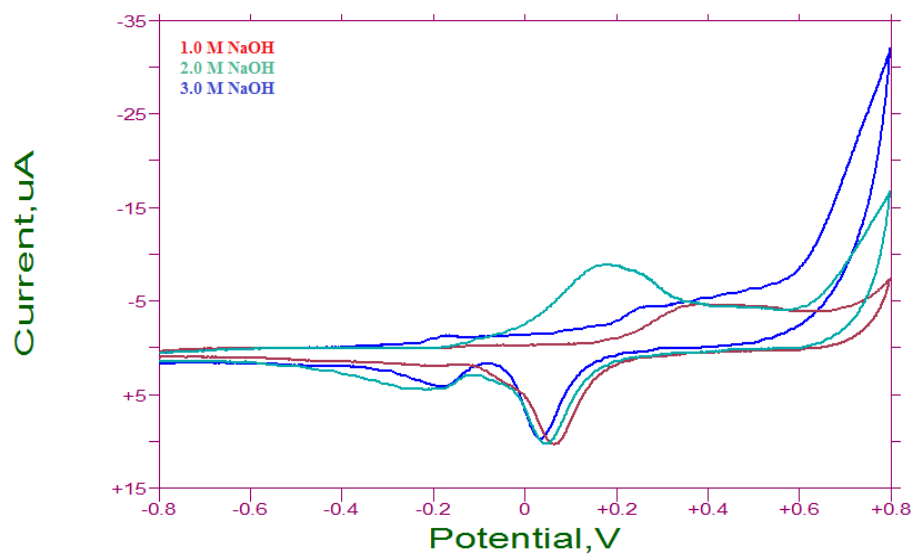
Figure 3.23 Cyclic voltammetric behaviour of polycrystalline Au disk electrode in alkaline solutions. The scan rate was 50 mV s^{-1}
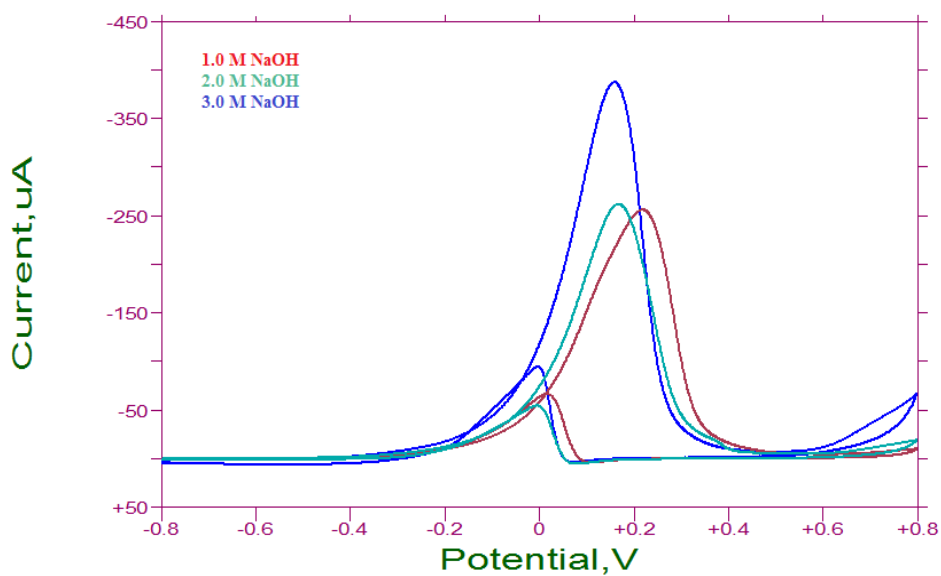
Figure 3.24 Cyclic voltammetric behaviour of polycrystalline Au disk electrode in the presence of 2.0 mol L^{-1} ethanol for different concentration of NaOH solutions. The scan rate was 50 mV s^{-1}

The oxidation peak current was linearly with increasing of ethanol concentration at 2.0 mol L^{-1} NaOH solution on both Pd and Au polycrystalline electrodes (Figure 3.25 and 3.26).

Figure 3.25 Cyclic voltammograms of ethanol oxidation at increasing concentration in presence of 2.0 mol L^{-1} NaOH with Pd disk electrode at 50 mV s^{-1} scan rate

Figure 3.26 Cyclic voltammograms of ethanol oxidation at increasing concentration in presence of 2.0 mol L^{-1} NaOH with Au disk electrode at 50 mV s^{-1} scan rate

By comparing the obtained results with Pd disk electrode, Pd disk was higher catalytic activity towards ethanol oxidation by means of peak potential at about -0.213 V and peak current for main oxidation peak. But in the case of reverse peak formation, the carbonaceous species can not strongly adsorb on the Au disk electrode surface compare with Pd disk electrode at all NaOH concentrations. These results shows that using of Au and Pd metal on the same electrode surface, the bimetallic electrode could be shown higher catalytic activity towards ethanol oxidaton.

3.3.2.2 Electrochemical behaviour of ethanol in the presence of alkaline solutions at Au, Pd and Ni nanoparticles modified multiwall carbon nanotubes/glassy carbon electrodes

The oxidation of ethanol on a bulk or polycrystalline noble metal electrodes is followed by the formation of CH_xO-like intermediates which are strongly adsorbed on the catalyst surface. These formations considerably reduce the electroactivity of ethanol. Electrochemical experiments have shown that carbon dioxide, acetaldehyde and acetic acid are produced in the oxidation of ethanol on polycrystalline noble metal electrodes. Noble metals are extremely rare and expensive metals for fuel cell systems. To overcome these problems, preparation of new noble metal containing modified electrodes has been proposed.

Metal nanoparticles especially noble metal nanoparticles on lots of substrates offer unique property as electrocatalyst towards electrocatalytic oxidation of small organic compounds. Therefore, Au, Pd and Ni nanoparticles modified MWCNT/GC electrodes were used in future studies for ethanol oxidation.

Our literature review reveals that Pd catalysts can be suitable for alkaline-type direct alcohol fuel cell (DAFC) (Liang et al., 2009). In this study, this alternative was evalutaed for ethanol oxidation using glassy carbon electrode modified with multiwall carbon nanotube electrodeposited with palladium nanoparticles ($Pd_{(10cyc)}$-MWCNT/GCE). The experiments were carried out in presence of 0.1-3.0 mol L^{-1} NaOH solutions.

Figure 3.27 shows the cyclic voltammograms for the Pd nanoparticle modified MWCNT/GCE in the concentration range of 0.1-3.0 mol L^{-1} NaOH solution. An oxidation signal was observed at more positive potential for Pd nanoparticles during the anodic potential scan. There was a reduction peak for pallaium oxide species in the reverse potential scan in all NaOH concnetrations and the peak characteristics were also varied with NaOH concentration. The peak current was increased by increasing of NaOH concentration while the reduction peak potential was shifted towards negative potential.
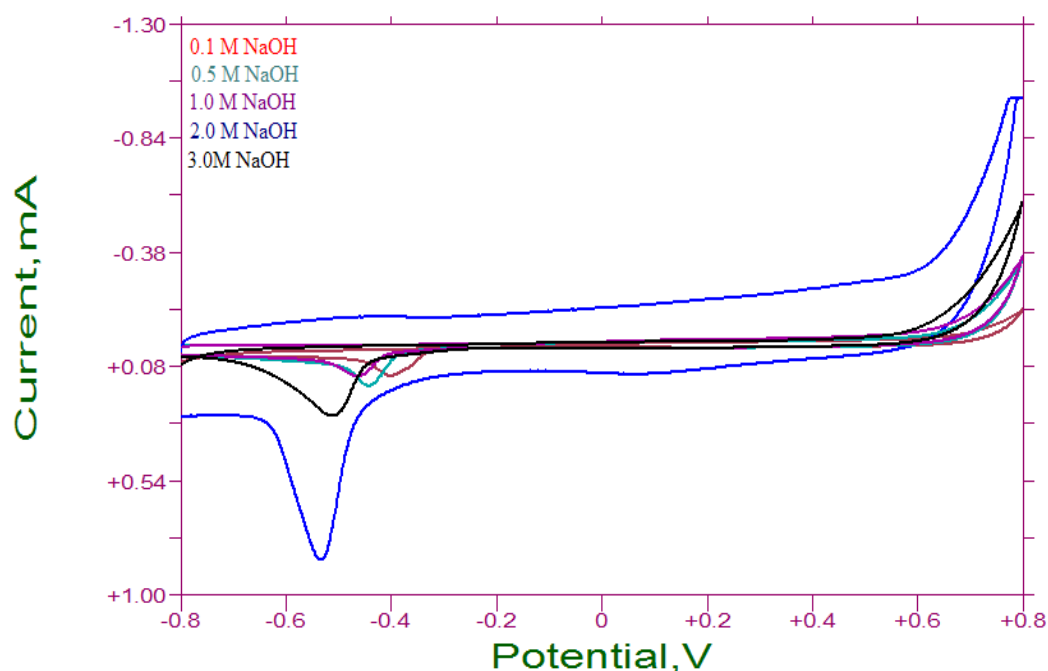
Figure 3.27 Cyclic voltammetric behaviour of Pd nanoparticles modified MWCNT/GC electrode in alkaline solutions as a supporting electrolyte. The scan rate was 50mV s^{-1}

Since the pH effect of supporting electrolyte solution on the ethanol oxidation on Pd nanoparticle modified MWCNT/GCE, it was important to study the effect of NaOH concentration on ethanol oxidation. The effect of NaOH concentration on ethanol oxidation on Pd nanoparticle modified MWCNT/GCE was studied in 2.0 mol L^{-1} ethanol with different NaOH concentration and the results were depicted in Figure 3.28. A well defined two oxidation peaks were observed in both anodic potential scan and cathodic potential scan which is called reverse oxidation peak. The oxidation peak potential was shifted to negative potential while peak current increased by increasing NaOH concentration. The reverse oxidation peak was occured due to the partial oxidation of ethanol and the formation of acetaldehyde, acetic acid or carbon monoxide, which can be easily adsorbed on the electrode surface and decrease its catalytic activity towards ethanol oxidation.

Figure 3.28 Cyclic voltammetric behaviour of Pd nanoparticles modified MWCNT/GC electrode in the presence of 2.0 mol L^{-1} etanol for different concentration of NaOH solutions. The scan rate was 50 mV s^{-1}

The variation of peak currents and peak potentials obtained with Pd-MWCNT/GCE for 1.0 mol L^{-1} ethanol was summarized in Table 3.1. Both the highest peak current and the lowest negative peak potential were obtained at 2.0 mol L^{-1} NaOH solution. Thus the supporting solutions were chosen as a most optimum supporting electrolyte.

Table 3.1 Change of peak currents and peak potentials obtained with Pd-MWCNT/GCE for 2.0 mol L^{-1} ethanol

NaOH Solution Concentration (mol L^{-1})	Peak Current (µA)	Peak Potential (V)
0.1	64.1	-0.067
0.5	109.0	-0.136
1.0	47.6	-0.142
2.0	**110.1**	**-0.187**
3.0	72.1	-0.186

3.3.2.3 Effect of glassy carbon electrode modified with multiwall carbon nanotube electrodeposited with gold nanoparticles (Au-MWCNT/GCE)

Over the years, it is well-known that gold nanoparticles are a highly active catalyst for many reactions of both industrial and environmental importance such as selective CO oxidation and hydrogenation reactions (Pitois et al., 2011). In addition to this, gold and some binary alloys of gold are promising active catalysts for alcohol oxidation in alkaline media (Ye et al., 2012). Thus, the probable catalytic effect of gold nanoparticles was investigated multiwall carbon nanotube modified with gold nanoparticles for ethanol oxidation in 2.0 mol L^{-1} NaOH solutions as supporting electrolyte (Figures 3.29). The ethanol oxidation was observed at +0.248 V for 0.5 mol L^{-1} ethanol. As it is expected the findings for the other modified electrodes discussed above, with increasing of ethanol concentration the oxidation potential shifted to more positive potential. On the other hand, the peak current obtained with Au-MWCNT/GCE was smaller than those of other modified electrodes.
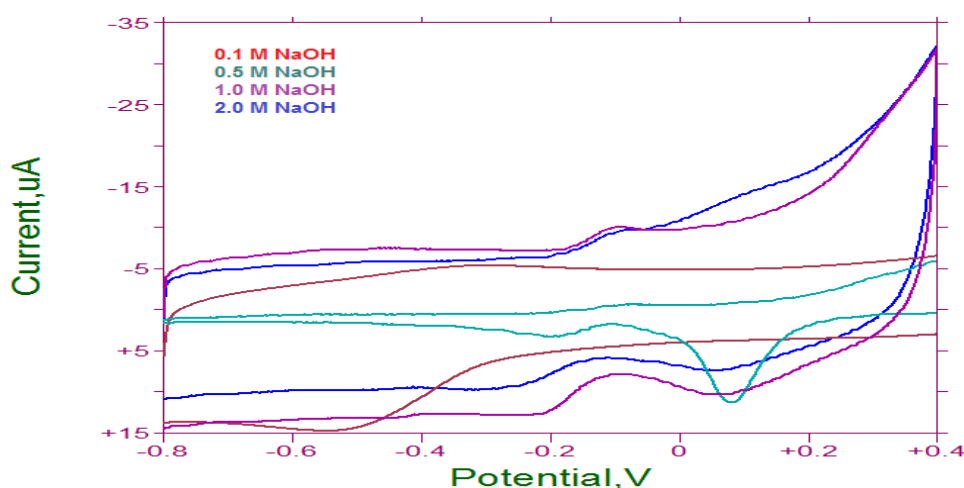
Figure 3.29 Cyclic voltammetric behaviour of Au nanoparticles modified MWCNT/GC electrode in alkaline solutions as a supporting electrolyte. The scan rate was 50 mV s^{-1}

The voltammetric behaviour of Au nanoparticle modified MWCNT/GCE was studied in presence of 2.0 mol L^{-1} ethanol in the concentration range of 0.1-2.0 mol L^{-1} NaOH (Figure 3.29). The ethanol oxidation on Au nanoparticle modified MWCNT/GCE was observed at higher positive potentials in comparison to both polycrystalline Au disk and Pd nanoparticle modified MWCNT/GC electrodes for all NaOH concentrations.

On the other hand, the peak current was increased by increasing NaOH concentration on the Au nanoparticle modified MWCNT/GCE (Figure 3.30).
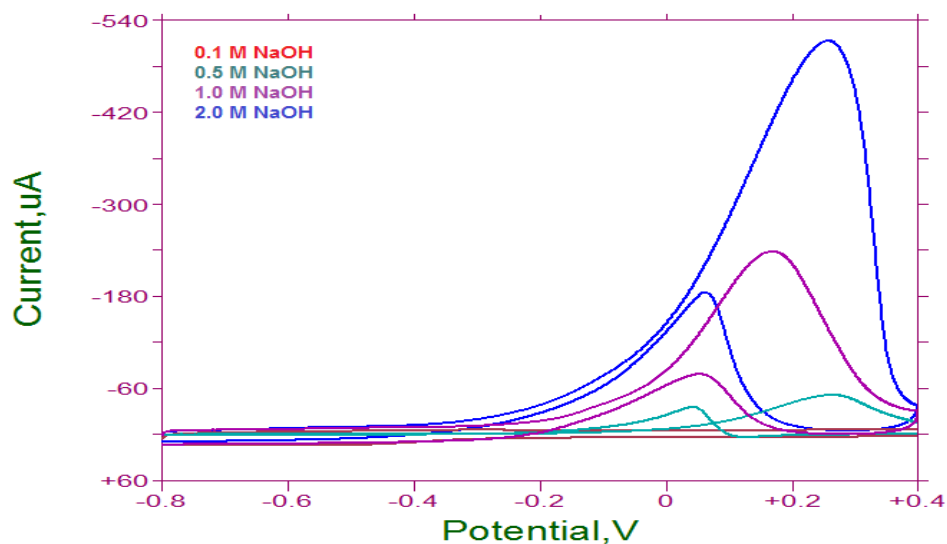
Figure 3.30 Cyclic voltammetric behaviour of Au nanoparticles modified MWCNT/GC electrode in the presence of 2.0 mol L^{-1} ethanol for different concentration of NaOH solutions. The scan rate was 50 mV s^{-1}

In alkaline media, increasing of ethanol concentration the peak potential was increased (Figure 3.31).

Figure 3.31 Cyclic voltammograms of ethanol oxidation at increasing concentration in presence of 0.5 mol L^{-1} NaOH with Au$_{(10cyc)}$-MWCNT/GCE at 50 mV s^{-1} scan rate

3.3.2.4 The electrocatalytic activity of Ni-MWCNT/GCE on ethanol oxidation in alkaline solutions

Ethanol oxidation in alkaline solutions occurs with the adsorption of acetyl species and the formation of stable intermediate products such as acetaldehyde and acetic acid. Generaly, on the Pd-sites adsorption and decomposition of ethanol take place and dissociative adsorption of water occurs on the Ni-sites. During the dissociative adsorption of ethanol on Pd-sites, Ni could be provided the O-species for the oxidation of CO-like species (He et al., 2011). To increase the electrocatliytic activity of Pd based catalysts on ethanol or methanol oxidation, binary or triple metal nanoparticles modified electrode have been used. Therefore, the electrocatalytic role of Ni nanoparticles on ethanol and methanol was examined with single Ni, binary Ni-Pd, Ni-Au and triple form of Pd-Au-Ni metal nanoparticles modified MWCNT/GCE.

The electrochemical behaviour of Ni-MWCNT/GCE was studied in the absence and presence of ethanol in 1.0 and 2.0 mol L^{-1} NaOH solutions. A higher background current was obtained in 1.0 mol L^{-1} NaOH solution compare with 2.0 mol L^{-1} NaOH solutions. A reduction signal was observed about -0.4 V due to the reduction of Ni oxide species which were formed during the anodic potential scan by partially oxidation of Ni nanoparticle on the MWCNT/GCE surface.
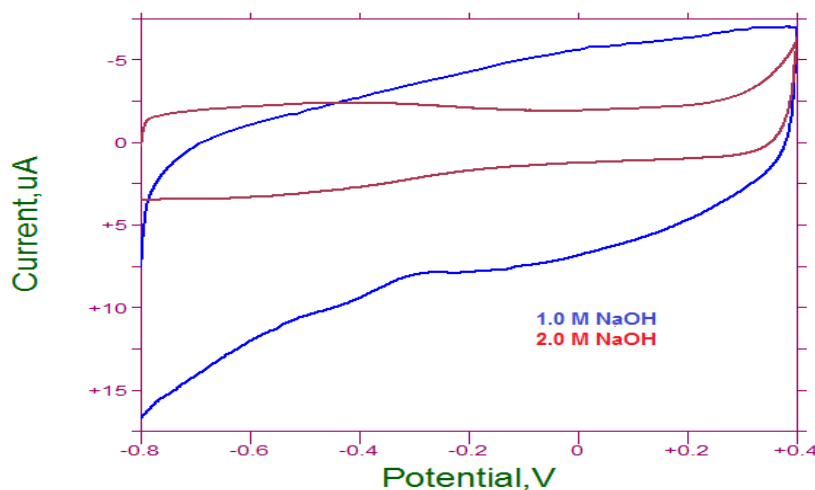
Figure 3.32 Cyclic voltammetric behaviour of Ni nanoparticles modified MWCNT/GC electrode in alkaline solutions as a supporting electrolyte. The scan rate was 50 mV s^{-1}

The electrocatalytic property of Ni-MWCNT/GCE for 2.0 mol L^{-1} ethanol oxidation was investigated by cyclic voltammograms in 1.0 and 2.0 mol L^{-1} NaOH solutions. It can be observed in Figure 3.32 that a typical ethanol oxidation peak appears at 0.07 V in both NaOH solutions. A higher peak current was found in 1.0 mol L^{-1} NaOH solution at Ni- MWCNT/GCE. A reduction peak was also formed during the backward potential sweep at -0.53 V due to the reduction of NiO in the presence conditions. The oxidation peak current was increased by increasing of ethanol concentration in 1.0 mol L^{-1} NaOH solution (Figure 3.33).
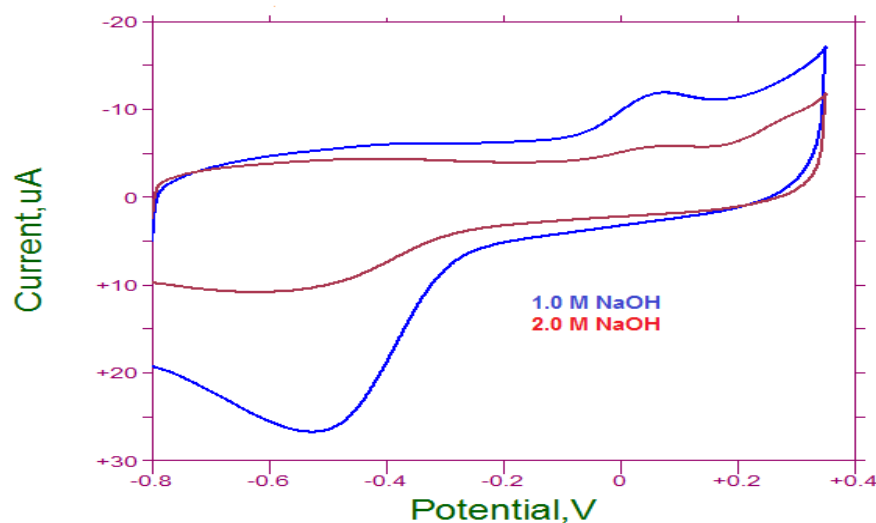
Figure 3.33 Cyclic voltammetric behaviour of Ni nanoparticles modified MWCNT/GC electrode in the presence of 2.0 mol L^{-1} ethanol for different concentration of NaOH solutions. The scan rate was 50 mV s^{-1}

The new catalyst which is nickel nanoparticles were tried with 1.0 mol L^{-1} NaOH as a supporting electrolyte. The electrochemical behaviour of Ni nanoparticles decorated Ni-MWCNT/GCE was studied by CV in 1.0 mol L^{-1} NaOH in the presence of different ethanol concentrations and the corresponding CVs are shown in Figure 3.34.

As shown in figure, forward potential scan has displayed a small oxidation paek at nearly 0.35 V while the reduction peak was observed at -0.580 V for Ni species reverse potential scan. Figure 3.34 showed Ni nanoparticles could not increase the electrocatalytic activity of MWCNT/GCE.
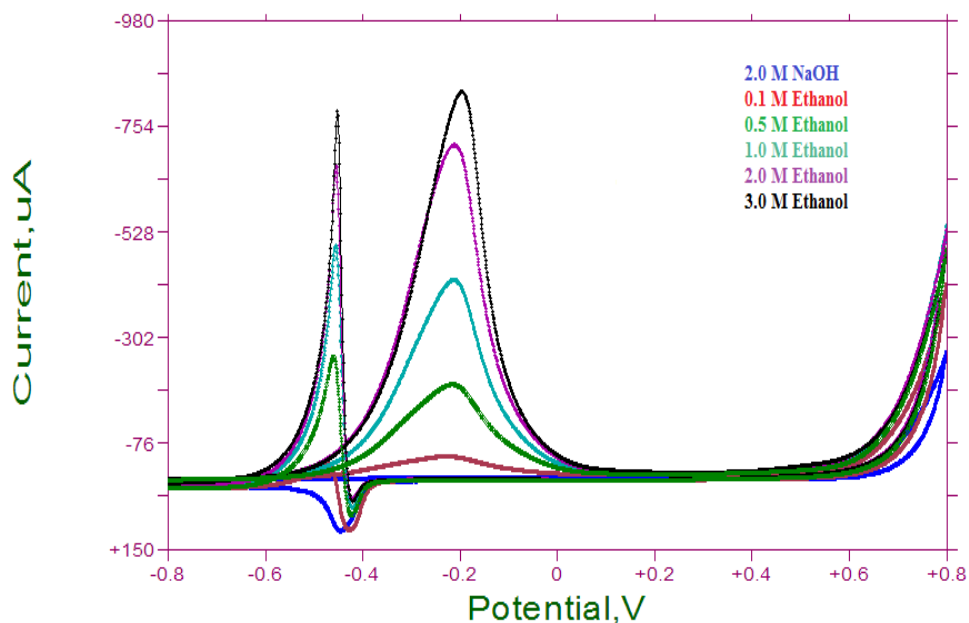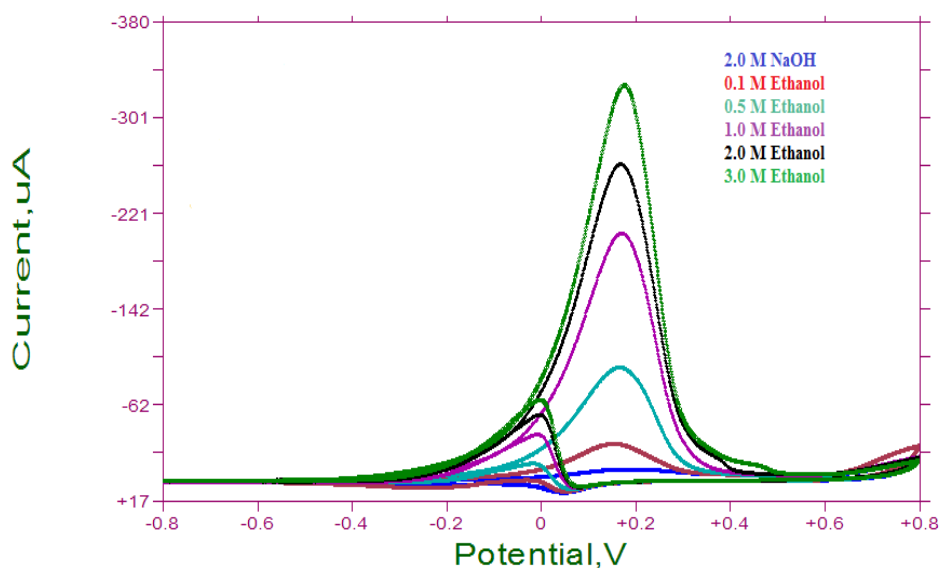
Figure 3.34 Cyclic voltammograms of ethanol oxidation at increasing concentration in presence of 1.0 mol L^{-1} NaOH with Ni$_{(10cyc)}$-MWCNT/GCE at 50 mV s^{-1} scan rate

3.3.2.5 The electrocatalytic activity of palladium-gold on ethanol oxidation in alkalinemedia

Based on the findings obtained with Pd-MWCNT/GC and Au-MWCNT/GCE for ethanol oxidation and according to literature survey, the catalytic performance of bimetallic Pd and Au nanoparticles was investigated in alkaline media. The synergic effect of the Pd and Au nanoparticles was examined using palladium electrodeposited on gold modified MWCNT/GCE.

Figures 3.35 and 3.36 show the electrochemical behaviour of Pd-Au-MWCNT/GCE in the absence and in the presence of ethanol in concentration range of 0.1-2.0 mol L^{-1} NaOH solutions. Two oxidation peaks were observed at about -0.351 V and 0.058 V respectively in anodic potential scan at higher NaOH concentrations due to the partialy oxidation of Pd and Au metal particles. In the reverse potential scan, two coincident reduction peaks were observed at 0.135 and -0.469 V for the reduction of Au and Pd oxides.
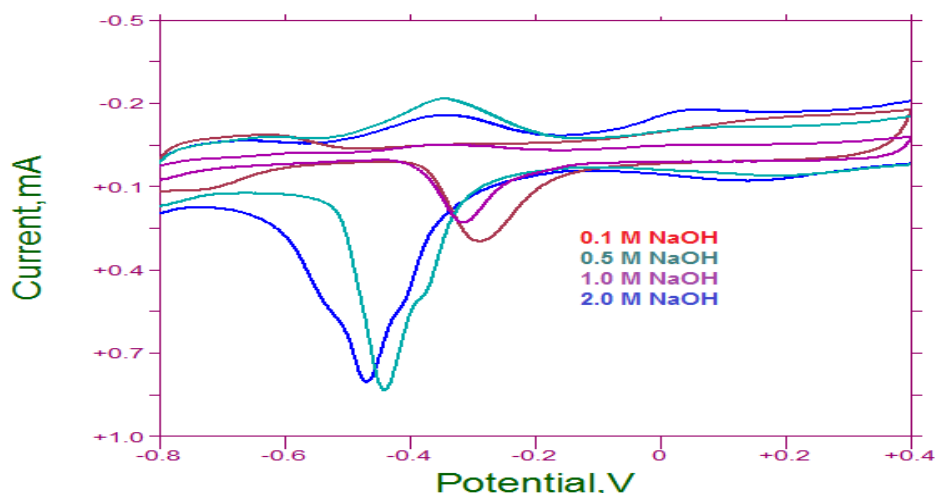
Figure 3.35 Cyclic voltammetric behaviour of Pd and Au nanoparticles modified MWCNT/GC electrode in alkaline solutions as a supporting electrolyte. The scan rate was 50 mV s^{-1}

The effect of NaOH concentration on the electrochemical behaviour of binary Pd-Au-MWCNT/GCE was studied in the presence of 0.1 mol L^{-1} ethanol NaOH and the obtained voltammograms were displayed in Figure 3.36. The oxidation peak potential and peak current were changed with NaOH concetration. The higher peak current and lower oxidation potential were obtained in the presence of 1.0 mol L^{-1} NaOH solution on Pd-Au-MWCNT/GCE.

The reverse oxidation peak formed during the cathodic potential scan was decreased compare to polycrystalline Pd disk and Pd nanoparticle modified MWCNT/GCE. This decreasing current value on the reverse oxidation peak can be expalined by sysnergistic effet of Pd-Au nanoparticles due to the suppersion of carbaneous species on the bimetalic particles modified MWCNT/GCE surface. The main oxidation peak current enhancements with increasing the NaOH concentration higher than 0.1 mol L^{-1} NaOH solution.

The results suggest that the kinetics of the ethanol oxidation reaction were improved by the greater availability of OH^{-} ions in solution and/or a higher OH^{-} coverage of the electrode surface (Yi et al., 2013). From different concentration of NaOH effect on ethanol oxidation studies, a favoriable peak characteristic were obtained in the presence of 1.0 mol L^{-1} NaOH solution. Therefore 1.0 mol L^{-1} NaOH was choosen as optimum supporting electrolyte solution for future studies.
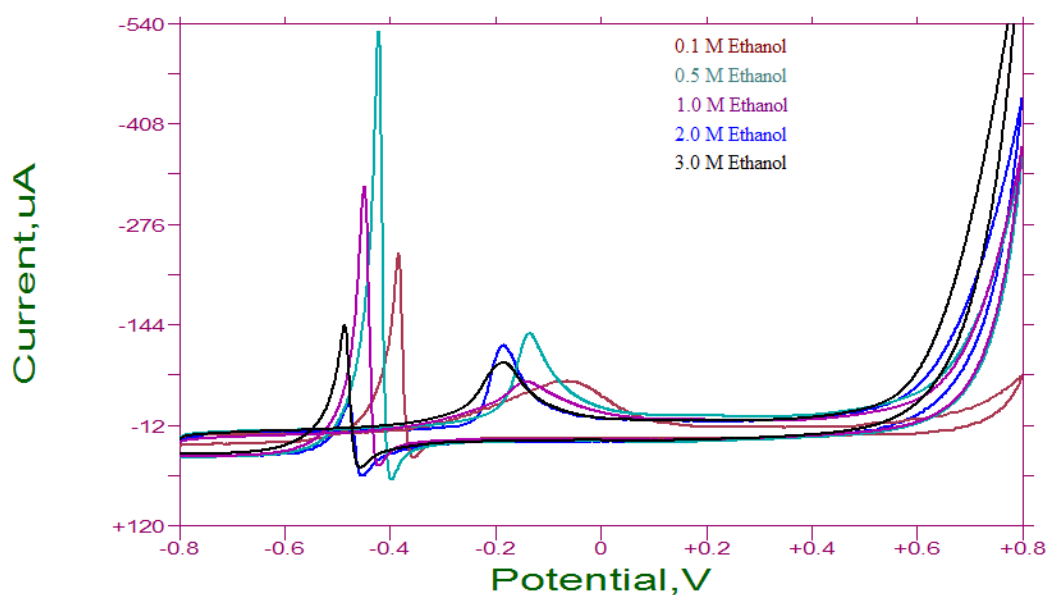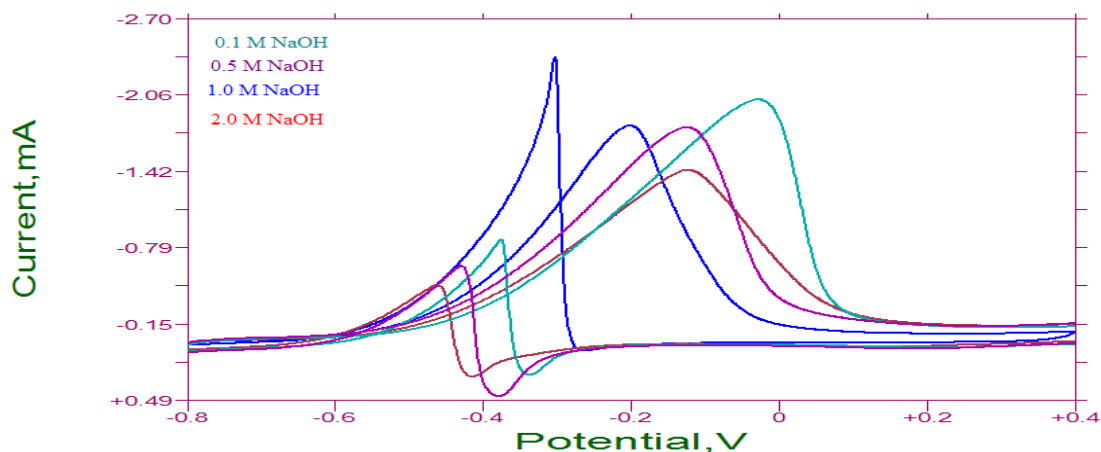
Figure 3.36 Cyclic voltammetric behaviour of Pd and Au nanoparticles modified MWCNT/GC electrode in the presence of 2.0 mol L^{-1} ethanol for different concentration of NaOH solutions. The scan rate was 50 mV s^{-1}

Table 3.2 The change of peak current and peak potential with increasing NaOH concentration for 0.1 mol L^{-1} ethanol with Pd-Au-MWCNT/GCE

NaOH Solution Concentration (mol L^{-1})	Peak Current (μA)	Peak Potential (V)
0.1	506.7	-0.078
0.5	870.3	-0.134
1.0	**1317.1**	**-0.205**
2.0	765.2	-0.067

From the cyclic voltammetric studies and Table 3.2, the optimum NaOH solution concentration was chosen as 1.0 mol L^{-1} NaOH for future studies at Pd-Au-MWCNT/GCE. The effect of electrodeposition potential cycle number of Pd and Au nanoparticles on MWCNT/GCE was examined by changing each metal potential cycle number.

The cycle number was changed in the range of 2-10 scale for each metal in the presence of 0.5 mol L^{-1} ethanol and 1.0 mol L^{-1} NaOH solution. The obtained results were given in Tables 3.3. The peak current characteristics were shown that the best cycle numbers of Pd and Au nanoparticles were found to be 10 cycles Pd-10 cycles Au (Au$_{(10cyc)}$-Pd$_{(10cyc)}$).

Table 3.3 Cycle number effect on oxidation of peak potentials of 0.1 mol L^{-1} ethanol with Pd-Au-MWCNT/GCE

	Cyc	mV	µA	Cyc	mV	µA	Cyc	mV	µA	Cyc	mV	µA
Pd	2	-125	287.9	2	-198	216.2	2	-190	307.6	2	-187	496.1
Au	4			6			8			10		
Pd	4	-134	144.5	4	-189	690.5	4	-144	573.1	4	-217	579.0
Au	4			6			8			10		
Pd	6	-104	822.5	6	-192	833.3	6	-157	669.0	6	-208	1055
Au	4			6			8			10		
Pd	8	-117	467.0	8	-184	937.4	8	-150	593.1	8	-202	1305
Au	4			6			8			10		
Pd	10	-133	849.6	10	-110	1678	10	-110	709.2	**10**	**-209**	**1455**
Au	4			6			8			**10**		

In order to confirm the electrode behaviour on the oxidation of ethanol, a series of cyclic volatmmograms were recorded at Pd$_{(10cyc)}$-MWCNT/GC electrode by varying potential scan rate. The oxidation peak current increased linearly with the square root of the scan rate (Figure 3.37), suggesting that ethanol oxidation reaction at this modified electrode was controlled by diffusion. The oxidation peak potential of ethanol shifted positive values with increasing the scan rate (Figure 3.38), indicating that the electron transfer was irreversible.
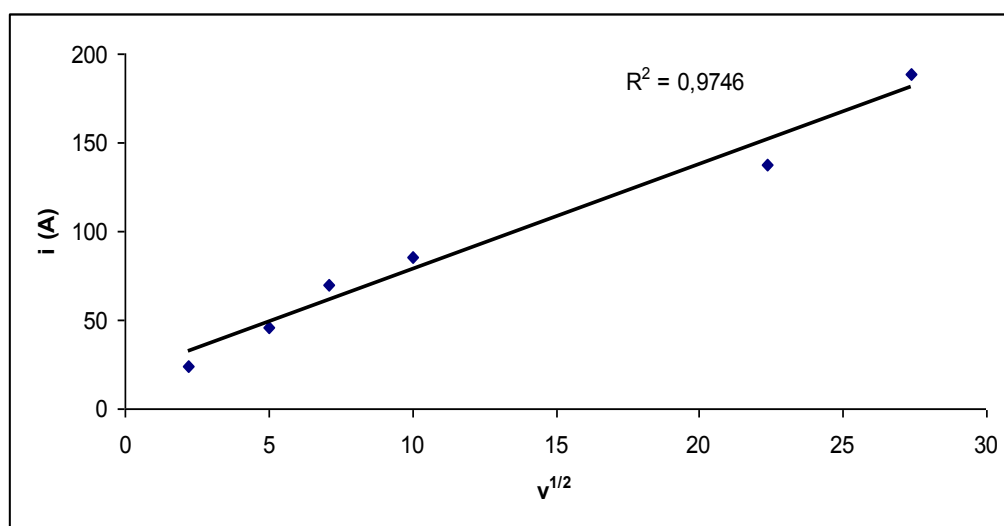
Figure 3.37 Dependence of scan rate on peak current of 0.5 mol L^{-1} ethanol at Pd-MWCNT/GCE in 2.0 mol L^{-1} NaOH
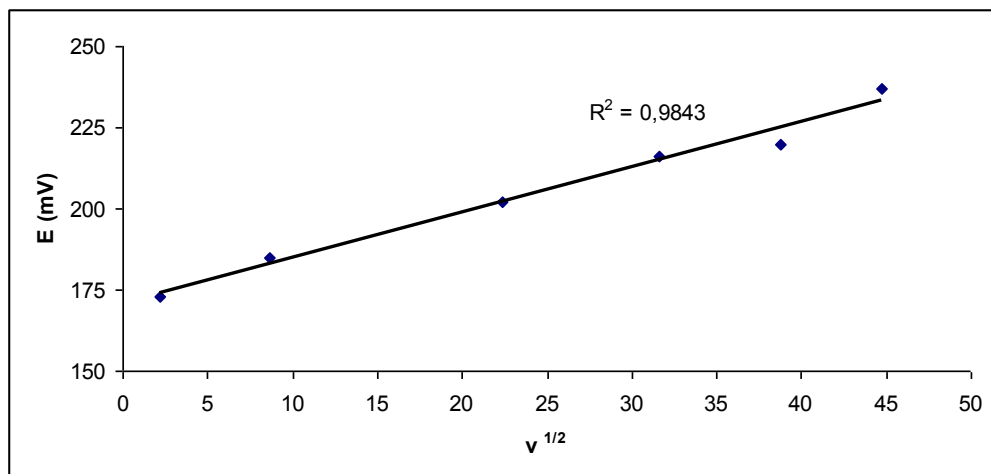
Figure 3.38 Dependence of scan rate on peak potential of 0.5 mol L^{-1} ethanol at Pd-MWCNT/GCE in 2.0 mol L^{-1} NaOH

3.3.2.6 The electrochemical behaviour of Au-Ni-MWCNT/GCE in the presence of ethanol in alkaline media

The cyclic voltammograms of the Au-Ni-MWCNT/GCE were recorded in different concentration of ethanol in 1.0 mol L^{-1} NaOH solution (Figure 3.39).
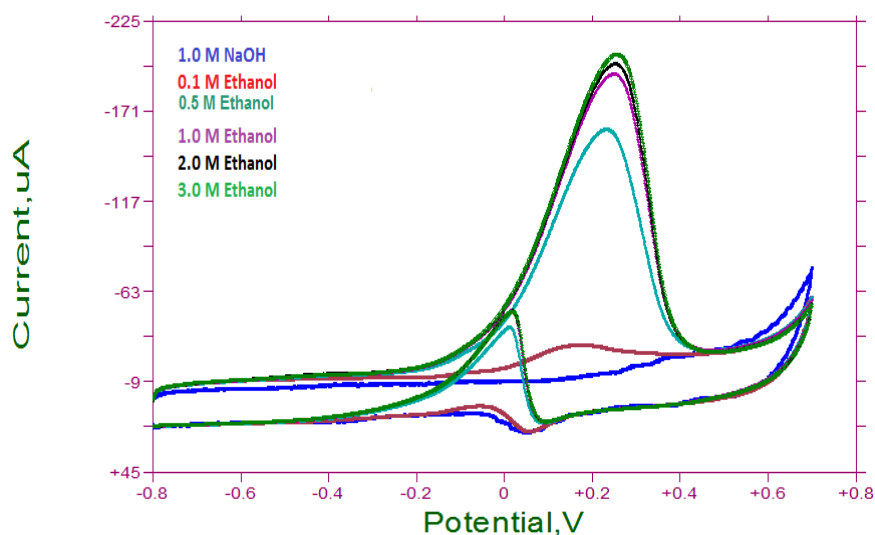
Figure 3.39 Cyclic voltammograms of ethanol oxidation at increasing concentration in the presence of 1.0 mol L^{-1} NaOH with Au$_{(10cyc)}$-Ni$_{(10cyc)}$-MWCNT/GCE at 50 mV s^{-1} scan rate

Ethanol oxidation takes place at 0.165 V on the Au-Ni-MWCNT/GCE (Figure 3.39). The results showed that the persence of Au has greater catalytic activity than Ni.

3.3.2.7 The electrochemical behaviour of Pd-Ni-MWCNT/GCE and Ni-Pd-MWCNT/GCE in the presence of ethanol in alkaline media

To investigate the bimetal catalytic activity of Pd and Ni or Ni and Pd nanoparticles deposition on the MWCNT/GCE, the ethanol oxidation was studied in 1.0 mol L^{-1} NaOH solution at both electrodes. Figure 3.40 shows, 0.5 mol L^{-1} ethanol oxidation takes place at -0.157 V on the Pd-Ni-MWCNT/GCE. The peak potential was shifted to positive potentials by increasing of ethanol concentration. On the other hand, the electrochemical behaviour of ethanol on Ni-Pd-MWCNT/GCE was shown in Figure 3.41. The oxidation peak was obtanied at -0.18 V on the anodic scan. In the reverse potential scan another oxidation peak was observed as reverse peak at -0.38 V due to the adsorption of ethanol oxidation product. The results indicated that, Pd-Ni nanoparticles modification has higer catalytic activity than Ni-Pd modified electrode.

Nickel nanoparticles coated after the Pd nanoparticles, the adsorption of intermediate was increased. This situation shows that the catalytic effect of electrode was protected.

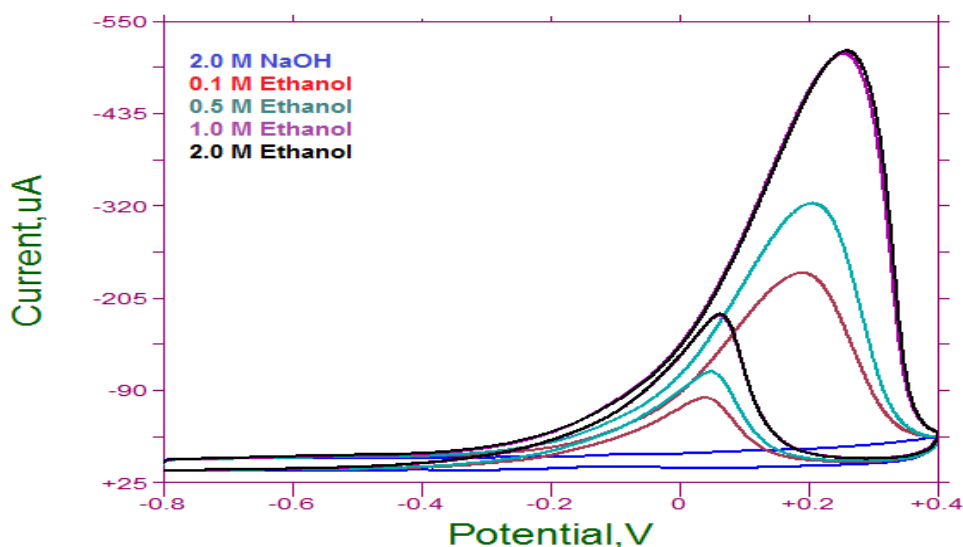**Figure 3.40 Cyclic voltammograms of ethanol oxidation at increasing concentration in presence of 1.0 mol L^{-1} NaOH with Ni$_{(10cyc)}$-Pd$_{(10cyc)}$-MWCNT/GCE at 50 mV s^{-1} scan rate**

On the other hand, Pd nanoparticles coated after the Ni nanoparticles the reverse oxidaiton peak was increased.

Figure 3.41 Cyclic voltammograms of ethanol oxidation at increasing concentration in presence of 1.0 mol L^{-1} NaOH with Pd$_{(10cyc)}$-Ni$_{(10cyc)}$-MWCNT/GCE at 50 mV s^{-1} scan rate

3.3.2.8 The electrochemical behaviour of triple metal nanoparticles modified MWCNT/GCEs in the presence of ethanol in alkaline media

To change the composition of metal nanoparticles on the electrode surface, MWCNT/GCE surface was modified with changing deposition sequence of three metal nanoparticles such as Ni-Pd-Au, Pd-Au-Ni, Pd-Ni-Au, Ni-Au-Pd and Au-Ni-Pd. The electrochemical behaviour of ethanol was studied with all metal nanoparticles modified electrodes in 1.0 mol L^{-1} NaOH solution.

The evalution and comparison of metal nanoparticle modified electrodes results above were discussed. Figure 3.42 shows the results obtained with three metalic nanoparticles modified electrodes prepared at changing deposition sequence and comparison of their results for 0.5 mol L^{-1} ethanol in 1.0 mol L^{-1} NaOH solutions. As can be seen from the voltammogram the higher catalytic activity can be observed with Pd-Au-Ni-MWCNT/GC electode.
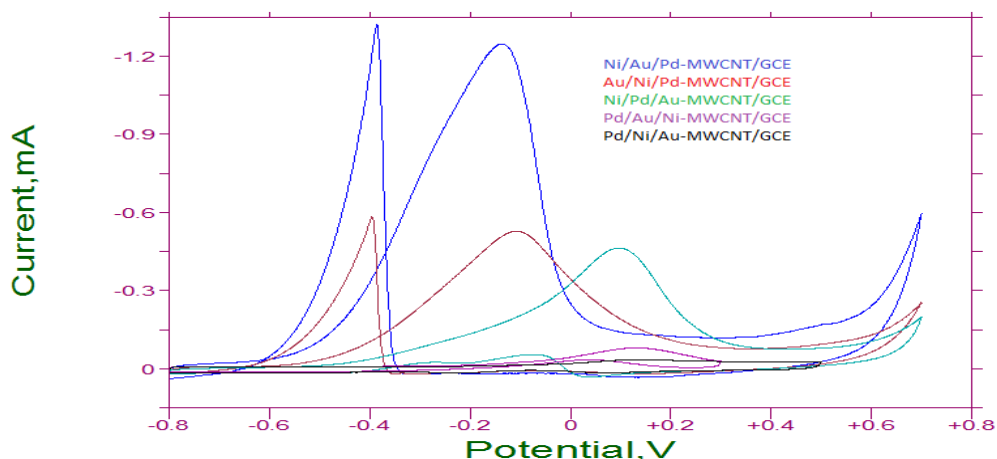
Figure 3.42 Comparison of the three metalic nanoparticles electrodes for 0.5 mol L^{-1} ethanol at a scan rate of 50 mV s^{-1} at 1.0 mol L^{-1} NaOH

Generally, two oxidation peaks were observed for both electrodes at -0.12 V with Au-Ni-Pd-MWCNT/GCE, at -0.15 V with Ni-Au-Pd-MWCNT/GCE, at 0.04 V with Ni-Pd-Au-MWCNT/GCE, at 0.13 V with Pd-Au-Ni-MWCNT/GCE and at 0.14 V with Pd-Ni-Au-MWCNT/GCE for anodic potential scan respectively and second reverse oxidation peak at -0.39 V for Au-Ni-Pd-MWCNT/GCE and -0.38 V for Ni-Au-Pd-MWCNT/GCE during the reverse current-potential scan.

From the results, Pd-Au-Ni MWCNT/GCE has higher electrocatalytic activity towards ethanol oxidation. The peak current was incraesed by increasing of ethanol concentration while the peak potential shifting towards positive values (Figure 3.43).
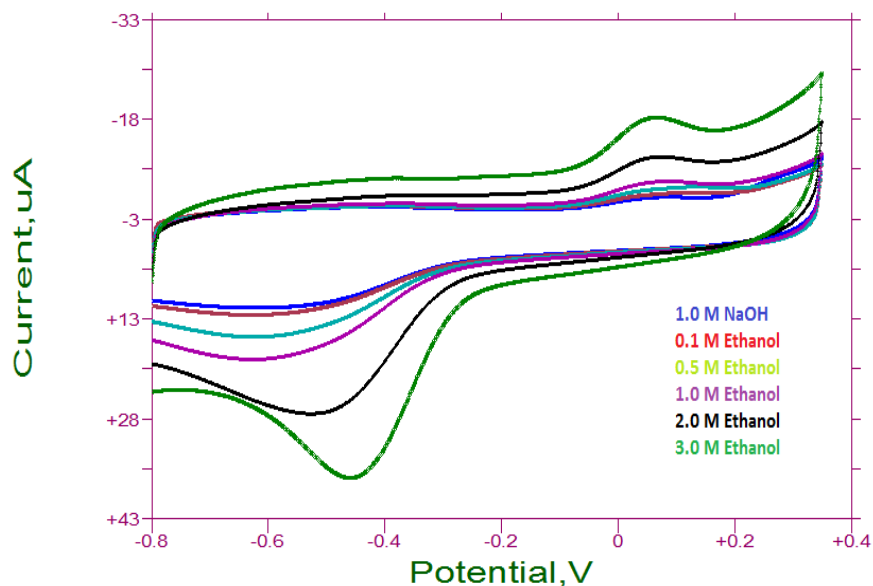

Figure 3.43 Cyclic voltammograms of ethanol oxidation at increasing concentration in presence of 1.0 mol L^{-1} NaOH with Pd$_{(10cyc)}$-Au$_{(10cyc)}$-Ni$_{(10cyc)}$-MWCNT/GCE at 50 mV s^{-1} scan rate

Table 3.4 shows peak potential and peak current values for each electrode. This means the high catalytic effect observed with Pd-Au-Ni-MWCNT/GCE for 0.5 mol L^{-1} ethanol in 1.0 mol L^{-1} NaOH solution.

Table 3.4 Current-Potential values of electrodes with different types of electrodes

Electrodes	Peak Potential (V)	Peak Current (µA)
Pd-MWCNT/GCE	0.102	16.4
Au-MWCNT/GCE	0.246	11.7
Ni-MWCNT/GCE	0.562	10.3
Pd-Ni-MWCNT/GCE	-0.164	448.0
Ni-Pd-MWCNT/GCE	-0.149	88.3
Pd-Au-MWCNT/GCE	-0.117	467.0
Au-Pd-MWCNT/GCE	0.213	330.9
Ni-Au-MWCNT/GCE	0.530	677.6
Au-Ni-MWCNT/GCE	0.213	82.7
Pd-Ni-Au-MWCNT/GCE	-0.126	219.9
Ni-Pd-Au-MWCNT/GCE	-0.118	22.2
Ni-Au-Pd-MWCNT/GCE	0.131	79.5
Au-Ni-Pd-MWCNT/GCE	0.143	35.3
Pd-Au-Ni-MWCNT/GCE	**-0.147**	**606.4**
Au-Pd-Ni-MWCNT/GCE	0.046	127.6

Table 3.5 shows that effect of cycle number on catalytic activity for ethanol. To change the cycle number in 1.0 mol L^{-1} NaOH solution 0.5 mol L^{-1} ethanol show that the best catalysts system was chosen as the $Pd_{(5cyc)}$-$Au_{(10cyc)}$-$Ni_{(5cyc)}$-MWCNT/GC electrode.

Table 3.5 Current-Potential values of Pd-Au-Ni-MWCNT/GCE different cycle number with 1.0 mol L^{-1} NaOH for 0.5 mol L^{-1} ethanol

Electrodes	Peak Potential (V)	Peak Current (μA)
15 Pd- 15 Au- 10 Ni	0.195	105.0
10 Pd - 10 Au- 15 Ni	-0.125	186.6
5 Pd - 5 Au- 5 Ni	0.070	964.7
10 Pd - 5 Au- 5 Ni	**-0.176**	**2086.0**
5 Pd- 10 Au -5 Ni	-0.165	1283.0
10 Pd- 10 Au- 5 Ni	-0.128	785.7
5 Pd - 5 Au- 10 Ni	-0.163	614.4
10 Pd - 5 Au- 10 Ni	-0.102	221.5
15 Pd - 5 Au- 15 Ni	0.203	406.7
5 Pd - 5 Au- 20 Ni	-0.022	904.7

3.3.3 Preparation of metal nanoparticles with chemical reduction methods and fabrication of metal nanoparticles modified multiwall carbon nanotubes/glassy carbon electrode for ethanol oxidation in alkaline solutions

To compare the catalytic activity of metal nanoparticles modified MWCNT/GCE which were prepared by electrochemically method on ethanol oxidation, the MWNTs decorated with metal nanoparticles catalyst, such as gold, nickel, palladium and their mixtures were prepared by chemically reduction method. For this aim, sodium borohydride and citric acid were used as reducing reagents. They were used as explained in section 2.3.4. The obtained results were discussed following sections.

3.3.3.1 The electrochemical behaviour of metal nanoparticles modified multiwall carbon nanotubes/glassy carbon electrode prepared with sodium borohydride for ethanol oxidation in alkaline media

The voltammetric behaviour of MWCNT/GCE, Pd-MWCNT/GCE, Au-MWCNT/GCE and Ni-MWCNT/GCE was investigated in the absence and in the presence of ethanol in the concentration range of 0.5-2.0 mol L^{-1} NaOH soluion. The obtained voltammograms were given in Figure 3.44-3.45. In Figure 3.44 characteristic small oxidation peak and reduction peaks were observed during the anodic and cathodic potential scan respectively in all NaOH solutions. The voltammograms shows that Pd, Au and Ni nanoparticles were sensitized on MWCNT.
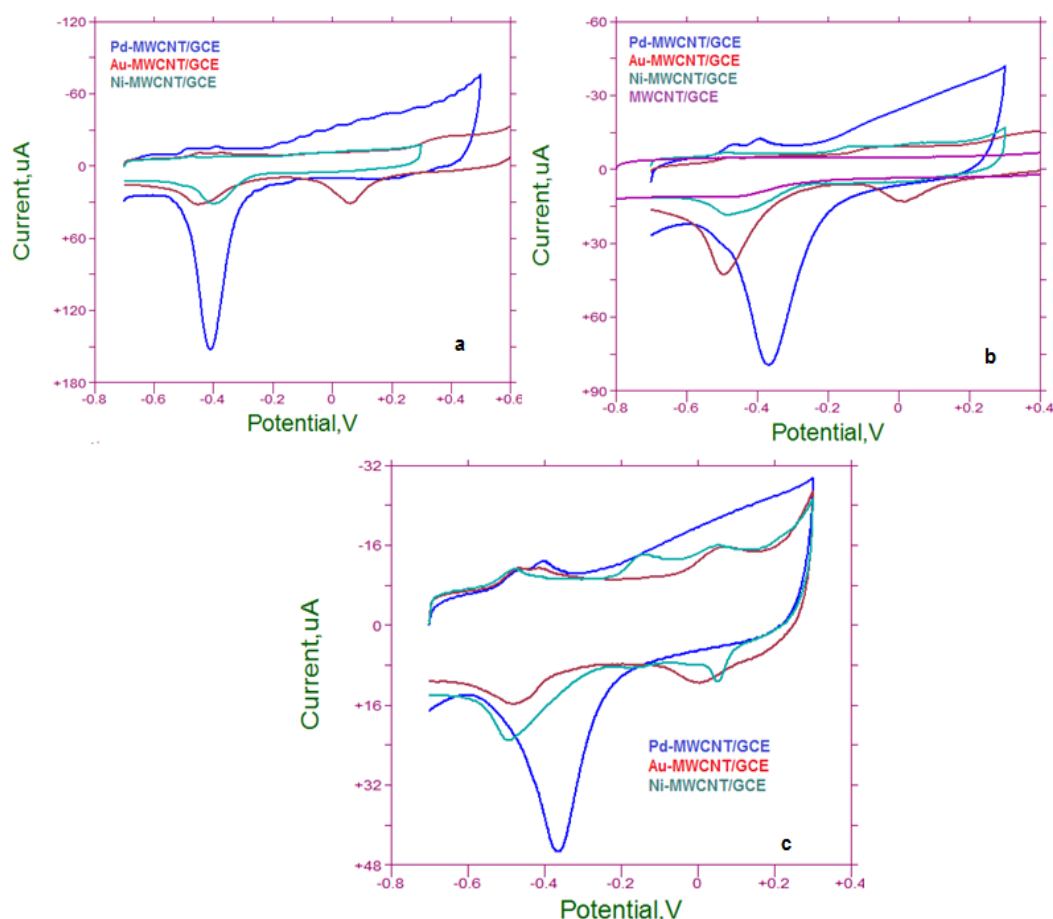
Figure 3.44 Cyclic voltammetric behaviour of Pd, Au and Ni nanoparticles modified MWCNT/GC electrodes in a) 0.5 mol L^{-1} b) 1.0 mol L^{-1} c) 2.0 mol L^{-1} NaOH solutions as a supporting electrolyte. The scan rate was 50 mV s^{-1}

In the presence of ethanol, only Pd-MWCNT/GCE and Au-MWCNT/GCE were shown eletrocatalytic activity towards ethanol oxidation while well defined two oxidation peaks were observed in both anodic potential scan and cathodic potential scan which was called revers oxidation peak. A more negative oxidation potentials as -0.18 V in 0.5 mol L^{-1} NaOH, -0.05 V in both 1.0 and 2.0 mol L^{-1} NaOH solutions were obtained with Pd nanoparticle then Au nanoparticle (ethanol oxidation take place at 0.36 V, 0.39 V and 0.4 V in 0.5 mol L^{-1}, 0.1 mol L^{-1} and 2.0 mol L^{-1} NaOH solutions, respectively on Au nanoparticles modified electrode). The oxidation peak potential was shifted to negative potential by increasing NaOH concentration. A higher reverse oxidation peak current at about -0.4 V was obtained at Pd-MWCNT/GCE compare with Au-MWCNT/GCE due to the partial oxidation of ethanol and the formation of acetaldehyde, acetic acid, or carbon monoxide, which can be easily adsorbed on the electrode surface and decrease its catalytic activity towards ethanol oxidation (Figure 3.45).
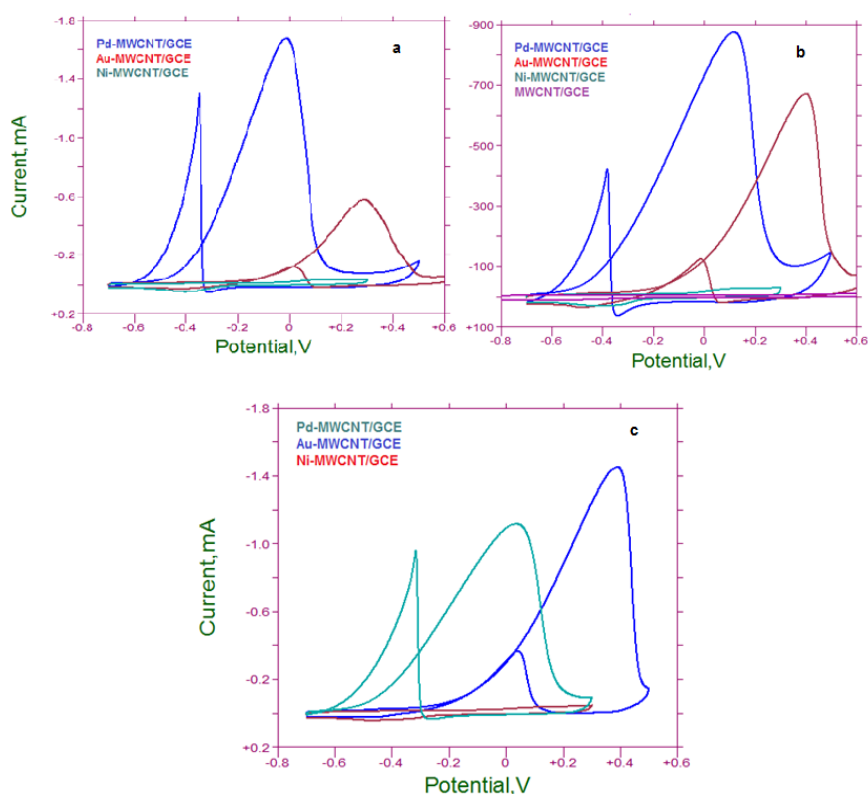
Figure 3.45 Cyclic voltammetric behaviour of Pd, Au and Ni nanoparticles modified MWCNT/GC electrode in the presence of 2.0 mol L^{-1} ethanol for a) 0.5 mol L^{-1} b) 1.0 mol L^{-1} c) 2.0 mol L^{-1} NaOH solutions. The scan rate was 50 mV s^{-1}

The peak current of ethanol oxidation was increased while peak potential shifting positive values with increasing ethanol concentration (Figure 3.46).

Figure 3.46 Cyclic voltammograms of ethanol oxidation at increasing concentration in presence of 1.0 mol L^{-1} NaOH with Pd-MWCNT/GCE at 50 mV s^{-1} scan rate

The Table 3.6 demonstrated that with Pd-MWNCT/GC electrode the higher catalytic activity observed in 2.0 mol L^{-1} NaOH solution. So that the following studies, 2.0 mol L^{-1} NaOH solution was chosen as a supporting electrolyte. The small voltammogram emphasized the supporting electolyte.

Table 3.6 Current-Potential table for 0.5 mol L^{-1} ethanol with Pd-MWNCT/GCE

NaOH Solution Concentration (mol L^{-1})	Peak Current (µA)	Peak Potential (V)
2.0	**118.5**	**-0.169**
1.0	106.5	-0.148
0.5	103.3	-0.172
0.1	76.2	+0.033

In the second step of chemical reduction procedure with sodium borohydride reaction, the binary mixtures of Pd-Au, Pd-Ni and Au-Ni metal nanoparticles modified MWCNT/GC electrodes were prepared and applied to electrocatalytic oxidation of ethanol in different concentration of NaOH solutions. The voltammetric behaviour of of Pd-Au, Pd-Ni and Au-Ni metal nanoparticles modified MWCNT/GC electrodes were performed in the absence and in the presence of ethanol. Typical voltammograms were obtained for Au, Pd and Ni species into binary mixture of metals on MWCNT/GCE surface (Figure 3.47).
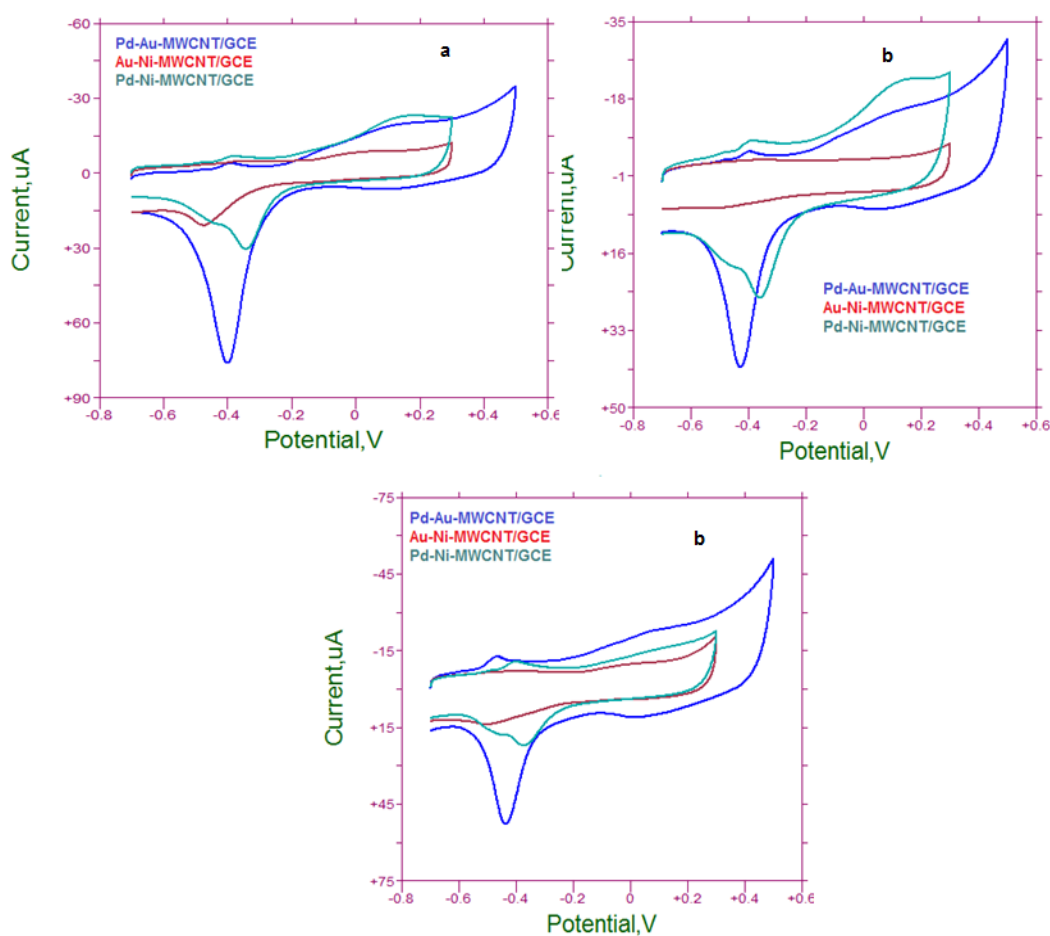
Figure 3.47 Cyclic voltammetric behaviour of Pd-Au, Au-Ni and Pd-Ni nanoparticles modified MWCNT/GC electrodes in a) 0.5 mol L^{-1} b) 1.0 mol L^{-1} c) 2.0 mol L^{-1} NaOH solutions as a supporting electrolyte. The scan rate was 50 mV s^{-1}

Figure 3.48 shows, 2.0 mol L^{-1} ethanol oxidation observed at almost same potential at about -0.150 V on the Pd-Au-MWCNT/GCE in all NaOH solutions during the anodic potential scan. The peak current was no also changed by changing NaOH concentration at this electrode. In the case of Pd-Ni-MWCNT/GCE, a small oxidation peak was observed accompanying positive peak potential compare Pd-Au-MWCT/GCE results. The peak potential was also almost constant at all NaOH media on Pd-Ni-MWCNT/GCE.

On the other hand, Ni-Au-MWCNT/GCE did not show any catalytic activity towards ethanol oxidaton in all NaOH solutions. In the reverse potential scan, a reverse oxidation peak was observed at -0.38 V on the Pd-Au-MWCNT/GCE and Pd-Ni-MWCNT/GCE due to the adsorption of ethanol oxidation product. The reverse oxidation peak current was higher on Pd-Au-MWCNT/GCE compare to Pd-Ni-MWCNT. Since the presence of Ni nanoparticle in binary mixture could be suppressed the adsorption of ethanol oxidation products.
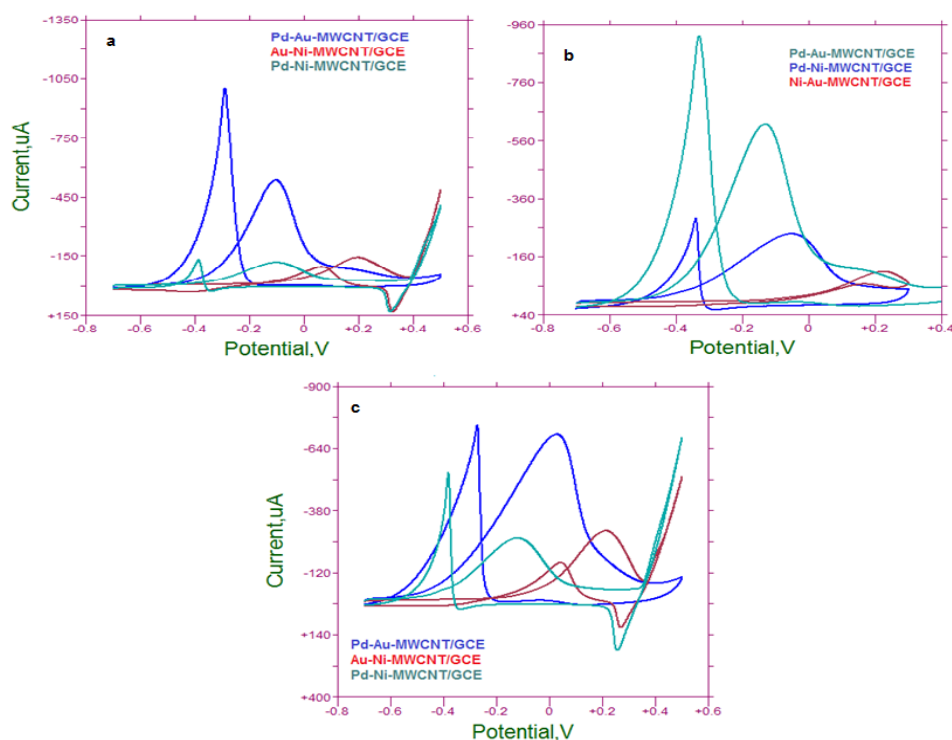
Figure 3.48 Cyclic voltammetric behaviour of Pd-Au, Au-Ni and Pd-Ni nanoparticles modified MWCNT/GC electrodes in the presence of 2.0 mol L^{-1} ethanol for a) 0.5 mol L^{-1} b) 1.0 mol L^{-1} c) 2.0 mol L^{-1} NaOH solutions. The scan rate was 50 mV s^{-1}

The peak current of ethanol oxidation was increased while peak potential shifting positive values with increasing of ethanol concentration on Pd-Au-MWCNT/GCE (Figure 3.49). The reverse peak current was also increased depending on ethanol concentration.
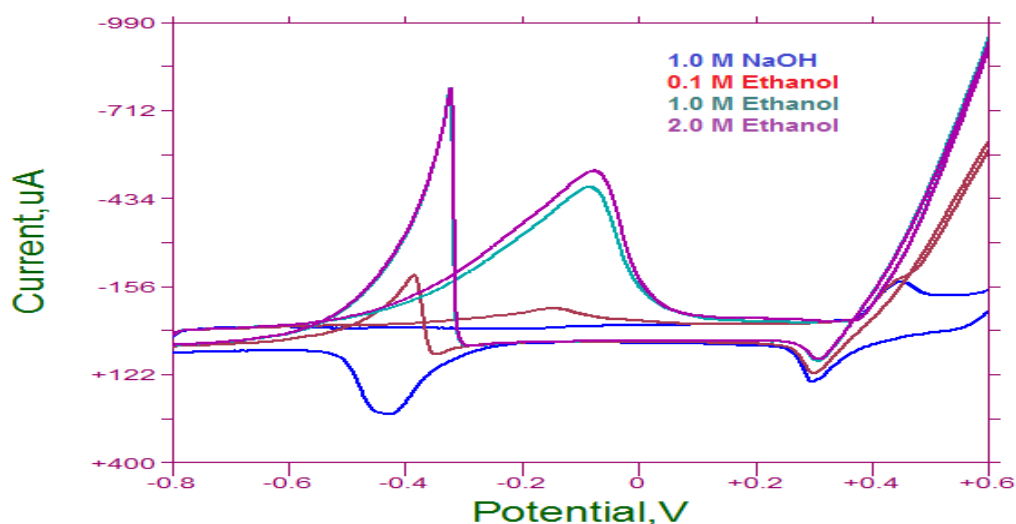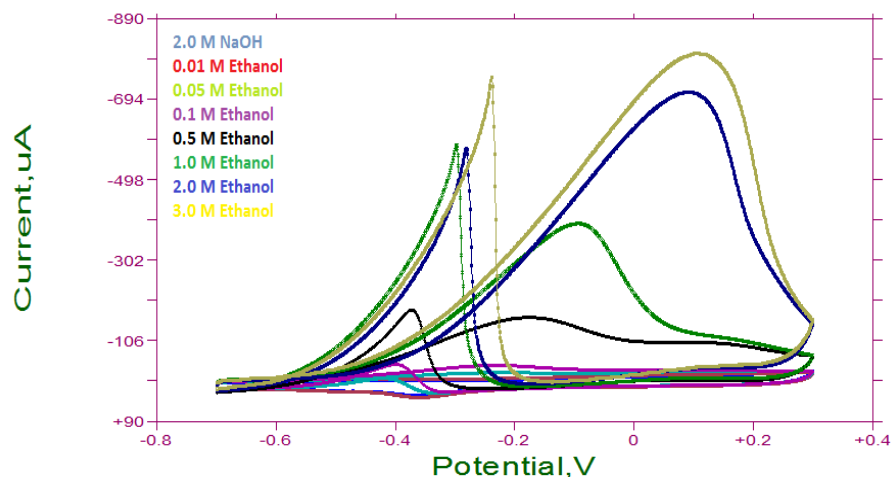

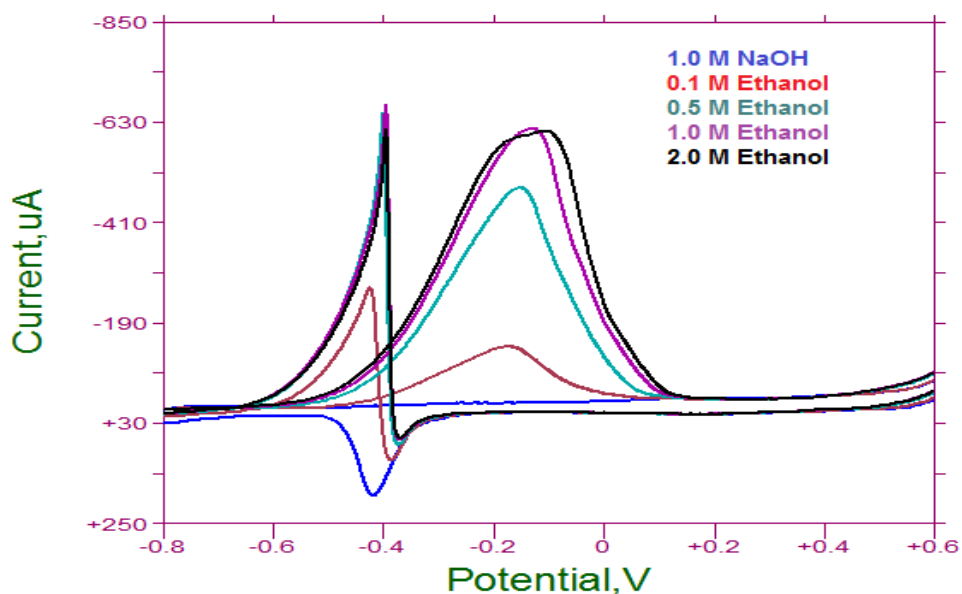**Figure 3.49 Cyclic voltammograms of ethanol oxidation at increasing concentration in presence of 2.0 mol L⁻¹ NaOH with Pd-Au-MWCNT/GCE at 50 mV s⁻¹ scan rate**

In the third step of chemical reduction procedure with sodium borohydride reaction, the binary mixtures of Pd-Au-Ni metal nanoparticles modified MWCNT/GC electrode was prepared and applied to electrocatalytic oxidation of ethanol in different concentration of NaOH solutions. The voltammetric behaviour of Pd-Au-Ni modified MWCNT/GC electrodes were studied in the absence and in the presence of ethanol. Typical voltammograms were obtained for Au, Pd and Ni species into mixture of metals on MWCNT/GCE surface (Figure 3.50).
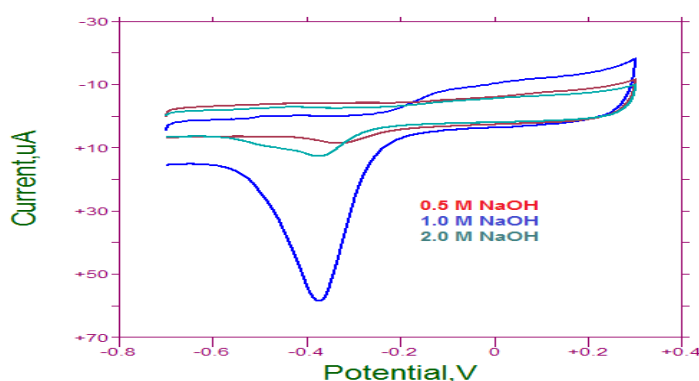
Figure 3.50 Cyclic voltammetric behaviour of Pd-Au-Ni nanoparticles modified MWCNT/GC electrode in alkaline solutions as a supporting electrolyte. The scan rate was 50 mV s⁻¹

The electrocatalytical oxidation of 2.0 mol L^{-1} ethanol was investigated at Pd-Au-Ni-MWCNT/GCE in different concentration of NaOH solutions (Figure 3.51). Two oxidation peaks at -0.180 V and 0.170 V were observed during the anodic potential sweep. Both peaks were formed by the oxidation of ethanol in two steps in the presence conditions. The reverse oxidation peak was also appeared in the cathodic potential scan as the reasons explained above for Pd based electrodes. But, the reverse peak current was much more compare with electrochemically prepared Pd based electrode results.
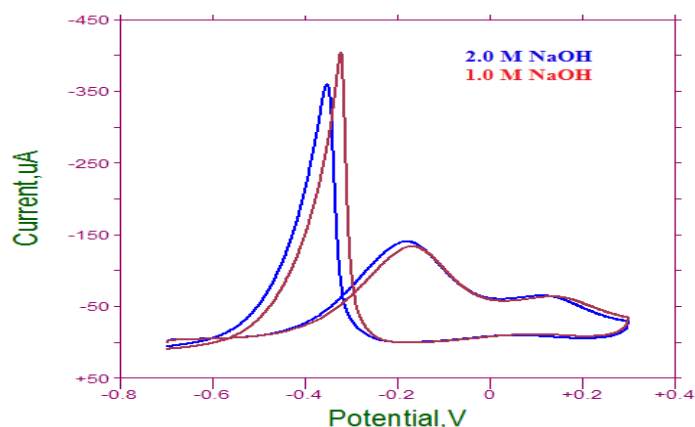
Figure 3.51 Cyclic voltammetric behaviour of Pd-Au-Ni-MWCNT/GC electrode in the presence of 2.0 mol L^{-1} ethanol for different concentration of NaOH solutions. The scan rate was 50 mV s^{-1}

The ethanol concentration dependence of both oxidation peaks and reverse oxidation peak currents were obtained linearly in 2.0 mol L^{-1} NaOH solution (Figure 3.52).
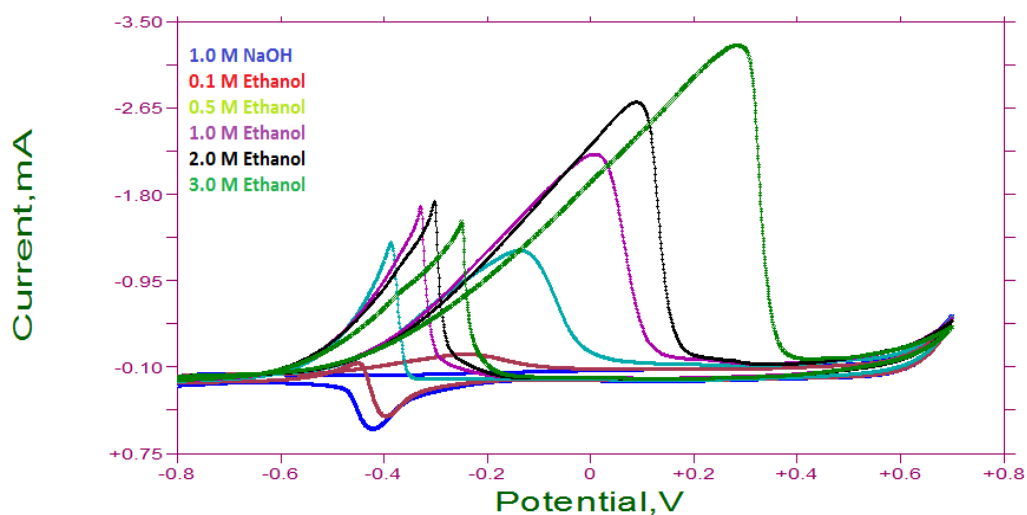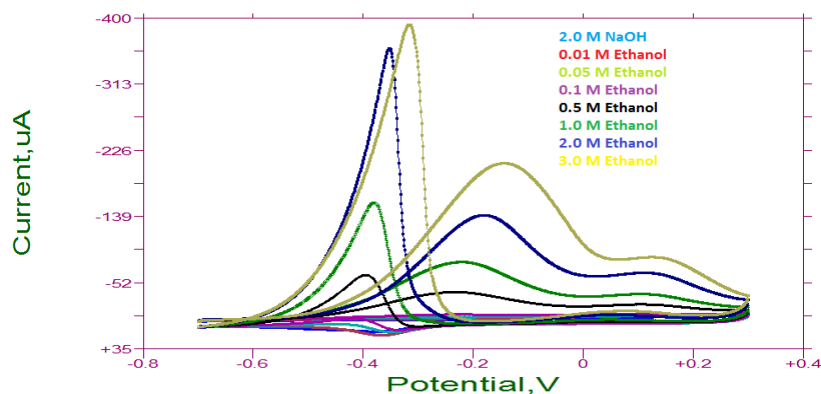

Figure 3.52 Cyclic voltammograms of ethanol oxidation at increasing concentration in presence of 2.0 mol L^{-1} NaOH with Pd-Au-Ni-MWCNT/GCE at 50 mV s^{-1} scan rate

The obtained results were summarized in Table 3.7 for oxidation of ethanol in the presence of 2.0 mol L^{-1} NaOH solution.

Table 3.7 Current-Potential table for 1.0 mol L^{-1} ethanol in 2.0 mol L^{-1} NaOH for different types of electrodes

Electrodes	Peak Current (μA)	Peak Potential (V)
Pd-MCNT/GCE	265.2	-0.155
Ni-MCNT/GCE	3.3	+0.063
Au-MCNT/GCE	374.6	+0.223
Pd-Ni-MCNT/GCE	93.6	-0.171
Pd-Au-MCNT/GCE	166.3	-0.110
Au-Ni-MCNT/GCE	61.8	0.174
Pd-Au-Ni-MCNT/GCE	**115.9**	**-0.226**

The Pd-Au-Ni-MWCNT/GCE electrode exhibits much higher catalytic activity for the electrooxidation of ethanol in comparison to the bare Pd, Ni and Au electrodes and also bi and tri metalic MWCNT/GCE. The peak potential is comparable for the all electrodes. However, the onset potential of the metalic electrode for ethanol oxidation is -0.22 V, much lower than that of the flat Pd electrode (-0.16 V). The shift of this onset potential to a more negative values means that metal nanoparticles can significantly enhance the electrooxidation kinetics of ethanol, which is important for its application in fuel cells.

The effect of NaOH concentration on the oxidation of ethanol, the concentration of NaOH solution was varied from 0.1 to 2.0 mol L^{-1}. The catalytic activity on ethanol oxidation was increased with increasing of NaOH concentration. The peak potential of ethanol was shifted towards positive potentials with increasing of NaOH concentration. The positive-shift in the peak potential suggests that the NaOH concentration has a favorable effect on the oxidation of ethanol. The table 3.8 demonstrated that with Pd-Au-Ni-MWNCT/GC electrode the higher catalytic activity observed on 2.0 mol L^{-1} NaOH solution.

Table 3.8 Current-Potential table for 1.0 mol L^{-1} etanol with Pd-Au-Ni-MWNCT/GCE

NaOH Solution Concentration (mol L^{-1})	Peak Current (μA)	Peak Potential (V)
2.0	**115.9**	**-0.226**
1.0	47.9	-0.221
0.5	8.3	-0.110
0.1	9.7	-0.098

3.3.3.2 The electrochemical behaviour of metal nanoparticles modified multiwall carbon nanotubes/glassy carbon electrode prepared with citric acid for ethanol oxidation in alkaline media

The cyclic voltammogram behaviour of ethanol was preliminarily investigated using metal and metal mixture nanoparticles decorated multiwalled carbon nanotubes prepared with citric acid**.** The results were given following sections.

3.3.3.2.1 Palladium nanoparticles decorated multiwall carbon nanotubes

The voltammetric behaviour of ethanol was studied at Pd-MWCNT/GCE in various concentration of NaOH as a supporting electrolyte. However, there is a sharp oxidation peak at -0.383 V on the positive potential scan and also a sharp reduction peak at -0.425 V due to the oxidation of Pd species formed during the anodic potential scan in the absence of ethanol.

Figure 3.53 Cyclic voltammograms of ethanol oxidation at increasing concentration in presence of 2.0 mol L^{-1} NaOH with Pd-MWCNT/GCE at 50 mV s^{-1} scan rate

There was a small oxidation at -0.082 V for 2.0 mol L^{-1} ethanol. At cathodic scan ethanol reduction peak was observed at -0.281 V (Figure 3.53).

3.3.3.2.2 Gold and nickel nanoparticles decorated multiwall carbon nanotubes

To increase the catalytic activity of nanoparticles modified electrodes, bimetallic active sites were formed at MWCNT/GCE surface, prepared by chemically reduction procedure with citrate solution. The gold and nickel nanoparticles modified electrodes were prepared.

Figure 3.54 indicates that at -0.384 V and -0.447 V the peaks belongs to oxidation of Ni and Au nanoparticles. At the same time, at -0.469 V and -0.425 V the peaks belongs to reduction of Ni and Au nanoparticles. As can be seen from the Figure 3.54, Au-Ni-MWCNT/GC electrode could not show any catalytic effect on oxidation of ethanol with chemical reduction method.
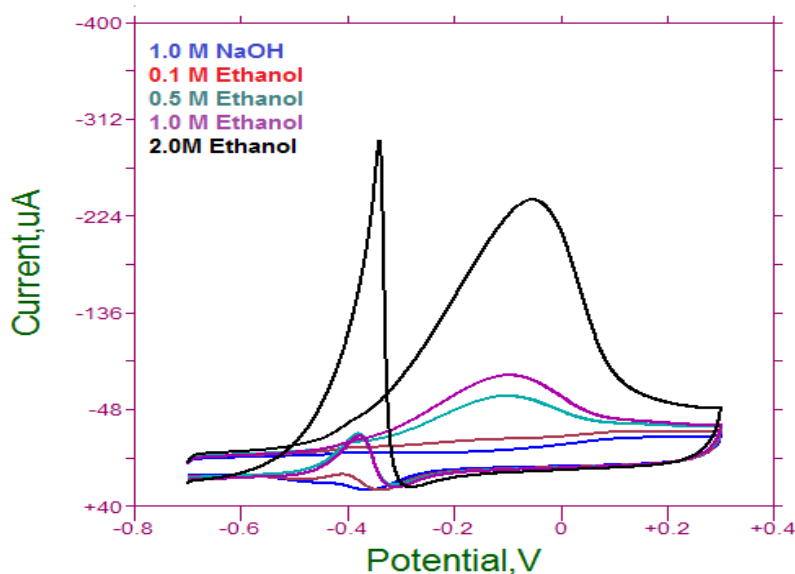
Figure 3.54 Cyclic voltammograms of ethanol oxidation at increasing concentration in presence of 2.0 mol L^{-1} NaOH with Au-Ni-MWCNT/GCE at 50 mV s^{-1} scan rate

3.3.3.2.3 Palladium, gold and nickel nanoparticles decorated multiwall carbon nanotubes

To increase the catalytic activity of modified electrodes, the electrode surfaces modified with trimetallic particles which were prepared by chemically reduction procedure. The electrocatalytical oxidation of 0.5 mol L^{-1} ethanol was investigated at Ni-Au-Pd-MWCNT/GCE (Figure 3.55).

Figure 3.55 Cyclic voltammograms of ethanol oxidation at increasing concentration in presence of 2.0 mol L^{-1} NaOH with Pd-Au-Ni-MWCNT/GCE at 50 mV s^{-1} scan rate

The Pd-Au-Ni-MWCNT/GC electrode could not exhibit any catalytic activity for the electrooxidation of ethanol in comparison to the flat Pd, Ni and Au electrodes and also bi and tri metalic MWCNT/GC electrodes.

3.4 Voltammetric Behaviour of Methanol

Direct methanol fuel cells (DMFCs) are known as one of the convenient power sources for increasing energy demand. However, it includes some deficiency:

1) the slow kinetics of methanol electrooxidation

2) a large rate of methanol crossover through the membrane proper heat and water management (Ko et al., 2010)

3) Considerable efforts in DMFC studies are needed to overcome these intrinsic flaws. Therefore, the development of high efficiency electrocatalysts is of vital importance for methanol oxidation reaction. In this thesis, the efficiency of GCE, MWCNT/GCE, Ni-MWCNT/GCE, Au-MWCNT/GCE, Pd-MWCNT/GCE, Pd-Au-MWCNT/GCE, Au-Ni-MWCNT/GCE, Pd-Ni-MWCNT/GCE and Pd-Au-Ni-MWCNT/GCE catalytic systems were researched for voltammetric behaviour of methanol.

3.4.1 Electrochemical behaviour of methanol in the presence of alkaline solutions at bare glassy carbon, MWCNT/GCE and gold, palladium and nickel nanoparticles modified multiwall carbon nanotubes/glassy carbon electrodes

The cyclic voltammetric behaviour of bare GCE, MWCNT/GCE and Pd, Au and Ni nanoparticle modified MWCNT/GCE in alkaline solution was also examined in the absence and presence of methanol oxidation. To see catalytic effect on methanol oxidation with those electrodes, $2.0 \ mol \ L^{-1}$ NaOH solutions was used as a supporting electrolyte The electrodes were prepared with electrochemical deposition methods. Figure 3.56 shows that on positive and negative potential scan, the oxidation peaks and reduction peaks related with Au and Pd species on Au-MWCNT/GCE and Pd-MWCNT/GCE.
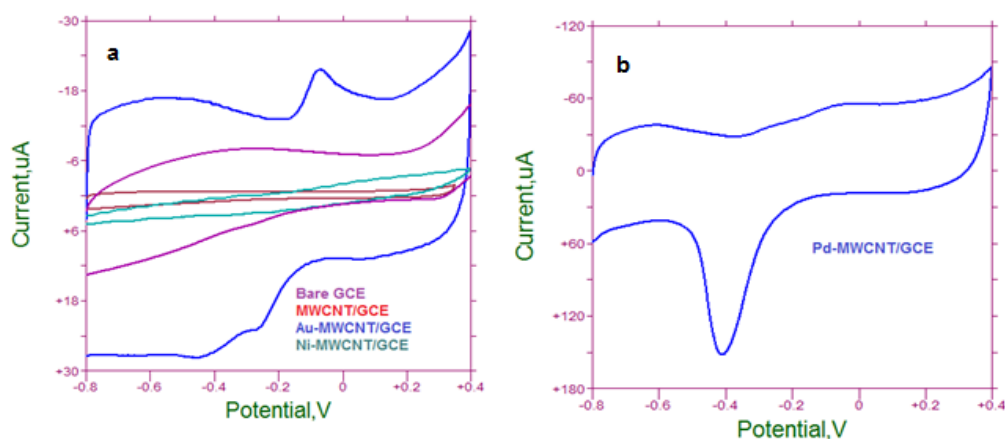
Figure 3.56 Cyclic voltammetric behaviour of a) bare GCE, MWCNT/GCE and Au, Ni nanoparticles modified MWCNT/GC electrodes d) Pd-MWCNT/GCE in 2.0 mol L^{-1} NaOH solutions as a supporting electrolyte. The scan rate was 50 mV s^{-1}
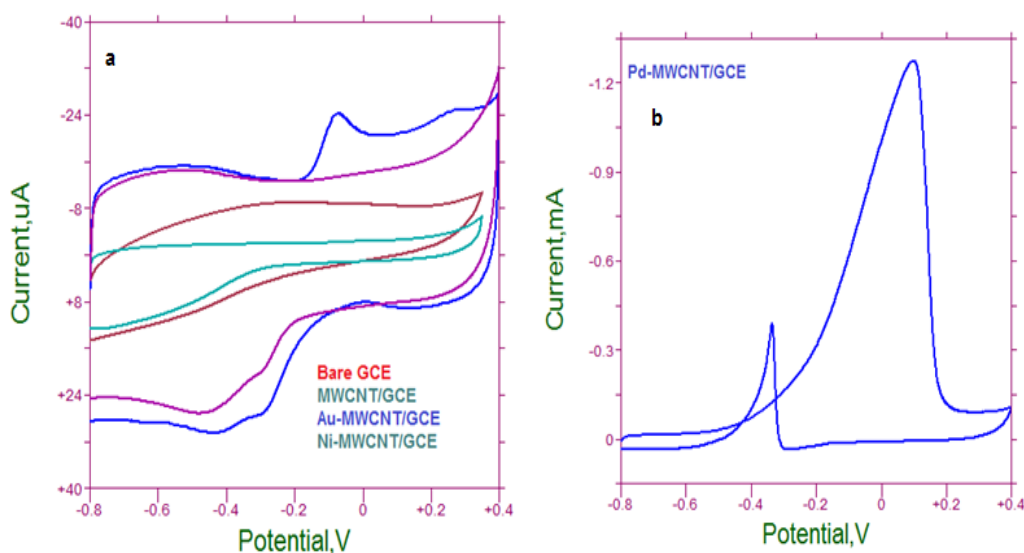
Figure 3.57 Cyclic voltammetric behaviour of a) bare GCE, MWCNT/GCE and Au, Ni nanoparticles modified MWCNT/GC electrode b) Pd-MWCNT/GCE in the presence of 2.0 mol L^{-1} methanol in 2.0 mol L^{-1} NaOH solutions. The scan rate was 50 mV s^{-1}

On the other hand, in the presence of methanol with Pd-MWCNT/GCE electrode shows higher catalytic activity for methanol oxidaiton. The methanol oxidation was observed at +0.1 V for 2.0 mol L^{-1} methanol in alkaline solution. Using Au-MWCNT/GCE, in the forward potential scan was showed a small oxidation paek at nearly 0.15 V while the reduction peak was observed at -0.25 V for Au species reverse potential scan. But, Au nanoparticles could not increase the electrocatalytic activity of MWCNT/GCE.

Moreover, the other electrodes could not show any catalytic effect by comparing Pd-MWCNT/GCE. Table 3.9 was summarized the change of peak currents and peak potentials. Both the highest peak current and the lowest negative peak potential were obtained at 2.0 mol L^{-1} NaOH solutions. Thus 2.0 mol L^{-1} NaOH solutions were chosen as a most convenient supporting electrolyte.

Table 3.9 Current-Potential table for 0.5 mol L^{-1} methanol with Pd-MWNCT/GCE

NaOH Solution Concentration (mol L^{-1})	Peak Current (µA)	Peak Potential (V)
2.0	**492.7**	**-0.159**
1.0	472.9	-0.097
0.5	297.4	-0.138
0.1	98.4	-0.082

2.0 mol L^{-1} NaOH solutions were choosen as supporting electrolyte for future studies. The peak current was increased by icreasing methanol concentration while peak potential shifting to positive values, indicating that an irreversible electrode reaction takes place on the Pd-MWCNT/GCE surface (Figure 3.58).

Figure 3.58 Cyclic voltammograms of methanol oxidation at increasing concentration in presence of 2.0 mol L^{-1} NaOH with Pd$_{(10cyc)}$-MWCNT/GCE at 50 mV s^{-1} scan rate

3.4.2 The electrocatalytic activity of palladium-gold and nickel-gold on methanol oxidation in alkaline solutions

To increase the catalytic activity of modified electrodes, the electrode surfaces modified with bimetallic particles which were prepared by electrochemical reduction method. The binary mixtures of Pd-Au and Au-Ni metal nanoparticles modified MWCNT/GC electrodes were prepared and applied to electrocatalytic oxidation of methanol in 2.0 mol L^{-1} NaOH solutions. The voltammetric behaviour of Pd-Au and Au-Ni metal nanoparticles modified MWCNT/GC electrodes were performed in the absence and in the presence of methanol in 2.0 mol L^{-1} NaOH solutions. Typical voltammograms were obtained for Au, Pd and Ni species into binary mixture of metals on MWCNT/GCE surface in absence of methanol (Figure 3.59).
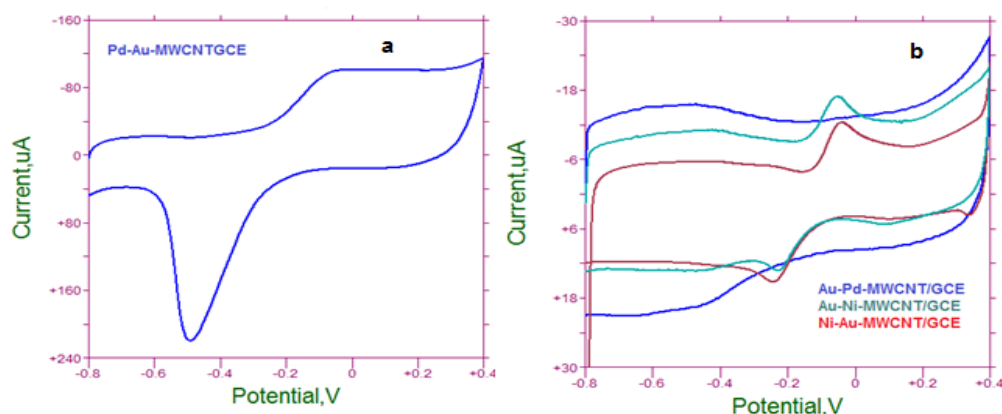
Figure 3.59 Cyclic voltammetric behaviour of a) Pd-Au-MWCNT/GCE b) Au-Pd-MWCNT/GCE, Au-Ni-MWCNT/GCE and Ni-Au-MWCNT/GC electrodes in 2.0 mol L^{-1} NaOH solutions as a supporting electrolyte. The scan rate was 50 mV s^{-1}

In the absence of methanol, there were small reduction and oxidation peaks at -0.105 V and -0.250 V which were concerning the presence of nickel and gold nanoparticles on $Au_{(10cyc)}$-$Ni_{(10cyc)}$-MWCNT/GCE or on Ni-Au-MWCNT/GC surfaces. The oxidation and reduction peaks at -0.055 V and -0.246 V belongs to oxidation and reduction of gold nanoparticles, respectively (Figure 3.59b). The synergic effect of the Pd and Au nanoparticles was tested using palladium electrodeposited on gold modified MWCNT/GCE and gold electrodeposited on palladium modified MWCNT/GCE.

For supporting electrolyte voltammogram, an oxidation peak at -0.04 V and a sharp reduction peak at -0.490 V is releated to Pd nanoparticles (Figure 3.59a). An irreversible electrode reaction was obtained for 2.0 mol L^{-1} methanol oxidation at 0.0 V on the Pd-Au-MWCNT/GCE in alkaline solution during the anodic potential scan (Figure 3.60). The other conbination of binary metalic electrodes could not show any catalitic effect on oxidation of methanol. The peak current was increased depending on methanol concentration accompanying positive shifting oxidation peak potential. With increasing of methanol concentration from Figure 3.61, the peak was increased but the peak potential shifted to positive side.
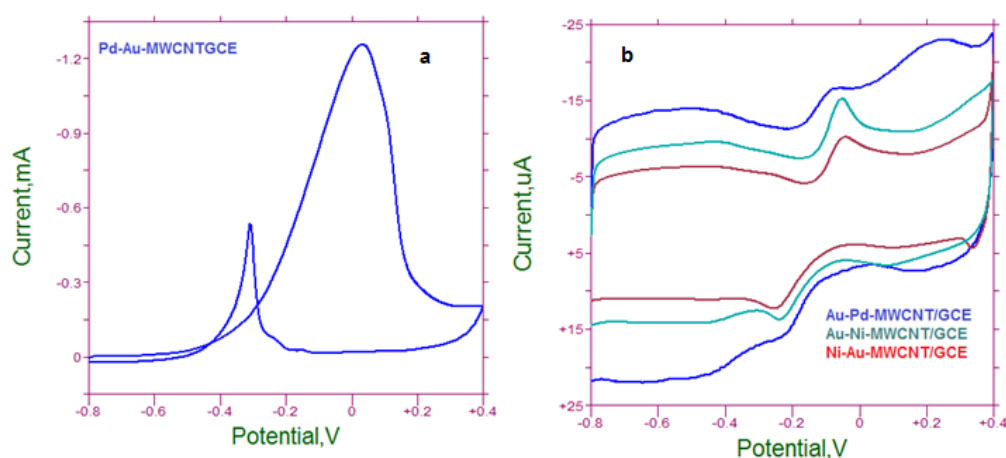
Figure 3.60 Cyclic voltammetric behaviour of a) Pd-MWCNT/GCE b) bare GCE, MWCNT/GCE and Au, Ni nanoparticles modified MWCNT/GC electrode in the presence of 2.0 mol L^{-1} methanol in 2.0 mol L^{-1} NaOH solutions. The scan rate was 50 mV s^{-1}
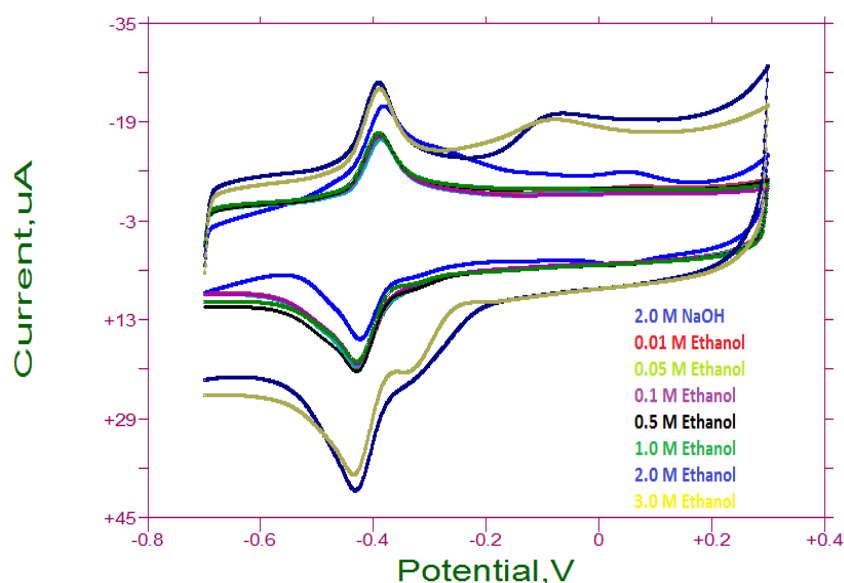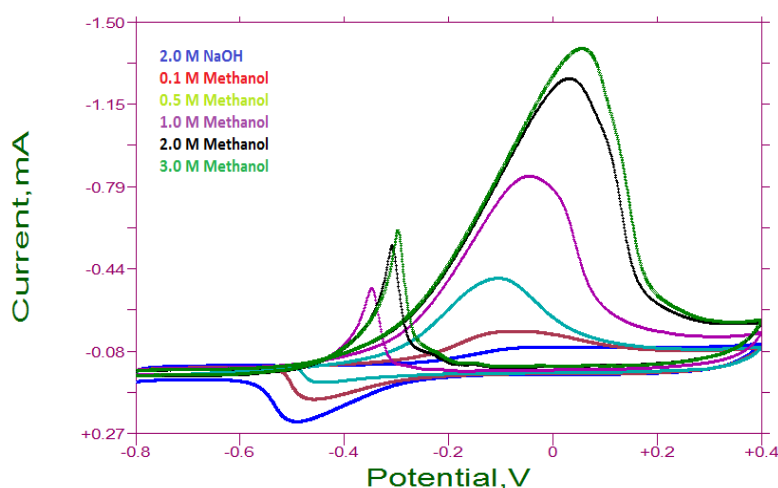

Figure 3.61 Cyclic voltammograms of methanol oxidation at increasing concentration in presence of 2.0 mol L^{-1} NaOH with Pd$_{(10cyc)}$-Au$_{(10cyc)}$-MWCNT/GCE at 50 mV s^{-1} scan rate

3.4.3 The electrocatalytic activity of palladium-gold-nickel on methanol oxidation in alkaline solutions

For methanol oxidation, to increase the catalytic activity, the MWCNT/GCE surface was modified with three metallic particles which were prepared by electrochemical reduction of Ni^{2+}, Au^{3+} and Pd^{2+} ions. The catalytic activity of Pd, Au, Ni nanoparticles were investigated Pd-Au-Ni nanoparticles modified MWCNT/GC electrode for methanol oxidation in the 1.0 and 2.0 mol L^{-1} NaOH solution (Figures 3.62). An oxidation peak was appeared at -0.150 V and a reduction peak at -0.400 V were related with metal Au, Pd and Ni species in the absence of methanol. The peak at -0.05 V was observed for methanol oxidation and a reverse oxidation peak was formed at -0.360 V due to the future oxidation of methanol oxidation products in the cathodic potential scan (Figure 3.63).

Figure 3.62 Cyclic voltammetric behaviour of Pd-Au-Ni nanoparticles modified MWCNT/GC electrode in alkaline solutions as a supporting electrolyte. The scan rate was 50 mV s^{-1}

Figure 3.63 Cyclic voltammetric behaviour of Pd-Au-Ni nanoparticles modified MWCNT/GC electrode in the presence of 2.0 mol L^{-1} methanol for different concentration of NaOH solutions. The scan rate was 50 mV s^{-1}

The effect of methanol concentration on peak current was also studied at Pd-Au-Ni-MWCNT/GCE. The peak current was increased with methanol concentration while peak potential shifting to positive values in the presence of 2.0 mol L^{-1} NaOH (Figure 3.64). The Pd-Au-Ni-MWCNT/GC electrode exhibits much higher catalytic activity for the electrooxidation of methanol in comparison to the polycrystalline Pd, Ni and Au disk electrodes and also bi and tri metalic MWCNT/GCE.

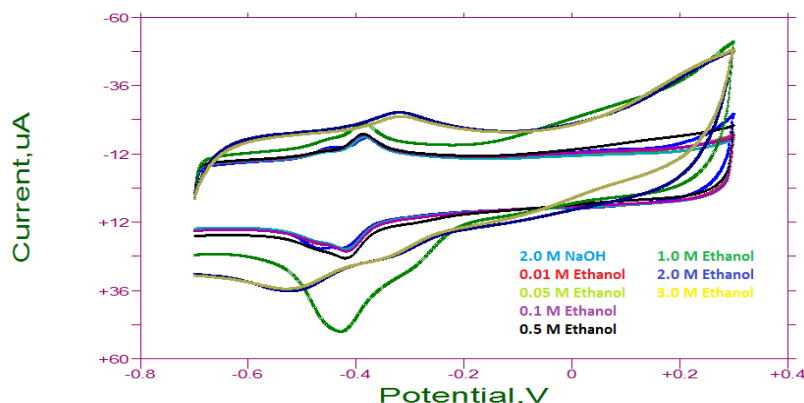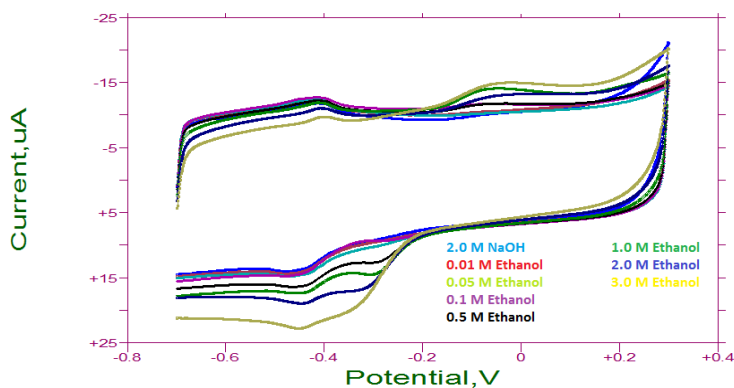**Figure 3.64 Cyclic voltammograms of methanol oxidation at increasing concentration in presence of 2.0 mol L^{-1} NaOH with Pd$_{(10cyc)}$-Au$_{(10cyc)}$-Ni$_{(10cyc)}$-MWCNT/GCE at 50 mV s^{-1} scan rate**

Table 3.10 Current-Potential values of 1.0 mol L^{-1} methanol in 2.0 mol L^{-1} NaOH with different types of electrodes

Electrodes	Peak Current (µA)	Peak Potential (V)
Pd-MWCNT/GCE	**492.7**	**-0.159**
Pd-Au-MWCNT/GCE	190.8	0.081
Pd-Au-Ni-MWCNT/GCE	245.9	-0.114

Table 3.11 shows that effect of cycle number on catalytic activity for methanol. To change cycle number, at 2.0 mol L^{-1} NaOH solution with different electrodes for 1.0 mol L^{-1} methanol. As can be seen from the Table 3.11, the best electrodes was choosen Pd$_{(5cyc)}$-Au$_{(5cyc)}$-Ni$_{(5cyc)}$-MWCNT/GC electrode.

Table 3.11 Current-Potential values of different cycle number for 1.0 mol L^{-1} methanol in 2.0 mol L^{-1} NaOH with Pd-Au-Ni-MWCNT/GCE

Electrodes	Peak Potential (V)	Peak Current (µA)
10 Pd - 10 Au- 10 Ni	0.006	646.8
10 Pd - 15 Au- 10 Ni	-0.112	580.8
5 Pd - 5 Au- 10 Ni	-0.096	583.4
10 Pd - 5 Au- 10 Ni	0.005	358.0
15 Pd - 15 Au- 15 Ni	-0.066	632.0
5 Pd - 5 Au- 15 Ni	-0.021	423.1
10 Pd - 5 Au- 15 Ni	-0.122	514.0
15 Pd - 10 Au- 5 Ni	0.009	600.7
10 Pd - 5 Au- 5 Ni	-0.113	589.1
5 Pd - 5 Au- 5 Ni	**-0.116**	**853.4**

3.4.4 Preparation of metal nanoparticles with chemical reduction methods and fabrication of metal nanoparticles modified multiwall carbon nanotubes/glassy carbon electrode for methanol oxidation in alkaline solutions

To compare the catalytic activity of metal nanoparticles modified MWCNT/GCE which were prepared by electrochemically method on methanol oxidation, the MWNTs decorated with metal nanoparticles catalyst, such as gold, nickel, palladium and their mixtures were prepared by chemically reduction method. For this aim, sodium borohydride and citric acid were used as reducing reagents. They were used as explained in section 2.3.4. The obtained results were discussed following sections.

3.4.4.1 The electrochemical behaviour of metal nanoparticles modified multiwall carbon nanotubes/glassy carbon electrode prepared with sodium borohydride for methanol oxidation in alkaline media

The voltammetric behaviour of Pd-MWCNT/GCE, Au-MWCNT/GCE and Ni-MWCNT/GCE was investigated in the absence and in the presence of methanol in the concentration range of 0.5-2.0 mol L^{-1} NaOH solution. The voltammograms were given in Figure 3.65 where the characteristic small oxidation and reduction peaks were observed during the anodic and cathodic potential scan in all concentrations of NaOH solutions. The voltammograms shows that Pd, Au and Ni nanoparticles were sensitized on MWCNT.

The voltammetric behaviour of methanol was studied at Pd-MWCNT/GCE in various concentration of NaOH as a supporting electrolyte. However, there was a small oxidation peak at -0.419 V on the positive potential scan (Figure 3.65), and also a reduction peak at -0.364 V due to the oxidation of Pd species formed during the anodic potential scan in the absence of methanol.
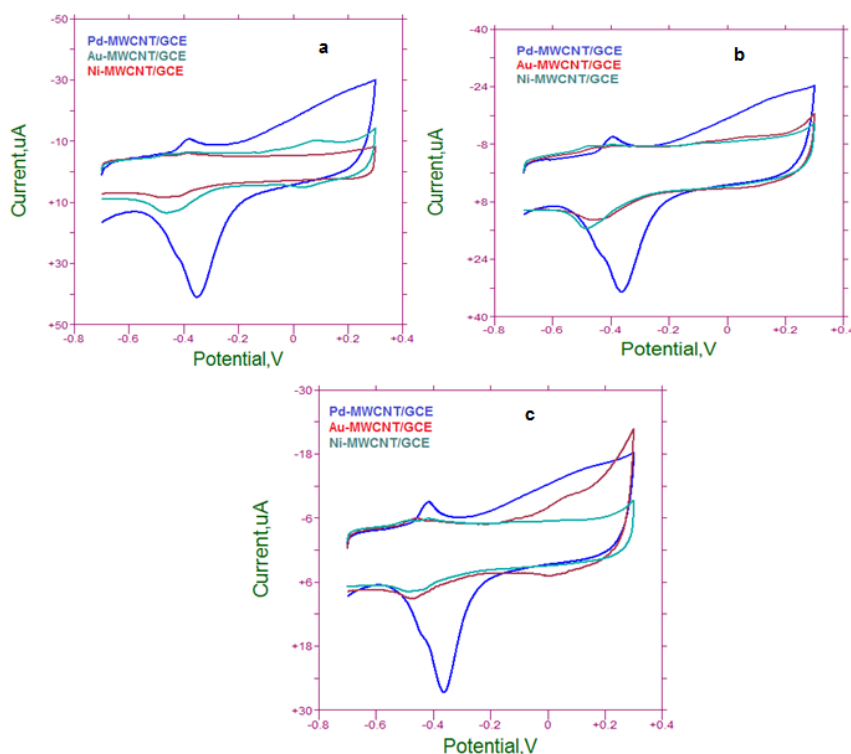
Figure 3.65 Cyclic voltammetric behaviour of Pd, Au and Ni nanoparticles modified MWCNT/GC electrodes in a) 0.5 mol L^{-1} b) 1.0 mol L^{-1} c) 2.0 mol L^{-1} NaOH solutions as a supporting electrolyte. The scan rate was 50 mV s^{-1}

Methanol oxidation took place at different potential by changing NaOH concentration (Figuer 3.66 and Table 3.12). The catalytic activity on methanol oxidation was increased with increasing of NaOH concentration depending on both peak current and peak potential values. In general, the peak potential of methanol was shifted towards low potentials with decreasing of NaOH concentration. The positive-shift in the peak potential suggests that the NaOH concentration has a favorable effect on the oxidation of methanol. The reverse peak was also formed almost same potentials as explained in above results.

Table 3.12 demonstrated that with Pd-MWNCT/GC electrode the higher catalytic activity observed on 2.0 mol L^{-1} NaOH solution. So that the following studies, 2.0 mol L^{-1} NaOH solutions were chosen as a supporting electrolyte.

There was an oxidation peak at -0.20 V for 0.5 mol L^{-1} methanol but the peak potential was shifted to positive potential by increasing methanol concentration for anodic potential scan (Figure 3.66). A reverse oxidation peak was observed during cathodic potential scan due to the adsorption of oxidized species of methanol during the anodic potential scan.

Table 3.12 Current-Potantial table for 0.5 mol L^{-1} methanol with

Pd-MWNCT/GCE

NaOH Solution Concentration (mol L^{-1})	Peak Current (μA)	Peak Potential (V)
2.0	**83.11**	**-0.200**
1.0	13.88	-0.032
0.5	43.05	-0.139
0.1	29.27	-0.110
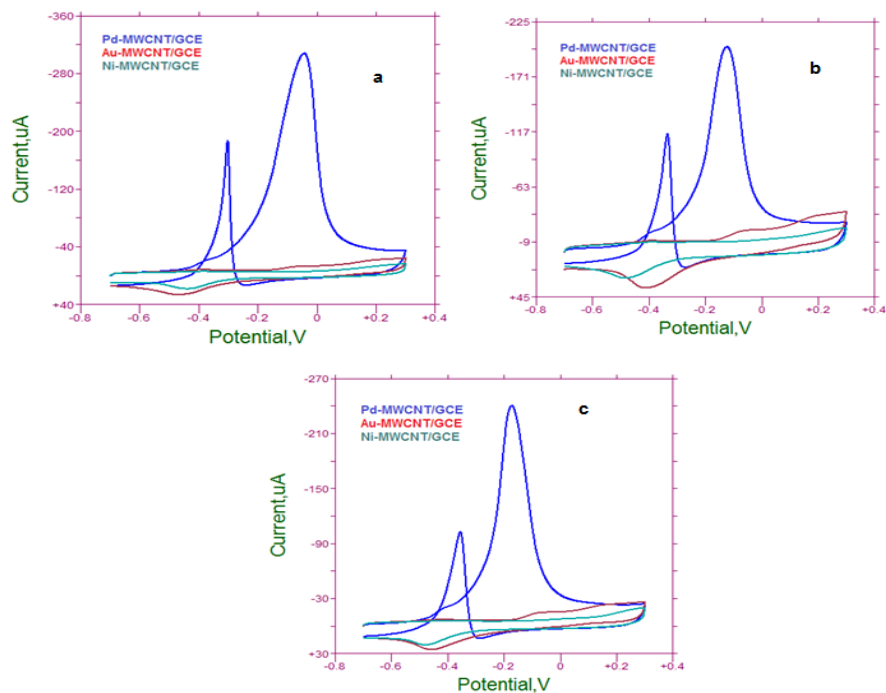
Figure 3.66 Cyclic voltammetric behaviour of Pd, Au and Ni nanoparticles modified MWCNT/GC electrode in the presence of 2.0 mol L^{-1} methanol for a) 0.5 mol L^{-1} b) 1.0 mol L^{-1} c) 2.0 mol L^{-1} NaOH solutions. The scan rate was 50 mV s^{-1}
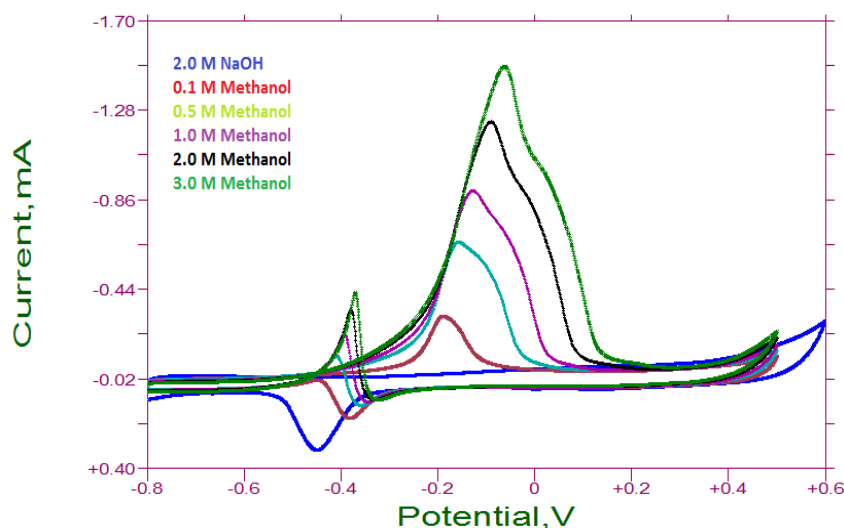

Figure 3.67 Cyclic voltammograms of methanol oxidation at increasing concentration in presence of 2.0 mol L^{-1} NaOH with Pd-MWCNT/GCE at 50 mV s^{-1} scan rate

The peak potential at -0.20 V in 2.0 mol L^{-1} NaOH solution was shifted to positive potential by increasing methanol concentration for anodic potential scan (Figure 3.67).

The second step of chemical reduction procedure with sodium borohydride reaction, the binary mixtures of Pd-Au, Pd-Ni and Au-Ni metal nanoparticles modified MWCNT/GC electrodes were prepared and applied to electrocatalytic oxidation of methanol in different concentration of NaOH solutions.

The voltammetric behaviour of Pd-Au, Pd-Ni and Au-Ni metal nanoparticles modified MWCNT/GC electrodes were performed in the absence and in the presence of ethanol. Typical voltammograms were obtained for Au, Pd and Ni species into binary mixture of metals on MWCNT/GCE surface (Figure 3.68).
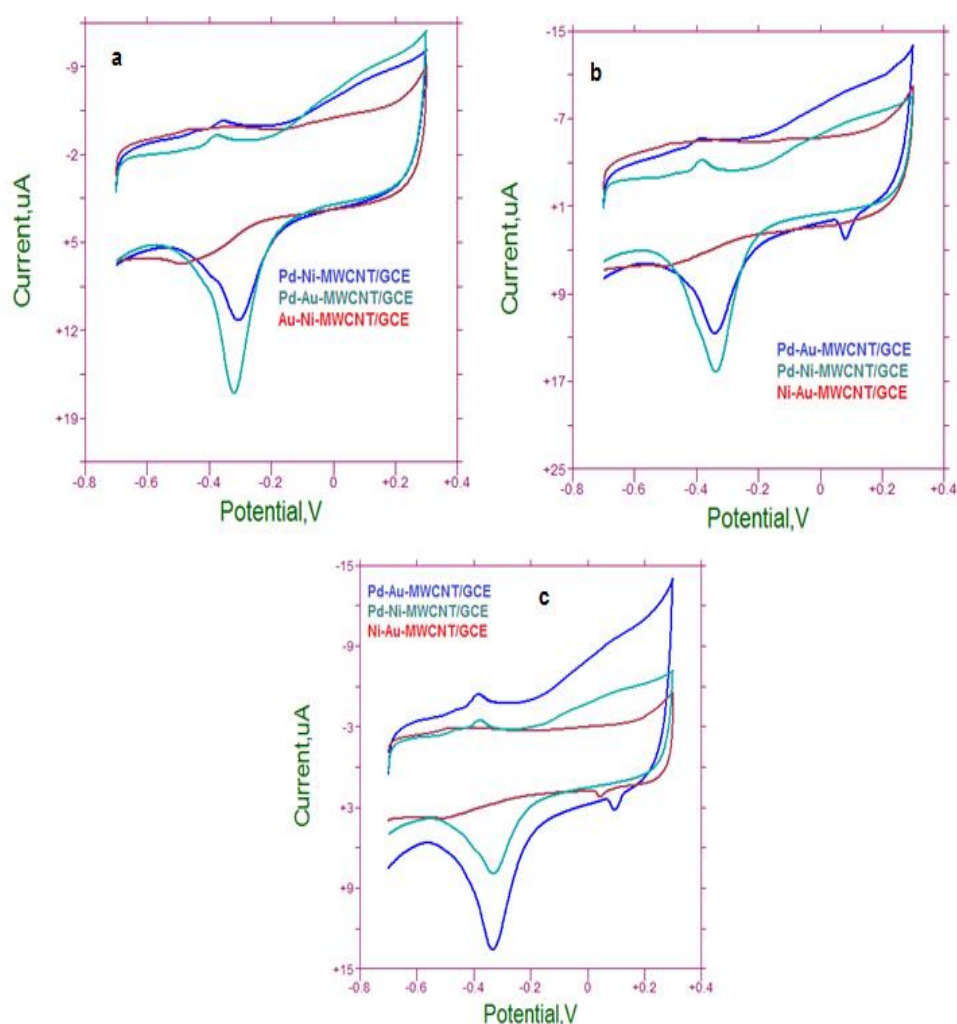
Figure 3.68 Cyclic voltammetric behaviour of Pd-Au, Au-Ni and Pd-Ni nanoparticles modified MWCNT/GC electrodes in a) 0.5 mol L^{-1} b) 1.0 mol L^{-1} c) 2.0 mol L^{-1} NaOH solutions as a supporting electrolyte. The scan rate was 50 mV s^{-1}
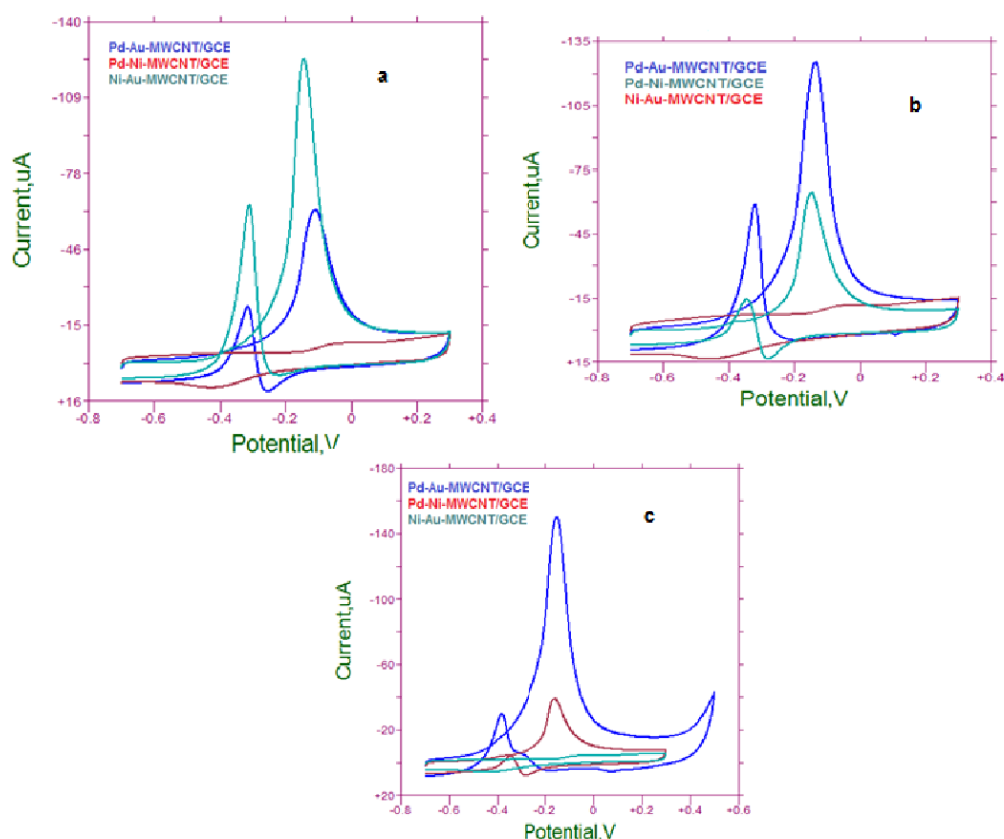
Figure 3.69 Cyclic voltammetric behaviour of Pd-Au, Au-Pd and Pd-Ni nanoparticles modified MWCNT/GC electrode in the presence of 2.0 mol L^{-1} methanol for a) 0.5 mol L^{-1} b) 1.0 mol L^{-1} c) 2.0 mol L^{-1} NaOH solutions. The scan rate was 50 mV s^{-1}

Figure 3.69 shows, 2.0 mol L^{-1} methanol oxidation was observed at almost same potential at about -0.150 V on the Pd-Au-MWCNT/GCE in all NaOH solutions during the anodic potential scan. The peak current was unchanged by increasing of NaOH concentration at those electrodes. In the case of Pd-Ni-MWCNT/GCE, a small oxidation peak was observed accompanying positive peak potential compare Pd-Au-MWCT/GCE results. The peak potential was also almost constant at all NaOH media on Pd-Ni-MWCNT/GCE. On the other hand, Ni-Au-MWCNT/GCE did not show any catalytic activity towards ethanol oxidaton in all NaOH solutions.

In the third step of chemical reduction procedure with sodium borohydride reaction, the binary mixtures of Pd-Au-Ni metal nanoparticles modified MWCNT/GC electrode was prepared and applied to electrocatalytic oxidation of methanol in different concentration of NaOH solutions.

The voltammetric behaviour of Pd-Au-Ni modified MWCNT/GC electrodes were studied in the absence and in the presence of ethanol. Typical voltammograms were obtained for Au, Pd and Ni species into mixture of metals on MWCNT/GCE surface (Figure 3.70).
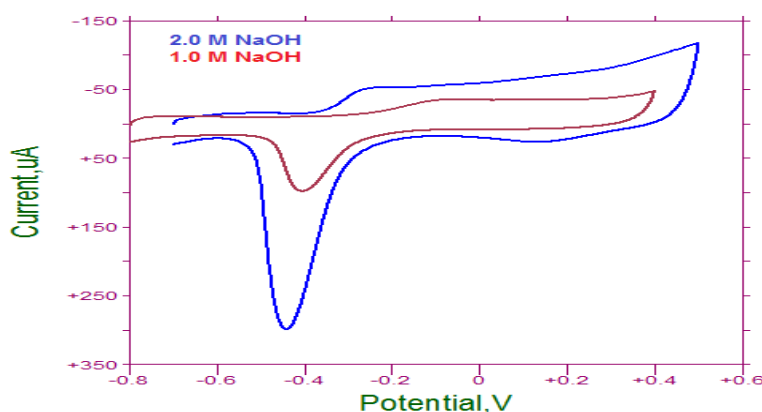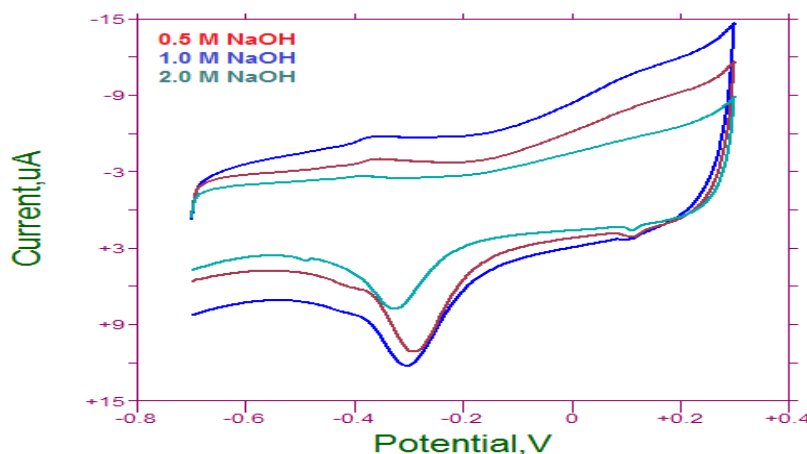

Figure 3.70 Cyclic voltammetric behaviour of Pd-Au-Ni nanoparticles modified MWCNT/GC electrode in alkaline solutions as a supporting electrolyte. The scan rate was 50 mV s^{-1}
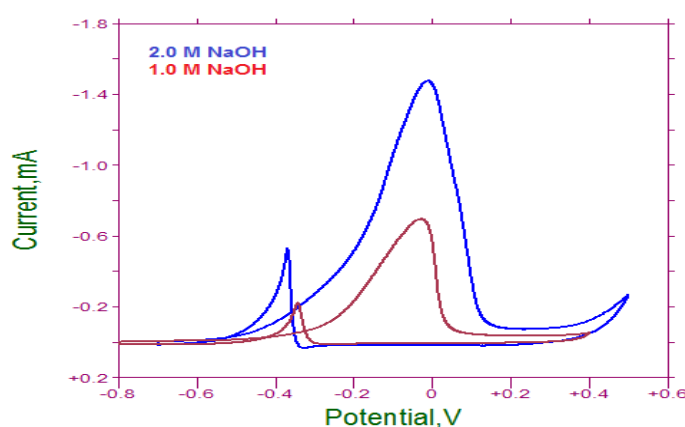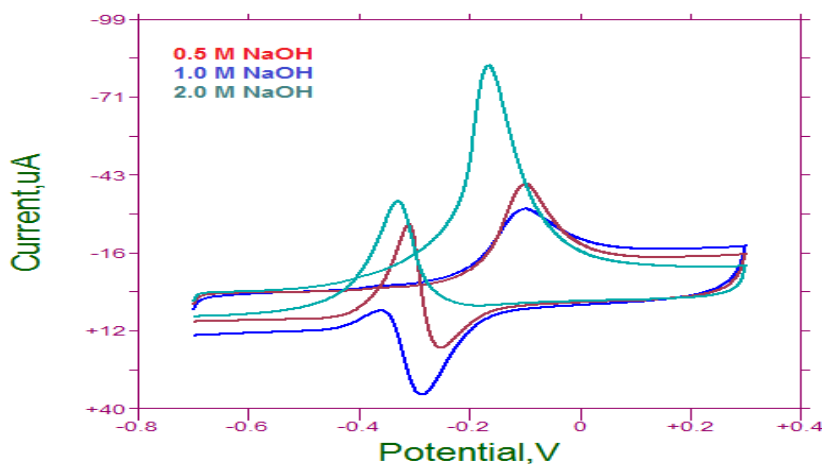

Figure 3.71 Cyclic voltammetric behaviour of Pd-Au-Ni-MWCNT/GC electrode in the presence of 2.0 mol L^{-1} methanol for different concentration of NaOH solutions. The scan rate: 50 mV s^{-1}

The electrocatalytical oxidation of 2.0 mol L^{-1} methanol was investigated at Pd-Au-Ni-MWCNT/GCE in different concentration of NaOH solutions (Figure 3.71). An oxidation peaks at -0.180 V was observed during the anodic potential sweep. The reverse oxidation peak was also appeared in the cathodic potential scan as the reasons explained above for Pd based electrodes.
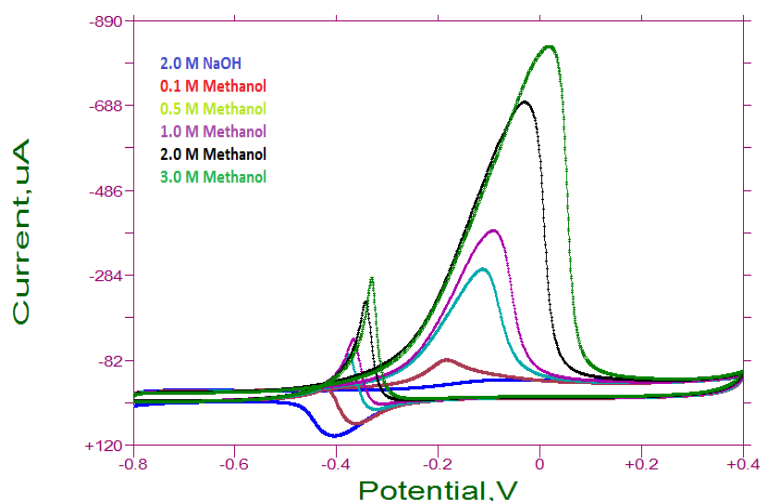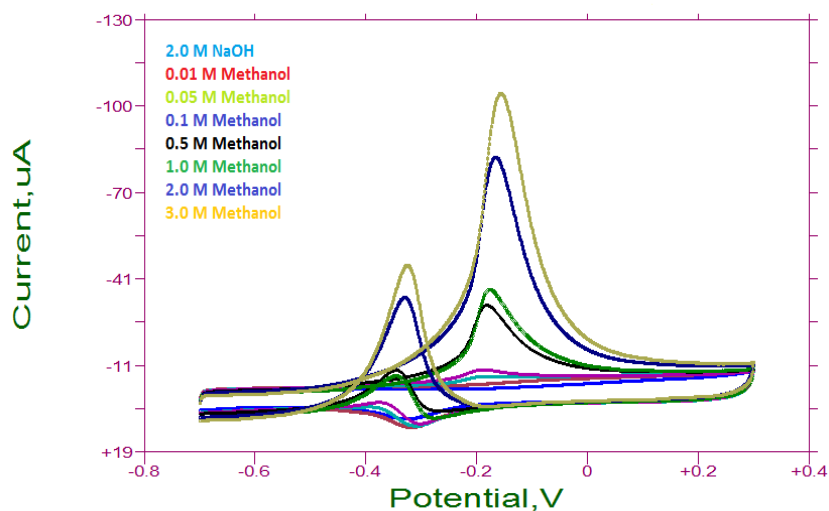
Figure 3.72 Cyclic voltammograms of methanol oxidation at increasing concentration in presence of 2.0 mol L^{-1} NaOH with Pd-Au-Ni-MWCNT/GCE at 50 mV s^{-1} scan rate

The Pd-Au-Ni-MWCNT/GC electrode exhibits much higher catalytic activity for the electrooxidation of methanol in comparison to the Pd, Ni and Au modified multiwall carbon nanotube electrodes and also bi and tri metalic MWCNT/GCE. The peak potential is comparable for the all electrodes. The shift of this onset potential to a more negative value means that metal nanoparticles can significantly enhance the electrooxidation kinetics of methanol, which is important for its application in fuel cells.
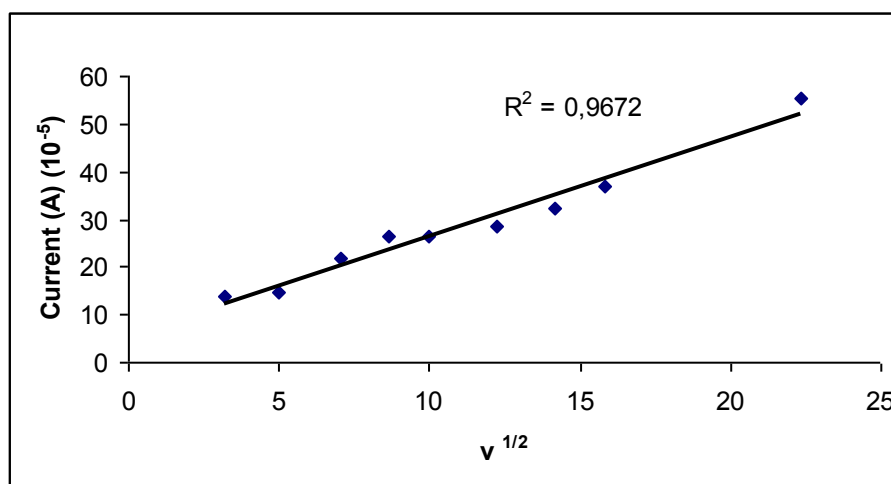
Figure 3.73 Dependence of scan rate on peak potential of 0.5 mol L^{-1} methanol at Pd-Au-Ni-MWCNT/GCE to 2.0 mol L^{-1} NaOH solution

The plots of 0.5 mol L^{-1} methanol oxidation in the presence of 2.0 mol L^{-1} NaOH peak current vs. (scan rate)$^{1/2}$ for Pd-Au-Ni-MWCNT/GCE were given in Figure 3.73. The peak current has shown a linear increase with the square root of the scan rate, indicating that a diffusion-controlled electrode process takes place at the Pd-Au-Ni-MWCNT/GCE surface. The peak potential was also shifted towards positive potential depending on increasing of (scan rate)$^{1/2}$ indicating an irreversible electrode reaction.

3.4.4.2 The electrochemical behaviour of metal nanoparticles modified multiwall carbon nanotubes/glassy carbon electrode prepared with citric acid for methanol oxidation in alkaline media

Citric acid as another reducing reagent in acidic solution was used to prepare metal nanoparticles decorated multiwalled carbon nanotube electrodes as well. The each electrode was investigated for methanol oxidation.

3.4.4.2.1 Gold nanoparticles decorated multiwall carbon nanotubes

The voltammetric behaviour of methanol was studied at Au-MWCNT/GCE in different concentrations of NaOH (2.0 mol L^{-1}, 1.0 mol L^{-1}, 0.5 mol L^{-1} and 0.1 mol L^{-1}) as a supporting electrolyte. The oxidation peak at -0.370 V and also a reduction peaks at -0.440 V releated to gold nanoparticles in the absences of methanol.
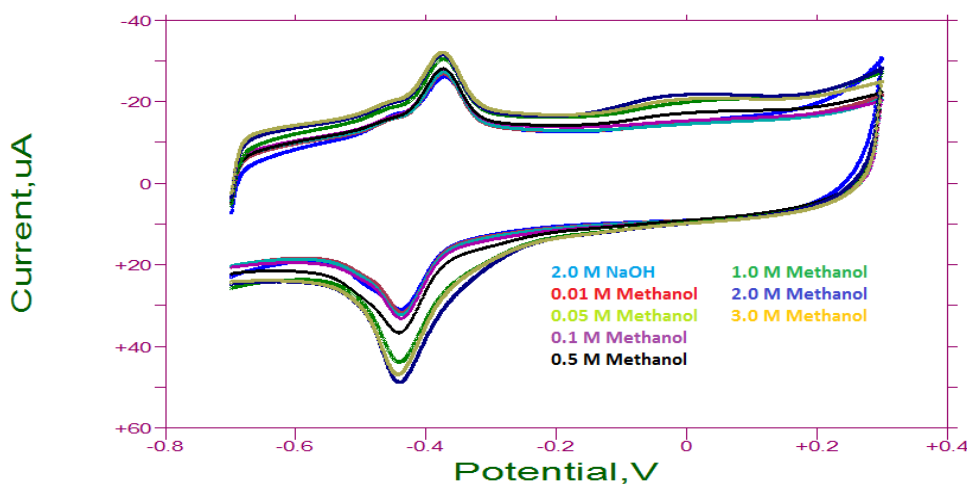
Figure 3.74 Cyclic voltammograms of methanol oxidation at increasing concentration in presence of 2.0 mol L^{-1} NaOH with Au-MWCNT/GCE at 50 mV s^{-1} scan rate

The electrochemical behaviour of gold nanoparticles decorated Au-MWCNT/GCE was studied by CV in 2.0 mol L^{-1} NaOH solution in the presence of different methanol concentration and the corresponding CVs are shown in Figure 3.88. The forward potential scan was showed an oxidation paek at nearly -0.370 V while the reduction peak was observed at -0.445 V for methanol reverse potential scan. Figure 3.74 showed Au nanoparticles could not increase the electrocatalytic activity of MWCNT/GCE.

3.4.4.2.2 Gold and nickel nanoparticles decorated multiwall carbon nanotubes

To increase the catalytic activity of nanoparticles modified electrodes, bimetallic active sites were formed at MWCNT/GCE surface, prepared by chemically reduction procedure with citric acid solution. Firstly, gold and nickel nanoparticles modified electrodes were prepared.

The cyclic voltammograms were recorded for Au-Ni-MWCNT/GCE in 2.0 mol L^{-1} NaOH supporting electrolyte. An oxidation peaks appared at -0.378 V at Au-Ni-MWCNT/GC electrode on the anodic potential scan and one broad reduction peak were observed -0.433 V which were releated to oxidation and reduction of gold and nickel nanoparticles.
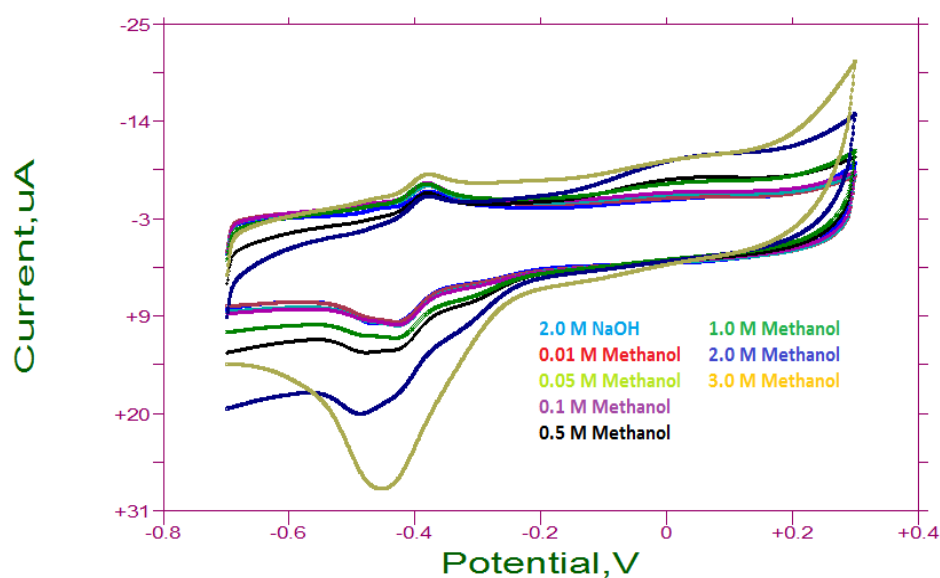
Figure 3.75 Cyclic voltammograms of methanol oxidation at increasing concentration in presence of 2.0 mol L^{-1} NaOH with Au-Ni-MWCNT/GCE at 50 mV s^{-1} scan rate

Bimetalic modified Au-Ni-MWCNT/GC electrodes could not show any catalic effect for methanol oxidation. The small and broad oxidation and reduction peaks were related to Au and Ni species (Figure 3.75).

3.4.4.2.3 Palladium, gold and nickel nanoparticles decorated multiwall carbon nanotubes

To increase the catalytic activity of modified electrodes, the electrode surfaces modified with trimetallic particles which were prepared by chemically reduction procedure with citrate solution. The electrocatalytical oxidation of 0.5 mol L^{-1} methanol was investigated at Pd-Au-Ni-MWCNT/GCE. Figure 3.76 shows that cyclic voltammograms of various 2.0 mol L^{-1} NaOH as a supporting electrolyte at Pd-Au-Ni-MWCNT/GC electrode. There was a broad oxidation at -0.391 V and at -0.365 V there was a reverse oxidation peak.
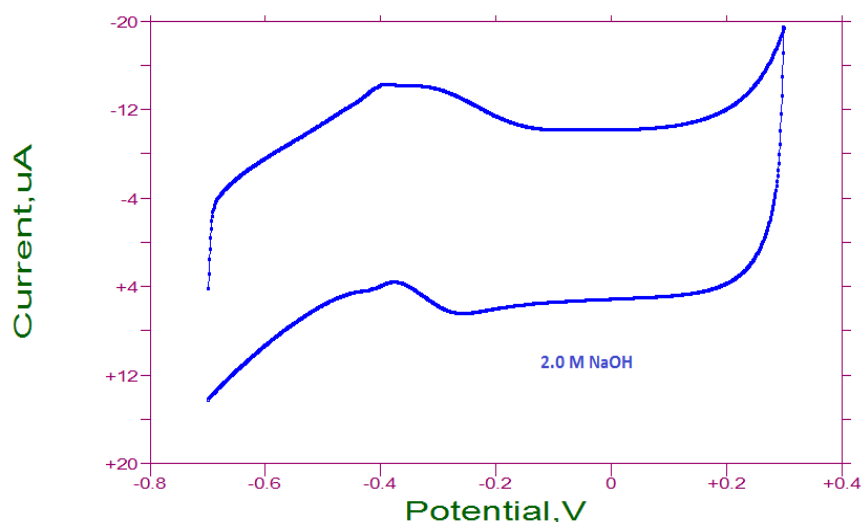
Figure 3.76 Cyclic voltammograms of 2.0 mol L^{-1} NaOH supporting electrolyte for Pd-Au-MWCNT/GCE with a scan rate of 50 mV s^{-1}

From the Figure 3.77, for 0.5 mol L^{-1} methanol the oxidation peak at -0.118 V was related to oxidation of methanol. The chemical reduction method with citrate solution could not exhibit catalytic activity for the electrooxidation of methanol comparison to electrochemical reduction method.
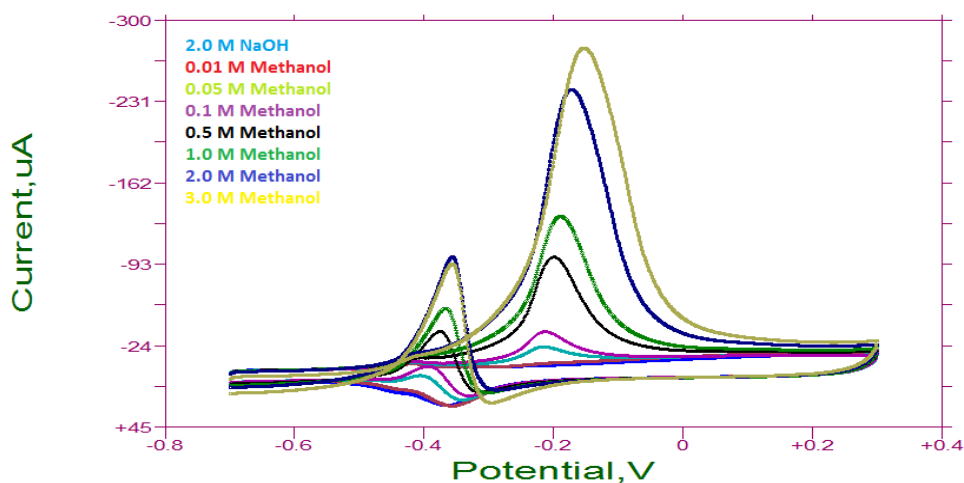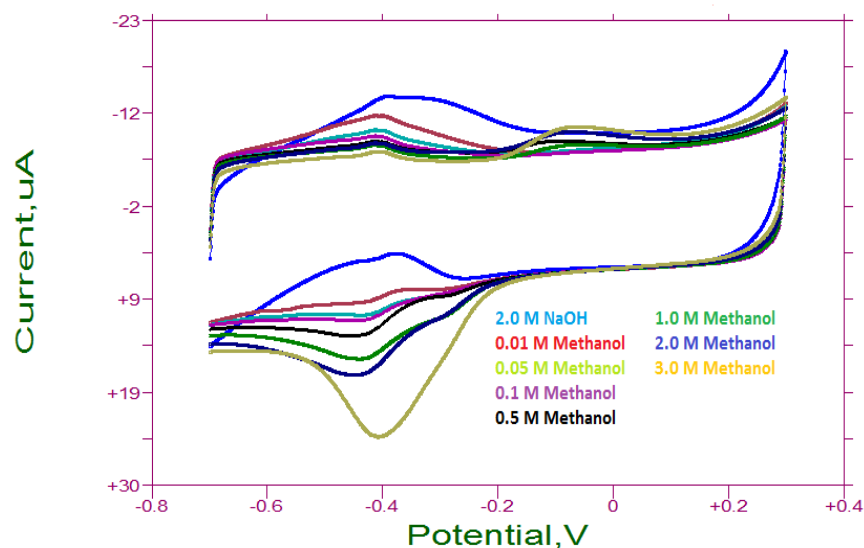
Figure 3.77 Cyclic voltammograms of methanol oxidation at increasing concentration in presence of 2.0 mol L^{-1} NaOH with Pd-Ni-MWCNT/GCE at 50 mV s^{-1} scan rate

3.4.5 Methanol Oxidation in Mixture of Gold, Palladium and Nickel

A mixture of gold, palladium and nickel solutions at 1.0×10^{-3} mol L^{-1} was prepared at volume ratio of 1:1:1. MWCNT/GC electrode surface was coated in the potential range of 1.0 V to -1.5 V at 50 mV s^{-1} for 10 cycles (Figure 3.78).
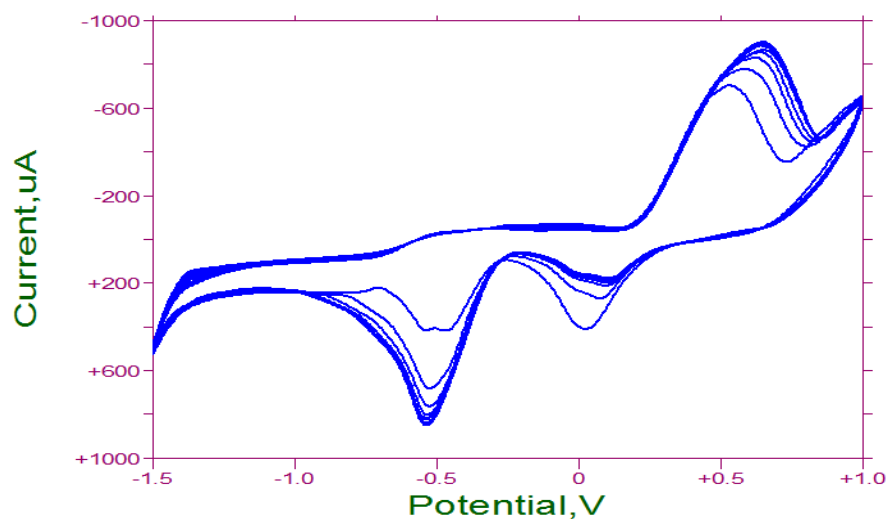
Figure 3.78 Consecutive cyclic voltammograms of palladium, gold and nickel nanoparticles on a MWCNT-GCE in a solution containing 1.0×10^{-3} $HAuCl_4$+0.1 mol L^{-1} HCl and 1.0×10^{-3} mol L^{-1} $PdSO_4$+1.0×10^{-3} mol L^{-1} $NiSO_4$+0.1 mol L^{-1} H_2SO_4 at 50 mV s^{-1} scan rate

The reduction and oxidation peaks for gold, palladium and nickel nanoparticles were obtained again (Figure 3.78). However, the peak current of methanol oxidation was lower than those obtained by the electrode coated with single nanoparticles, given in Figures 3.1, 3.2 and 3.3. The oxidation potential of methanol was observed at little more positive potential. But this electrode was not investigated in detail, after these results (Figure 3.79).
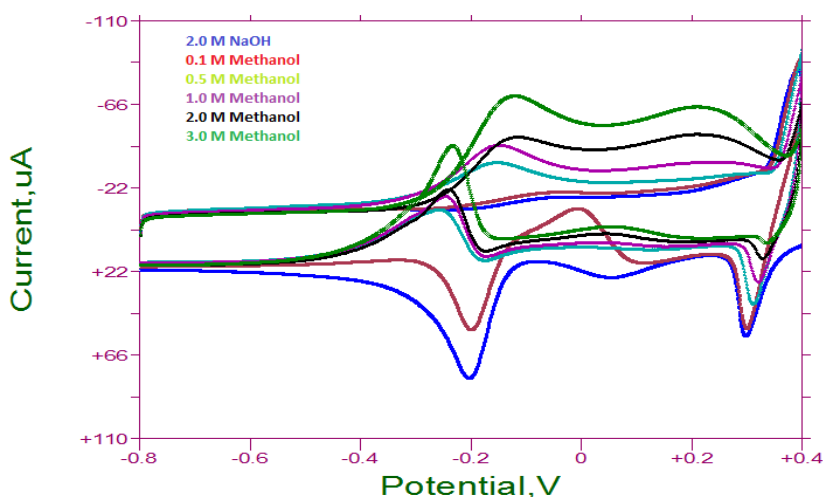
Figure 3.79 Cyclic voltammograms of methanol oxidation at increasing concentration in presence of 2.0 mol L^{-1} NaOH with Pd-Au-Ni-MWCNT/GCE at 50 mV s^{-1} scan rate

3.4.6 Electrooxidation of methanol and ethanol by chronoamperometry

In order to investigate the electrocatalytic performance of the Pd-MWCNT/GCE, Pd-Au-MWCNT/GCE and Pd-Au-Ni-MWCNT/GCE for methanol and ethanol oxidation, chronoamperometric (CA) measurements were performed by applying different potential steps inside the ethanol and methanol oxidation potential region for 120.0 seconds.

The chronoamperometric curves of Pd-MWCNT/GCE, Pd-Au-MWCNT/GCE and Pd-Au-Ni-MWCNT/GCE electrocatalysts systems in the electrolyte solution of 2.0 mol L^{-1} NaOH solution as a supporting electrolyte for 0.5 mol L^{-1} methanol were shown in Figure 3.80. The initial current values in all the curves for all catalysts systems have decreased quickly in a short time followed by a slow decay rate and finally approached nearly steady current. The chronoamperometry results showed that Pd-MWCNT/GCE electrocatalyst showed low activity for ethanol oxidation.

However, the addition of Au nanoparticles increased the catalytic activity of the Pd-Au-MWCNT/GCE catalyst. In addition to this, adding Ni nanoparticles the catalytic activity was increased.
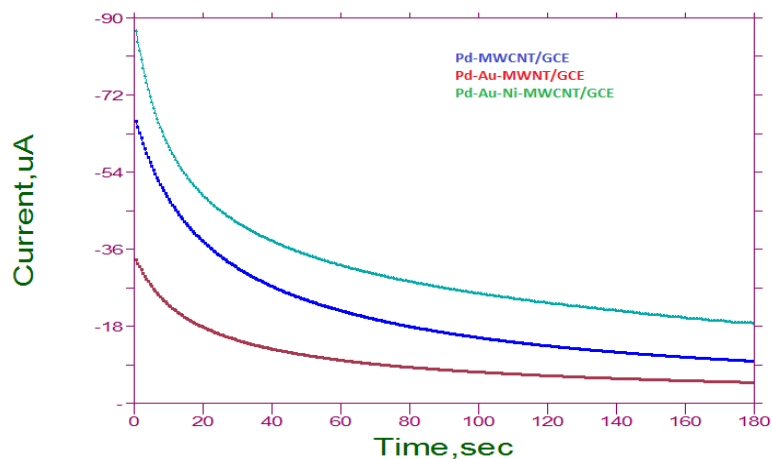
Figure 3.80 Chronoamperometric Curves at 0.03 V in 0.5 mol L^{-1} Methanol solution in 2.0 mol L^{-1} NaOH for the electrocatalysts

Chronoamperometric curves of Pd-MWCNT/GCE, Pd-Au-MWCNT/GCE and Pd-Au-Ni-MWCNT/GCE electrocatalysts systems in the electrolyte solution of 1.0 mol L^{-1} NaOH solution as a supporting electrolyte for 0.5 mol L^{-1} ethanol at room temperature was given in Figure 3.81. It can be seen in Figure 3.81, all current-time curves an initial current values were dropped rapidly until 20.0 seconds which can be explained by fast surface poisoning by adsorbed intermediate product. After the 20.0 seconds, the CA curves became relatively stable. Pd-Au-Ni-MWCNT/GC electrode show stable currents for ethanol oxidation after 20.0 seconds while the Pd-MWCNT/GC alone catalyst continue its decay towards zero current.
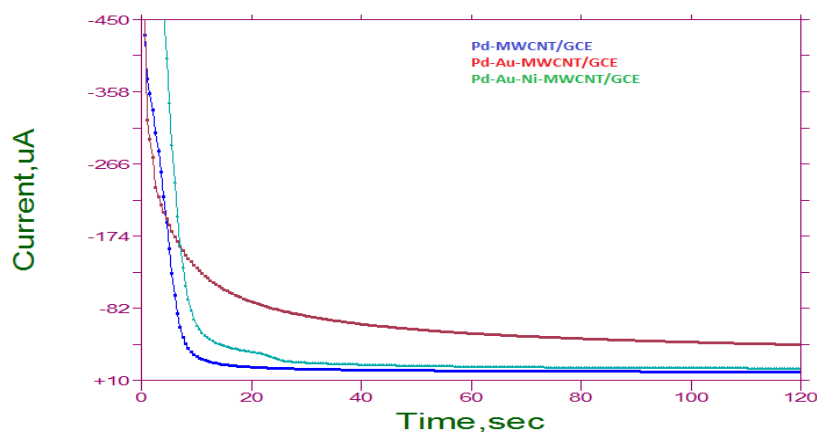
Figure 3.81 Chronoamperometric Curves at 0.1 V in 0.5 mol L^{-1} Ethanol solution in 0.5 mol L^{-1} NaOH for the electrocatalysts

3.4.7 Electrochemical impedance spectroscopy

Electrochemical impedance spectroscopy (EIS) is a method consisting of the application of a small current or voltage to an electrochemical system and monitoring the response of the system. Electrode properties were characterized using Nyquist plots from EIS measurements to better elucidate the interaction between the electrolyte, electrode surface, and the charge transfer within catalytic structure. In impedance measurements, a sinusoidal potential variation is applied to the under studied electrodes such as; Pd-MWCNT/GCE, Au-MWCNT/GCE, Ni-MWCNT/GCE, Pd-Au-MWCNT/GCE, Au-Ni-MWCNT/GCE and Pd-Au-Ni-MWCNT/GCE. Electrochemical impedance spectra were established by scanning 0.1 Hz up to 500 kHz at room temperature. Impedance diagrams are normally expressed as Nyquist and Bode plots. In this study, the Nyquist plot was used for the impedance versus the real part of the impedance. The Nyquist plots were obtained by 0.1 mol L^{-1} KCl as a supporting electrolyte including 5.0×10^{-3} mol L^{-1} for both $K_4Fe(CN)_6$ and $K_3Fe(CN)_6$.

The electrochemical impedance spectra for all the electrodes (excepct of Pd-MWCNT and Pd-Au-Ni-MWCNT/GCE) include a semicircular and a linear portion. The semicircle shapes in the spectra shows that there is a charge transfer process through the electrode and the coated nanoparticles at high frequency. On the other hand, in the low frequencies diffusion process is responsible for the electron transfer. The semicircle diameter presents the magnitude Rct at electrode surface. The EIS data were fitted with an equivalent circuit. This equivalent circuit consists of the ohmic resistance (Rs) of the electrolyte solution, the double layer capacitance (Cdl), electron-transfer resistance (Rct) resulting from the diffusion of ions from the bulk of the electrolyte to the interface.

In the case of GCE, MWCNT/GCE, Pd-MWCNT/GCE, Au-MWCNT/GCE, Ni-MWCNT/GCE, Ni-Au-MWCNT/GCE, Pd-Au-MWCNT/GCE and Pd-Au-Ni-MWCNT/GCE, the anode impedances were found to be 636.04 Ω, 11.82 kΩ, 22.83 kΩ, 4.98 kΩ, 7.06 kΩ, 9.53 kΩ, 1.17 kΩ, 11.91 kΩ, respectively (Figures 3.82-3.83). This behaviour shows that the semicircle corresponds to the charge transfer process through the GCE to metal nanoparticles modified carbon nanotubes electrodes at high frequencies, in contrast, the second step was due to the diffusion process in the low frequencies.

The diameter of the semicircle represents the magnitude of R_{ct} at the electrode surface. This equivalent circuit consists of the ohmic resistance (Rs) of the electrolyte solution, the double layer capacitance (Cdl), electron-transfer resistance (Rct) resulting from the diffusion of ions from the bulk of the electrolyte to the interface. The results of EIS measurements were detailed in Table 3.13. This reveals a slow ethanol oxidation reaction rate due to intermediates, which are strongly adsorbed onto Pd, blocking incessant adsorption and dehydrogenation of ethanol.

Table 3.13 EIS results for R_{ct}, W and C_{dl} obtained after fitting the electrochemical impedance spectra with the equivalent circuit

Electrodes	R_{ct} (Ω)	W (mMho)	C_{dl} (F)
GCE	636.04 Ω	0.46	618.0 nF
MWCNT/GCE	11.82 kΩ	1.78	900.0 fF
Pd-MWCNT/GCE	22.83 kΩ	8.53	900.0 fF
Au-MWCNT/GCE	4.98 kΩ	1.28	900.0 fF
Ni-MWCNT/GCE	7.06 kΩ	11.81	1.1 pF
Ni-Au-WCNT/GCE	9.53 kΩ	10.94	900.0 fF
Pd-Au-MWCNT/GCE	1.17 kΩ	5.28	3.9 mF
Pd-Au-Ni-MWCNT/GCE	11.91 kΩ	9.31	900.0 fF
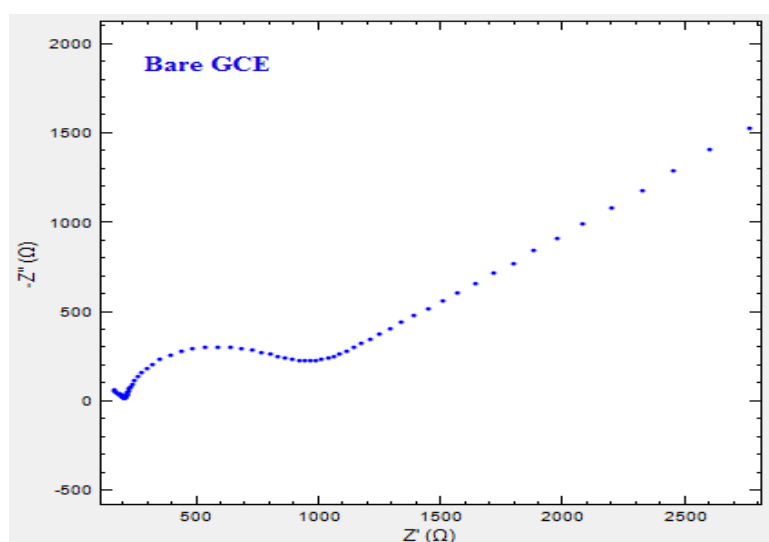
Figure 3.82 Electrochemical impedance spectroscopy of bare GCE. Supporting electrolyte, 5.0×10^{-3} mol $L^{-1} K_3Fe(CN)_6/K_4Fe(CN)_6$ in 0.1 mol L^{-1} KCl
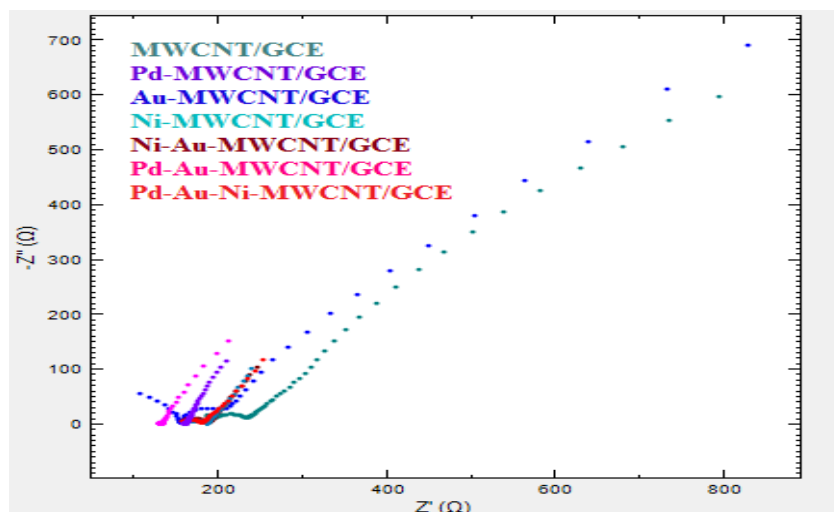
Figure 3.83 Electrochemical impedance spectroscopy of the different electrodes Pd-Au-Ni-MWCNT/GCE, MWCNT/GCE, Pd-MWCNT/GCE, Au-MWCNT/GCE, Ni-MWCNT/GCE, Pd-Au-MWCNT/GCE, Ni-Au-MWCNT/GCE modified electrodes. Supporting electrolyte, 5.0×10^{-3} mol $L^{-1} K_3Fe(CN)_6 / K_4Fe(CN)_6$ in 0.1 mol L^{-1} KCl

3.5 Voltammetric Determination of Lead and Cadmium by Different Modified Carbon Paste Electrodes

Stripping voltammetric techniques are among most popular methods for the determination of heavy metal ions at trace levels, due to their speed, acceptable analytical sensitivity, simplicity, relatively low instrumental cost and minimum sample pretreatment etc. However, voltammetric determination of trace metals after their preconcentration at modified electrodes is one of the important current research areas in electrochemical analysis.

In order to improve sensitivity, accuracy, precision and speed of voltammetric determination, moreover, recently, the developing of the new modified carbon paste electrodes (MCPEs) have received significant attention (Keawkim et al., 2013; Mousavi et al., 2001). The modified electrodes are inexpensive and possess many advantages such as low background current, wide range of used potential and easy fabrication. These can enhance the analytical sensitivity and selectivity of the electrodes by preconcentration of analytes onto the modified electrode surface in the accumulation step. Until now, many modifiers such as hydroxyapatite, zirconium phosphated amorphous silica, multiwall carbon nanotubes have been used in the construction of MCPEs (Li et al., 2009; Shams and Torabi 2006; Wu et al., 2003).

In this section of the thesis, six different modified carbon pasta and multiwall carbon nanotubes on glassy carbon electrodes were prepared using Potassium Ferrocyanide-Carbon Nanotubes, Calcium Phosphate, $Ca_3(PO_4)_2+ZrO(H_2PO_4)_2$, $Ca_3(PO_4)_2+Cu_2Fe(CN)_6$, Bismuth-Antimony film and Bismuth-Tin film as a modifier and tested for voltammetric quantitative determinations of lead and cadmium.

3.5.1 Anodic stripping voltammetric determination of Lead(II) with potassium ferrocyanide-carbon nanotubes modified carbon paste electrode

A carbon paste modified electrode for determination of trace amount of lead was prepared using MWCNTs, potassium ferrocyanide and silicate to the sensitive determeination of lead. MWCNTs have a good conductivity which helps the transduction of the signal in CPEs (Ganjali et al., 2010).

3.5.1.1 Effect of the mass ratio of carbon paste to multiwall carbon nanotubes, potassium ferrocyanide and silicate

In initial experiments, the carbon paste electrodes were modified with silicate, silicate+potassium ferrocyanide and silicate+potassium ferrocyanide+carbon nanotubes. The modifications of carbon paste electrodes are given following;

1. 70.0 % graphite + 30.0 % mineral oil

2. 65.0 % graphite + 25.0 % mineral oil + 10.0 % silicate

3. 65.0 % graphite + 25.0 % mineral oil + 5.0 % silicate + 5.0 % $K_4Fe(CN)_6$

4. 64.0 % graphite + 25.0 % mineral oil + 5.0 % silicate + 5.0 % $K_4Fe(CN)_6$ + 1.0 % carbon nanotubes

5. 65.0 % carbon nanotubes + 25.0 % mineral oil + 5.0 % silicate + 5.0 % $K_4Fe(CN)_6$

The differential pulse anodic stripping voltammetric behaviour of Pb(II) was performed using $K_4Fe(CN)_6$ immobilized silica modified CPE during 300.0 seconds accumulation time at -0.80 V deposition potential from the 3.0×10^{-8} mol L^{-1} Pb(II) ions containing solution on the modified electrode surface. Generally, after the anodic depostion of metallic Pb from the Pd(II) ions containing solution, it was oxidized at -0.55 V at modified carbon paste electrode.

All voltammograms were obtained in the presence 0.2 mol L^{-1} acetic acid soluion. The acetic acid concentration was choosen from the literature (Tesarova et al., 2009).The electrodes were evaluated in 0.2 mol L^{-1} CH$_3$COOH supporting electrolyte media. Figure 3.84 shows that the mixture of 64.0 % graphite + 25.0 % mineral oil + 5.0 % silicate + 5.0 % K$_4$Fe(CN)$_6$ + 1.0 % carbon nanotube electrode was the best electrode composition for Pb(II) determination as it gives the highest peak current for lead.
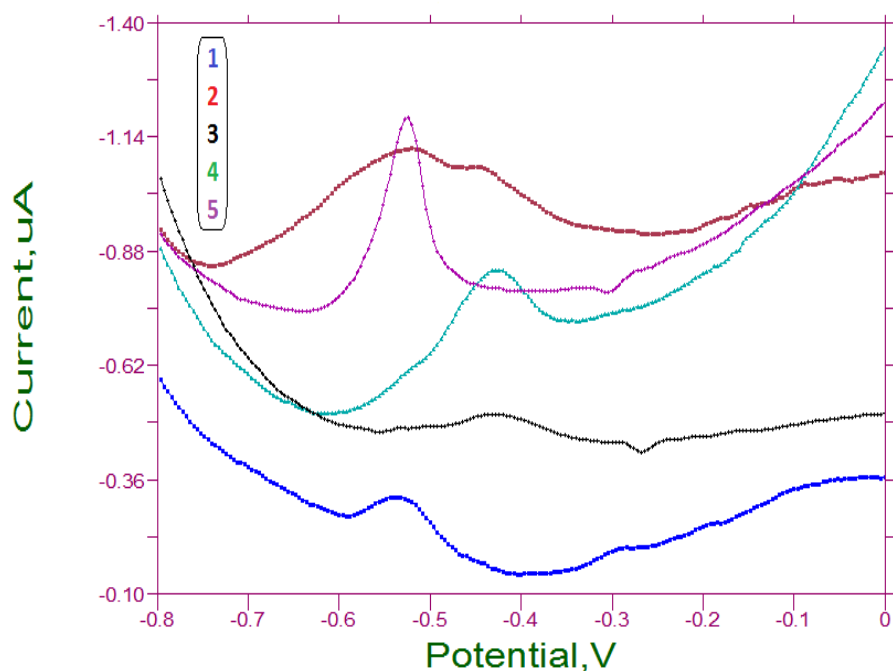
Figure 3.84 Comparison of the five electrodes at 0.2 mol L^{-1} CH$_3$COOH depending on 300 seconds accumulation time of 3.0×10^{-8} mol L^{-1} Pb(II) solution

In addition, the numeric data for the evaluation results of electrode were summarized tabulated in Table 3.14. With comparison of peak currents, the best electrode was selected 64.0 % graphite + 25.0 % mineral oil + 5.0 % silicate + 5.0 % K$_4$Fe(CN)$_6$ + 1.0 % CNT. According to the plain carbon pasta electrode, the peak current was increased almost five times by the modification.

Table 3.14 Peak current values of different types of electrodes

Number	Electrodes	Peak Current(μA)
1	70.0 % graphite + 30.0 % mineral oil	0.0857
2	65.0 % graphite + 25.0 % mineral oil + 10.0 % silicate	0.0112
3	65.0 % carbon nanotubes + 25.0 % mineral oil + 5.0 % silicate + 5.0 % $K_4Fe(CN)_6$	0.0568
4	65.0 % graphite + 25.0 % mineral oil + 5.0 % silicate + 5.0 % $K_4Fe(CN)_6$	0.1871
5	**64.0 % graphite + 25.0 % mineral oil + 5.0 % silicate + 5.0 % $K_4Fe(CN)_6$ + 1.0 % CNT**	**0.4178**

3.5.1.2 Effect of accumulation time

To improve the sensitivity of the modified electrode for lead determination, the accumulation time in ranging of 120.0-300.0 seconds were evaluated using the $K_4Fe(CN)_6$ immobilized silica modified CPE in acidic medium. The results were shown in Figure 3.85. The optimum accumulation time at -0.80 V deposition potential was 300.0 seconds (Table 3.15).
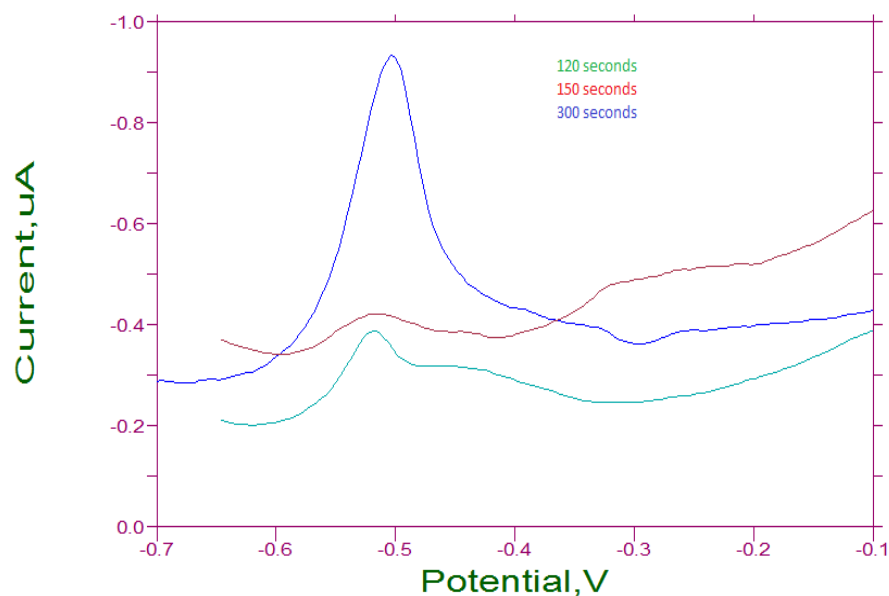
Figure 3.85 Differential pulse anodic stripping voltammograms recorded at $K_4Fe(CN)_6$ immobilized silica modified CPE in 0.2 mol L^{-1} CH_3COOH depending on accumulation time of 1.0×10^{-8} mol L^{-1} Pb(II) solution

Table 3.15 Effect of accumulation time on peak current for 1.0×10^{-8} mol L^{-1} Pb(II)

Time (Second)	Peak Current (µA)
120.0	0.065
150.0	0.178
300.0	**0.628**

3.5.1.3 Calibration curve

Under the optimum experimental condition, a linear peak current versus Pb(II) concentration was obtained at about -0.55 V during the metallic Pb(II) oxidation which were electrodeposited at -0.80 V deposition potential for the range of 1.0×10^{-9}-6.0×10^{-7} mol L^{-1} with 0.9877 regression coefficient (Figure 3.86). The detection limit was calculated as 5.0×10^{-9} mol L^{-1} for Pb(II) ions.
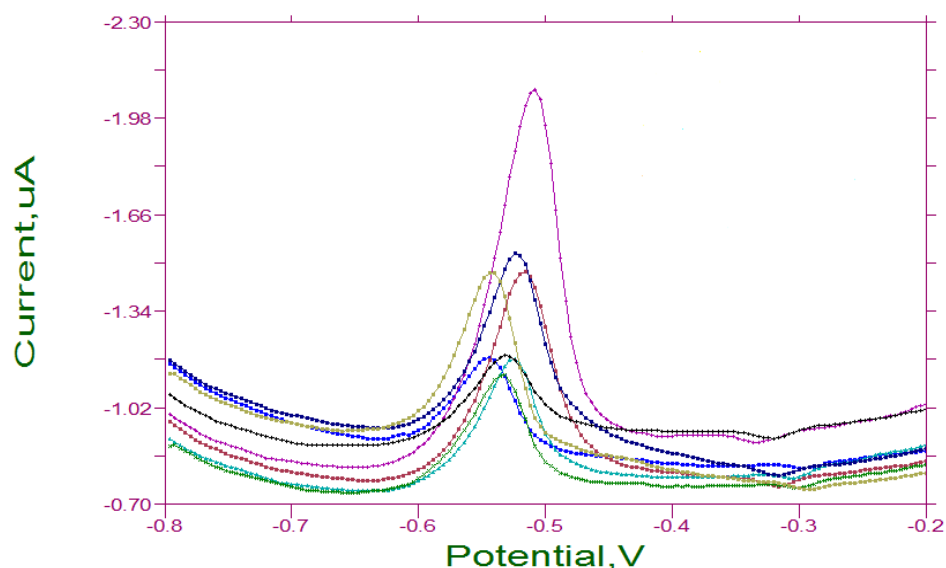
Figure 3.86 DPASVs of K$_4$Fe(CN)$_6$ immobilized silica modified CPE, for increasing concentrations of Pb(II) in 0.2 mol L^{-1} CH$_3$COOH solution: deposition time, 5 min; pulse amplitude, 10 mV; range of scan potential, -0.80 to -0.20 V and scan rate, 20.0 mV s^{-1}, Pb(II) concentrations: 1.0×10^{-9} M, 2.0×10^{-9} M, 6.0×10^{-9} M, 3.0×10^{-8} M, 6.0×10^{-8} M, 9.0×10^{-8} M, 3.0×10^{-7} M, 6.0×10^{-7} M
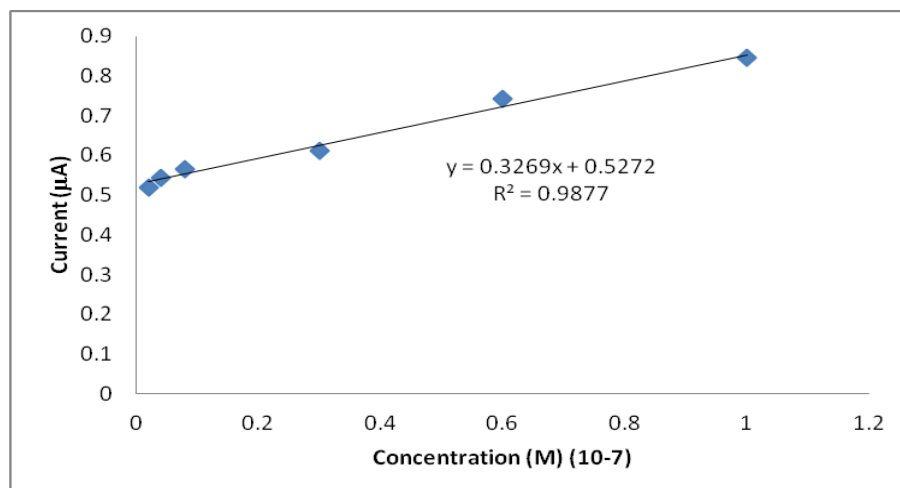
Figure 3.87 The calibration curve of Pb(II) with K$_4$Fe(CN)$_6$ immobilized silica modified CPE

3.5.1.4 Determination of lead in black tea sample

The proposed method was applied to the determination of Pb(II) ion in a black tea sample. For this, one gram of the dry tea sample (dried at 110°C) was placed in a 50.0 mL beaker and followed by the addition of 7.0 mL of concentrated nitric acid. The beaker was covered with a watch glass and allowed to stand overnight. Then the contents were heated at 150 ^{o}C, for 15 min. Eight milliliter of perchloric acid was added into the cooled sample and the mixture was heated again at 200°C until the solution became clear for about one hour. The watch glass was removed and the acid was evaporated till dryness at 150 ^{o}C.

The residue was completely dissolved in 5.0 mL of 1.0 mol L^{-1} nitric acid and the solution was transferred to a 100.0 mL volumetric flask. The solution was neutralized with NaOH solution and diluted to the mark with pure water. The content of Pb(II) was determined by differential pulse anodic stripping voltammetry with potassium ferrocyanide-carbon nanotubes modified carbon paste electrode. The determination of Pb(II) was carried out using standard addition method (Figure 3.88).

In the application of K$_4$Fe(CN)$_6$ immobilized silica modified CPE in the black tea sample using standart addition method for the determination of Pb(II) ions, an aliquot of 0.50 mL tea sample solution from the prepared tea solution above was placed in the voltammetric cell containing 9.50 mL supporting electrolyte. The current-potential curve was recorded in the potential ragne of -0.8-(-0.10) V.

Then, the increasing amounts of standart lead solutions were injected into voltammetric cell which is containing samlpe solution and the I-E curves were recorded (Figure 3.88). The current value at -0.55 V was evalutaed for the determination of lead in sample and standart solutions. The procedure was validated with Inductively Coupled Plasma-Mass Spectrometry (ICP-MS) and lead concentration was determined as 45.0 ppb (2.17×10^{-7} mol L^{-1} Pb(II)) with modified CPE and 52.0 ppb (2.51×10^{-7} mol L^{-1} Pb(II)) with ICP-MS. The relative error was found to be -13.5 %.
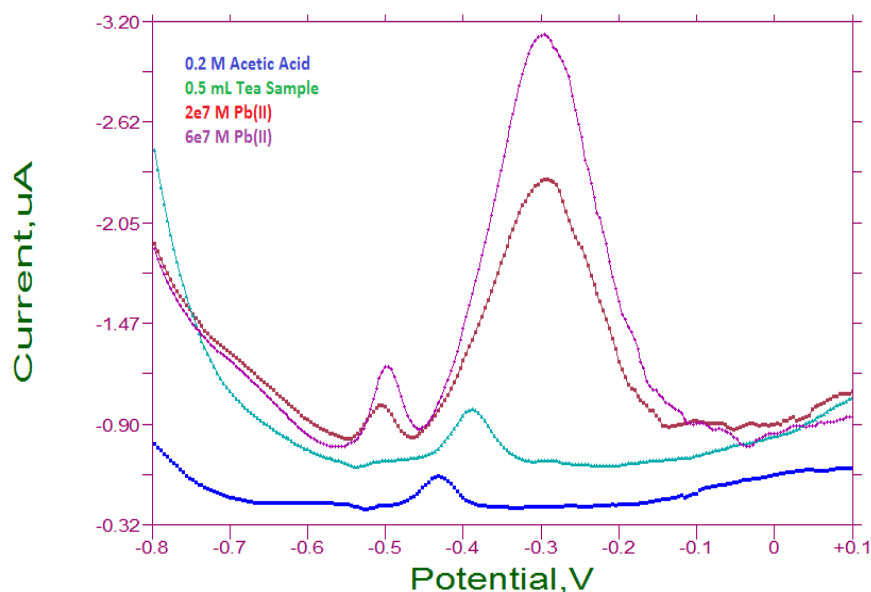
Figure 3.88 The voltammograms of tea samples with standart addition methods. DPASVs of $K_4Fe(CN)_6$ immobilized silica modified CPE, electrodeposition of lead in 0.2 mol L^{-1} CH_3COOH solution: deposition time, 5 min; pulse amplitude 10 mV; range of scan potential -0.80 to +0.10 V and scan rate: 20.0 mV s^{-1}

3.5.2 Voltammetric behavior of Lead(II) at calcium phosphate modified carbon paste electrode

The literature survey showed that the determination of lead using a carbon paste electrode modified with hydroxyapatite as a phosphorous compound was improved when compared to unmodified CPE (Mhammedi et al., 2009). The analytical performance of hydroxyapatite $Ca_{10}(PO_4)_6(OH)_2$ (HAp) modified-platinum for the determination of lead was evaluated using cyclic voltammetry and differential pulse voltammetry (Zejli et al., 2006). These studies encourage to investigate the the use of phosphate compounds to modify carbon paste electrode for determination of lead.

According to our literature survey, there is no study based on use of $Ca_3(PO_4)_2$ nanocrystals including calcium as a modifier. Thus, we tried to obtain $Ca_3(PO_4)_2$ nanocrystals using a mixture of calcium nitrate tetrahydrate and diammonium hydrogen phosphate. The analytical performance of carbon paste electrode modified with $Ca_3(PO_4)_2$ nanocrystals was evaluated for the determination of lead using differential pulse anodic stripping voltammetry. The measuring range of modified CPE includes the linear part of the calibration voltammograms as shown in Figure 3.89. The electrodeposited lead at -0.80 V was oxidized at -0.52 V during the anodic stripping on the of $Ca_3(PO_4)_2$ modified carbon paste electrode. The acumulation time effect was studied and 120.0 seconds was choosen as optimum depotion time at -0.80 V on $Ca_3(PO_4)_2$ modified carbon paste electrode (the results were not given in the thesis).
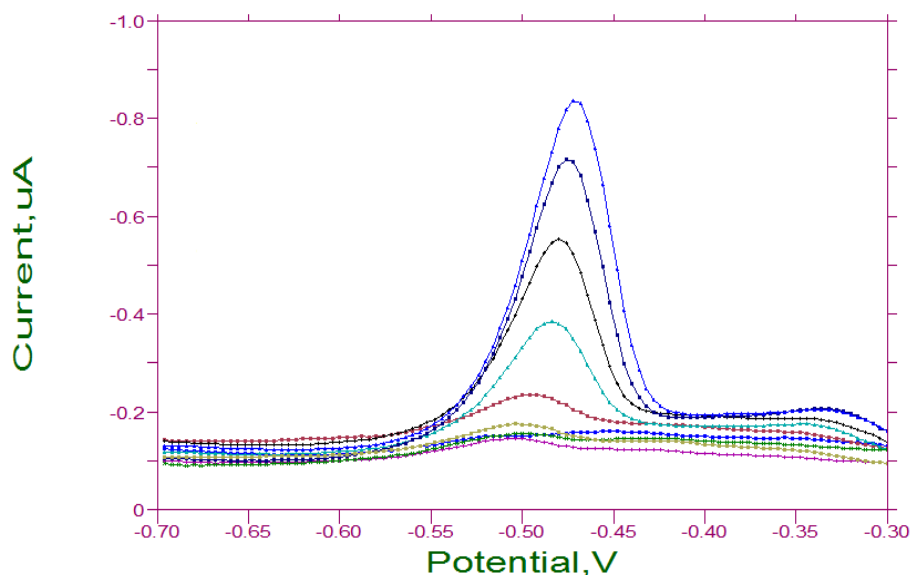
Figure 3.89 The voltammograms of tea samples with standart addition methods. DPASVs of $Ca_3(PO_4)_2$ modified CPEs, electrodeposition of lead in 0.2 mol L^{-1} CH_3COOH solution: deposition time, 5 min; pulse amplitude 10 mV; range of scan potential -0.80 to +0.10 V and scan rate: 20.0 mV s^{-1}

To obtain calibration curve for Pb(II) ions, the differential pulse voltammetric behaviour of Pb(II) was performed using $Ca_3(PO_4)_2$ modified CPE for 120.0 seconds accumulation time and -0.80 V deposition potential. Under the optimum experimental condition, a linear peak current versus Pb(II) concentration was obtained for the concentration range of $4.0x10^{-8}$-$1.0x10^{-6}$ mol L^{-1} Pb(II) with 0.9921 regression coefficient (Figure 3.90). The detection limit was found to be $2.0x10^{-8}$ mol L^{-1} Pb(II).

Figure 3.90 The calibration curve of Pb(II) with Ca$_3$(PO$_4$)$_2$ modified CPE

3.5.3 Voltammetric behaviour of calcium phosphate and zirconium phosphate nanocrystals modified carbon paste electrode in acidic media

To improve the analytical performance of Ca$_3$(PO$_4$)$_2$ modified carbon paste electrode for Pb(II) ions, the mixture of Ca$_3$(PO$_4$)$_2$ and ZrO(H$_2$PO$_4$)$_2$ nanocrystals as a modifier was used into CPE. It is well known that zirconium phosphated and zirconiumdioxide have good properties as a modifier for carbon paste electrode which have been used for the determination of lead (Shamsa and Torabi, 2006; Nguyen and Lunsford, 2012).

The electrodeposited Pb metallic form at -0.80 V was oxidized during the anodic stripping of lead from the Ca$_3$(PO$_4$)$_2$ and ZrO(H$_2$PO$_4$)$_2$ nanocrystals modified carbon paste electrode surface. The depence of metallic formed Pb oxidation peak on Pb(II) concentration was given in Figure 3.91. Under the optimum experimental conditions such as -0.80 V deposition potential and 120.0 s deposition time, the peak current was changed linearly by increasing of Pb(II) concentration in the range of 4.0×10^{-8}-2.0×10^{-7} mol L^{-1} with 0.9872 regression coefficient (Figure 3.92). But the linear part did not pass to the intersection point. From the calibration curve slope, the detection limit was found to be 2.0×10^{-8} mol L^{-1} Pb(II).
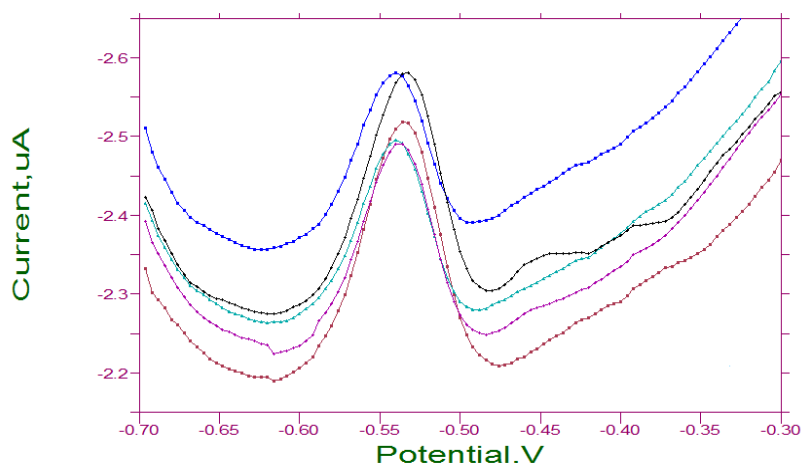
Figure 3.91 DPASVs of Ca$_3$(PO$_4$)$_2$ and ZrO(H$_2$PO$_4$)$_2$ nanocrystals modified CPEs, for increasing concentrations of lead in 0.2 mol L^{-1} CH$_3$COOH solution: deposition time 2 min; pulse amplitude 10 mV; range of scan potential -0.70 to -0.30 V and scan rate: 20 mVs^{-1}, Pb(II) concentrations: 4.0x10^{-8} M, 6.0x10^{-8} M, 8.0x10^{-8} M, 1.0x10^{-7} M, 2.0x10^{-7} M
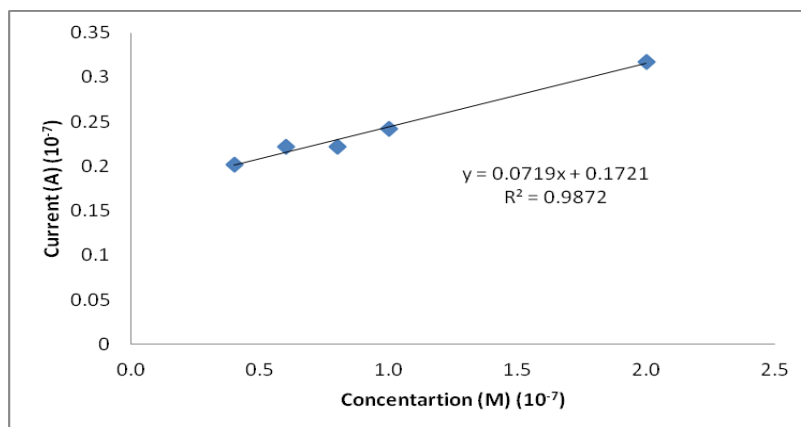
Figure 3.92 Calibration curve of Pb(II) with Ca$_3$(PO$_4$)$_2$+ZrO(H$_2$PO$_4$)$_2$ modified CPE

3.5.4 Voltammetric behaviour of calcium phosphate and copper (II) ferrocyanide modified carbon paste electrode in acidic media and analytic application

Up to now, ferrocyanide for modification of carbon paste electrode has been used for different purposes because of its good catalytic properties. However, according to our best knowledges, it was not used to modify carbon paste electrode for the determination of lead (Raoof et al., 2004; Arribas et al., 2005). To provide the synergic effect, ferrocyanide as a Cu$_2$Fe(CN)$_6$ was mixed with Ca$_3$(PO$_4$)$_2$ nanocrystal and the mixture was used to modify bare carbon pasta electrode.

The effect of deposition time was investigated for 1.0×10^{-7} mol L^{-1} Pb(II) using 0.2 mol L^{-1} CH$_3$COOH solution as a supporting electrolyte. As can be seen from Figure 3.93, the highest current was obtained on 360.0 s. Thus 240.0 second was choosen as the deposition time in further experiments.
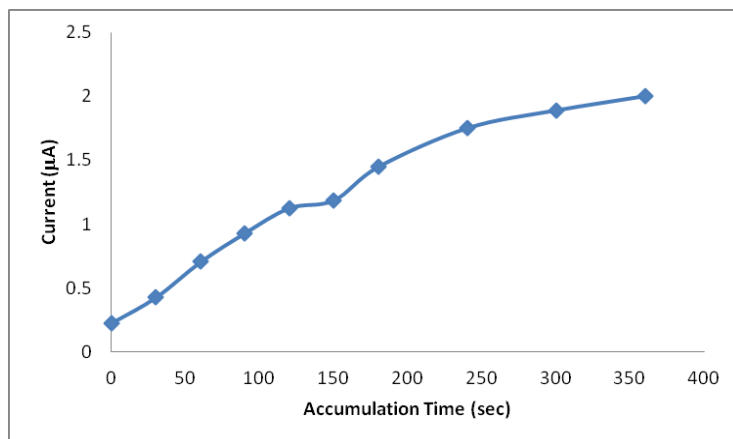
Figure3.93 Influence of accumulation time of 1.0×10^{-7} mol L^{-1} Pb(II) in 0.2 mol L^{-1} CH$_3$COOH solution with Ca$_3$(PO$_4$)$_2$+Cu$_2$Fe(CN)$_6$ modified carbon paste electrode

The differential pulse anodic stripping voltammograms at different concentrations of Pb(II) ions under optimum conditions are shown in Figure 3.94.
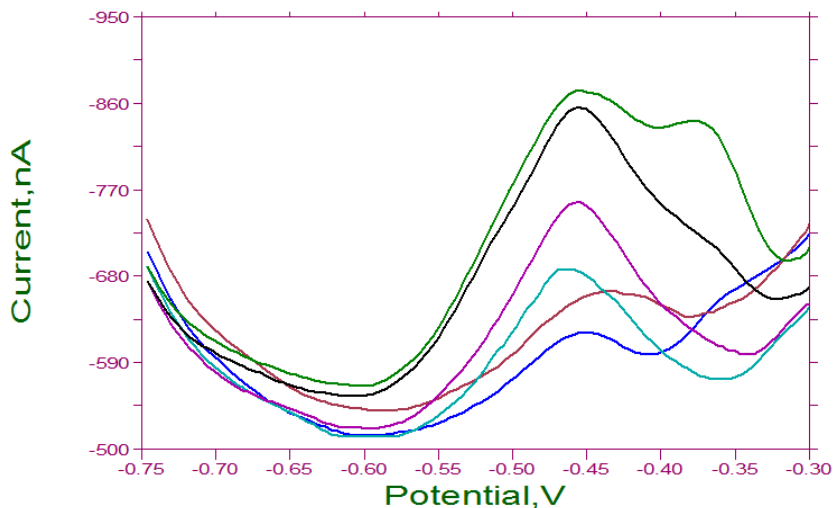
Figure 3.94 DPASVs of Ca$_3$(PO$_4$)$_2$+Cu$_2$Fe(CN)$_6$ modified carbon paste electrodes, for increasing concentrations of lead in 0.2 mol L^{-1} CH$_3$COOH solution, deposition time 240 s., pulse amplitude 10 mV, range of scan potential -0.750 to 0.30 V and scan rate: 20 mV s^{-1}, Pb(II) concentrations: 1.0×10^{-9} M, 2.0×10^{-9} M, 3.0×10^{-8} M, 6.0×10^{-8} M, 9.0×10^{-8} M, 1.0×10^{-7} M

To obtain calibration curve for lead, the differential pulse voltammetric behaviour of Pb(II) was performed using mixture of $Ca_3(PO_4)_2$ and $Cu_2Fe(CN)_6$ modified CPE during 240.0 seconds accumulation time of the electrode into the Pb(II) containing voltammetric cell. Under the optimum experimental condition, a linear peak current versus Pb(II) concentration was obtained for the range of $1.0x10^{-9}$-$1.0x10^{-7}$ mol L^{-1} with 0.993 regression coefficient (Figure 3.95). The detection limit was found to be $0.5x10^{-9}$ mol L^{-1} (n=3) Pb(II).
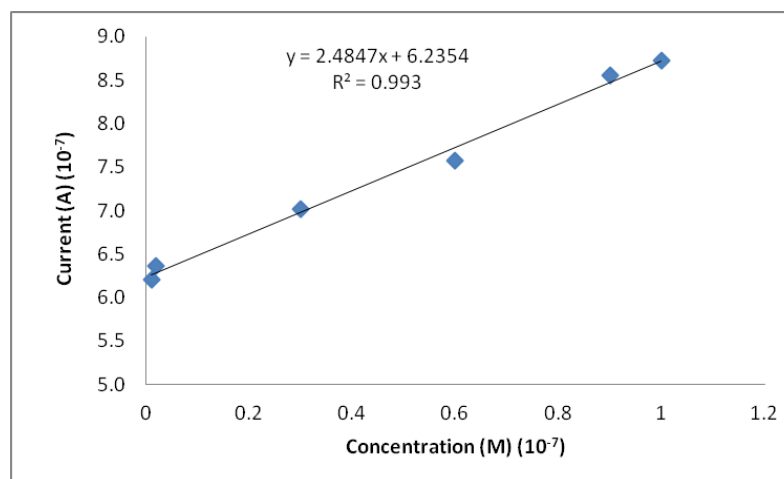
Figure 3.95 Calibration curve of Pb(II) with $Ca_3(PO_4)_2$+$Cu_2Fe(CN)_6$ modified CPE

In order to evaluate the performance of modified carbon paste electrode in practical analytical applications, lead in a tap water sample was determined using standard addition method (Figure 3.96).
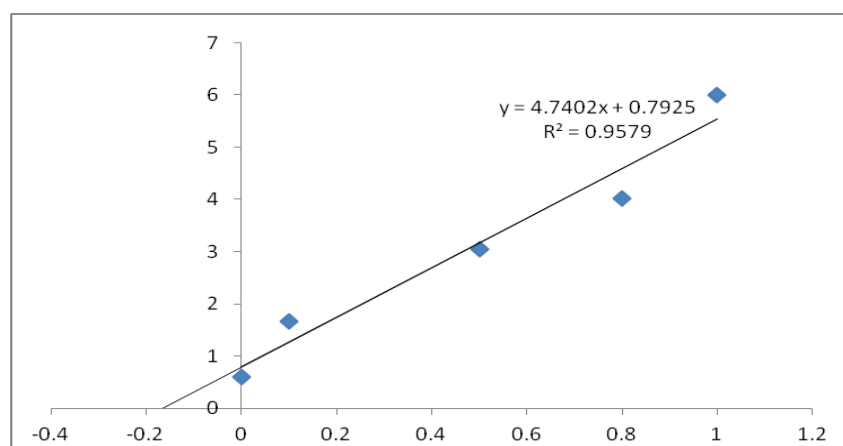
Figure 3.96 Standard addition graph of tap water sample with $Ca_3(PO_4)_2$+$Cu_6Fe(CN)_6$ modified CPE

The plot of peak current against lead concentration was linear (r^2=0.9579). The concentration of lead in the diluted tap water sample (1/1 ratio) was found to be 0.167×10^{-6} mol L^{-1}, which gave the concentration of 0.334×10^{-6} mol L^{-1} (69.28 µg L^{-1}) Pb(II) in the tab water. The detection limit was found to be 8.351×10^{-8} mol L^{-1} (n=3) Pb(II) ions.

3.5.5 Voltammetric behaviour of bismuth–antimony film electrode for lead determination

Since the year 2000, the electrodes modified with bismuth, bismuth-antimony and bismuth/poly (p-aminobenzene sulfonic acid film have become an attractive new electroanalytical research field for determination of some heavy metals at trace level (Wu et al., 2008; Xu et al., 2008).

These film electrodes have been considered as a good alternative to mercury-based electrodes which is toxic. Furthermore the electrodes have provided a good selectivity for simultaneous analysis of heavy metals. The bare glassy carbon electrode modified with bismuth-antimony film has been used for cadmium determination (Yi et al., 2012). Also antimony and bismuth have been seperately and together used to modify the bare galssy carbon electrode (Yi et al., 2012) and carbon paste electrode (Ashrafi and Vytras, 2011).

Nevertheless, there is no any report regarding the application of a Bi-Sb film electrode for determination of lead by square wave anodic stripping voltammetry. In addition the Bi-Sb film has been not used to modify the surface of MWCNTs coated bare glassy carbon electrode. Therefore, the electrochemical behaviour of Bi-Sb film used to coat the multiwall carbon nanotubes on bare glassy carbon electrode was investigated for determination of lead.

Bi-Sb film electrode has been applied in acidic media such as acetic acid, hydrocloric acid and suitable acidic buffer. In our initial experiments regarding the the film we tested acetic acid buffer and tartaric acid solutions. Acetic acid buffer at pH 4.5 generated hydrogen gas on the electrode surface. This phenomen dropped the multiwall carbon nanotubes from the glassy carbon electrode surface. The tartaric acid supporting electrolyte worked better than acetic acid buffer.

To prepare potassium hydrogen tartrate (KHT) solution as a supporting electrolyte, the defined amounts of tartaric acid (4.007 g) and potassium carbonate (4.563 g) were mixtured. The mixture was dissolved in 250.0 mL ultrapure water. The prepared pH of the solution was 3.65. This solution was used as a supporting electrolyte during the Bi–Sb film electrode studies. In order to establish the suitable experimental conditions for the square wave anodic stripping voltammetry (SWASV) measurement of Pb(II) by using the Bi-Sb Film Electrode, the proper proportion between Sb(III) and Bi(III) concentrations and the deposition time were optimized.

3.5.5.1 Optimization of Sb(III) and Bi(III) concentration

To obtain best highest oxidation peak current of Pb(II) by GCE modified with MWCNT, firstly the effect of Sb(III) concentrations in the electrolyte including 500.0 $\mu g\ L^{-1}$ Bi(III) was investigated. The results are given Table 3.16. The highest oxidation current in the examined range of Sb(III) concentration was obtained with 400.0 $\mu g\ L^{-1}$ Sb(III) concentration for lead determination.

Table 3.16 Effect of increasing Sb(III) concentration on oxidation current of Pb(II) at costant Bi(III) concentration

500.0 $\mu g\ L^{-1}$ Bi(III)	
Concentration of Sb (III) ($\mu g\ L^{-1}$)	**Current (μA)**
50.0	2.243
100.0	1.362
300.0	3.041
400.0	**4.228**
500.0	2.589

The effect of Bi(III) concentration in the electrolyte solution on the lead determination was examined at constant Sb(III) concentration as 500.0 $\mu g\ L^{-1}$ (Table 3.17).

The highest oxidation current for Pb(II) was obtained with 300.0 μg L^{-1} Bi(III) concentration. As a result, in our study the concentration of Bi(III) and Sb(III) concentration in the electrolyte solution were taken to be 300.0 μg L^{-1} and 500.0 μg L^{-1}, respectively.

Table 3.17 Effect of increasing Bi(III) concentration on oxidation current of Pb(II) at costant Sb(III) concentration

500.0 μg L^{-1} Sb(III)	
Concentration of Bi (III) (μg L^{-1})	**Current (μA)**
50.0	4.06
100.0	57.94
300.0	**56.74**
400.0	38.13
500.0	2.59

3.5.5.2 Effect of deposition time

The effect of deposition time was investigated for 5x10^{-7} mol L^{-1} Pb(II) using potassium hydrogen tartrate (KHT) solution as a supporting electrolyte, including 500.0 μg L^{-1} Sb(III) and 300.0 μg L^{-1} Bi(III). As can be seen from Figure 3.97, the highest current was obtained on 240.0 s. However the obtained current time for 240.0 s was not repeatable. Because, the different peak currents were obtained under same working conditions. Thus 180.0 second was choosen as the deposition time in further experiments.
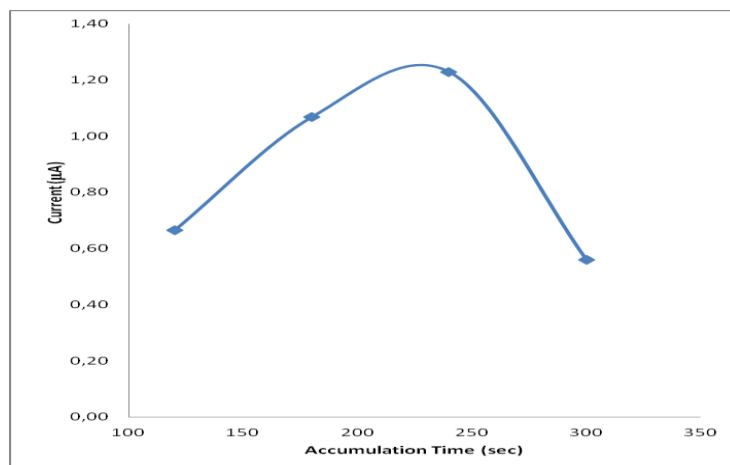
Figure 3.97 Influence of accumulation time of 5.0x10^{-7} mol L^{-1} Pb(II) in the electrolyte including 500.0 µg L^{-1} Sb(III) and 300.0 µg L^{-1} Bi(III)

3.5.5.3 Calibration data for Lead ions
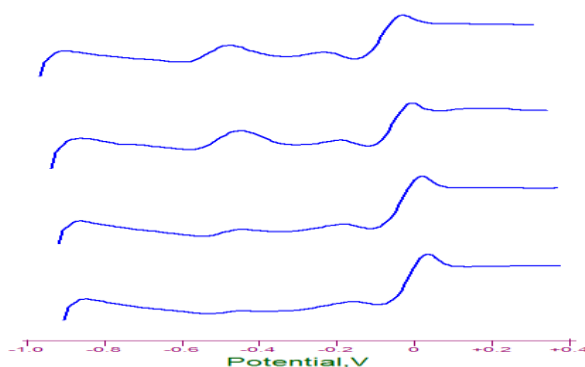
Figure 3.98 SWASV responses of increasing concentrations Pb(II) in KHT solution (pH 3.65) for 500.0 µg L^{-1} Sb(III) with Sb-FE. Deposition potential -0.90 V; deposition time: 180 s, range of scan potential -0.90 to +0.40 V, quiet time 20 s, frequency 15.0 Hz, pulse amplitude 25.0 mV, Pb(II) concentrations: 1.0x10^{-6} M, 2.0x10^{-6} M, 4.0x10^{-6} M, 8.0x10^{-6} M

There is a close fit to linearity from 1.0x10^{-6} to 8.0x10^{-6} mol L^{-1}. The correlation coefficient is 0.9936. The lower concentration of lead could be detected.
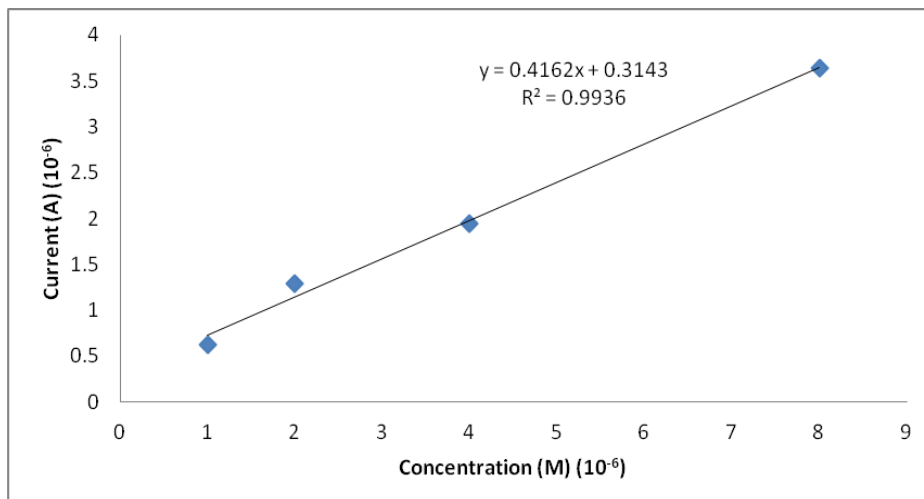
Figure 3.99 The calibration curves for the determination of Pb(II) of different concentrations with in situ 500.0 μg L^{-1} Sb-FE

Square wave anodic stripping voltammetry experiments at the bismuth-film electrode (Bi-FE) were performed and the peak currents increased with increasing Pb(II) concentration. The obtained voltammograms are shown in Figure 3.100.
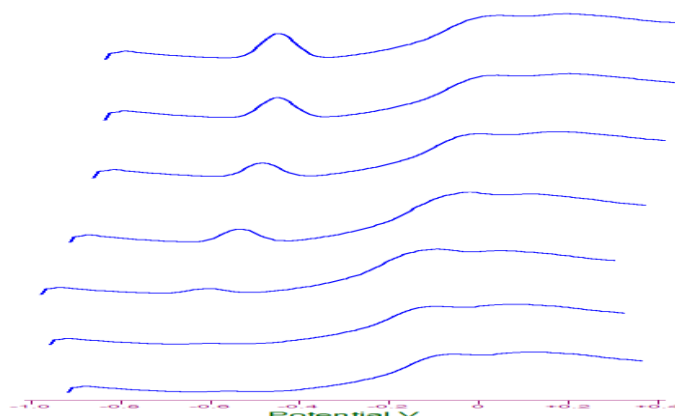
Figure 3.100 SWASV responses of increasing concentrations Pb(II) in KHT solution (pH 3.65) for 300.0 μg L^{-1} Bi(III) at Bi-FE. Deposition potential -0.90 V, deposition time 180 s, range of scan potential -0.90 to +0.40 V, quiet time 20 s, frequency 15.0 Hz, pulse amplitude 25.0 mV, Pb(II) concentrations: 8.0×10^{-8} M, 1.0×10^{-7} M, 2.0×10^{-7} M, 4.0×10^{-7} M, 6.0×10^{-7} M, 8.0×10^{-7} M, 1.0×10^{-6} M

There is a close fit to linearity from 8.0×10^{-8} to 1.0×10^{-6} mol L^{-1}. The correlation coefficient is 0.9941. The use of Bi-FE provided the determination of lower concentration of lead than that of Sb-FE (Figure 3.101).

155
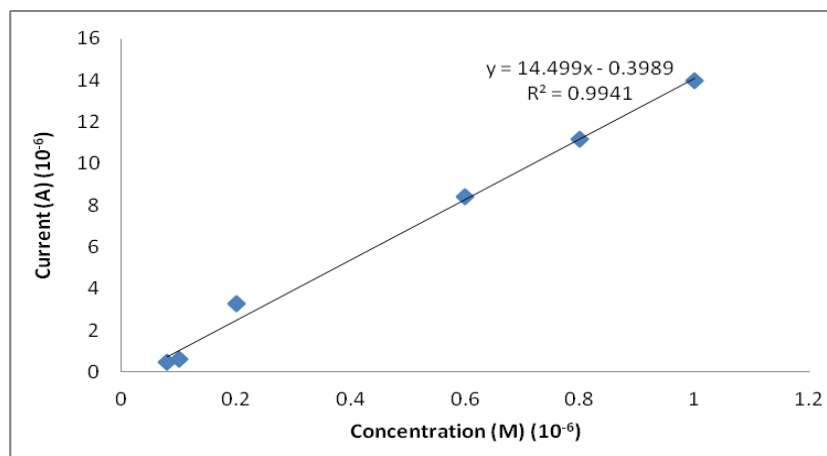
Figure 3.101 The calibration curves for the determination of Pb (II) of different concentrations with in situ 300.0 μg L^{-1} Bi-FE

To achieve the determination of lower concentration of lead, than discussed concentration above, the supporting electrolyte including both Sb(III) and Bi(III) was also studied in the presence of selected concentration of Pb(II) ions. For this, the voltammograms were obtained with increasing of concentration of lead (Figure 3.102).
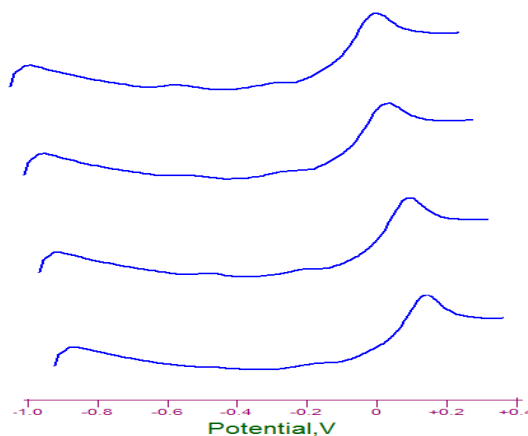
Figure 3.102 SWASV responses of increasing concentrations Pb(II) in KHT solution (pH 3.65) for 500.0 μg L^{-1} Sb(III) and 300.0 μg L^{-1} Bi (III) at Sb-Bi-FE. Deposition potential -0.90 V, deposition time 180 s, range of scan potential -0.90 to +0.40 V, quiet time: 20 s, frequency 15.0 Hz, pulse amplitude 25.0 mV, Pb(II) concentrations: 4.0x10^{-7} M, 6.0x10^{-7} M, 8.0x10^{-7} M, 1.0x10^{-6} M

There was a close fit to linearity from 4.0x10^{-7} to 1.0x10^{-6} mol L^{-1}. The correlation coefficient was 0.9953 (Figure 3.103). As a result as it was expected the determination of lead at the lowest concentration could be not carried out using Sb-Bi film electrode. The lowest concentration of lead was determined with Bi-FE.
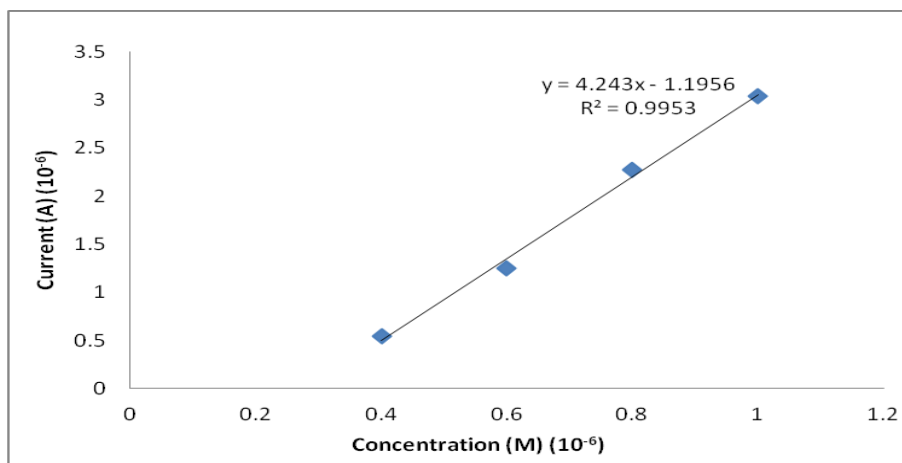
Figure 3.103 The calibration curves for the determination of Pb(II) with in situ 500.0 µg L⁻¹ Sb(III) ana 300.0 µg L⁻¹ Bi(III) film electrode

3.5.6 Voltammetric behaviour of bismuth–tin film electrode for cadmium and lead ions determination

Tin-film electrode (Sn-FE) based on glassy carbon and carbon paste substrates have been used for the heavy metal determination using anodic stripping voltammetry (Tian et al., 2009; Li et al., 2012). The sensitivities of carbon paste and glassy carbon electrodes have been improved significantly for cadmium determination. According to our best literature survey, there is no any published paper for the determination of both Cd(II) and Pb(II) species on Bi-Sn film electrode. In this study, Bi-FE, Sn-FE and Bi-Sn-film on carbon paste electrode surfaces were investigated for the determination of Cd(II) and Pb(II) species by square wave anodic stripping voltammetry. Parameters such as pH, effect of the Sn(II) and Bi(III) concentration, accumulation time, carbon nanotubes amount, calibration curves and interferences that affects the voltammetric peak current were tested as described below.

3.5.6.1 Effect of pH on the voltammetric behaviour of Cd(II) at Bi-Sn-FE

The effect of pH on the voltammetric responses of the Bi-Sn/MWCNTs-CP-FE was studied at different pH of acetate buffer solution in the pH range of 3.75–5.76 for 5.0×10^{-7} mol L⁻¹ Cd(II) ions and -1.0 V depsition potential and 210.0 sec accumulatiin time. The electrodeposited Cd metal was oxidized at -0.75 V during the anodic stripping step.

At the same conditions, the peak current increased until the pH 4.5 and then suddenly the peak current was decrased after the pH 4.5 and almost reached fixed up to pH 5.0 (Figure 3.104). From pH effect studies, the optimum suppotring electrolyte pH was choosen as 4.5 for the proposed electrode and future studies.
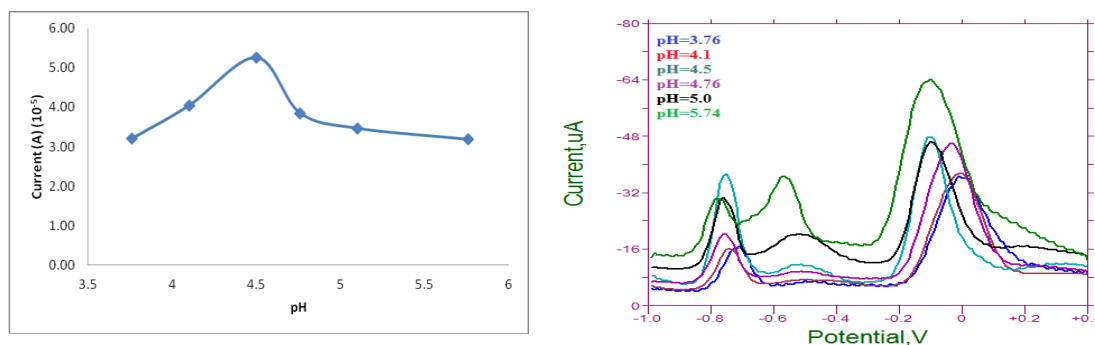
Figure 3.104 Effect of pH on the voltammetric response for 5.0x10^{-7} mol L^{-1} Cd(II) solutions with Bi-Sn/MWCNTs-CP-FE

3.5.6.2 Effect of the Sn(II) and Bi(III) concentration on the Cd(II) voltammetric response

To obtain highest peak current of Cd(II) by carbon paste electrode modified with tin and bismuth, the concentration of both Sn(II) and Bi(III) were changed as 500.0 µg L^{-1} constant Sn(II) concentrations and varying concentration of Bi(III) in the range of 50.0-500 µg L^{-1} Sn(II) and then the Bi(III) concentration was kept constant as 500.0 µg L^{-1} and the varying of Sn(II) concentration in the range 50.0-500.0 µg L^{-1}. The obtained results at -0.75 V oxidation peak were given Table 3.18. The highest oxidation currents for Cd(II) was obtained with the electrolyte including both 500.0 µg L^{-1} Bi(III) and Sn(II) concentrations.

Table 3.18 Effect of increasing tin and bismuth concentration on peak current for 1×10^{-6} mol L^{-1} Cd(II)

500.0 µg L^{-1} Sn (II)		500.0 µg L^{-1} Bi(III)	
Concentration of Bi(III) (µg L^{-1})	Peak Current (µA)	Concentration of Sn(II) (µg L^{-1})	Peak Current (µA)
50.0	21.24	50.0	56.35
100.0	22.13	100.0	43.12
200.0	27.00	200.0	51.72
300.0	41.76	300.0	29.90
400.0	29.07	400.0	33.72
500.0	**59.27**	**500.0**	**59.27**
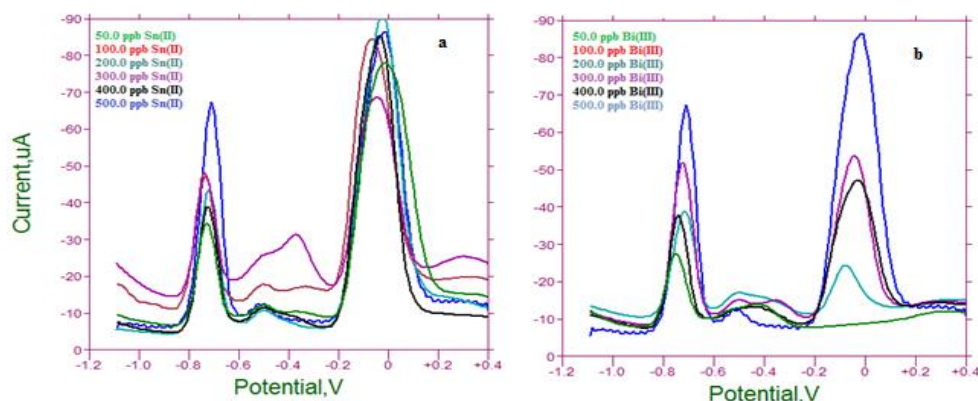
Figure 3.105 SWASVs recorded at Bi-Sn/MWCNTs-CP-FE in pH=4.5 CH$_3$COOH/CH$_3$COONa buffer a) constant Bi(III) b) Sn(II) ions for 1.0×10^{-6} mol L^{-1} Cd(II) solution

3.5.6.3 Effect of accumulation time on the Cd(II) voltammetric response on Bi-Sn/MWCNTs-CP-FE

The accumulation time effect on the 5.0×10^{-7} mol L^{-1} Cd(II) ion concentration was studied in the range of 30.0-360.0 second on Bi-Sn/MWCNTs-CP-FE in the presence of pH 4.5 acetate buffer solution (Figure 3.105). It was found that the peak current at -0.75 V was increased with increasing accumulation time until 210.0 seconds.

This indicates that an enhancement of Cd(II) uptake was improved at the electrode surface. The results showed that the attainment of a steady-state accumulation time of Cd(II) ions were 210.0 seconds (Table 3.20). The peak current was decreased up to 240.0 seconds and almost maintains the value of current for the subsequent accumulation times.
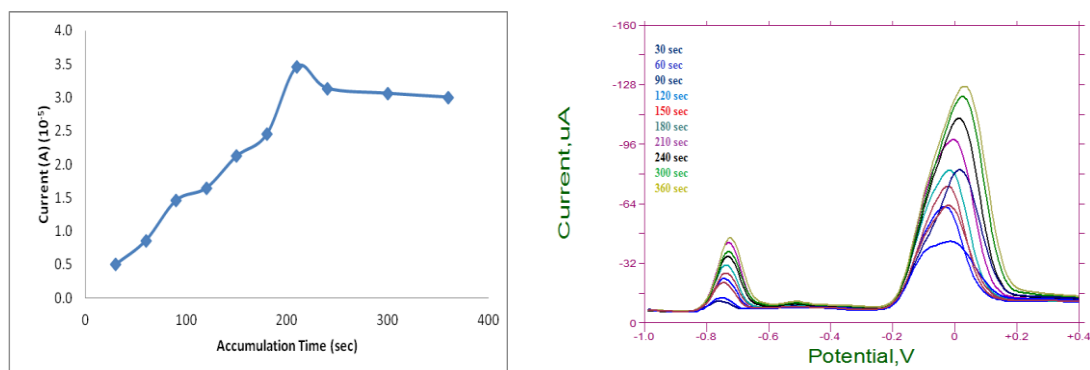
Figure 3.106 SWASVs recorded at Bi-Sn/MWCNTs-CP-FE in pH=4.5 CH$_3$COOH/CH$_3$COONa buffer depending on accumulation time of 5.0x10^{-7} mol L^{-1} Cd(II) solution

Table 3.19 Effect of accumulation time on peak current for 5.0x10^{-7} mol L^{-1} Cd(II)

Time (Second)	Peak Current (µA)
30.0	0.501±0.030
60.0	0.859±0.090
90.0	1.459±0.015
120.0	1.644±0.047
150.0	2.120±0.092
180.0	2.449±0.021
210.0	**3.459±0.010**
240.0	3.136±0.021
300.0	3.060±0.028
360.0	3.003±0.023

3.5.5.4 Optimization of square wave frequency for Cd(II) voltammetric behaviour on the Bi-Sn/MWCNTs-CP-FE

The effect of square wave frequency on the peak current of Cd(II) ions was performed in the range of 5.0-35.0 hertz (Table 3.20). From the square wave voltammetric results, the optimum frequency parameter was obtained as 25.0 Hertz for future studies.

Table 3.20 Changes of frequency-current

Frequency (Hertz)	Current (µA)
15.0	18.41
25.0	**34.99**
35.0	34.19

3.5.5.5 The effect carbon nanotubes amount in the carbon paste on the Cd(II) voltammetric response on Bi-Sn/MWCNTs-CP-FE

The effect of the carbon nanotubes amount into CPE was investigated in the Cd(II) ion containing pH 4.5 acetat buffer solution on Bi-Sn/MWCNTs-CP-FE. The percentage of mineral oil was fixed at 30.0 % (m/m) while the percentage of carbon nanotubes was varied from 0.0-20.0 (Figure 3.106). From obtaining voltammetric response of $5.0x10^{-7}$ mol L^{-1} Cd(II), the optimum CNT was obtained as 7.0 % (m/m) into CP.
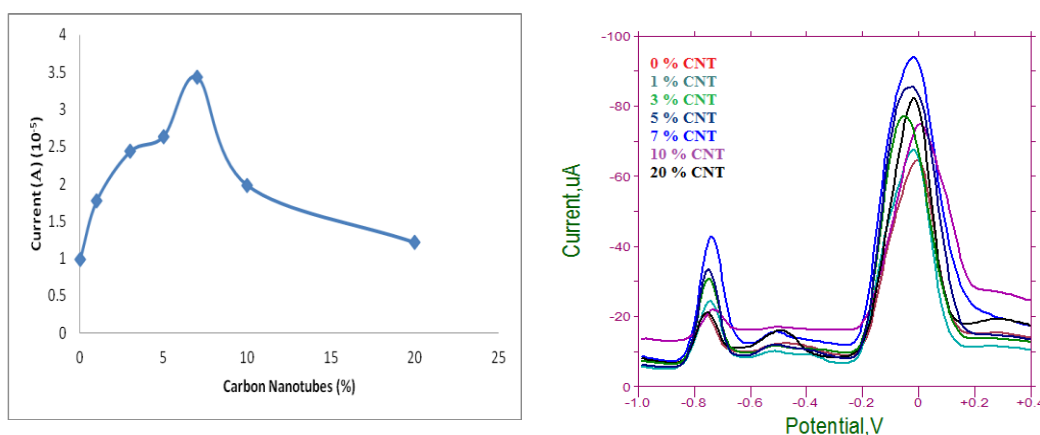
Figure 3.107 Anodic peak currents obtained by SWASV as function of the percentage of CNT in the CPE for $5.0x10^{-7}$ mol L^{-1} Cd(II) solution

3.5.5.6 Calibration curves and detection limit

The square wave anodic stripping voltammograms at different concentrations of Cd(II) ions under the optimum conditions were taken to obtain calibration curves by Bi/MWCNTs-CP-FE, Sn/MWCNTs-CP-FE and Bi-Sn/MWCNTs-CP-FE given Figures 3.108, 3.110 and 3.112, respectively. The peak currents increased linearly with increasing concentration of Cd(II) ions, using three different electrodes described above.

Figure 3.108 shows the square wave anodic stripping voltammograms obtained with Bi/MWCNTs-CP-FE at pH 4.5 of acetat buffer solution. The first oxidation peak of two peaks in the voltammograms belongs to oxidation of cadmium. The second peak shows oxidation of bismuth.

Figure 3.108 SWASVs obtained with Bi/MWCNTs-CP-FE, increasing concentration of Cd(II) ions in pH=4.5 CH$_3$COOH/CH$_3$COONa buffer solution, deposition time 210 s, range of scan potential -1.0 to +0.40 V, SW amplitude 25 mV, SW frequency 25 Hz and quite time 15 s, Cd(II) concentrations: 1.0x10^{-7} M, 2.0x10^{-7} M, 4.0x10^{-7} M, 6.0x10^{-7} M, 8.0x10^{-7} M, 1.0x10^{-6} M

A linear calibration graph was obtained in the concentration range 1.0x10^{-7}-1.0x10^{-6} mol L^{-1} Cd(II) (r^2=0.9929) using Bi/MWCNTs-CP-FE (Figure 3.109). The detection limit was found to be 5.0x10^{-8} mol L^{-1} (n=3) Cd(II).
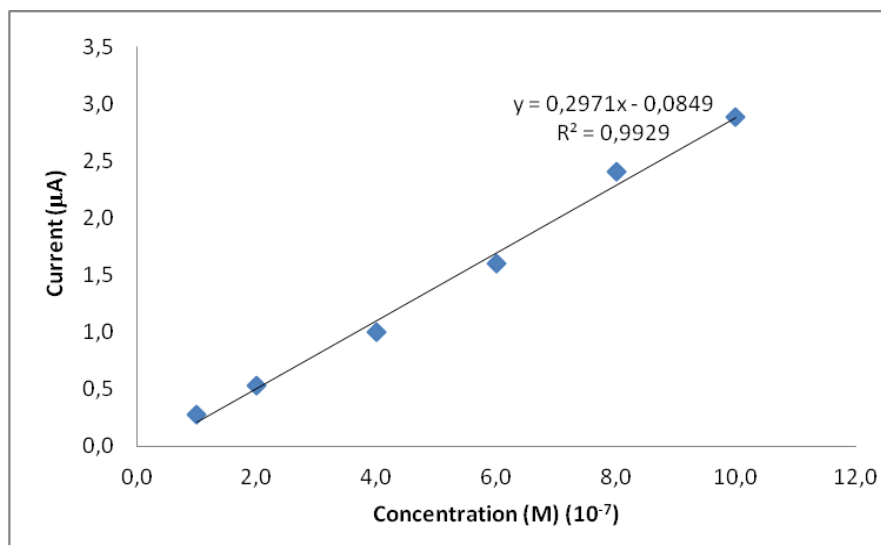
Figure 3.109 Calibration Curve of Cd(II), obtained with Bi/MWCNTs-CP-FE

Figure 3.110 shows the square wave anodic stripping voltammograms obtained with Sn/MWCNTs-CP-FE at pH 4.5 CH_3COOH/CH_3COONa buffer solution. The oxidation peak in the voltammograms belongs to oxidation of cadmium. The oxidation current of tin was too much low.
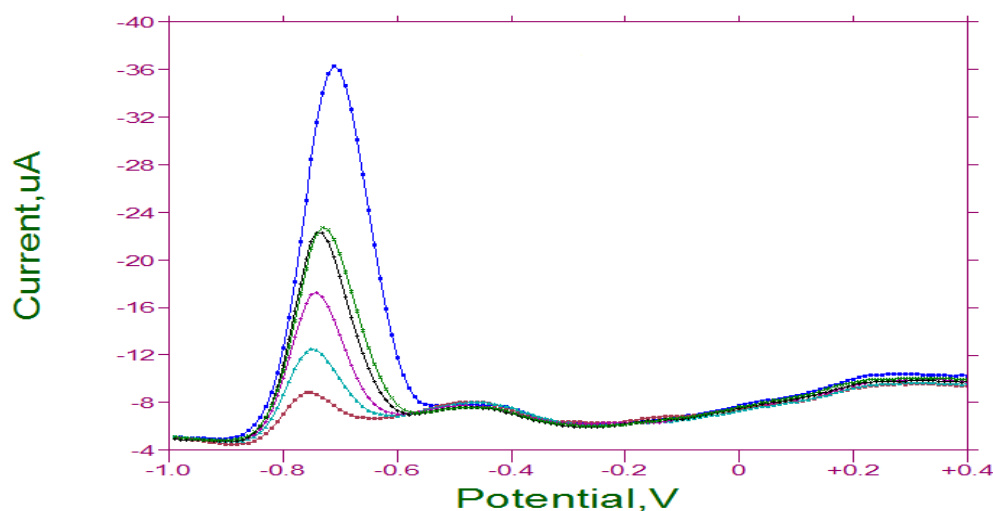
Figure 3.110 SWASVs obtained with Sn/MWCNTs-CP-FE, increasing concentration of Cd(II) ions in pH=4.5 CH_3COOH/CH_3COONa buffer solution, deposition time 210 s, range of scan potential -1.0 to +0.40 V, SW amplitude 25 mV, SW frequency 25 Hz and quite time 15 s, Cd(II) concentrations: $2.0x10^{-7}$ M, $4.0x10^{-7}$ M, $6.0x10^{-7}$ M, $8.0x10^{-7}$ M, $1.0x10^{-6}$ M, $2.0x10^{-6}$ M

A linear calibration graph was obtained in the concentration range 20.0×10^{-7}-2.0×10^{-6} mol L^{-1} Cd(II) (r^2=0.9837) using Sn/MWCNTs-CP-FE (Figure 3.111). The detection limit was found to be 1.0×10^{-7} mol L^{-1} (n=3) Cd(II).
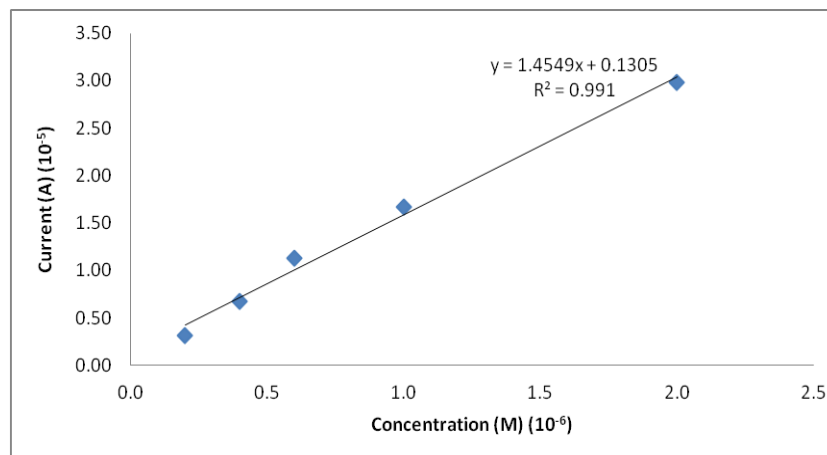
Figure 3.111 Calibration Curve of Cd(II), obtained with Sn/MWCNTs-CP-FE

Figure 3.112 shows the square wave anodic stripping voltammograms obtained with Bi-Sn/MWCNTs-CP-FE at pH 4.5 CH_3COOH/CH_3COONa buffer solution. The oxidation peak in the voltammograms belongs to oxidation of cadmium. The second peak belongs to tin, like Figure 3.110.
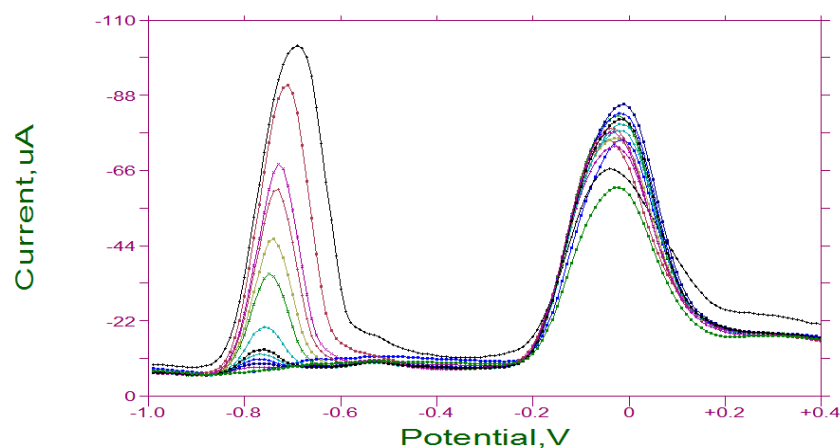
Figure 3.112 SWASVs obtained with Bi-Sn/MWCNTs-CP-FE, increasing concentration of Cd(II) ions in pH=4.5 CH_3COOH/CH_3COONa buffer solution, deposition time 210 s, range of scan potential -1.0 to +0.40 V, SW amplitude 25 mV, SW. frequency 25 Hz and quite time 15 s, Cd(II) concentrations: 1.0×10^{-8} M, 2.0×10^{-8} M, 4.0×10^{-8} M, 6.0×10^{-8} M, 8.0×10^{-8} M, 1.0×10^{-7} M, 2.0×10^{-7} M, 4.0×10^{-7} M, 6.0×10^{-7} M, 8.0×10^{-7} M, 1.0×10^{-6} M, 2.0×10^{-6} M, 4.0×10^{-6} M
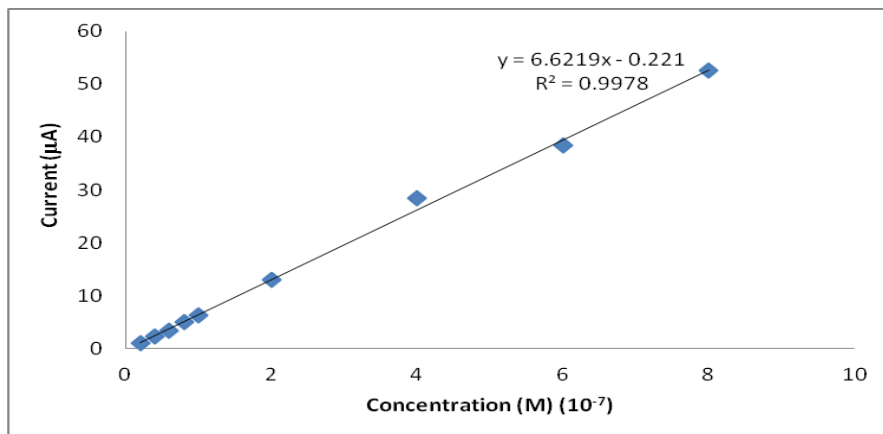
Figure 3.113 Calibration Curve of Cd(II), obtained with Bi-Sn/MWCNTs-CP-FE

There is a close fit to linearity from 1.0×10^{-8} to 4.0×10^{-6} mol L^{-1}. The correlation coefficient is 0.9978 using Bi-Sn/MWCNTs-CP-FE (Figure 3.113). The detection limit was found to be 5.0×10^{-9} mol L^{-1} (n=3) Cd(II). By comparision of three film electrode discussed above, the best sensitivity was obtained using Bi-Sn/MWCNTs-CP film electrode. Also its lineerity was better than those of others. The concentration range of cadmium for the calibration curve was changed from 1.0×10^{-8} to 4.0×10^{-6} mol L^{-1} and larger. The dedectable lowest concentration of Cd(II) was achieved with Bi-Sn/MWCNTs-CP film electrode.

Table 3.22 indicates that the comparison of the film modified carbon paste electrodes for cadmium determination. Bi-Sn/MWCNTs-CP film electrode show the best sensitivity for Cd(II) determination by using square wave anodic stripping voltammetry, among the three film electrode.

Table 3.21 The comparison of the film modified carbon paste electrodes

Electrodes	Linear Range (mol L^{-1})	Correlation Coefficient
Bi/MWCNTs-CP-FE	1.0×10^{-7}-1.0×10^{-6}	0.9929
Sn/MWCNTs-CP-FE	1.0×10^{-7}-2.0×10^{-6}	0.9837
Bi-Sn/MWCNTs-CP-FE	**1.0×10^{-8} to 4.0×10^{-6}**	**0.9978**

3.5.5.7 Interferences studies

In the analysis of real sample, the interference of foreign ions in the sample is most important for the accuracy of the results. So, the influence of Al(III), Ba(II), Ca(II), Cu(II), Fe(III), K(I), Mg(II), Na(I), Ni(II), Pb(II) and Zn(II) in the Cd(II) peak current has been evaluated and the results are presented in Table 3.21. The tolerable concentration ratio of (concentration of foreign ion/concentration of analyte) Cd(II) to foreign was defined as ±5.0% current change by foreign ion.

Table 3.22 The effect of foreign ions on the square wave voltammetry of 5.0x10^{-7} mol L^{-1} Cd(II) at Bi-Sn/MWCNTs-CP-FE

Foreign Ions	Tolerable Ratio	Recovery (%)	RE (%)
Al(III) as chloride salt	0.1	91.2	-8.8
Ba(II) as chloride salt	1.0	90.9	-9.1
Ca(II) as chloride salt	0.1	150.9	+50.9
Cu(II) as nitrate salt	1.0	57.5	-42.5
Fe(III) as chloride salt	1.0	193.3	+93.3
K(I) as chloride salt	1.0	84.1	-15.9
Mg(II) as chloride salt	0.1	79.7	-20.3
Na(I) as chloride salt	100	71.1	-29.6
Ni(II) as chloride salt	0.5	136.7	+36.7
Pb(II) as nitrate salt	1.0	129.6	+29.6
Zn(II) as nitrate salt	0.5	81.9	-18.0

It can be seen from Table 3.22 that Al(III) and Ba(II) have little interference. The peak current of Cd(II) decreases in the presence of Cu(II) ions. This interference might be explained by the formation of intermetallic compounds between cadmium and copper (Jiang et al., 2010). Probably, there is also a competion between cadmium and copper on surface active sites of the film electrode.

3.5.5.8 Voltammetric behaviour of bismuth–tin film electrode for lead determination

3.5.5.8.1 Effect of pH

The effect of pH on the voltammetric responses of the electrode was tested for 5.0×10^{-7} mol L^{-1} Pb(II) ions. The peak current increased until pH 4.5 and then decreased (Table 3.22). As a result, the best working pH was choosen 4.5 for the proposed electrode.

Table 3.23 The efffect of pH with Sn-Bi/MWCNTs-CP-FE for 5×10^{-7} M Pb(II) ions

pH	Peak Currnet (μA)	Peak Potential (V)
0.1 M HClO4	9.64	-0.530
3.76 CH_3COOH/CH_3COONa	47.51	-0.480
4.0 CH_3COOH/CH_3COONa	1.08	-0.510
4.5 CH_3COOH/CH_3COONa	**65.72**	**-0.530**
5.0 CH_3COOH/CH_3COONa	44.53	-0.540
5.2 CH_3COOH/CH_3COONa	20.54	-0.560

The concentration range from 1.0×10^{-8} to 1.0×10^{-6} mol L^{-1} was investigated for proportionality of the Bi-Sn/MWCNTs-CP-FE signal with concentration of lead by analyzing model solutions containing appropriate additions of Pb(II). Square wave anodic stripping voltammograms obtained with Bi-Sn/MWCNTs-CP-FE at different concentration of Pb(II) ions under the optimized working conditions are shown in Figure 3.114.
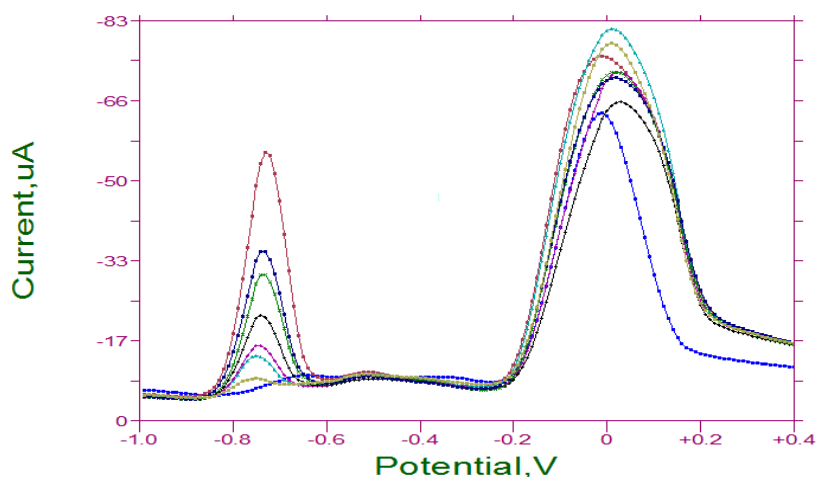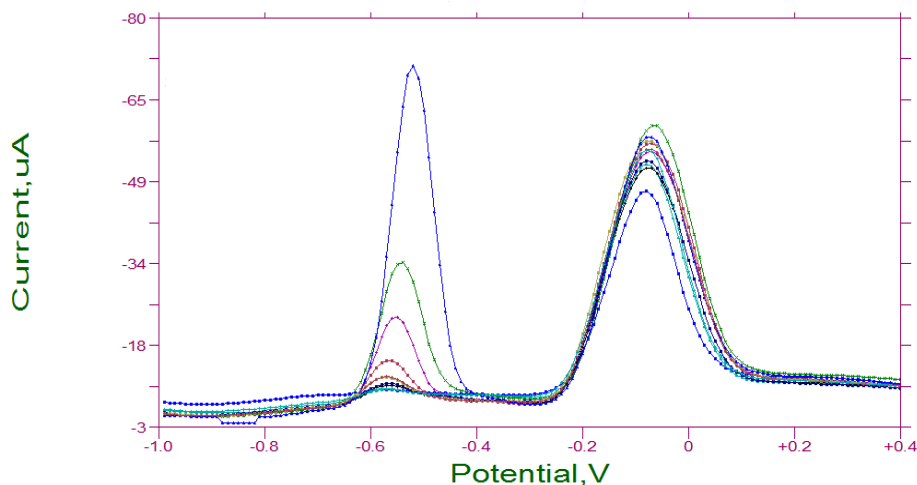
Figure 3.114 SWASVs obtained with Bi-Sn/MWCNTs-CP-FE, increasing concentration of Pb(II) ions at pH=4.5 CH₃COOH/CH₃COONa buffer solution, deposition time 210 s, range of scan potential -1.0 to +0.40 V, SW amplitude 25 mV, S.W. frequency 25 Hz and quite time 15 s, Pb(II) concentrations: $1.0x10^{-8}$ M, $2.0x10^{-8}$ M, $4.0x10^{-8}$ M, $6.0x10^{-8}$ M, $8.0x10^{-8}$ M, $1.0x10^{-7}$ M, $2.0x10^{-7}$ M, $4.0x10^{-7}$ M, $6.0x10^{-7}$ M, $8.0x10^{-7}$ M, $1.0x10^{-6}$ M

The linear calibration curve was graphted in Figure 3.115. The peak current increased linearly with increasing concentration up to $1.0x10^{-6}$ mol L^{-1}.
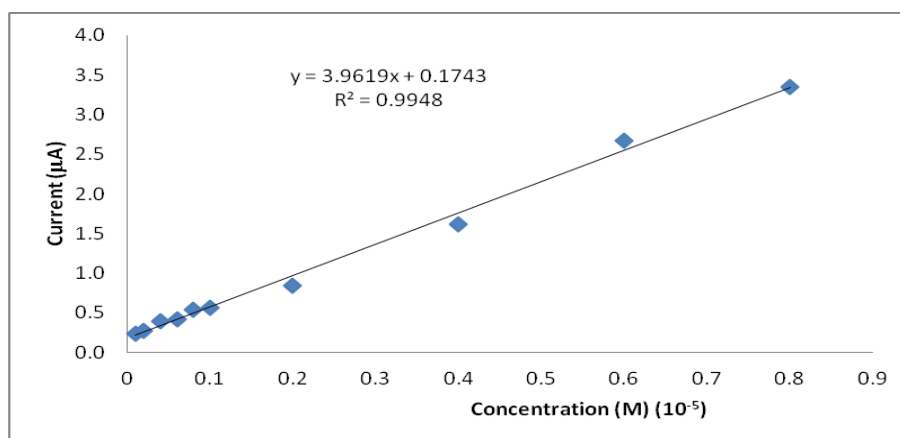
Figure 3.115 Calibration curve of Pb(II), obtained with Bi-Sn/MWCNTs-CP-FE

Figure 3.116 shows the voltammograms of Pb(II) and Cd(II) for a 210.0 seconds preconcentration period in a mixture of Pb(II) and Cd(II) solution at the same concentration range above. The Pb(II) and Cd(II) ions peaks appeared at -0.55 and -0.80 V, respectively.

Figure 3.116 SWASVs obtained with Bi-Sn/MWCNTs-CP-FE, increasing concentrations of Pb (II) and Cd(II) ions in pH= 4.5 CH$_3$COOH/CH$_3$COONa buffer solution, deposition time 210 s, range of scan potential -1.0 to +0.40 V, S.W. amplitude 25 mV, SW. frequency 25 Hz and quite time 15 s, Pb(II) concentrations: 1.0x10^{-8} M, 2.0x10^{-8} M, 4.0x10^{-8} M, 6.0x10^{-8} M, 8.0x10^{-8} M, 1.0x10^{-7} M, 2.0x10^{-7} M, 4.0x10^{-7} M, 6.0x10^{-7} M, 8.0x10^{-7} M, Cd(II) concentrations: 4.0x10^{-8} M, 6.0x10^{-8} M, 8.0x10^{-8} M, 1.0x10^{-7} M, 2.0x10^{-7} M, 4.0x10^{-7} M, 6.0x10^{-7} M, 8.0x10^{-7} M

The simultaneous voltammetric siganal of both analytes were increased by increasing each Pb(II) and Cd(II) concentrations in the range of 1.0x10^{-8}-8.0x10^{-7} mol L^{-1} and 4.0x10^{-8} mol L^{-1}-8.0x10^{-7} mol L^{-1} respectively. At the obtaining oxidation potentials, the calibration curves of Pb(II) and Cd(II) in their mixture soluiton were constructed in Figure 3.117.

Limit of dedection of Pb(II) ions was 0.1584x10^{-7} mol L^{-1}±0.035 (X$_{ort}$±3S) and limit of quantitaion of Pb(II) ions was 0.528x10^{-7} mol L^{-1}±0.172 (X$_{ort}$±10S) for Sn-Bi Film modified carbon paste electrode. Limit of dedection of Cd(II) ions was 1.2654x10^{-7}mol L^{-1}±0.042 (X$_{ort}$±3S) and limit of quantitaion of Cd(II) ions was 4.218x10^{-7} mol L^{-1}±0.196 (X$_{ort}$±10S) for Sn-Bi Film modified carbon paste electrode.
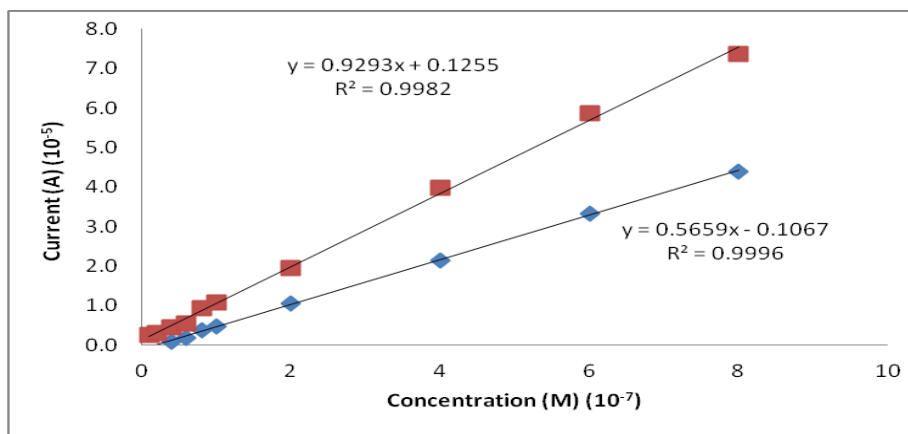
Figure 3.117 Standard addition graph of Pb(II) and Cd(II), obtained with Bi-Sn/MWCNTs-CP-FE

3.5.5.9. Analytical application

To determine the relevancy of the Bi-Sn/MWCNTs-CP-FE, the electrode was applied to determine Cd(II) concentration in water samples by the standard addition method under the optimized conditions. Recovery experiments were also carried out in order to evaluate the interference of matrix effects of the tap water samples on the detection of Cd(II) ions with Bi-Sn/MWCNTs-CP-FE. Results obtained for percentage recovery for the samples spiked with 5×10^{-7} mol L^{-1} cadmium was 107.7%. also 5×10^{-8} mol L^{-1} lead was 67.7%, respectively. The results presented satisfactory values for the proposed electroanalytical methods indicating thus the suitability of the proposed method for use in tap water samples.
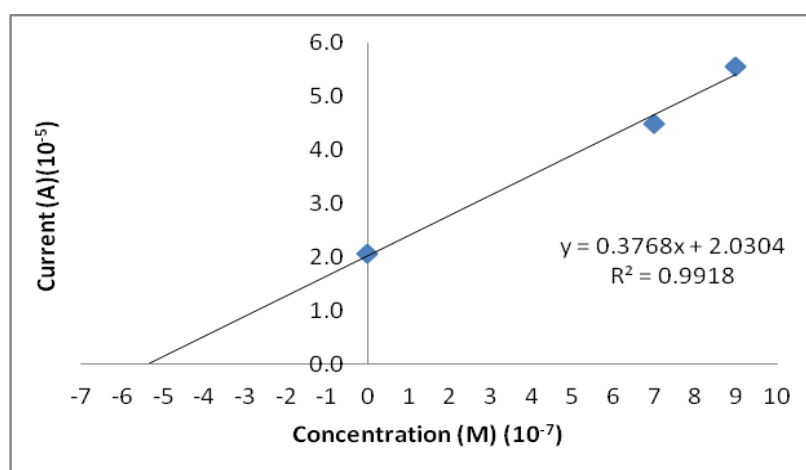
Figure 3.118 Standard addition graph of tap water for Cd(II) obtained with Bi-Sn/MWCNTs-CP-FE

$$y = 0,8944x + 0,277$$
$$R^2 = 0,9976$$
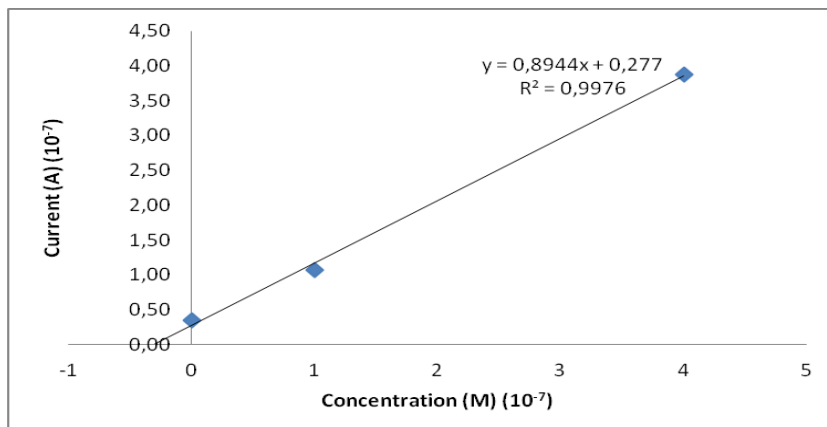
Figure 3.119 Calibration graph of tap water for Pb(II), obtained with Bi-Sn/MWCNTs-CP-FE

3.5.5.10 Characterization of modified carbon paste electrodes by scanning electron microscopy images

Figures 3.120 show the typical SEM images of the MWCNTs-CPE, Bi/MWCNTs-CP-FE, Sn/MWCNTs-CP-FE and Bi-Sn/MWCNTs-CP-FE. By comparing the SEM images of the three electrode surface, it is understood that there is a significant difference between them. The MWCNTs-CPE coated with Bi includes fine distrubition of relatively white dots related to bismuth ions. The white dots are smiliar scattering snow particles. On the other hand, the surface of MWCNTs-CP-FE coated with Sn was more smooth, like bright film shell, than that of Bi/MWCNTs-CP-FE.

The surface of MWCNTs-CP electrode coated with Sn and Bi simultaneously shows a difference structure image with the bright clean white snow particles from bismuth on the shell film form tin.
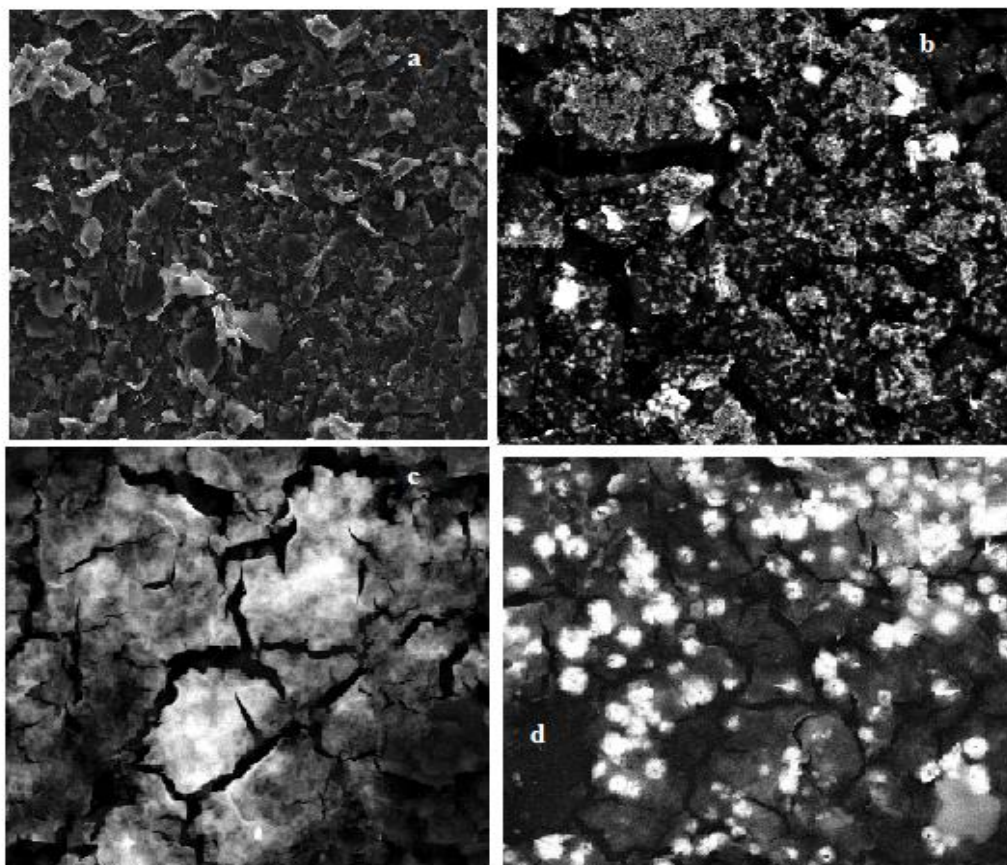
Figure 3.120 SEM images of a) Bare MWCNTs-CPE b) Bi/MWCNTs-CP-FE c) Sn/MWCNTs-CP-FE d) Bi-Sn/MWCNTs-CP-FE

3.5.5.11 X-Ray photoelectron spectroscopic measurements

The formation of Bi-Sn film on the MWCNTcontaining CPE was also characterized by XPS as shown in Figure 3. 121 a-b. The XPS spectrum of the Bi-Sn on the MWCNT displays the Bi 4f7/2 with binding energy of 163.0 eV, and the Sn 3d with a binding energy of 487.5 eV, which were typically characteristic of Bi and Sn. Finally, it can be claimed that the Bi-Sn alloy film on MWCNT containing carbon pasta electroe can easily be prepared via the proposed technique.
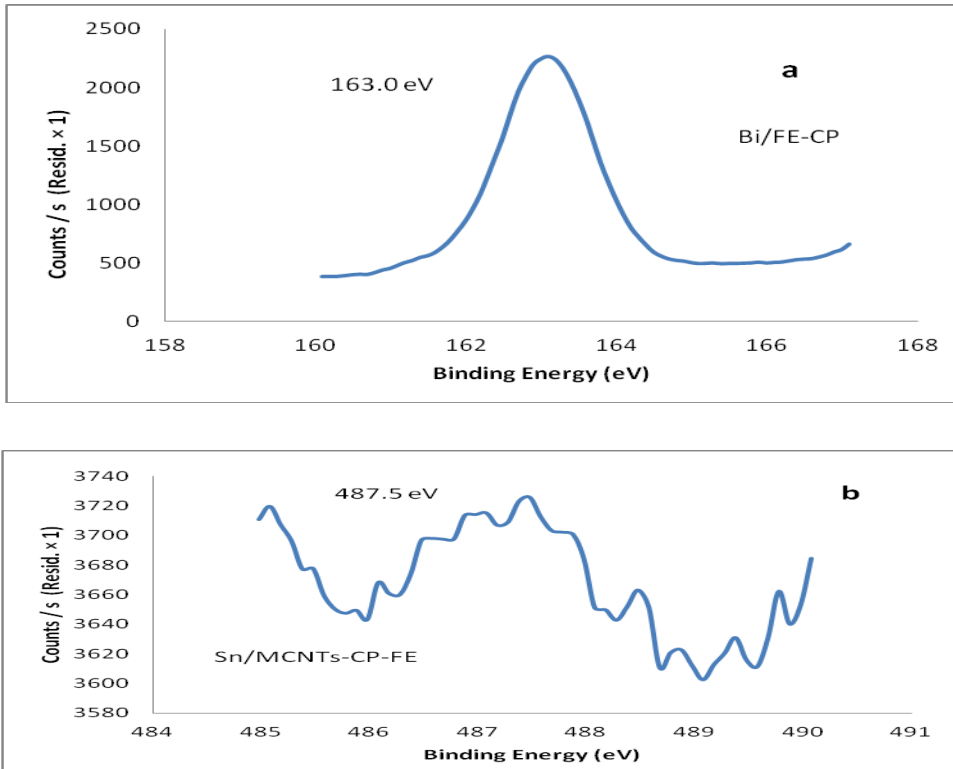
Figure 3.121 XPS of a) Bi/MWCNTs-CP-FE b) Sn/MWCNTs-CP-FE

4. GENERAL DISCUSSIONS AND CONCLUSIONS

Direct alcohol fuel cells are very promising as a portable power because of their high energy densities ease of available ethanol and methanol fuels and operation at low temperature. In general, the performance of direct alcohol fuels cells is not excellent because those small alcohols still need higher catalytic activity of electrodes to improve the oxidation kinetics. Therefore, to obtaine the best catalysts for small alcohols as fuel, lots of research groups have been focused on this type of researchs.

In the first section of this thesis, to increase the electrode performance the use of various catalysts was systematically evaluated for direct ethanol oxidation. For this aim, multiwall carbon nanotubes, metal nanoparticles such as palladium, gold and nickel and their mixtures as the potential catalysts materials were used to modify the bare glassy carbon electrode. The modified MWCNT covered GCEs were used to both direct ethanol and methanol electrochemistry.

To evaluate the performance of those electrodes, the oxidation peak potential and peak current were compared with those of bare GCE, MWCNT/GCE and Au, Pd polycystalline electrodes. The electrochemical preparation method for Pd, Au and Ni metal nanoparticles offer high-purtity on the electrode surface. Therefore, bimetallic or tri metallic particles containing electrode surfaces have higher catalytic activity towards ethanol and methanol oxidation. Generally in the fuel cells, a completed oxidation reaction is expecting on the electrode surface. Especially, in the case of ethanol and methanol, the final oxidation product should be carbon dioxide. But, there was no catalyts to achive the oxidation reaction in fuel cell technology until today. Therefore, the uncompleted oxidation reaction is still main problem on the electrode surfaces.

Since the uncompleted oxidation step could be poisoned the catalytic electrode surface by the adsorption of intermediate products of oxidation reaction. Thus the reverse oxidation peak formed during the cathodic potential scan. The peak current indicates the amount of intermediate products of the carbonaceous species on the electrode (catalyst) surface. This reverse peak formation have been observed on Pd based catalsyts compare with Au or Ni based electrodes in both ethanol and methanol oxidation in electrochemistry.

However, Pd based electrodes have higher catalytic activity towards small alcohol molecules while reverse peak formation due to the adsorption of carbonaceous species which were decreased the catalytic activity in the present conditions. To overcome this problem on the Pd based electrode surface, the Pd containing surfaces have been modified with another metal particle such as Au, Ni and Sn. In this thesis, to improve the catalytic activity of Pd based MWCNT/GC electrodes were modified with binary and tri metallic form of Pd-Au, Pd-Ni, Pd-Au-Ni particles modified MWCT/GCE and higher catalytic activity was obatined for both ethanol and methanol at Pd-Au-Ni-MWCNT/GCE. The supporting electrolyte (NaOH) concentration was also effected positively of the catalytic activity of the Pd-Ni, Pd-Au-Ni particles modified MWCT/GCE towards ethanol and methanol oxidation. From our results, 1.0 and 2.0 mol L^{-1} NaOH solution concentrations could be choosen as supporting electrolytes for alkaline fuel cells in the case of Pd-Au-Ni catalyts using as anode material in fuel cell.

One of the important results of the thesis is that the electrochemically reduction procedure could be offer high-purity electrode surface for higher catalytic activity towards ethanol oxidation compare with the same catalysts containing surfaces prepared by chemically reduction method. Because, after the chemical reduction of metal ions in the presence of MWCNT or another substrates, the oxidation product of reductive chemicals generally adsorp on the both metal nanoparticles and substrate surface. Alhough, sodium borohydride has been the most popular reducing regeant for the preparation of metal nanoparticles for fuel cell pre-eletrochemical studies, but the boron species are known as surface active compounds. This phenomenal could be decreased the intereaction between the alcohol molecules with metal nanoparticles. Therefore, the catalytic activity of chemically reduced metal nanoparticles was obtained lower to ethanol oxidation by evaluating of peak potential and peak current compare with results obtained with electrochemically prepared electrode surfaces.

On the other hand, a diffusion controlled electrode reactions were obtained for both ethanol and methanol oxidation on the Pd-Au-Ni modified MWCNT/GCE. Ni-, Au-, Pd-, Au-Ni-, Pd-Ni-, Pd-Au- and Pd-Au-Ni-MWCNT/GC electrodes prepared by citric acid as a reduction reagent do not show any catalytic activity for both ethanol and methanol oxidation due to the adsoption of the chemical reaction products to the metal nanoparticles surface.

The higher electrocatalytic activity can be also explained by the electrochemical impedance spectra results. The electrochemical impedance spectra for all the electrodes (except of Pd-MWCNT and Pd-Au-Ni-MWCNT/GCE) include a semicircular and a linear portion. The semicircle shapes in the spectra shows that there is a charge transfer process through the electrode and the coated nanoparticles at high frequency. On the other hand, in the low frequencies diffusion process is responsible for the electron transfer. The Rct for the bare GCE and MWCNT/GCE were higher than Pd, Au, Ni or their bimetallic or three metallic modified electrodes. This low R_{ct} values for metal nanoparticles modified electrodes implies that the charge transfer process is relatively fast compared to bare GCE and MWCNT/GCE.

In second chapter of the thesis, the determinations of lead and cadmium ions in water samples and tea sample were carried out by differantial pulse and square wave anodic stripping voltammetric techniques. For this purpose, five types of modified CPE were prepared using potassium ferrocyanide-carbon nanotubes, calcium phosphate, $Ca_3(PO_4)_2+ZrO(H_2PO_4)_2$, $Ca_3(PO_4)_2+Cu_2Fe(CN)_6$ and bismuth-tin film. Bismuth-Antimony film modified multiwall carbon nanotubes on glassy carbon electrodes were also used.

The carbon paste electrodes modified with silicate, silicate+potassium ferrocyanide and silicate+potassium ferrocyanide+carbon nanotubes were investigated to increase peak current of lead obtained by differential pulse anodic stripping voltammetry. The peak currents of lead achieved with the each electrodes were compared each others. As a result, the mixture of 64.0 % graphite +25.0 % mineral oil+5.0 % silicate+5.0 % $K_4Fe(CN)_6$ +1.0 % carbon nanotubes modified electrode provided the highest sensitivity for lead with accumulation time of 300.0 seconds. Under the optimum experimental condition, the prosedure was applied to analysis of tea sample solution and the concentraiton of lead was to be 45.0 ppb.

The carbon paste electrode modified with the mixture of $Ca_3(PO_4)_2+Cu_2Fe(CN)_6$ nanocrystals was optimized and then used for the determination of lead ions in tap water, using standard addition method. Both phosphate and ferrocyanide active sides offer high interaction between Pb(II) ion and electrode surface. Thus sensitive Pb(II) can be determined compare with CPE, $Ca_3(PO_4)_2$ modified CPE and $Cu_2Fe(CN)_6$ modified CPE.

The prepared modified electrode was succesfully applied to determination of Pb(II) ions in real water samples and the Pb(II) was obtained as 69.28 $\mu g\ L^{-1}$ Pb(II) in the tap water.

The others electrodes were evaluated analytically. The linear ranges of $Ca_3(PO_4)_2$ modified carbon paste, Bi-Sb film and $Ca_3(PO_4)_2 + ZrO(H_2PO_4)_2$ electrodes were found to be $4.0x10^{-8}-1.0x10^{-6}\ mol\ L^{-1}$, $4.0x10^{-7}-4.0x10^{-6}\ mol\ L^{-1}$ and $4.0x10^{-8}-2.0x10^{-7}\ mol\ L^{-1}$ for lead, respectively.

In our experiments, Bi and Sn film electrodes have provided better analytical performance for cadmium and lead determinations. Therefore, bismuth-tin film modified carbon pasta electrodes (Bi-Sn/MWCNTs-CP-FE) were investigated in detail in this thesis.

The pH dependence of Cd(II) and Pb(II) voltammetric response was observed on the Bi-Sn film-MWCNT containig CPE. The pH 4.5 acetat buffer solution was choosen as working medai for both Cd(II) and Pb(II) ions. From our voltammetric studies, both analytes signals were shown a dependency to the initial concentration of Sn(II) and Bi(III) in voltammetric cell and 500.0 ppb was optimum concentration for each modifier. The electrochemical deposition potential and depotion time was obtained as -1.0 V and 210.0 s for the sensitive determination of both Cd(II) and Pb(II) ions.

A new Bi-Sn codeposited film electrodes show well-defined stripping signals for both cadmium(II) and lead(II) and thus present another interesting alternative to mercury electrodes in electrochemical stripping analysis with a sensitivity that is significantly higher than those observed for single (pure) Sn or Bi films-based electrodes.

To obtain the good accuracy in the analysis of real sample, the influences of Al(III), Ba(II), Ca(II), Cu(II), Fe(III), K(I), Mg(II), Na(I), Ni(II), Pb(II) and Zn(II) as probable matrix ions have been evaluated and the tolerable concentration ratios were obtained. The most interference ions were Fe(III), Ca(II), Ni(II) as positivily effect by increasing peak currents, and Cu(II) negatively effect by decreasing peak current of Cd(II).

On the optimum experimental conditions, the Bi-Sn-MWCNT/CPE was used for the determination Pb(II) in tap water. Anodic stripping voltammetry coupled with Bi-Sn/MWCNTs-CP film electrode applied to tap water. The recovery was found 107%. Also with same electrode system Pb(II) ions were investigated and the calibration curve was linner in the range of 1.0×10^{-8} to 1.0×10^{-6} mol L^{-1}.

4.1 Overall Evaluation of Surface Characterizations

In this thesis, the surface morphologies under studied electrodes were characterized by scanning electron microscopy (SEM), energy dispersive X-Ray spectroscopy (EDX) and X-Ray photoelectron spectoscopy (XPS). In general, the deposition of metal nanoparticles modified multiwall carbon nanotube on bare glassy carbon by electrochemical and chemical deposition methods were determined with comporison of carbon nanotube electrodes and the modified electrode surface.

In SEM image studies with electrochemical deposition method, the SEM images of single metallic, bimetalllic and trimetallic nanoparticle modified electrodes surfaces decorated muliwall carbon nanotubes were compared each other to see the differences of their surfaces. It can be concluded that the each modified surface was covered as uniform in the different form. For example, the SEM images showed that gold and palladium nanoparticles modified on multiwall carbon nanotube surface were observed on the end of MWCNT ropes and over the ropes of MWCNT, respectively. The SEM image of Pd-Au-MWCNT explains that the aggregate of gold on the end of the MWCNT ropes is grown because of palladium deposition and again palladium is placed over the ropes. The SEM image of Pd-Au-Ni-MWCNT indicated the nickel dots over the carbon nanotube ropes and gold of bright round-shaped aggregates end of the carbon nanotube ropes were grown because of palladium deposition on them. At the same time, it was observed that the rope pieces between nickel dots and gold aggregates were coated with palladium nanoparticles.

In contrast to the electrochemical deposition method, the SEM images of the electrode surface prepared with chemical deposition method were different than those of electrochemical deposition method. For example, nickel nanoparticle modified electrode surface obtained with chemical deposition method were more homogeneous than that of Ni-MWCNT using electrochemical deposition method.

Distributions of gold and palladium over the carbon nanotube ropes were homogeneous, but at the same time included a few aggregates observed in the SEM images.

The presence of Pd, Au and Ni nanoparticles decorating on MWCNT/GCE, with the electrochemical deposition was confirmed by EDX study and Pd, Au and Ni metallic formation on the MWCNT/GCE were proved with XPS.

The SEM images of MCNTs-CP-FE, Bi-MCNTs-CP-FE, Sn- MCNTs-CP-FE and Bi-Sn-MCNTs-CP-FE have been given in Figure 3.119. By comparing the SEM images of the four electrode surfaces, it is seen that there are important differences between them. These SEM images show that a well-coated Bi- Sn film formation was prepared on the MCNTs-CPE. The XPS results proved that Bi and Sn film covered the electrode surface as their metallic forms.

REFERENCES

Abid, A.D., Anderson, D.S., Das, G.K., Winkle, L.S.V. and Kennedy, I.M., 2013, Novel lanthanide-labeled metal oxide nanoparticles improve the measurement of in vivo clearance and translocation, *Particle and Fibre Toxicology*, 10(1), 10p.

Antiochia, R., Lavagnini, I., Magno, F., Valentini F. and Palleschi, G., 2004, Single-Wall Carbon Nanotube Paste Electrodes: a Comparison with Carbon Paste, Platinum and Glassy Carbon Electrodes via Cyclic Voltammetric Data, *Electroanalysis*, 16(17), 1451p.

Ardakani, M.M., Beitollah, H., Amini, M.K., Mirkhalaf, F. and Alibeik, M.A., 2010, New strategy for simultaneous and selective voltammetric determination of norepinephrine, acetaminophen and folic acid using ZrO2 nanoparticles-modified carbon paste electrode, *Sensors and Actuators B*, 151, 243p.

Arepalli, S., Nikolaev, P., Gorelik, O., Hadjiev, V. Holmes, W., Files, B. and Yowell, L., 2004, Protocol for the characterization of single-wall carbon nanotube material quality, *Carbon*, 42(8-9), 1783p.

Arribas, A.S., Vazquez, T., Wang, J., Mulchandani, A. and Chen, W., 2005, Electrochemical and optical bioassays of nerve agents based on the organophosphorus-hydrolase mediated growth of cupric ferrocyanide nanoparticles, *Electrochemistry Communications*, 7, 1371p.

Ashrafi, A.M., Vytras, K., 2011, Stripping voltammetric determination of mercury(II) at antimony-coated carbon paste electrode, *Talant*a, 85, 2700p.

Azizia, S.N., Ghasemib, S. and Chiania, E., 2013, Nickel/mesoporous silica (SBA-15) modified electrode: An effective porous material for electrooxidation of methanol, *Electrochimica Acta*, 88, 463p.

Babaei, A., Zhang, L., Liu, E. and Jiang, S.P., 2012, Performance and carbon deposition over Pd nanoparticle catalyst promoted Ni/GDC anode of SOFCs in methane, methanol and ethanol fuels, *International Journal of Hydrogen Energy*, 37, 15301p.

Bakır, C.C., 2010, Preparation and characterization of metal nanoparticles modified carbon nanotube and polymer film electrodes and their analytical applications, MSc Thesis, Ege univercity, 147p.

Bambagioni, V., Bianchini, C., Marchionni, A. and Filippi, J., 2009, Pd and Pt–Ru anode electrocatalysts supported on multi-walled carbon nanotubes and their use in passive and active direct alcohol fuel cells with an anion-exchange membrane (alcohol=methanol, ethanol, glycerol), *Journal of Power Sources*, 190, 241p.

Banks, C.E., Davies, T.J., Wildgoose, G.G. and Compton, R.G., 2005, Electrocatalysis at graphite and carbon nanotube modified electrodes: edge-plane sites and tube ends are the reactive sites, *Chemical Communication*, 7, 829p.

REFERENCES(continued)

Barker, G.C. and Jenkin, I.L., 1952, Square-wave polarography, Analyst, 77, 685p.

Baughman, R.H., Zakhidov, A. and Heer, W.A., 2002, Carbon nanotubes-the route toward applications, *Science*, 297(5582), 787p.

Bera, D., Kuiry, S.C., McCutchen, M., Kruize, A., Heinrich, H., Meyyappan, M. and Seal, S., 2004, In-situ synthesis of palladium nanoparticles-filled carbon nanotubes using arc-discharge in solution, *Chemical Physical Letters*, 386, 364p.

Bethune, D.S., Kiang, C.H., Vries, M.S., Gorman, G., Savoy, R., Vazuez, J. and Beyers, R., 1993, Cobalt-catalyzed growth of carbon nanotubes with single-atomic-layer walls, *Nature*, 363, 305p.

Binnig, G., Quate C.F. and Gerber C.H., 1986, Atomic Force Microscope, Physical Review Letters, 56, 930p.

Calvillo, L., Celorriob, V., Molinerb, R., Garciac, A.B., Cameanc, I., Lazarob, M.J., 2013, Comparative study of Pt catalysts supported on different high conductive carbon materials for methanol and ethanol oxidation, *Electrochimica Acta*, 102, 19p.

Cao, L., Jia, J. and Wang, Z., 2008, Sensitive determination of Cd and Pb by differential pulse stripping voltammetry with in situ bismuth-modified zeolite doped carbon paste electrodes, *Electrochimica Acta*, 53, 2177p.

Casella, I.G. and Contursi, M., 2006, Characterization of bismuth adatom-modified palladium electrodes The electrocatalytic oxidation of aliphatic aldehydes in alkaline solutions*, Electrochimica Acta*, 52, 649p.

Chaudhuri, R.G. and Paria, S., 2012, Core/Shell Nanoparticles: Classes, Properties, Synthesis Mechanisms, Characterization, and Applications, Chem. Rev., 112, 2373p.

Chen, Y., Zhang, G., Mab, J., Zhou, Y., Tang, Y. and Lu, T., 2010, Electro-oxidation of methanol at the different carbon materials supported Pt nano-particles, *International Journal of Hydrogen Energy*, 35, 10109p.

Dai, Y.Q. and Shiu, K.K., 2004, Glucose Biosensor Based on Multi-Walled Carbon Nanotube Modified Glassy Carbon Electrode, *Electroanalysis*, 16(20), 1697p.

Danaee, I., Jafarian, M., Forouzandeh, F., Global, F. and Mahjani, M.G., 2008, Electrocatalytic oxidation of methanol on Ni and NiCu alloy modified glassy carbon electrode, *International journal of hydrogen energy*, 33(16), 4367p .

Denysenko, I., Ostrikov, K., Cvelbar, U., Mozetic, M. and Azarenkov, N.A., 2008, Carbon nanofiber growth in plasma-enhanced chemical vapor deposition, *Journal of Applied Physics*, 104, 073301p.

REFERENCES(continued)

Derycke, V., Martel, R., Appenzeller, J. and Avouris, P., 2001, Carbon Nanotube Inter- and Intramolecular Logic Gates, *Nano Letters*, 1(9), 453p.

Doria, G., Conde, J., Veigas, B., Giestas, L., Almeida, C., Assunção, M., Rosa, J. and Baptista, P.V., 2012, Noble Metal Nanoparticles for Biosensing Applications, *Sensors*, 12, 1657p.

Ebbesen (by editor), T.W., 1997, Carbon Nanotubes: preparartion and properties, CRC Lewis Publishers, 296p.

Ehsani, A., Mahjani, M.G., Jafarian, M. and Naeemy, A., 2012, Electrosynthesis of polypyrrole composite film and electrocatalytic oxidation of ethanol, *Electrochimica Acta*, 71, 128p.

Eres, G., Puretzky, A.A., Geohegan, D.B. and Cui, H., 2004, *In situ* control of the catalyst efficiency in chemical vapor deposition of vertically aligned carbon nanotubes on predeposited metal catalyst films, *Applied Physical Letters*, 84, 1759p.

Estevez-Hernandez, O., Naranjo-Rodrıguez, I., Hidalgo-Hidalgo de Cisneros, J.L. and Reguera, E., 2007, Evaluation of carbon paste electrodes modified with 1-furoylthioureas for the analysis of cadmium by differential pulse anodic stripping voltammetry, *Sensors and Actuators B. Chemical*, 123, 488p.

Fernandez, C.L., 2009, Electro-Catalytic Reactions, Ph D Thesis, Hull University, England.

Ganjali, M.R., Kazamia, N.M., Faridbod, F., Khoeec, S. and Norouzi, P., 2010, Determination of Pb^{2+} ions by a modified carbon paste electrode based on multi-walled carbon nanotubes (MWCNTs) and nanosilica, *Journal of Hazardous Materials*, 173, 415p.

Ghiaci, M., Rezaei, B.and Kalbasi, R.J., 2007, High selective SiO_2-Al_2O_3 mixed-oxide modified carbon paste electrode for anodic stripping voltammetric determination of Pb(II), *Talanta*, 73, 37p.

Ghosh, S.K. and Pal, T., 2007, Interparticle Coupling Effect on the Surface Plasmon Resonance of Gold Nanoparticles: From Theory to Applications. Chem. Rev., 107, 4797p.

Gomez, Y., Fernandez, L., Borras, C., Mostany, J. and Scharifker, B., 2011, Characterization of a carbon paste electrode modified with tripolyphosphate-modified kaolinite clay for the detection of lead, *Talanta*, 85, 1357p.

Gooding, J.J., 2005, Nanostructuring electrodes with carbon nanotubes: A review on electrochemistry and applications for sensing, *Electrochimica Acta*, 50, 3049p.

REFERENCES(continued)

Guo, D.J. and Li, H.L., 2005, Highly dispersed Ag nanoparticles on functional MWNT surfaces for methanol oxidation in alkaline solution, *Carbon*, 43, 1259p.

Guo, R., Song, Y., Wang, G. and Murray, R.W., 2005, Does Core Size Matter in The Kinetics of Ligand Exchanges of Monolayer-Protected Au Clusters?, *Journal of American Chemical Society*, 127, 2752p.

Ha, B. and Han, O.H., 2013, Platinum-catalyzed carbon nanotubes for durability enhancement of low-temperature fuel cells, *Journal of Power Sources*, 223, 246p.

Hall, S.C., Subramanian, V., Teeter, G. and Rambabu, B., 2004, Influence of metal-support interaction in Pt/C on CO and methanol oxidation reactions, *Solid State Ionics*, 175, 809p.

He, Z., Zhan, L., Wang, Q., Song, S., Chen, J., Zhu, K., Xu, X. and Liu, W., 2011, Increasing the activity and stability of chemi-deposited palladium catalysts on nickel foam substrate by electrochemical deposition of a middle coating of silver, *Separation and Purification Technology*, 80(3), 526p

Hester, J.R. and Louchevet, O.A., 2002, Nanoparticle-templated carbon nanotube ring nucleus formation, *Applied Physical Letters*, 80, 2580p.

Houston, D.K. and Johnson, M.A., 1999, Blood Lead Level is Associated with Elevated Blood Pressure in Blacks, Nutr. Rev. 57 (9 Part 1), 277p.

Hu, F. and Chen, W., 2011, End-opened carbon nanotube array supported Pd as anode for alkaline fuel cell, *Electrochemistry Communications*, 13, 955p.

Hwanga, G.H., Hana, W.K., Parkb, J.S. and Kanga, S.G., 2008, Determination of trace metals by anodic stripping voltammetry using a bismuth-modified carbon nanotube electrode, *Talanta*, 76, 301p.

Iijima, 2002.

Iijima, S. and Ichihashi, T., 1993, Single-shell carbon nanotubes of 1-nm diameter *Nature*, 363, 603p.

Iijima, S., 1991, Helical microtubules of graphitic carbon, *Nature*, 354, 56p.

Jang, A., Seo, Y.W. and Bishop, P.L., 2005, The removal of heavy metals in urban run off by sorption on mulch, *Environmental Pollution*, 133, 117p.

Jha, M.K., Kumar, V., Jeong, J. and Lee, J.C., 2012, Review on solvent extraction of cadmium from various solutions, *Hydrometallurgy*, 111, 1p.

REFERENCES(continued)

Jiang, H., Zhu, L., Moon, K. and Wong, C.P., 2007, The preparation of stable metal nanoparticles on carbonnanotubes whose surfaces were modified during production, *Carbon*, 45, 655p.

Jiang, L., Wang, Y., Ding, J., Lou, T. and Qin, W., 2010, An ionophore–Nafion modified bismuth electrode for the analysis of cadmium(II), *Electrochemistry Communications*, 12, 202p.

Jiang, L., Zang, H., Sun, G. and Xin, Q., 2006, Influence of Preparation Method on the Performance of PtSn/C Anode Electrocatalyst for Direct Ethanol Fuel Cells, *Chinese Journal of Catalysis*, 27, 15p.

Kang, S.J., Kocabas, C., Ozel, T., Shim, M., Pimparkar, N., Alam, M.A., Rotkin, S.V. and Rogers, J.A., 2007, High-performance electronics using dense, perfectly aligned arrays of single-walled carbon nanotubes, *Nature Nanotechnology*, 2, 230p.

Keawkim, K., Chuanuwatanakul, S., Chailapakul, O. and Motomizu, S., 2013, Determination of lead and cadmium in rice samples by sequential injection/anodic stripping voltammetry using a bismuth film/crown ether/Nafion modified screen-printed carbon electrode, *Food Control*, 31, 14p.

Kim, J.H., Nam, K.W., Ma, S.B. and Kim, K.B., 2006, Fabrication and electrochemical properties of carbon nanotube film electrodes, *Carbon*, 44, 1963p.

Kim, S.N., Rusling, J.F. and Papadimitrakopoulos, F., 2007, Adv. Material, 19, 3214p.

Ko, C.J., Lee, C.Y., Ko, F.H., Chen, H.L. and Chu, T.C., 2004, Microelectron. Eng., 570, 73p.

Ko, J., Chippar P. and Ju, H., 2010, A one-dimensional, two-phase model for direct methanol fuel cells – Part I: Model development and parametric study, *Energy*, 35, 2149p.

Kokkinos, C., Economou, A., Raptis, I. and Efstathiou, C.E., 2008, Lithographically fabricated disposable bismuth-film electrodes for the trace determination of Pb(II) and Cd(II) by anodic stripping voltammetry, *Electrochimica Acta*, 53, 5294p.

Kounaves, S.P., 1997, Voltammetric techniques, in Handbook of Instrumental Techniques for Analytical Chemistry, Settle, F. A., chapter 37, Prentice Hall PTR.

Kumar, L.V., Ntim, S.A., Khow, O.S., Janardhana, C., Lakshminarayananc, V. and Mitrab, S., 2012, Electro-catalytic activity of multiwall carbon nanotube-metal (Pt or Pd) nanohybrid materials synthesized using microwave-induced reactions and their possible use in fuel cells, *Electrochimica Acta*, 83, 40p.

REFERENCES(continued)

Larsen, J.L, Tune, D.D., Kemppinen, P., Winzenberg, K.N., Watkins, S.E. and Shapter, J.G., 2012, Increased performance of single walled carbon nanotube photovoltaic cells through the addition of dibenzo[b,def]chrysene derivative, *Journal of Photochemistry and Photobiology A: Chemistry,* 235, 72p.

Lawrence, N.S., Deoa R.P. and Wang, J., 2004, Detection of homocysteine at carbon nanotube paste electrodes, *Talanta*, 63, 443p.

Lee, E., 2010, Development of anode catalysts for direct alcohol fuel cells, Dissertation, the graduate school of the university of texas at Austin, Austin, USA.

Lee, K.Y., Kim, M., Lee, Y.W., Lee, J.J. and Woo, S., 2007, Han Fabrication of metal nanoparticles–carbon nanotubes composite materials in solution, *Chemical Physics Letters*, 440, 249p.

Li, B.L., Wu, Z.L., Xiong, C.H., Luo, H.Q. and Li, N.B., 2012, Anodic stripping voltammetric measurement of trace cadmium at tin-coated carbon paste electrode, *Talanta,* 88, 707p.

Li, D., Jia, J. and Wang, J., 2010, Simultaneous determination of Cd(II) and Pb(II) by differential pulse anodic stripping voltammetry based on graphite nanofibers–Nafion composite modified bismuth film electrode, *Talanta,* 83, 332p.

Li, T.X., Lee, J.H., Wang, R.Z., Kang, Y.T., 2013, Enhancement of heat transfer for thermal energy storage application using stearic acid nanocomposite with multi-walled carbon nanotubes, *Energy*, 55, 752p.

Li, Y., Liu, X., Zeng, X., Liu, Y., Liu, X., Wei, W. and Luo, S., 2009, Simultaneous determination of ultra-trace lead and cadmium at a hydroxyapatite-modified carbon ionic liquid electrode by square-wave stripping voltammetry, *Sensors and Actuators B*, 139, 604p.

Liang, Z.X., Zhao, T.S., Xu, J.B. and Zhu, L.D., 2009, Mechanism study of the ethanol oxidation reaction on palladium in alkaline media, *Electrochimica Acta*, 54, 2203p.

Lin, X.Q., He, J.B. and Zha, Z.J., 2006, Simultaneous determination of quercetin and rutin at a multi-wall carbon-nanotube paste electrodes by reversing differential pulse voltammetry, *Sensors and Actuators B: Chemical*, 119, 608p.

Lin, Y., Zhang, S., Yan, S. and Liu, G., 2012, The effect of Sn content in Pt–SnO2/CNTs for methanol electro-oxidation, *Electrochimica Acta*, 66, 1p.

Liu, Z., Li, Z., Wang F., Liu, J., Ji, J., Wang, J., Wang, W., Qin, S. and Zhang, L., 2011, Synthesis of multi-walled carbon nanotube supported nickel catalysts by hydrazine reduction and their electrocatalytic activity on ethanol electro-oxidation**,** *Materials Letters*, 65, 3396p.

REFERENCES(continued)

Long, N.V., Hien, T.D., Asaka, T., Ohtaki, M. and Nogami, M., 2011,Synthesis and characterization of Pt–Pd alloy and core-shell bimetallic nanoparticles for direct methanol fuel cells (DMFCs): Enhanced electrocatalytic properties of well-shaped core-shell morphologies and nanostructures, *International Journal of Hydrogen Energy*, 36, 8478p.

Louchev, O.A. and Growth, C.J., 2002, Transport-kinetical phenomena in nanotube growth, 237(1), 65p.

Luo, H.X., Shi, Z.J., Li, N.Q., Gu, Z.N. and Zhuang, Q.K., 2001, Investigation of the electrochemical and electrocatalytic behavior of single-wall carbon nanotube film on a glassy carbon electrode, *Analytical Chemistry*, 73, 915p.

Luque, R., Varma Rajender, S., Rajender, S., Varma, J.H., Clark, G. and Kraus, A., 2008, Sustainable Preparation of Metal Nanoparticles: Methods and Applications, Chapter 3, RCSpublishing, NY.

Lyons, M.E.G. and Keeley, G.P., 2008, Carbon nanotube based modified electrode biosensors: Electrochemical studies of the flavin group redox kinetics at SWCNT/glucose oxidase composite modified electrodes, *International. Journal of Electrochemical Science*, 3, 819p.

Mahapatra, S.S. and Datta, J., 2011, Characterization of Pt-Pd/C Electrocatalyst for Methanol Oxidation in Alkaline Medium, *International Journal of Electrochemistry*, 2011, 16p.

Martinez, R.H. and Blasco, I.N., 2012, Estimation of dietary intake and content of lead and cadmium in infant cereals marketed in Spain, *Food Control*, 26, 6p.

Mhammedi, M.A., Achak, M., and Chtaini, A., 2009, $Ca_{10}(PO_4)_6(OH)_2$-modified carbon-paste electrode for the determination of trace lead(II) by square-wave voltammetry, *Journal of Hazardous Materials*, 161, 55p.

Moulder, J.F., Stikle, W.F., Sobol, P.E. and Bomben, K.D., Handbook of X-ray Photoelectron Spectroscopy. Perkin-Elmer, USA, 1992.

Mousavi, M.F., Rahmani, A., Golabi, S.M., Shamsipur, M. and Sharghi, H., 2001, Differential pulse anodic stripping voltammetric determination of lead(II) with a 1,4-bis(prop-2′-enyloxy)-9,10-anthraquinone modified carbon paste electrode, *Talanta,* 55, 305p.

Musameh, M., Wang, J., Merkoci, A. and Lin, Y., 2002, Low-potential stable NADH detection at carbon-nanotube-modified glassy carbon electrodes, *Electrochemical Communication*, 4, 743p.

REFERENCES(continued)

Nair, A.S., Tom, R.T., Kumar, V.R.R., Subramaniam, C. and Pradeep, T., 2007, Chemical Interactions at Noble Metal Nanoparticle Surfaces-Catalysis, *Sensors and Devices*, Cosmos, 3(1), 103p.

Nenkova, R., Ivanova, D., Vladimirova, J. and Godjevargova, T., 2010, New amperometric glucose biosensor based on cross-linking of glucose oxidase on silica gel/multiwalled carbon nanotubes/polyacrylonitrile nanocomposite film, *Sensors and Actuators B*, 148, 59p.

Nguyen, P.K.Q. and Lunsford, S.K., 2012, Electrochemical response of carbon paste electrode modified with mixture of titanium dioxide/zirconium dioxide in the detection of heavy metals: Lead and cadmium, *Talanta*, 101, 110p.

Oliveira, M.C., Rego, R., Fernandes, L.S., Tavares, P.B., 2011, Evaluation of the catalytic activity of Pd–Ag alloys on ethanol oxidation and oxygen reduction reactions in alkaline medium, *Journal of Power Sources*, 196, 6092p.

Osteryoung, J. and Osteryoung, R., 1985, Square wave voltammetry, Analytical Chemistry, 57, 101p.

Parra, M.R., Garcia, T., Lorenzo, E. and Parientei, F., 2008, Electrocatalytic oxidation of methanol and other short chain aliphatic alcohols on glassy carbon electrodes modified with conductive films derived from Ni(II)-(N,N-bis(2,5-dihydroxybenzylidene)-1,2-diaminobenzene, *Sensors and Actuators B*, 130, 730p.

Parvin, M.H., Golivand, M.B., Najafi, M. and Shariaty, S.M., 2012, Carbon paste electrode modified with cobalt nanoparticles and its application to the electrocatalytic determination of chlorpromazine, *Journal of Electroanalytical Chemistry*, 683, 31p.

Pedano, M.L. and Rivas, G.A., 2004, Adsorption and electrooxidation of nucleic acids at carbon nanotubes paste electrodes, *Electrochemical Communication*, 6, 10p.

Pereira, P.F., Sousa, R.M.F., Munoz, R.A.A. and Richter, E.M., 2013, Simultaneous determination of ethanol and methanol in fuel ethanol using cyclic voltammetry, *Fuel*, 103, 725p.

Pitois, A., Pilenga, A., Pfrang, A. and Tsotridis, G., 2011, Temperature-dependent CO desorption kinetics on supported gold nanoparticles: Relevance to clean hydrogen production and fuel cell systems, *International Journal of Hydrogen Energy*, 36(7), 4375p.

Qu, B., Xu, Y.T., Lin, S.J., Zheng, Y.F. and Dai, L.Z., 2010, Fabrication of Pt nanoparticles decorated PPy–MWCNTs composites and their electrocatalytic activity for methanol oxidation, *Synthetic Metals*, 160, 732p.

REFERENCES(continued)

Qu, J., Shen, Y., Qu, X. and Dong, S., 2004, Electrocatalytic Reduction of Oxygen at Multi-Walled Carbon Nanotubes and Cobalt Porphyrin Modified Glassy Carbon Electrode, *Electroanalysis*, 16(17), 1444p.

Rao, V., 2007, Electro-oxidation of ethanol at gas diffusion electrodes a DEMS study, *Journal. of the Electrochemical. Society*, 154, 1138p.

Raoof, J.B., Ojani, R. and Nadimi, S.R., 2004, Preparation of polypyrrole/ferrocyanide films modified carbon paste electrode and its application on the electrocatalytic determination of ascorbic acid, *Electrochimica Acta*, 49, 271p.

Raoof, J.B., Ojani, R. and Hosseini, S.R., 2011, Electrochemical fabrication of novel Pt/poly (m-toluidine)/Triton X-100 composite catalyst at the surface of carbon nanotube paste electrode and its application for methanol oxidation, *International Journal of Hydrogen Energy*, 36, 52p.

Reimer L. and Kohl, H., 2008, Transmission electron microscopy: physics of image formation, 5th edition, Springer.

Rubianes, M.D. and Rivas, G.A., 2003, Carbon nanotubes paste electrode, *Electrochemistry Communications*, 5, 689p.

Saadeh, S.M., Abu-Shawish, H.M., Abed-Almonem, K.I., Baraka, A., Mkhada, A. and Safi, W., 2012, A new potentiometric thiosalicylamide-functionalized polysiloxane carbon paste electrode for lead(II) determination, *Journal of Electroanalytical Chemistry*, 687, 11p.

Sánchez, A., Zarcero, S.M., Quintanilla, D.P., Hierro, I. and Sierra, I., 2013, A comparative study on carbon paste electrodes modified with hybrid mesoporous materials for voltammetric analysis of lead (II), *Journal of Electroanalytical Chemistry*, 689, 76p.

Sarkar, S., Guibal, E., Quignard, F. and Gupta, A.K.S., 2012, Polymer-supported metals and metal oxide nanoparticles: synthesis, characterization, and applications, *J Nanopart Res*. 14, 715p.

Schwarz, M.W. and Irving, S., 1964, Theory of stationary electrode polarography: single scan and cyclic methods applied to reversible, irreversible, and kinetic systems, *Analytical Chemistry*, 36, 706p.

Senthilkumar, S. and Saraswathi, R., 2009, Electrochemical sensing of cadmium and lead ions at zeolite-modified electrodes: Optimization and field measurements Original Research Article, *Sensors and Actuators B: Chemical*, 141, 65p.

Shah, A., 2010, Redox Behavior and DNA binding studies of some electroactive compounds, Ph D Thesis, Quaid-i-Azam University, Islamabad, Pakistan.

REFERENCES(continued)

Shahrokhian, S. and Fotouhi, L., 2007, Carbon paste electrode incorporating multi-walled carbon nanotube/cobalt salophen for sensitive voltammetric determination of tryptophan, *Sensors and Actuators B: Chemical*, 123, 942p.

Shams, E. and Torabi, R., 2006, Determination of nanomolar concentrations of cadmium by anodic-stripping voltammetry at a carbon paste electrode modified with zirconium phosphated amorphous silica, *Sensors and Actuators B*, 117, 86p.

Sherigara, B., Kutner, S. and D'Souza, W.F., 2003, Electrocatalytic properties and sensor applications of fullerenes and carbon nanotubes, *Electroanalysis*, 15(9), 753p.

Taurino, I., Carrara, S., Giorcelli, M., Tagliaferro, A. and Michelia, G., 2011, Comparing sensitivities of differently oriented multi-walled carbon nanotubes integrated on silicon wafer for electrochemical biosensors, *Sensors and Actuators B*, 160, 327p.

Tayal, J., Rawat, B. and Basu, S., 2011, Bi-metallic and tri-metallic Pt–Sn/C, Pt–Ir/C, Pt–Ir–Sn/C catalysts for electro-oxidation of ethanol in direct ethanol fuel cell, *International Journal of Hydrogen Energy*, 36, 14884p.

Tesarova, E., Baldrianovaa, L., Hocevar, S.B., Svancarab, I., Vytrasb, K. and Ogorevc, B., 2009, Anodic stripping voltammetric measurement of trace heavy metals at antimony film carbon paste electrode, *Electrochimica Acta*, 54, 1506p.

Tian, Y.Q., Li, N. B. and Luo, H.Q., 2009, Simultaneous Determination of Trace Zinc(II) and Cadmium(II) by Differential Pulse Anodic Stripping Voltammetry Using a MWCNTs–NaDBS Modified Stannum Film Electrode, *Electroanalysis*, 21(23), 2584p.

Türker, A.R., 2012, Separation, Preconcentration and Speciation of Metal Ions by Solid Phase Extraction, Separation & Purification Reviews, 41, 169p.

Ulubay, S., 2008, Preparation of metal nano-particles modified polypyrrole film electrodes and investigations of their electrocatalytic activity., MSc Thesis, Ege univercity, 138p.

US EPA, National Primary Drinking Water Regulations, 2009, EPA 816-F-09-0004.

Valentini, F., Amine, A., Orlanducci, S., Terranova, M.L. and Palleschi, G., 2003, Carbon nanotube purification: preparation and characterization of carbon nanotube paste electrodes, *Analytical Chemistry*, 75, 5413p.

REFERENCES(continued)

Velázquez-Palenzuela, A., Brillas, E., Arias, C., Centellas, F., Garrido, J.A., Rodríguez, R.M., Cabot, P.L., 2013, Structural analysis of carbon-supported Ru-decorated Pt nanoparticles synthesized using forced deposition and catalytic performance toward CO, methanol, and ethanol electro-oxidation, *Journal of Catalysis*, 298, 112p.

Venkataramanı, K., 2010, Non-contact atomic force microscopy studies of metal oxide surfaces and oxide supported metal nanoclusters, PhD Thesis, Aarhus University, Denmark.

Vigier, F., Rousseau, S., Coutanceau, C., Leger, J.M. and Lamy, C., 2006, Electrocatalysis for the direct alcohol fuel cell, Topics in Catalysis, 40(1-4), 111p.

Vijayaraghavan, A., Blatt, S., Weissenberger, D., Oron-Carl, M., Hennrich, F., Gerthsen, D., Hahn, H. and Krupke, R., 2007, Ultra-large-scale directed assembly of single-walled carbon nanotube devices, *Nano Letters*, 7(6), 1556p.

Wang, J., 2000, Analytical electrochemistry, Chapter 2, John Wiley and Sons, NY.

Wang, J.X., Li, M.X., Shi, Z.J., Li N.Q. and Gu, Z.N., 2002, Investigation of the electrocatalytic behavior of single-wall carbon nanotube films on an Au electrode, *Microchemical Journal*, 73, 325p.

Wang, J.X., Li, M.X., Shi, Z.J., Li, N.Q. and Gu, Z.N., 2002, Direct electrochemistry of cytochrome c at a glassy carbon electrode modified with single-wall carbon nanotubes, *Anal. Chem.*, 74(9), 1993p.

Wang, L., Zhao, J., He, X., Gao, J., Li, J., Wan, C. and Jiang, C., 2012, Electrochemical impedance spectroscopy (EIS) study of LiNi1/3Co1/3Mn1/3O2 for Li-ion batteries, *International Journal of Electrochemical Science*, 7, 345p.

Wang, M., Liu W. and Huang, C., 2009, Investigation of PdNiO/C catalyst for methanol electrooxidation, *International Journal of Hydrogen Energy*, 34, 2758p.

Wang, Z., Liang, Q., Wang, Y., Luo and G.A., 2002, Carbon nanotube-modified electrodes for the simultaneous determination of dopamine and ascorbic acid, *Analyst*, 127(5):653p.

White, R.J., Luque, R., Budarin, V.L., Clark, J.H. and Macquarrie, D.J., 2009, Supported metal nanoparticles on porous materials,. *Methods and applications Chemical. Society*, 38, 481p.

Wongyao, N., Therdthianwong, A. and Therdthianwong, S., 2011, Performance of direct alcohol fuel cells fed with mixed methanol/ethanol solutions, *Energy Conversion and Management*, 52(7), 2676p.

REFERENCES(continued)

Wonsawat, W., Chuanuwatanakul, S., Dungchai, W., Punrat, E., Motomizu, S. and Chailapakul, O., 2012, Graphene-carbon paste electrode for cadmium and lead ion monitoring in a flow-based system, *Talanta*, 100, 282p.

Wu, K., Hu, S., Fei, J., Bai, W., 2003, Mercury-free simultaneous determination of cadmium and lead at a glassy carbon electrode modified with multi-wall carbon nanotubes, *Analytica Chimica Acta*, 489, 215p.

Wu. Y., Li, N.B. and Luo, H.Q., 2008, Simultaneous measurement of Pb, Cd and Zn using differential pulse anodic stripping voltammetry at a bismuth/poly(p-aminobenzene sulfonic acid) film electrode, *Sensors and Actuators B: Chemical*, 133, 677p.

Xu, H., Zeng, L., Huang, D., Xian, Y.and Jin L., 2008, A Nafion-coated bismuth film electrode for the determination of heavy metals in vegetable using differential pulse anodic stripping voltammetry: An alternative to mercury-based electrodes, *Food Chemistry*, 109, 834p.

Xu, J., Hua, K., Sun, G., Wang, C., Lv, X. and Wang, Y., 2006, Electrooxidation of methanol on carbon nanotubes supported Pt–Fe alloy electrode*, Electrochemistry Communications*, 8, 982p.

Xu, J.B., Zhao, T.S., Li, Y.S. and Yang, W.W., 2010, Synthesis and characterization of the Au-modified Pd cathode catalyst for alkaline direct ethanol fuel cells**,** *International Journal of Hydrogen Energy*, 35, 9693p.

Xu, K., Pierce, D.T., Li, A. and Zhao, J.X., 2008, Nanocatalysts in Direct Methanol Fuel Cell Applications, Synthesis and Reactivity in Inorganic, *Metal-Organic, and Nano-Metal Chemistry*, 38, 394p.

Yan, Z., Meng, H., Shi, L., Li, Z.P. and Shen, K., 2010, Synthesis of mesoporous hollow carbon hemispheres as highly efficient Pd electrocatalyst support for ethanol oxidation, *Electrochemistry Communications*, 12, 689p.

Yanez-Sedeno, P., Riu, J., Pingarron, J.M., Rius, F.X., 2010, Electrochemical sensing based on carbon nanotubes, *Trends in Analytical Chemistry*, 29(9).

Yang, X., Zheng, J., Zhen, M., Meng, X., Jiang, F., Wang, T., Shu, C., Jiang, L. and Wang, C., 2012, A linear molecule functionalized multi-walled carbon nanotubes with well dispersed PtRu nanoparticles for ethanol electro-oxidation, *Applied Catalysis B: Environmental*, 121-122, 57p.

Yantasee, W., Lin, Y., Fryxell, G.E. and Busche, B.J., 2004, Simultaneous detection of cadmium, copper, and lead using a carbon paste electrode modified with carbamoylphosphonic acid self-assembled monolayer on mesoporous silica (SAMMS), *Analytica Chimica Acta*, 502, 207p.

REFERENCES(continued)

Ye, W., Kou, H., Liu, Q., Yan, J., Zhou, F. and Wanga, C., 2012, Electrochemical deposition of Au–Pt alloy particles with cauliflower-like microstructures for electrocatalytic methanol oxidation*, International Journal of Hydrogen Energy*, 37(5), 4088p.

Yi, Q., Sun, L., Liu, X. and Nie, H., 2013, Palladium–nickel nanoparticles loaded on multi-walled carbon nanotubes modified with β-cyclodextrin for electrooxidation of alcohols, *Original Research Article Fuel*, 111, 88p.

Yi, W.J., Li, Y., Ran, G., Luo, H.Q. and Li, N.B., 2012, Determination of cadmium(II) by square wave anodic stripping voltammetry using bismuth–antimony film electrode, *Sensors and Actuators B*, 166-167, 544p.

Yun, Y.H., Shanov, V., Tu, Y., Subramaniam, S. and Schulz, M.J., 2006, Growth mechanism of long aligned multiwall carbon nanotube arrays by water-assisted chemical vapor deposition, *Journal of Physical Chemistry. B*, 110, 23920p.

Zejli, H., Temsaman, K.R., Cisneros, H., Rodriguez, I.N. and Sharrock, P., 2006, Electrochemical micro-extraction of lead (II) at a hydroxylapatite modified platinum electrode, *Electrochemistry Communications*, 8, 1544p.

Zhang, M., Su, L. and Mao, L., 2006, Surfactant functionalization of carbon nanotubes (CNTs) for layer-by-layer assembling of CNT multi-layer films and fabrication of gold nanoparticle/CNT nanohybrid, *Carbon*, 44, 276p.

Zhang, M., Yan, Z. and Xie, J., 2012, Core/shell Ni-Pd nanoparticles supported on MWCNTs at improved electrocatalytic performance for alcohol oxidation in alkaline media, *Electrochimica Acta*, 77, 237p.

Zhang, W.X., 2003, Nanoscale iron particles for environmental remediation: An overview, J Nanopart Res., 5, 323p.

Zhou, Y., Li, Y.S., Meng, X.Y., Zhang, Y.Y., Yang, L., Zhang, J.H., Wang, X.R., Lu, S.Y., Ren, H.L. and Liu, Z.S., 2013, Development of an immunochromatographic strip and its application in the simultaneous determination of Hg(II), Cd(II) and Pb(II), *Sensors and Actuators B*, 183, 303p.

Zhu, H.W., Xu, C.L., Wu, D.H., Wei, B.Q., Vajtai, R. and Ajayan, P.M., 2002, Direct Synthesis of Long Single-Walled Carbon Nanotube Strands, *Science*, 296, 884p.

Zhu, Z., Wang, J., Munir, A. and Zhou, H.S., 2010, Electrocatalytic activity of Pt nanoparticles on bamboo shaped carbon nanotubes for ethanol oxidation, *Electrochimica Acta*, 55, 8517p.

CURRICULUM VITAE

Name   :Aydan ELÇİ

Date of Birth   :August, 08, 1978

Place of Birth   :Manisa, Turkey

Nationality   :Republic of Turkish

Marital Status   :Single

Adress   :1846 Sok. Barış Apt. Karşıyaka/İzmir

Phone Number   :+90 536 6668583

E-mail   :aydan.elci@ege.edu.tr

Education   :1996-2000, BSc Degree in Chemisty Department of
Erciyes University, Kayseri, Turkey

2000-2003, MSc Degree in Chemistry Department of
Pamukkale University,

Denizli, Turkey